AD-A035 329 SOLAR SAN DIEGO CALIF F/G 21/5
APPLICATION OF CERAMIC NOZZLES TO 10KW ENGINE.(U)
AUG 76 J C NAPIER, A G METCALFE DAAK02-75-C-0138
UNCLASSIFIED RDR-1797-16 NL

1 OF 2
AD
A035 329

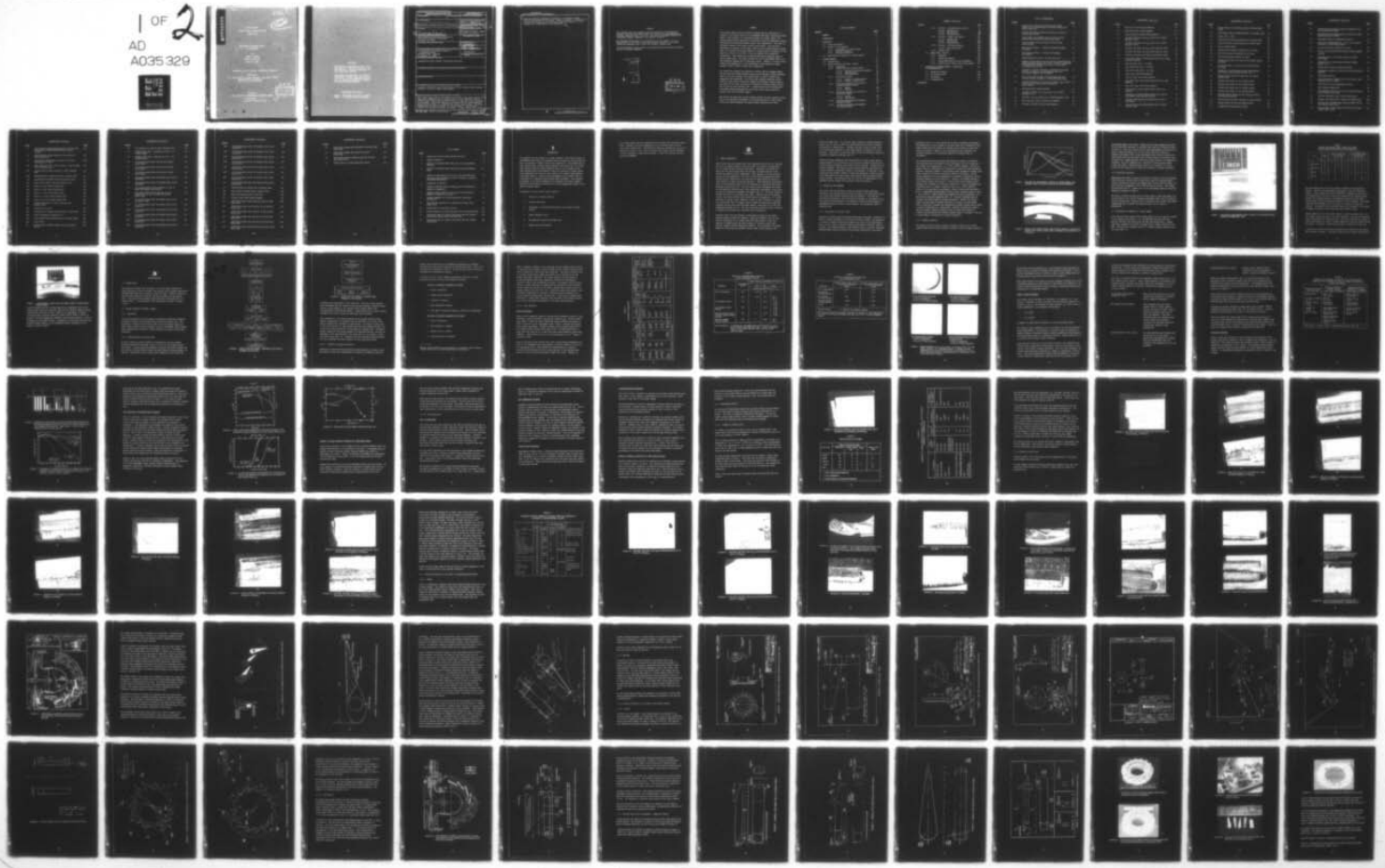

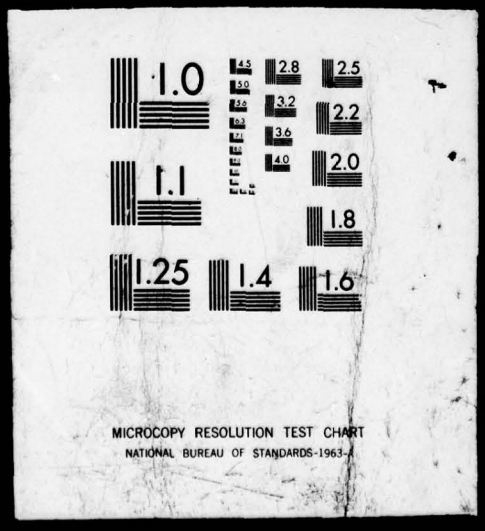

NDR 1797-16
S.O. 6-4375-7

INTERIM REPORT

Contract Number DAAK02-75-C-0138

AUGUST 1976

APPLICATION OF CERAMIC NOZZLES TO 10KW ENGINE

BY

JAMES C. NAPIER

ARTHUR G. METCALFE

THOMAS E. DUFFY

PREPARED FOR

U.S. Army Mobility Equipment Research & Development Command
Laboratory 3000 - CRDFB-EM
Fort Belvoir, Virginia 22060

Prepared by

SOLAR DIVISION OF INTERNATIONAL HARVESTER COMPANY

PO Box 80966

San Diego, California 92138

Disclaimer

The findings in this report are not
construed as an official Department
Army position, unless so designat
other authorized documents.

The citation of trade names and na
manufacturers in this report are not
construed as official Government in
ment or approval of commercial pro

SECURITY CLASSIFICATION OF THIS PAGE (When Data Entered)

REPORT DOCUMENTATION PAGE

READ INSTRUCTIONS BEFORE COMPLETING FORM

1. REPORT NUMBER
2. GOVT ACCESSION NO.
3. RECIPIENT'S CATALOG NUMBER

4. TITLE (and Subtitle)

(6) Application of Ceramic Nozzles to 10kW Engine.

5. TYPE OF REPORT & PERIOD COVERED

(9) Interim Report. 7 Mar 75 - 17 Aug 76

6. PERFORMING ORG. REPORT NUMBER

(14) RDR-1797-16

7. AUTHOR(s)

(10) J.C. Napier and A.G. Metcalfe

8. CONTRACT OR GRANT NUMBER(s)

(15) DAAK02-75-C-0138 new

9. PERFORMING ORGANIZATION NAME AND ADDRESS

Solar Division of International Harvester
2200 Pacific Highway, PO Box 80966
San Diego, CA 92138

10. PROGRAM ELEMENT, PROJECT, TASK AREA & WORK UNIT NUMBERS

11. CONTROLLING OFFICE NAME AND ADDRESS

(11) 12. REPORT DATE

August 1976

13. NUMBER OF PAGES

(12) 192p.

14. MONITORING AGENCY NAME & ADDRESS (if different from Controlling Office)

U.S. Army Mobility Equipment Research & Development Command
Laboratory 3000 - CRXFB-EM
Ft. Belvoir, VA 22060

15. SECURITY CLASS. (of this report)

Unclassified

15a. DECLASSIFICATION/DOWNGRADING SCHEDULE

16. DISTRIBUTION STATEMENT (of this Report)

Approved for Public Release; Distribution Unlimited

17. DISTRIBUTION STATEMENT (of the abstract entered in Block 20, if different from Report)

18. SUPPLEMENTARY NOTES

19. KEY WORDS (Continue on reverse side if necessary and identify by block number)

Ceramics, Gas Turbine, Nozzle Vanes, Nozzle Shrouds, Thermal Shock, Erosion, Corrosion, Joining, Relaxing Glass Adhesive

20. ABSTRACT (Continue on reverse side if necessary and identify by block number)

This report covers work for application of ceramics to the nozzle section of the small radial MERADCOM 10kW gas turbine engine. Engine simulator tests of a HPSi$_3$N$_4$ ceramic-vane/superalloy-shroud nozzle for improved erosion resistance are described. Engine test results of the same nozzle are also documented. Engine simulator tests of a simplified all-ceramic nozzle section, including HPSi$_3$N$_4$ vanes and RBSi$_3$N$_4$ shrouds are also documented. Special glass adhesives for joining of ceramics are studied. Program results show thermal

→over

DD FORM 1 JAN 73 1473 EDITION OF 1 NOV 65 IS OBSOLETE

UNCLASSIFIED 326 550

SECURITY CLASSIFICATION OF THIS PAGE (When Data Entered)

shock and corrosion resistance of ceramics to be adequate to meet operating environment of the engine. Erosion resistance of HPSi$_3$N$_4$ vanes has been shown to be one to two orders of magnitude superior to 713LC superalloy at 1700°F turbine inlet temperature.

PREFACE

This interim report was prepared by The Solar Division of International Harvester under Contract Number DAAK02-75-C-0138 for the Electromechanical Division, Laboratory 3000, of the U.S. Army Mobility Equipment Research and Development Command, (MERADCOM), Fort Belvoir, Virginia.

The Principal Investigator for the program is Mr. J.C. Napier. Dr. A.G. Metcalfe and Mr. T.E. Duffy are Project Technical Advisors. This report covers work conducted from 7 March 1975 through 17 August 1976.

The work described in this report was conducted under the technical direction of Mr. F.D. Jordan, MERADCOM.

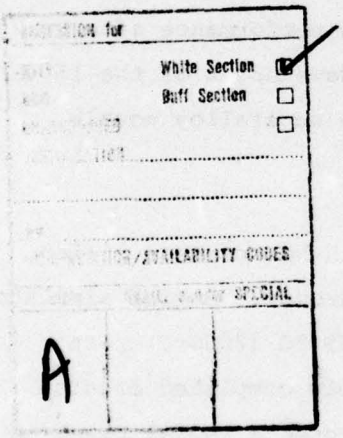

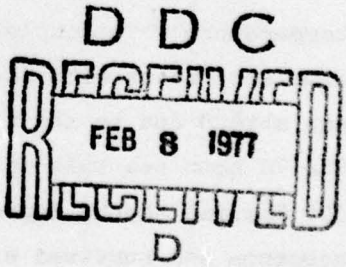

SUMMARY

This interim report covers 16 months of project work for application of ceramics to the nozzle section of the MERADCOM 10kW radial inflow gas turbine engine. The objective is to introduce ceramics for better engine life through higher erosion resistance of the nozzle vanes and subsequently better performance by facilitating higher turbine inlet temperature. Two steps for including ceramics in the nozzle section were planned. The first was replacement of sections of the nozzle vanes with hot pressed silicon nitride, which is projected from program results to increase erosion resistance of the nozzle by a factor of at least 16 over the standard 713LC superalloy construction. This concept was carried through engine simulator tests to actual engine tests. The nozzle suffered no loss in performance after a 25 hour operating sequence and 50 start/stop cycles. However, 5 of the 15 vanes suffered some damage due to yield deformation of the superalloy nozzle shrouds at 871°C (1600°F) turbine inlet temperature.

The second step involved the testing of a nozzle with hot pressed silicon nitride vanes and reaction bonded silicon nitride shrouds. Engine simulator tests for erosion, corrosion and thermal shock to 1093°C (2000°F) part temperature were completed. The first nozzle assembly completed erosion simulator tests with no significant damage but developed a radial crack in one shroud due to short circuiting of insulation by molten products during the 70 hour sea salt corrosion test. A second nozzle set was subjected to 500 thermal shocks representative of the most severe engine operating sequence and survived without damage.

This effort has shown that silicon nitride ceramics can most probably survive the hot end operating environment in the nozzle section of a small radial inflow gas turbine assuming that proper design precautions are taken.

TABLE OF CONTENTS

CONTENTS (Continued)

LIST OF ILLUSTRATIONS

ILLUSTRATIONS (Continued)

ILLUSTRATIONS (Continued)

ILLUSTRATIONS (Continued)

ILLUSTRATIONS (Continued)

ILLUSTRATIONS (Continued)

ILLUSTRATIONS (Continued)

ILLUSTRATIONS (Continued

LIST OF TABLES

1

INTRODUCTION

The objective of this program is to apply ceramics to the nozzle section of the MERADCOM 10kW engine for increased erosion resistance and to provide the means of achieving a higher turbine inlet temperature. The program work to date, reported here, includes engine simulator and engine test of a ceramic vane section nozzle and engine simulator test of an all-ceramic nozzle. Other programs which are necessary to meet the objective of higher turbine inlet temperature and relate to this project are a ceramic 10kW combustor development project, a ceramic rotor development project and/or work for development of a compressor wheel/turbine wheel monorotor. The successful development of the above components will establish the primary elements required to show technical feasibility of a high temperature version of the 10kW gas turbine engine.

Development of an all-ceramic nozzle requires:

1. Selection of ceramic material
2. Analysis and design
3. Development of specialized fabrication and ceramics joining methods
4. Engine simulator tests
5. Re-design and analysis for engine test
6. Engine test and evaluation.

All of these steps have been completed for the ceramic vane (section) nozzle. Steps 1 through 4 have been completed for an all-ceramic nozzle concept using simple shroud forms. Reiteration of steps one through four, as well as completion of steps 5 and 6 will be required with ceramic shroud components to solve problems of engine-related design. A plan for this work has been proposed to MERADCOM.

2

BACKGROUND

2.1 SERVICE EXPERIENCE

Small radial flow gas turbines have found widespread use by the U.S. Army and Air Force in ground generator sets and as APU's for service in essentially all U.S. Army and Navy transport helicopters. Experience in service has shown that the nozzle guide vanes are the most vulnerable portion of the turbine and suffer the most degradation. There appears to be two principal sources of this degradation. The first results from the ingestion of dust because service conditions do not allow use of highly effective filters or other devices to remove particulate materials. This problem was particularly acute in the Vietnam war where the dust generated at take-off by helicopters seriously affected APU life. The dust caused erosion throughout the engine but coatings were readily found to give significant improvement in the cooler sections as described by Shoemaker and Shumate (Ref. 1). No really effective coating was found for the nozzle guide vanes. However, even in the absence of dust, the nozzle suffers from a second source of degradation. It is more difficult to design a small combustor to have as high efficiency as a large one, particularly when the engine must be capable of operation by unskilled personnel and must keep operating under adverse conditions such as the dust ingestion described earlier. Hot spots and carbon particles result from loss of combustor performance and accelerate nozzle degradation.

Extensive effort has been devoted to developing solutions to the nozzle erosion problem in small gas turbines. Larger gas turbines, such as those used for propulsion do not present quite the same problem. First, the exposure to ingested dust and other erodants is limited to quite short periods, primarily during landing and take-off. And secondarily, the added weight of a dust particle separator does not make a major change in the

thrust-to-weight ratio. In contrast, small radial gas turbine generators used by the U.S. Army for APU's and ground generator sets may be exposed continuously to ingested dust. Further, the power output-to-weight ratio would be affected adversely in these small engines by addition of a dust separator. Some types of solution to dust erosion in propulsion engines are described by Connors and Murphy (Ref. 2).

Exclusion of dust separators from consideration for small radial engines caused attention to be directed to use of erosion resistant materials that would be used in monolithic form rather than as coatings. Ceramics were an obvious candidate. Work began on Solar internal programs and showed that ceramics offered a potential solution to the problem. In addition, it was recognized that ceramics offered a longer term advantage in terms of higher inlet temperatures and hence higher power outputs from the engine without weight increase. The background work at Solar and its application to the MERADCOM 10kW gas turbine are described in the next sections.

2.2 EROSION IN GAS TURBINES

The initial work was directed to tests of selected ceramic materials, selection of hot pressed silicon nitride and tests in an engine where three cast N-155 vanes had been replaced with this material. This work was sufficiently promising so that the difficult problems of replacement of all the vanes and of replacement of the metallic shrouds could be proposed to MERADCOM and became the basis of this program. The preliminary work is described here.

2.2.1 Requirements for Nozzle Vanes

Materials for nozzle guide vanes must possess many properties. Resistance to thermal cycling, resistance to hot spots and thermal flashes, and resistance to erosion by carbon and particulate matter are a few of the requirements. These, in turn, lead to specific property requirements including: high hot strength, low thermal expansion, good oxidation and hot corrosion resistance, minimum dynamic oxidation effects, high thermal conductivity, good impact

resistance, and so on. Good design must be used to minimize the demands on the material and, in this regard, it has been found that a mechanical joint between shroud and vane reduces the thermal stress problem in these small radial gas turbines. However, once the design has been optimized, the intrinsic properties of the materials impose the ultimate limit on performance.

The high pattern factor associated with small gas turbines, particularly those operated under unfavorable service conditions, has led to adoption of low turbine inlet temperatures, e.g., 927°C (1700°F) maximum. This has an adverse effect on efficiency but is warranted to permit the high reliability required. Materials capable of withstanding higher temperature flashes would permit increase of TIT with a beneficial effect on efficiency. Silicon nitride appeared to have the combination of strength at temperature and low expansion required for this application. However, the greatest problem in field service results from erosion. Erosion opens up the critical nozzle openings with a decrease of efficiency revealed by a rise in the exhaust gas temperature until it exceeds a specified value [e.g., 565°C (1050°F)]. Because of its importance on performance, several studies have been made at Solar to understand the mechanism of erosion and to evaluate materials (Refs. 1, and 3 thru 5). These studies have permitted the basic mechanisms to be identified for metallic materials (Ref. 4). Strength, hardness and heat treatment had little effect on erosion resistance. Indeed, the erosion weight loss was found to deviate less than $\pm$ 10 percent for many common metallic materials, although the differences in density between metals result in greater differences on a volume basis. However, non-metallic, elastic materials showed a markedly different rate of erosion that varied in a different way than metals when measured against angle of incidence. Data due to Finnie (Ref. 6) illustrate this point in Figure 1.

2.2.2 Erosion in Service

The erosion of nozzle vanes in service is shown in Figure 2 for a Titan turbine nozzle after 68 hours service in Vietnam. Note the severe erosion at

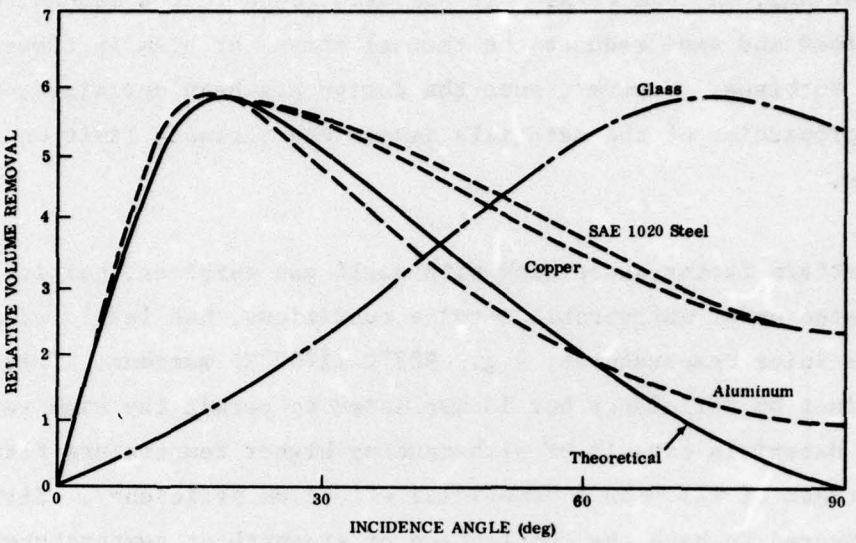

FIGURE 1. PREDICTED AND EXPERIMENTAL VARIATION OF VOLUME REMOVAL WITH INCIDENCE ANGLE FOR VARIOUS DUCTILE AND BRITTLE MATERIALS

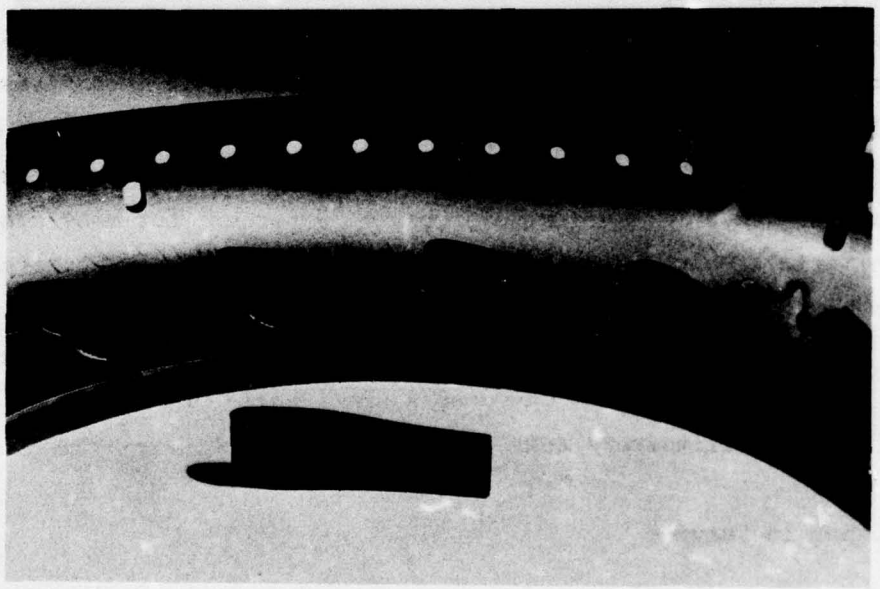

FIGURE 2. TYPICAL TITAN TURBINE NOZZLE VANES AFTER 68 HOURS OF VIETNAM DUST EROSION (Note Eroded, Curled Edge as Compared to Uneroded Vane in Foreground.

the trailing edges of the vanes. Similar wear has been induced in the test cell by controlled ingestion of -140 mesh silica dust for 10 hours as shown in Figure 3. Such wear results from low angle impingements and reference to Figure 1 shows that metals are at their worst under such conditions. Shoemaker and Shumate (Ref. 1) had investigated hard, brittle coatings for nozzle guide vanes but had found little success because of porosity in some coatings (e.g., plasma sprayed), spalling of dense coatings, or inadequacy of thickness. The work suggested that a monolithic ceramic material might provide the answer. Published data attested to the adequacy of silicon nitride in most respects but no data were available on erosion resistance.

2.2.3 Materials Evaluation

Measurements were made to compare the erosion resistance of the two principal forms of silicon nitride with a typical metal (type 410 stainless steel). Arizona road dust was used in the standard Solar erosion test rig (Refs. 1, 4 and 5) and was accelerated by air to 600-700 feet per second. The loading was 80 mg dust per ft^3. Results for the two impingement angles of 30 and 90 degrees are compared in Table 1.

The porous, reaction sintered silicon nitride shows a small improvement over the 410 steel at the critical 30-degree impingement angle, but not enough to warrant consideration. However, the hot pressed silicon nitride shows almost unmeasurable loss of weight and should increase the life nearly a hundred-fold.

2.3 APPLICATION OF CERAMICS TO A RADIAL ENGINE

Solar supplies eight separate Titan engine models for use on various versions of four military helicopters, i.e., the CH46 Navy Sea King, CH47 Army Chinook, CH53 Navy Sea Stallion and the CH54 Army Flying Crane. Ceramic vanes were evaluated on the T62T-27 engine used on various versions of the CH53. This work was performed as part of a product support program for the U.S. Navy (Ref. 7).

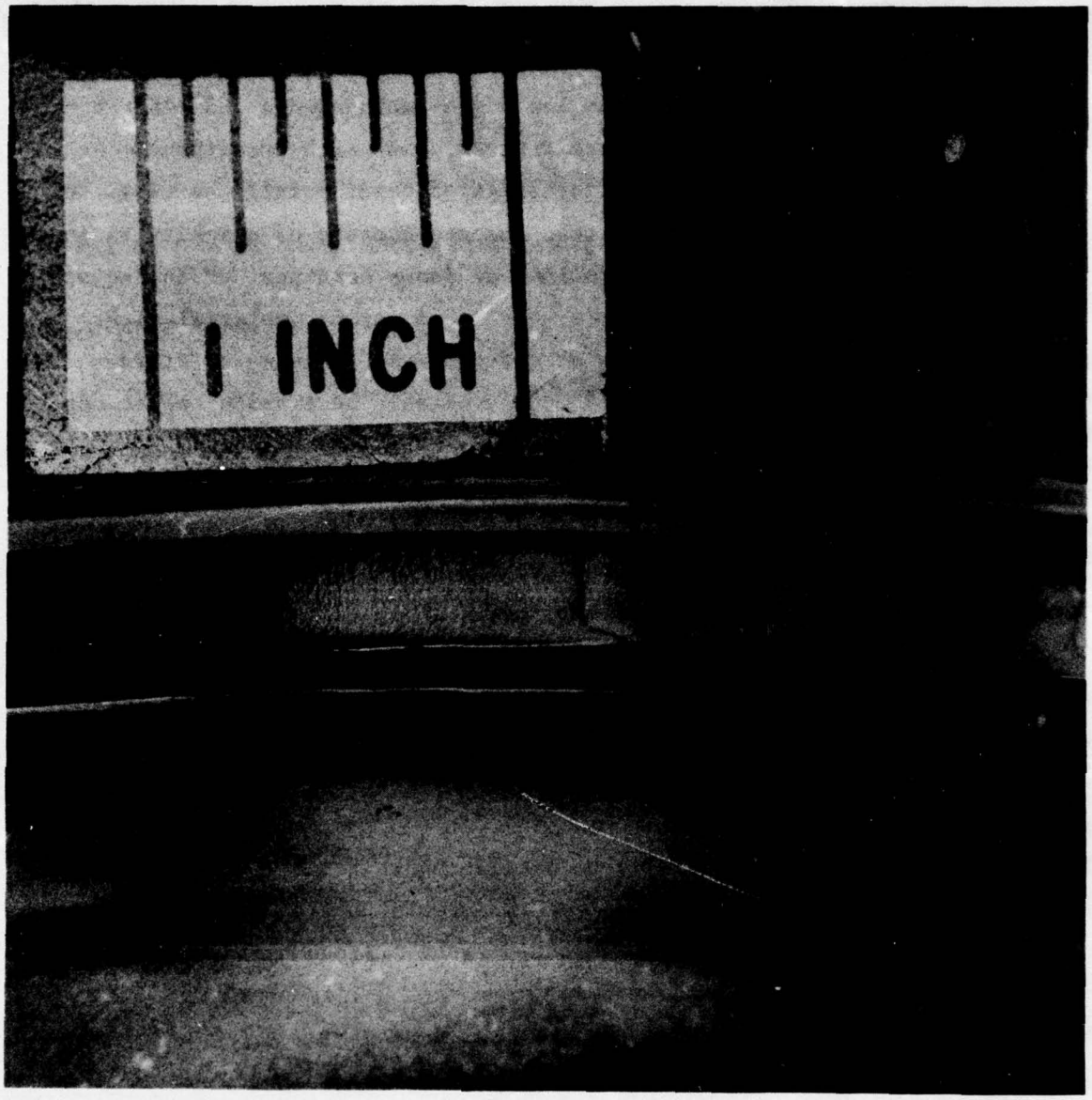

FIGURE 3. TITAN NOZZLE VANE ASSEMBLY AFTER 10 HOURS OF TEST SHOWING SEVERE EROSION OF CONVENTIONAL VANES

TABLE 1

EROSION TEST RESULTS USING ARIZONA ROAD DUST
(Average Velocity 600-700 fps, 80 mg dust/ft^3)

Material	Particle Size	30-Degree Impingement Angle Average Volume Loss x 10^3 cc For Time in Minutes			90-Degree Impingement Angle Average Volume Loss x 10^3 cc For Time in Minutes		
		5	10	15	5	10	15
410 SS	43-74	0.16	0.92	3.7	0.28	0.47	1.9
Reaction Sintered Si_3N_4	43-74	--	0.47	2.2	1.1	2.1	5.6
Reaction Sintered Si_3N_4	-43	--	--	2.3	--	--	4.5
Hot Pressed Si_3N_4	43-74	--	--	0.06	0.10	0.10	0.13
Hot Pressed Si_3N_4	-43	--	--	0.00	--	--	0.03

The nozzle guide vane in the Titan engine is shown in the foreground in Figure 2. The hole allows mechanical attachment of the outer and inner shrouds. Such a design would not be suitable for ceramics, so that in the first engine tests, only three vanes were replaced by hot pressed silicon nitride with reliance placed on the mechanical fasteners at the other metallic vanes to hold the silicon nitride in place in recesses. The method of mechanical attachment used in the Titan is to upset or rivet each fastener. Although the silicon nitride vane was not fastened in this manner, attachment of adjacent vanes caused some small cracks to form.

The T62 engine was run in the normal manner at 61,300 rpm except that 4.4×10^{-5} pounds of dust per pound of air was introduced. The dust was -140 mesh silica and required 172.5 grams per hour. The first erosion test extended 10 hours during which time nearly 4 pounds (1800 gms) of dust was passed through the engine. No special precautions were taken at light-off in this test.

A comparison of an N-155 vane with the adjacent hot pressed silicon nitride vane is shown in Figure 4. The small fracture in the silicon nitride vanes

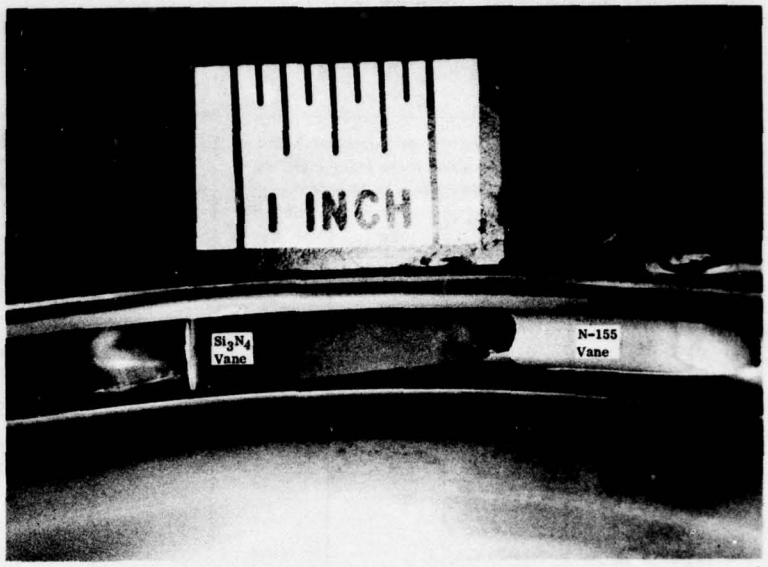

FIGURE 4. SILICON NITRIDE (LEFT) AND N-155 VANES (RIGHT) IN TITAN ENGINE AFTER TESTING

occurred because the thin trailing edges did not completely float in the recesses under operating conditions, and will be avoided by improved design as discussed in the next section. However, the improvement in erosion resistance under operating conditions at 898 to 927°C (1650 to 1700°F) is similar to the room temperature laboratory tests reported earlier. There is an absence of any general erosion. Preservation of the sharp fracture edges provides further support for the remarkable erosion resistance of this material at 927°C (1700°F).

3

PROGRAM RESULTS

3.1 PROGRAM PLAN

This program is divided into two phases. The first phase culminates in engine simulator rig test of ceramic vane section and all-ceramic nozzles and includes background steps required to reach this goal: material evaluation and selection; analysis and design; fabrication studies and preliminary tests. The second phase includes design fabrication and engine test of a ceramic nozzle. A block diagram of the program plan is shown in Figures 5 and 6.

3.2 ENGINE SIMULATOR RIG TESTS - PHASE I

3.2.1 Objectives

This program phase was for the purpose of generating background information necessary to design a part-ceramic nozzle suitable for engine test. The feasibility of using silicon nitride parts for an all-ceramic nozzle in a small radial engine hot end environment was also investigated. Both of these nozzle concepts were subjected to engine simulator rig tests to meet these objectives.

3.2.2 Ceramic Material Selection Study

Silicon nitride and silicon carbide are recognized as the best ceramic materials commercially available today for use in the gas turbine hot end environment. A paper study was conducted at program initiation to select the best material and fabrication process for nozzle vanes and nozzle shrouds. In addition, experimental erosion studies were conducted at Solar since this

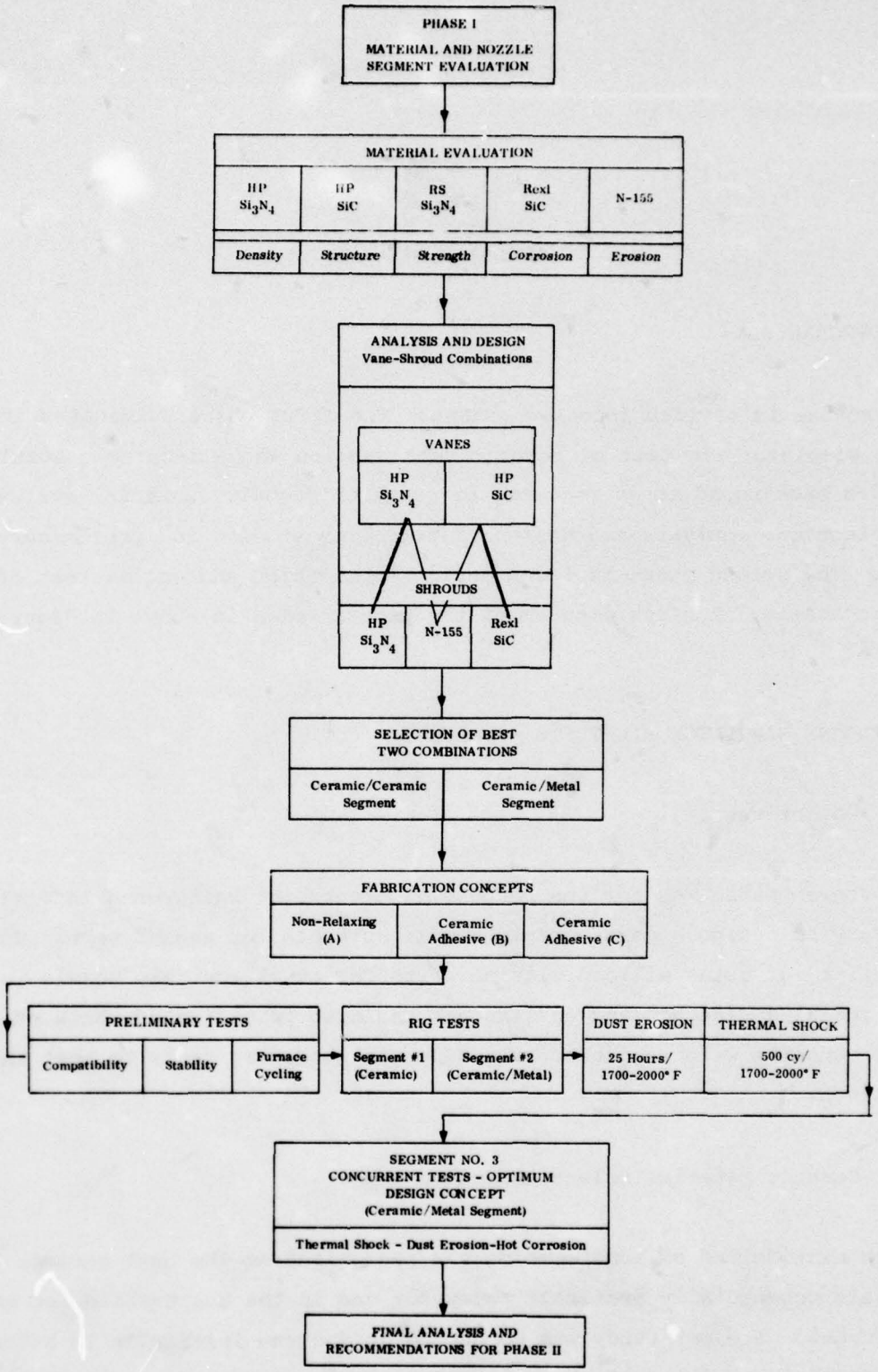

FIGURE 5. WORK PLAN FOR PHASE I - MATERIAL AND NOZZLE SEGMENT EVALUATION

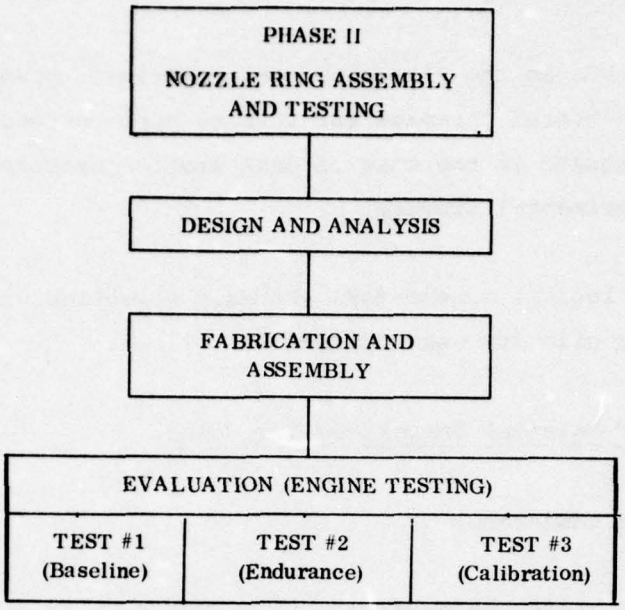

FIGURE 6. WORK PLAN FOR PHASE II - NOZZLE RING ASSEMBLY AND TESTING

information was unavailable in the literature. The four primary material forms considered were hot pressed silicon nitride ($HPSi_3N_4$), reaction bonded silicon nitride ($RBSi_3N_4$), hot pressed silicon carbide (HPSiC) and recrystallized silicon carbide (RCSiC). Another variation on silicon carbide considered was silicon filled recrystallized silicon carbide.

Since submission of the program proposal no new ceramic materials which warrant consideration for turbines have been developed to the point where they are commercially available for application. For example, Sialon (Ref. 8) shows the potential of good strength and fabrication characteristics, but is not fully characterized and is unavailable in finished form. Sinterable silicon carbide has also shown promise as an excellent material, but has not developed or been characterized to the point where it is practical to make gas turbine parts (Ref. 9). Therefore the above candidate ceramic materials are still considered the best available for this application study.

3.2.2.1 Criteria For Material Selection

Selection of silicon nitride and silicon carbide materials for Phase I vane and shroud rig tests was accomplished by considering fundamental materials

property data available in the literature and experience of numerous researchers who have tested ceramics for turbine application. Data in the literature was inadequate in the case of dust erosion properties and was supplemented by experimental studies.

In order to allow a logical scheme for materials selection, relevant properties and their priority were defined as follows:

Priority of Material Properties for Vanes

1. Erosion resistance
2. Thermal shock resistance*
3. Corrosion resistance
4. High temperature strength
5. High impact strength and energy of fracture at temperature

Priority of Material Properties for Shrouds

1. Ease of fabrication
2. High temperature strength
3. Thermal shock resistance
4. Erosion/corrosion resistance

---

*Thermal shock resistance relates primarily to strength, elastic modulus, thermal conductivity, thermal expansivity and plasticity.

Table 2 presents a summary of the properties for hot pressed silicon nitride, hot pressed silicon carbide, reaction bonded silicon nitride, recrystallized silicon carbide and 713LC nickel base superalloy. The data on ceramics refer to the most recent Norton Company materials, NC-132, NC-203, NC-350 and NC-400 except where indicated. The recent materials are the result of process refinement rather than composition variation of the materials reported in many of the references given here. For example, NC-132 Silicon Nitride is nearly identical in composition and structure to HS-130 Silicon Nitride except that the NC-132 has higher strength due to better control of maximum internal void size (Ref. 10). Properties, other than strength, such as thermal conductivity or corrosion resistance would be expected to be nearly identical between these two materials. In the case of thermal shock resistance or Charpy impact strength, data available on the former materials are at least qualitatively comparable to the most recent materials.

3.2.2.2 Vane Materials

Erosion Resistance

Tables 3 and 4 summarize results of erosion tests conducted at Solar on 713LC superalloy, reaction sintered Si_3N_4 and hot pressed Si_3N_4. The hot pressed Si_3N_4 shows at least one order of magnitude superior erosion resistance to 713LC in both 90° and 30° impingement tests. Figure 7 pictures test samples after erosion experiments. Further evidence of good erosion properties of hot pressed silicon nitride can be seen in Figure 4 which shows both H.P. Si_3N_4 and N-155 vanes run in a Solar T62 Titan engine exposed to severe dust injection. (Each pound of inlet air was injected with 4.4×10^{-5} pounds of -140 mesh silica.)

Reaction sintered silicon nitride shows only a slight erosion advantage over 713LC at 30° impingement angle and inferior erosion in relation to 713LC at a 90° impingement angle. This disqualifies consideration of a reaction sintered silicon nitride for use as a vane material in this program since erosion is the first priority material property for vanes. (However, it

TABLE 2

MATERIAL PROPERTIES

Material	Flexural Strength kPa (psi) 3 Pt. Bend at 982°C (1800°F)	Tensile Strength kPa (psi) at 982°C (1800°F)	Modulus of Elasticity kPa (psi) at 25°C (77°F)	Density gm/cc	Thermal Expansion Coefficient $°C^{-1}$ 20-1000°C (1832°F)	Thermal Conductivity W/m°C (BTU/Hr ft °F) at 25°C	Specific Heat Cal/gm °C at 25°C	Thermal Stress Resistance Parameter R_1 Rapid Temperature Variation $°C^{-1}$	Thermal Stress Resistance Parameter R_2 Slow Temperature Variation Cal/cm $°C^2$	1000 Hr Stress Rupture at Temperature kPa (psi)
Hot Pressed Silicon Nitride	869000 (126000)	294000 (42,600) HS-130 (Ref. 16)	317×10^6 (46×10^6) (Ref. 20)	3.2	3.2×10^{-6} (Ref. 10) (3.73×10^{-6} at 1800°F) (Ref. 27)	28 (17) (Ref. 20)	0.17 (0.30 at 1800°F) (Ref. 20)	650 (Ref. 21) Lucas Material	26 (Ref. 21)	138000 (20,000) HS-130 at 1149°C (2100°F) (Ref. 19)
Hot Pressed Silicon Carbide	676000 (98000)	239000 (34,700) (Ref. 16)	441×10^6 (64×10^6) (Ref. 20)	3.2	4.3×10^{-6} (Ref. 20)	81 (47) (Ref. 20)	0.15	144 (Ref. 21) Norton Material	23 (Ref. 21)	(only 619 hrs) 103000 (15,000) at 1260°C, (2300°F) (Ref. 28)
Reaction Bonded Silicon Nitride	317000 (46000)	--	172×10^6 (25×10^6)	2.4	3.2×10^{-6} (Ref. 20)	15.5 (9) (Ref. 20)	0.17	256 (Ref. 21) Lucas Material	5 (Ref. 21)	--
Recrystallized Silicon Carbide	186000 (27000)	--	207×10^6 (30×10^6) (Ref. 20)	2.6	4.3×10^{-6} (Ref. 20)	43 (25) (Ref. 20)	0.15	92 (Ref. 21) Norton Material	5 (Ref. 21)	--
713LC Nickel Base Superalloy	--	(68400) 19.7% elongation (Ref. 26)	206×10^6 (29.9×10^6) (Ref. 26)	7.91 (Ref. 26)	16.4×10^{-6} (Ref. 26)	21 (12) (Ref. 26)	--	Do not Apply to Ductile Materials		96500 (14000) at 982°C (1800°F) (Ref. 26)

*All information from Reference 17 unless indicated otherwise.

TABLE 3

Erosion of Candidate Nozzle Materials
Versus Impingement Velocity

Material	Impingement Angle	Mean Particle Impingement Velocity, fps		
		190	520	840
		Erosion Volume Loss x 10^3 cc		
713 LC Superalloy	30°	0.09	2.60	- -
	90°	0.21	1.79	30.0 26.8
Hot Pressed Silicon	90°	-	0.12	0.22 0.63 0.56
Hot Pressed Silicon Carbide	90°	-	0.32	1.59 1.28 1.34
Recrystallized Silicon Carbide, Silicon Filled (NC-430)	90°	0	0.39	2.34 3.08
Reaction Bonded Silicon Nitride	90°	0	2.88	21.7 28.2

Test Conditions: 15 minutes at room temperature with 80 mg/ft^3 of 43-74 micron Arizona road dust and 3/8 in. (0.95 cm) diameter nozzle. Gas velocity 200 fps (190), 600 fps (520), 1000 fps (840)

TABLE 4

Erosion of Candidate Nozzle Materials
Versus Impingement Angle

Material	Erosion Volume Loss x 10^3 cc 30 Degree Impingement Angle	Erosion Volume Loss x 10^3 cc 90 Degree Impingement Angle
713 LC Superalloy	2.60	1.79
Hot Pressed Silicon Nitride	0	0.12
Hot Pressed Silicon Carbide	0.04	0.32
Reaction Bonded* Silicon Nitride	1.65**	2.88
NC-430	0.08	0.39

*Ground surface. ** Derived from previous results.

[520 fps mean particle impingement velocity, 15 minutes at room temperature, 80 mg/ft^3 of 43-74 Micron Arizona road dust and 3/8 in. (0.95 cm) diameter nozzle]

713 LC Nickel-Base Superalloy
0.017 in. Penetration
30.3 cc x 10^{-3} Volume Removal

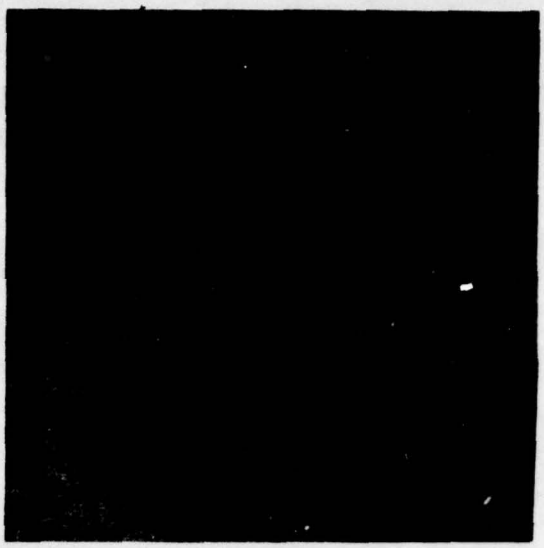

Hot Pressed Silicon Nitride
0.0003 in. Penetration
0.6 cc x 10^{-3} Volume Removal

Hot Pressed Silicon Carbide
0.0007 in. Penetration
1.3 cc x 10^{-3} Volume Removal

Silicon Filled Recrystallized Silicon Carbide (NC 430)
0.0013 in. Penetration
2.3 cc x 10^{-3} Volume Removal

FIGURE 7. ERODED SURFACES OF 713 LC HP Si_3N_4, HP SiC and NC 430; 3/8 Inch Nozzle Diameter; 90° Impingement Angle; 15 Minutes at Room Temperature; 840 fps Particle Velocity; and 80 mg/ft^3 of 43-74 Micron Arizona Road Dust. (Volume Removal and Penetration Calculated from Weight Changes.)

should resist erosion acceptably as a shroud material since the lower gas velocity at most surfaces of shrouds makes erosion less critical. Also, particle impingement angles to shrouds are very low near nozzle throat and turbine contour regions where gas velocities are higher.)

HPSiC shows slightly less erosion resistance compared to HPSi_3N_4 but is still considerably superior to 713LC superalloy under these test conditions. The silicon filled recrystallized silicon carbide has surprisingly good erosion resistance for a low density ceramic.

Thermal Stress Resistance

Good thermal stress resistance is considered to be important for a vane material. Reference 11 cites two thermal stress resistance parameters for ceramics, R_1 and R_2, which depend upon bend strength, σ_B, elastic modulus, E, thermal expansivity, α, and thermal conductivity k.

$$R_1 = \sigma_B/E\alpha$$

$$R_2 = k\sigma_B/E\alpha$$

R_1 applies to rapid thermal cycling and R_2 to slow thermal cycling.

The values of these parameters are given in Table 2 for the four materials under consideration. The terms are in indices of relative resistance to thermal stresses of different ceramic materials assuming the same geometry and surface heat loading in a monolithic structure. Larger values of R_1 or R_2 suggest greater thermal stress resistance.

Based upon the values of R_1 and R_2 listed in Table 2, hot pressed silicon nitride would be expected to perform better than the other materials under rapid or slow thermal transient conditions. This is in good agreement with thermal shock experiments conducted by a number of researchers, including Solar. Even though experimental thermal shock performance of hot pressed silicon carbide is substantially less than that of hot pressed silicon

nitride, the parameter R_1 best describes its relative merit for gas turbine applications. R_1 also agrees with experimental evidence which shows both reaction bonded silicon carbide and recrystallized silicon carbide to have inferior thermal shock resistance to either hot pressed form.

Beck (Ref. 12) reported results from comparative thermal shock tests of the four ceramic types in Table 2. Each of these materials was fabricated into simulated airfoil sections with various edge radii and exposed to a 1316°C (2400°F) maximum temperature laboratory thermal shock schedule with the following results.

Hot Pressed Silicon Nitride (Grades 130 & 110)	Both survived all tests for all radii (grade HS-130 (Norton Co.) provided better oxidation resistance).
Hot Pressed Silicon Carbide	Crack sensitive with one of four possible radii to 1316°C (2400°F). Survived all tests to 1260°C (2300°F). Oxidation resistance good only for short term exposure. Vane tests conducted later on an improved grade (NC-203) showed good oxidation resistance but continued subcritical cracking when exposed to peak temperatures.
Reaction Bonded Silicon Nitride	One grade exhibited poor thermal shock resistance for all size radii. A second grade performed well in thermal shock but considerable edge loss (oxidation) was exerienced for all test specimens.

Recrystallized Silicon Carbide	Showed an early tendency toward cracking but little progression of cracks. Oxidation resistance was good.

Mumford and Booker (Westinghouse, Ref. 13) reported simultaneous high temperature (1371°C [2500°F]) thermal shock tests of hot pressed silicon nitride and hot pressed silicon carbide vanes. (The maximum surface heat transfer coefficient on the vane airfoils was about 2840 W/M^2 degree C (500 Btu/hr sq. ft degree F.)

After three cycles the silicon carbide airfoils were cracked whereas the nitride parts were undamaged. Subsequent failure of the combustor impacted both types of vanes with metal debris. All of the silicon carbide vanes were shattered while the silicon nitride vanes remained intact.

Simulated gas turbine environment thermal shock tests to 1200°C (2200°F) conducted by Sanders and Probst (Ref. 14) are shown in Table 5. (Figure 8 summarizes these findings in the form of a bar chart for clarity.)

These data support the concept that the hot pressed silicon nitride is superior in high temperature thermal shock to the other three ceramic forms considered here, and that hot pressed silicon carbide performs better than reaction bonded silicon nitride or recrystallized silicon carbide. Refel SiC shows good thermal shock resistance, possibly better than HPSiC.

Corrosion Resistance

Figure 9 taken from Reference 15 gives corrosion-erosion behavior of hot pressed Si_3N_4 and SiC compared to that of commonly used superalloys, X-45 and Udimet-500. The ceramic materials were exposed to 1093°C (2000°F) diesel oil combustion gas containing S, Na, V and Mg. The superalloys showed greater weight loss even though they were exposed to a lower temperature of 908°C (1650°F). No appreciable degradation in strength was noted for either of the ceramics.

TABLE 5

Summary of Test Results for SiC and Si_3N_4 Simulated Vane Shape Specimens Evaluated at 1200°C in a Mach 1 Simulated Gas Turbine Environment.

Materials reaching 100 cycle goal	Materials failing in thermal fatigue (cycle range to failure)	Materials failing in mechanically in holder (cycle range to failure)
Norton HP SiC	A.C.E. HP SiC (41-43)	Norton low-fired RS SiC (26)
U.K.A.E.A. (Refel) RS SiC	AVCO HP SiC (1-47)	A.M.E. RS Si_3N_4 (7-49)
Norton HP HS130 Si_3N_4	Ceradyne HP SiC (1-11)	Norton NC350 RS Si_3N_4 (54-92)
Ceradyne HP Si_3N_4	Carborundum-KT-RS SiC (1-10)	U.K.A.E.A. (Refel) RS SiC (89)
AVCO HP Si_3N_4	Norton low-fired RS SiC (22)	E.R.C. CVD SiC (1-52)
	Norton high-fired RS SiC (0-1)	
	A.M.E. RS Si_3N_4 (9-24)	
Test Cycle: 1 hour at 1200°C, 5 minute still air cool (Ref. 14)		

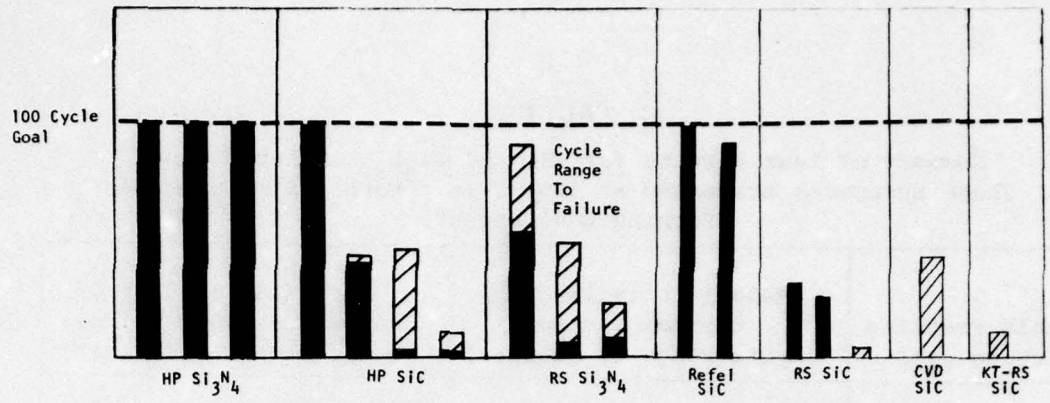

FIGURE 8. SUMMARY OF TEST RESULTS FOR SiC and Si_3N_4 SIMULATED VANE SHAPE SPECIMENS EVALUATED AT 1200°C IN A MACH 1 SIMULATED GAS TURBINE ENVIRONMENT. TEST CYCLE: 1 HR AT 1200°C, 5 MINUTES STILL AIR COOL (Ref. 14).

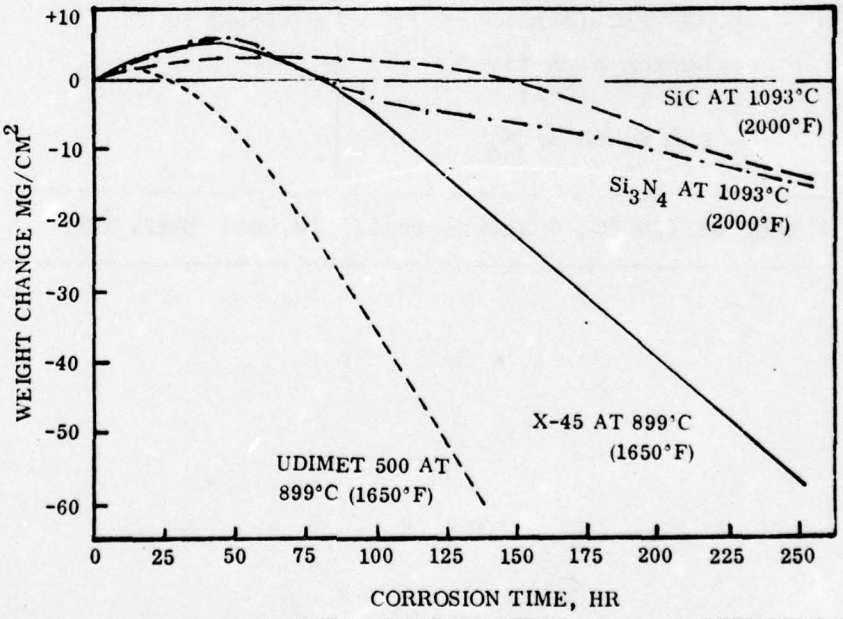

FIGURE 9. CORROSION OF VARIOUS MATERIALS IN TURBINE TEST PASSAGE, EXPOSED TO COMBUSTOR GAS CONTAMINATED WITH 0.5% S, 5 PPM Na, 2PPM V, AND 0.6 PPM Mg

Later work by the same researchers (Ref. 16) determined that barium introduced into the diesel fuel to inhibit smoke and prevent gum formation played a major role in accelerating corrosion-erosion behavior. Tests with a barium free fuel showed corrosion-erosion weight loss to be even less than corrosion weight loss alone cited in Figure 9. On the basis of these results, corrosion (plus mild erosion) are not expected to present a problem with the assumption that certain deleterious additions are not present in fuels.

High Temperature Strength/Fracture Strength

Figure 10 (from Ref. 17 and 18) includes the flexural strength (3 point bend) of hot pressed silicon carbide (NC-132), hot pressed silicon carbide (NC-350), and tensile strength of 713LC superalloy as a function of temperature. High temperature bend strengths are superior to the tensile strengths of high temperature turbine alloys. (Tensile strengths of ceramic materials are typically less than bend strengths as can be seen from data in Table 2. This is due to the statistical nature of failure in these materials. A tensile specimen has more potential sites for failure under load than a bend sample, therefore failure is more probable at a lower stress. However, bend test results are appropriate for consideration in this program for nozzle vanes since pure tensile loads are not expected to be encountered.) A failure probability curve shown in Figure 11 for hot pressed silicon nitride and silicon carbide taken from Reference 19 shows that despite high mean failure stresses, ceramic materials must be designed to a lower stress which depends upon the statistical nature of failure.

Figure 12 (Ref. 20) gives unnotched Charpy impact strengths for HP SiC (NC-203) and HP Si_3N_4 (NC-130) as a function of temperature. The difference in the high temperature impact strength between these materials is substantial, and offers a possible correlation to better thermal shock resistance in HP Si_3N_4.

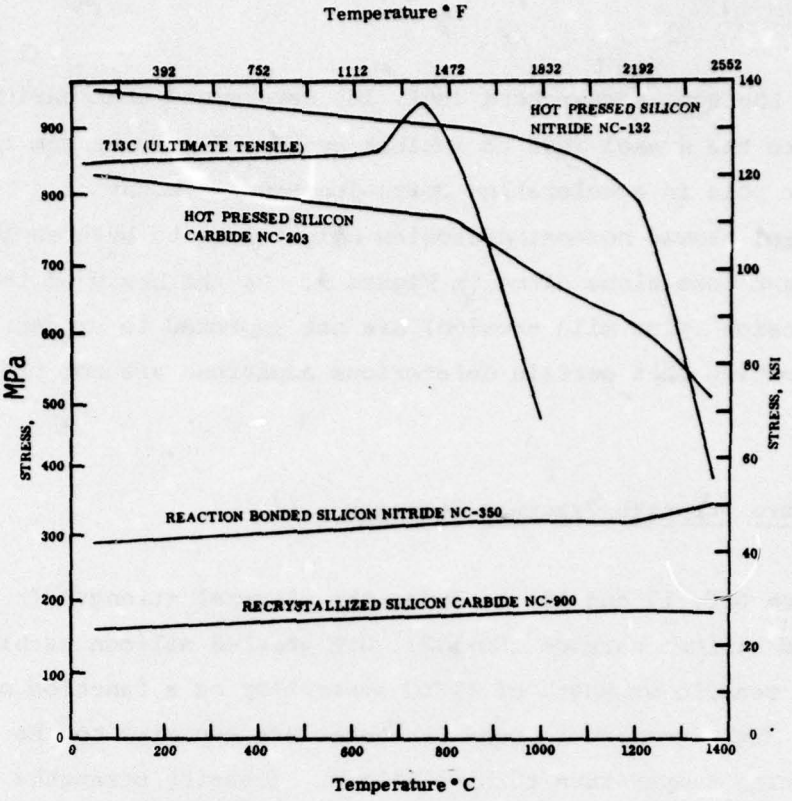

FIGURE 10. THREE POINT BEND STRENGTH OF CERAMIC MATERIALS AND ULTIMATE TENSILE STRENGTH OF 713LC NICKEL BASE ALLOY

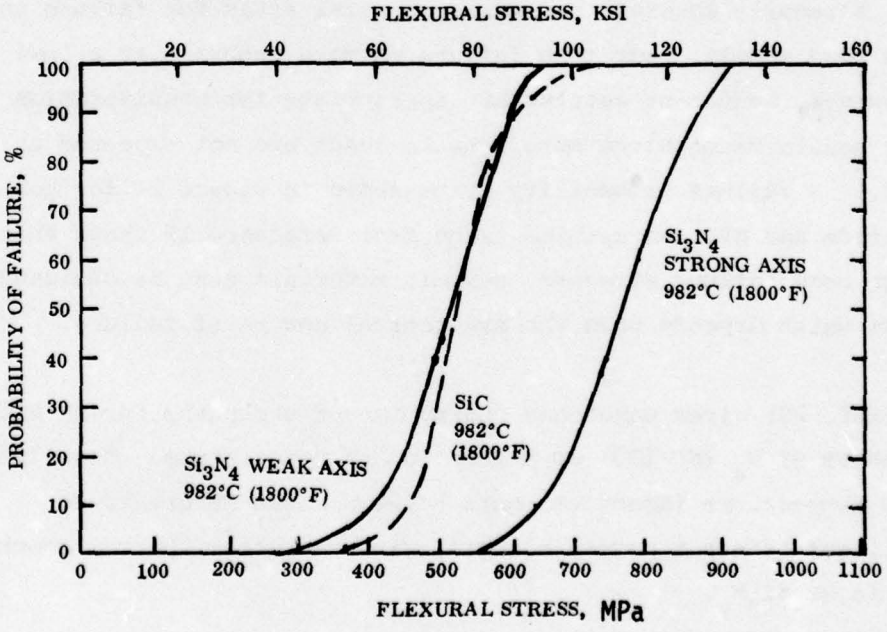

FIGURE 11. FAILURE PROBABILITY FOR NORTON HOT PRESSED Si_3N_4, HS-130, AND NORTON HOT PRESSED SILICON CARBIDE AT 982°C (1800°F) (REF. 19).

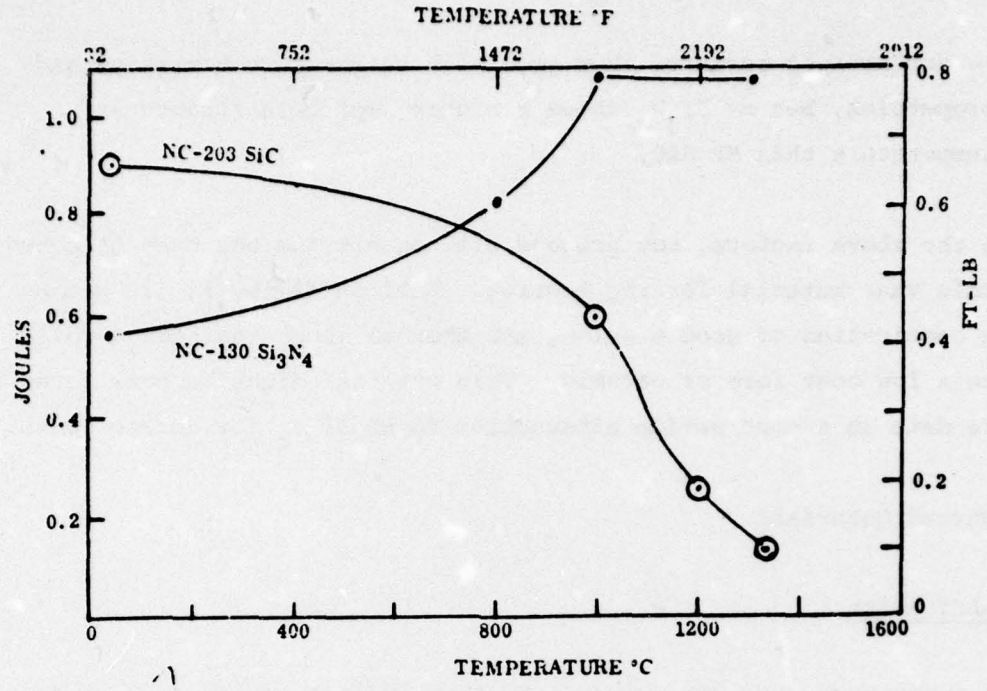

FIGURE 12. UNNOTCHED CHARPY IMPACT STRENGTH (REF. 20).

Summary of Ceramic Material Selection for 10kW Nozzle Vanes

Good erosion resistance is the highest priority material selection factor for ceramic vane materials to be considered in rig tests. Hot pressed Si_3N_4 has superior erosion resistance whereas reaction bonded Si_3N_4 offers no improvement over metals. $RBSi_3N_4$ is therefore eliminated from consideration for vane materials on this basis. HP SiC and silicon filled RC SiC both resist erosion well.

Thermal shock resistance is the next important material selection factor. HP Si_3N_4 appears to be significantly more resistant to thermal shock than the other ceramics considered. Refel SiC (similar to silicon filled RC SiC) shows good thermal shock characteristics, possibly better than HP SiC.

Both of the hot pressed ceramics show good high temperature corrosion and strength properties, but HP Si_3N_4 shows a higher impact resistance at elevated temperature than HP SiC.

Based upon the above factors, hot pressed silicon nitride has been selected as the nozzle vane material for rig testing. Silicon filled RC SiC has an attractive combination of good erosion, and thermal shock resistance while still being a low cost form of ceramic. This material might be considered at some future date as a cost saving alternative to HP Si_3N_4 for nozzle vanes.

3.2.2.3 Shroud Materials

Ease of Fabrication

Since both inner and outer shrouds for the 10kW are relatively large and are complex shapes compared to vanes, they must be made from materials capable of being fabricated easily to avoid prohibitive costs. Reaction bonded silicon nitride has the advantage over hot pressed forms because it can be fabricated by injection molding and other low cost fabrication methods. Injection molding is a convenient and inexpensive fabrication method in relation to hot pressing. Lower strength forms of silicon carbide also offer good fabrication properties since they can be slip cast or formed by some other means prior to final firing.

RB Si_3N_4 offers advantages over RC SiC because of very minimal distortion or shrinkage upon firing. Because of higher firing temperatures SiC has a tendency to slump during this process. In addition, surface finish is very poor. Si_3N_4 can be fired to a very good surface finish with negligible distortion of any type.

Hot pressing of either SiC or Si_3N_4 requires graphite dies which must function at temperatures in the range of 1700°C (3092°F) and 1800°C (3272°F) and pressures of 3000 to 4000 psi for 1 to 2 hours (Ref. 21). Usually parts

must be diamond ground after hot pressing because of process limitations. There is a significant difference in the cost and capabilities of these two techniques (Refs. 10 and 21).

High Temperature Strength

Strength of reaction bonded silicon nitride and recrystallized silicon carbide is substantially less than hot pressed forms (see Fig. 10). This is primarily due to porosity in these materials with approximate nominal material densities of 75 percent of theoretical (25% porosity) for reaction bonded Si_3N_4 (NC-350) and 80 percent of theoretical (20% porosity) for recrystallized silicon carbide. In the case of reaction bonded silicon nitride there is some advantage over hot pressed at very high temperatures [>1400°C (2552°F)] because it is free of grain boundary silicates resulting from the addition of MgO necessary as a bonding agent in the hot pressed silicon nitride. However, within the temperature range to be studied in this program, strength is still inferior to dense hot pressed materials since they typically contain no more than 1 percent porosity. This is not expected to hinder the use of $RBSi_3N_4$ or RCSiC for shrouds because their increased fabrication capability is expected to allow flexibility in design leading to lower stresses.

Thermal Shock Resistance

Experimental evidence cited in "Thermal Stress Resistance" shows the porous forms of Si_3N_4 and SiC to be less resistant to thermal shock in bench tests. This information may be slightly misleading, because the bench tests cited (Ref. 12 and 14) employed test conditions with relatively high heat transfer film coefficients. These conditions are much more severe than those imposed on 10kW engine shrouds.

Erosion/Corrosion Resistance

Very little erosion resistance is required for the 10kW turbine shrouds since very little, if any, damage is observed here due to dust ingestion. Vanes typically suffer most of the erosion damage.

Shrouds experience low angle of impingement from dust particles traveling at low velocities. Erosion studies at Solar indicated in Table 3 show that reaction sintered silicon nitride performs at least as well as 713LC superalloy at low impingement angles.

Reference 12 indicates poor oxidation resistance for reaction bonded silicon nitride and good oxidation resistance for recrystallized silicon carbide in laboratory thermal shock tests with temperature excursions up to 1316°C (2400°F). Oxidation tests to 1316°C (2400°F) conducted at Solar on reaction bonded silicon nitride showed excellent oxidation resistance. In contrast, references 20 and 21 report oxidation resistance for reaction bonded silicon nitride as 5 to 10 times as great as for hot pressed silicon nitride.

Results derived from corrosion or oxidation tests are heavily dependent upon test conditions and therefore it is very difficult to make a direct comparison between materials considered here. However, data that are available seem to support the idea that reaction bonded silicon nitride and recrystallized silicon carbide will have acceptable corrosion or oxidation performance in the 10kW engine nozzle environment.

Summary of Material Selection for 10kW Turbine Shrouds

Reaction bonded silicon nitride was selected as the candidate shroud material to be tested in Phase I rig tests. This selection was primarily based upon ease of fabrication, capability of making more complex shapes with good tolerance control and resultant lower final cost. Other properties such as strength and thermal shock resistance are lower for RB Si_3N_4 than for hot pressed forms, but increased fabrication capability and less severe material requirements allow consideration of RB Si_3N_4 as a shroud material.

Erosion and corrosion properties of these less dense materials are also inferior to hot pressed forms but are anticipated to at least equal the durability of the current shroud material, 713LC, and therefore perform acceptably.

3.2.3 Fabrication Studies

The objective of fabrication studies was to develop ceramic joining methods for the nozzle vane to shroud interface which could be evaluated in rig testing. The joint is expected to perform two functions: (1) seal gas leakage around ceramic inserts; and (2) provide uniform support of ceramic parts such that localized stress concentrations are avoided.

3.2.3.1 Ceramic to Ceramic Joint

"T" samples, as pictured in Figure 13 were used to evaluate bonds. The samples were fired and then evaluated for strength and stability after 60 hr air furnace exposure at 1093°C (2000°F).

The "T" samples consisted of RBSi$_3$N$_4$ pieces (corresponding to shrouds) with dimensions of 1 in. x 0.25 in. x 0.180 in. and HPSi$_3$N$_4$ pieces (corresponding to vanes) with dimensions of 1 in. x 0.25 in. x 0.15 in. The shroud pieces used 0.170 in. wide 0.020 in. deep lengthwise slots to contain the test joint material and vane pieces.

The glass mixture compositions were mixed from dry weights of basic glass ingredients shown in Table 6. Distilled water was added in appropriate amounts to make a thick slurry. The slurry was applied to both surfaces to be joined after they were cleaned by light bead blasting. The assembly was oven dried and then fired for one hour in air at the specified firing temperature.

Table 7 lists the eight types of relaxing glass joint materials that were studied.

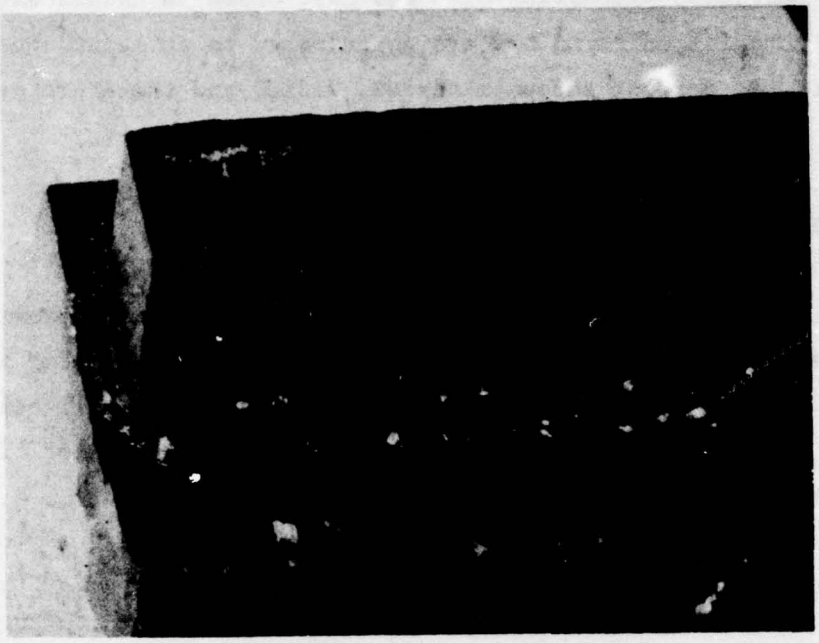

FIGURE 13. 40% GN19, 20% B402, 40% Cr_2O_3 AFTER 60 HR, 2000°F EXPOSURE IN AIR ($RBSi_3N_4$ TO $HPSi_3N_4$)

TABLE 6

PREPARATION OF GLASSES

Glass Type	Weight of Constituents (gm)			Milling Time (Hrs)
	Glass Frit	*Green Label Clay	KNO_2	
*S5210	300	18	-	6
†B402	95	5	-	1.5
†GN-19	95	5	-	4
Pyrex	95	5	1	1.5
x332	95	5	-	1.5

* Ferro Corporation Designation

† Solar Designation

x National Bureau of Standards Designation

TABLE 7

SUMMARY OF $RBSi_3N_4$ SHROUD TO $HPSi_3N_4$ VANE FILL MATERIALS EXPOSED TO TEMPERATURE

Fill Material	Firing Temperature °C (°F)	As-Fired Condition	After Exposure 60 hrs @ 1093°C (2000°F)	Bond Quality at Room Temperature After Exposure
B402, 20% Cr_2O_3	1093 (2000)	OK	Unstable	Good
50% GN19, 50% B402	1093 (2000)	OK	Good	Stronger than $RBSi_3N_4$
Pyrex	1149 (2100)	OK	Unstable	Good
Si (325 mesh)	1100 (2012) 40 min.; 1400 (2552) 16 hrs; in N_2 atmosphere	OK	Good	Weak
30% GN19, 30% B402, 40% Cr_2O_3	982 (1800)	OK	Unstable	Fair
40% GN19, 20% B402, 40% Cr_2O_3	1038 (1900)	OK	Good	Good
GN19	1149 (2100)	OK	Unstable	Weak
GN19, 40% Cr_2O_3	1149 (2100)	OK	Good	Good

The joint materials that are underlined, i.e., 40% GN19, 20% B402, 40% Cr_2O_3, and 60% GN19, 40% Cr_2O_3 were selected as the materials to be used for rig test joints. They are stable and have good bond quality. Joints made from these materials are shown in Figures 13 and 14.

The nonrelaxing silicon bond type joint also considered here was the most promising direct Si_3N_4 joining procedure developed in Reference 23. This bond was discounted for use in rig tests because of poor strength.

Figures 15 through 21 show as-fired and after-exposure conditions of the joints corresponding to joining materials listed in Table 7. B402 with 20% Cr_3O_3 shown in Figure 15 was rejected because of instability and 50% GN19 with 50% B402 shown in Figure 16 was rejected because it lacked a filler material to prevent extrusion from the joint under pressure. Both Pyrex and GN19 (Figs. 17 and 18) were unstable at temperature and silicon sintering was rejected because it offers no relaxation and relatively low strength (see Fig. 19). Thirty percent GN19, 30% B402 with 40% Cr_2O_3 also showed instability in the bond surface (see Figs. 20 and 21) and was eliminated.

The mixtures chosen for rig testing show little tendency to deteriorate with time at temperature. They contain a significant amount of filler material and have relatively strong bonds at room temperature.

3.2.3.2 Ceramic to Metal Joint

Ceramic to metal joint filler materials were considered here to find three types suitable for rig testing.

The test samples consisted of $HPSi_3N_4$ pieces which simulate vanes and 713LC superalloy shroud material with a 0.030 in. depth groove to receive the simulated vane.

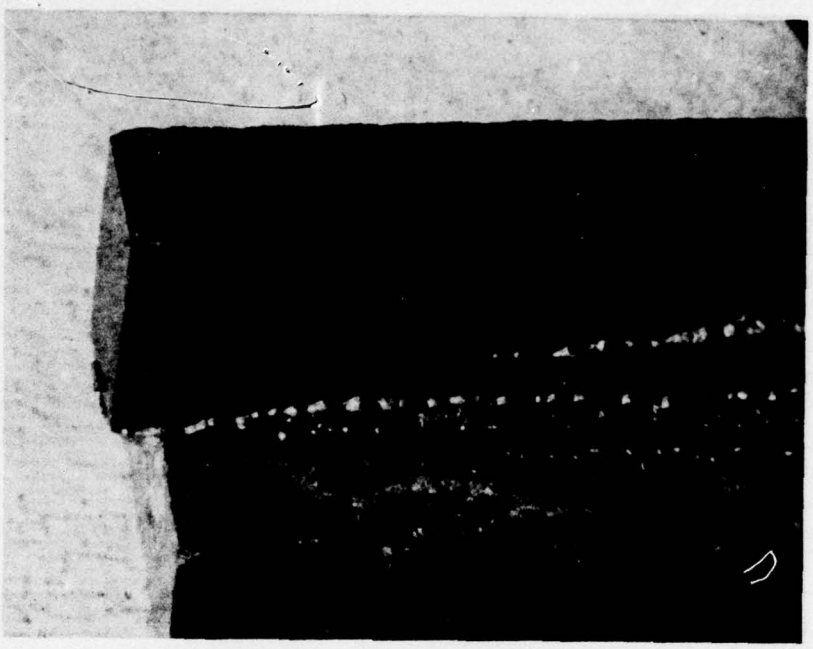

FIGURE 14. 60% GN19, 40% Cr_2O_3 AFTER 60 HR, 2000°F EXPOSURE IN AIR ($RBSi_3N_4$ TO $HPSi_3N_4$)

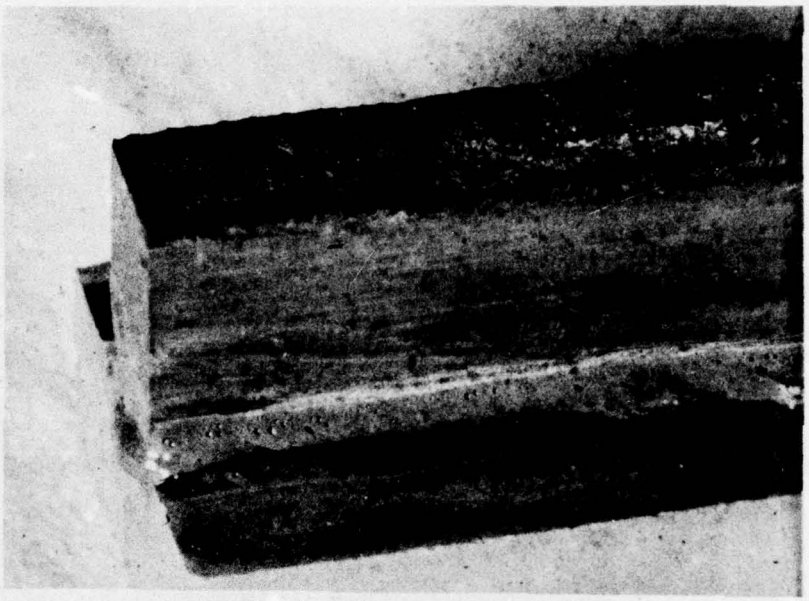

(a)

(b)

FIGURE 15. B402, 20% Cr_2O_3 FILL (a) AS FIRED (b) AFTER EXPOSURE ($RBSi_3N_4$ TO $HPSi_3N_4$)

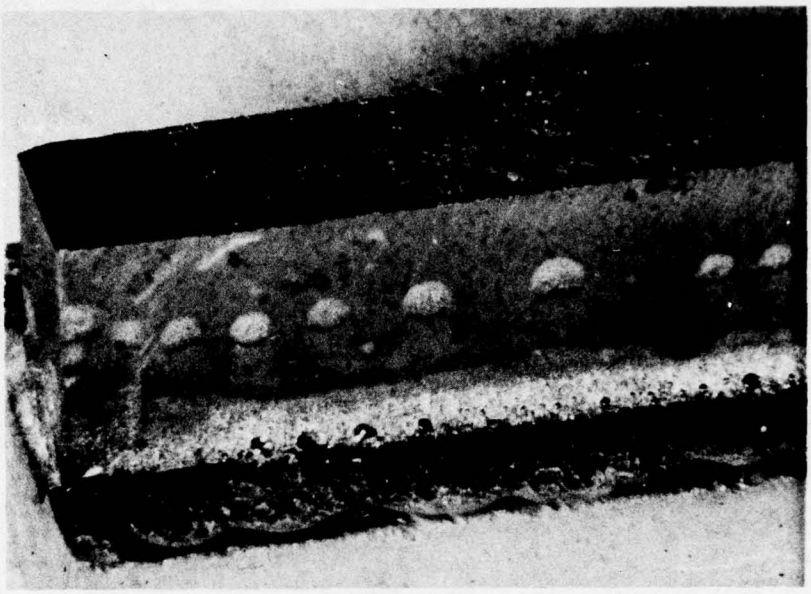

(a)

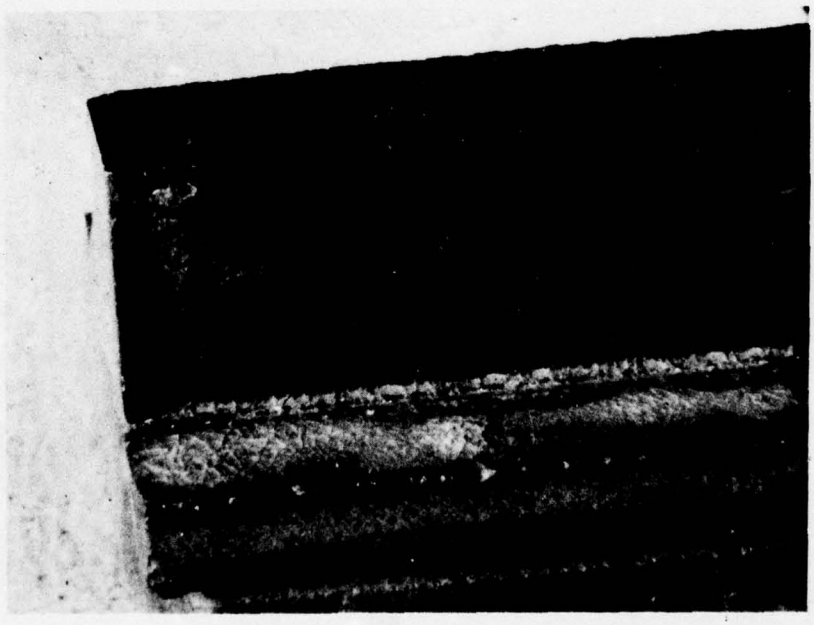

(b)

FIGURE 16. 50% GN19, 50% B402 (a) AS FIRED (b) AFTER EXPOSURE ($RBSi_3N_4$ TO $HPSi_3N_4$)

(a)

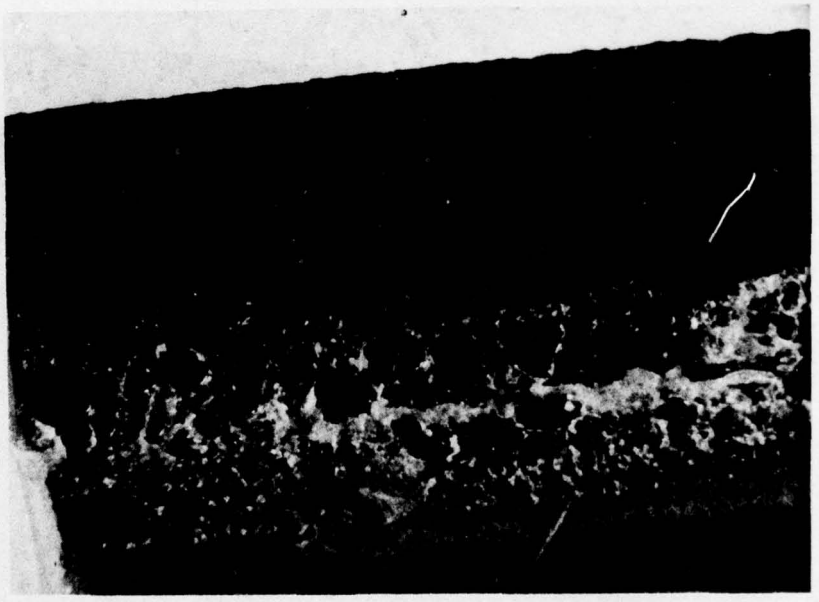

(b)

FIGURE 17. PYREX FILL (a) AS FIRED (b) AFTER EXPOSURE ($RBSi_3N_4$ TO $HPSi_3N_4$)

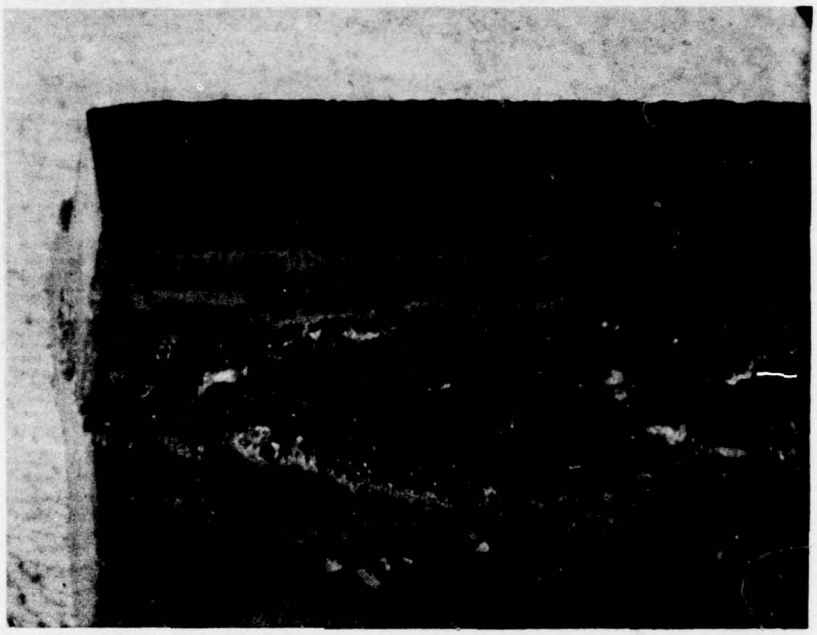

FIGURE 18. GN19 AFTER 60 HR, 2000°F EXPOSURE ($RBSi_3N_4$ TO $HPSi_3N_4$)

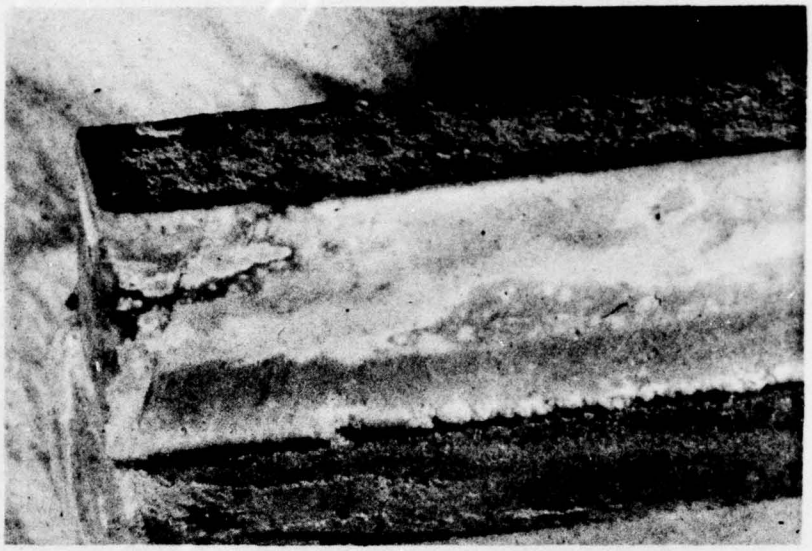

(a)

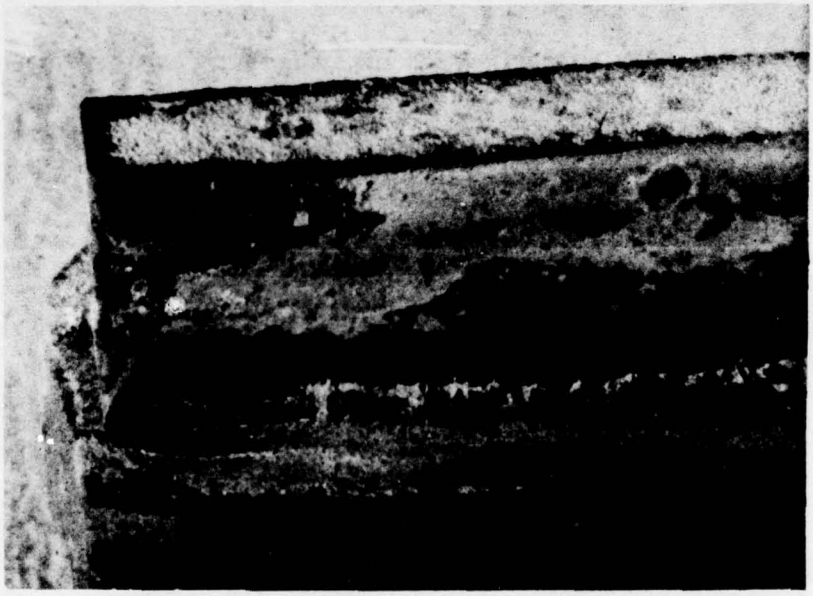

(b)

FIGURE 19. SILICON BOND (a) AS SINTERED (b) AFTER EXPOSURE ($RBSi_3N_4$ TO $HPSi_3N_4$)

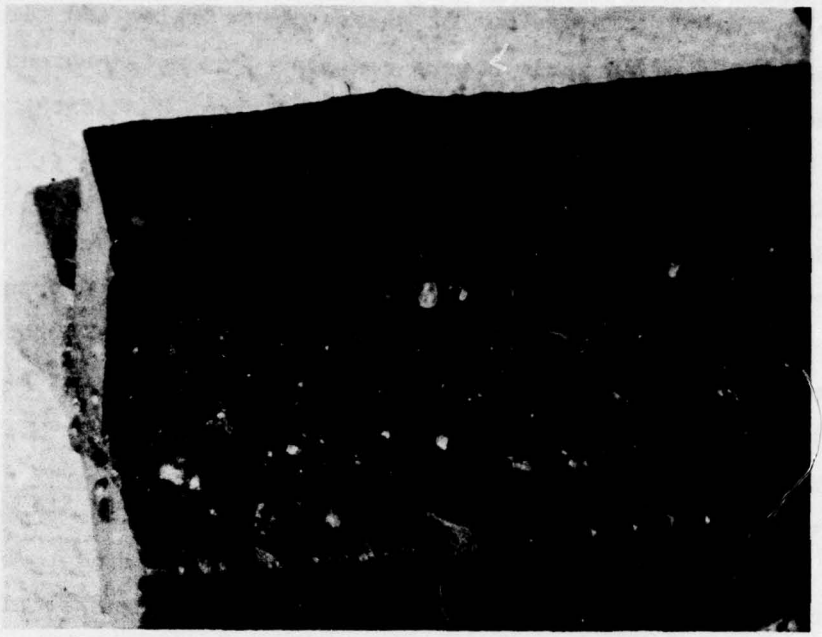

FIGURE 20. 30% GN19, 30% B402, 40% Cr_2O_3 AFTER 60 HR, 2000°F EXPOSURE IN AIR ($RBSi_3N_4$ TO $HPSi_3N_4$)

FIGURE 21. 30% GN19, 30% B402, 40% Cr_2O_3 AFTER 60 HR, 2000°F EXPOSURE IN AIR (BOND SURFACE) ($RBSi_3N_4$ TO $HPSi_3N_4$)

Twentythree different combinations of glass, glass filler and firing temperatures as listed in Table 8 were considered as metal-shroud ceramic-vane rig test candidate materials. The three candidates shown in Figures 22 to 24 which include: 30% B402, 30% GN19, 40% Cr_2O_3, 1093°C (2000°F) fire; 35% B402, 35% GN19, 30% Cr_2O_3, 1093°C (2000°F) fire; and 20% GN19, 40% B402, 40% Cr_2O_3, 927°C (1700°F) fire, show promise in meeting all of the functional requirements of a glass filler and were selected for rig test. The two basic material requirements are to seal gas leakage around ceramic inserts and to provide uniform contact surface for ceramic parts such that localized stress concentrations are avoided. The three compositions above appear capable of meeting sealing requirements since they survived differential strains associated with temperature cycling, as shown in Table 8, without severe cracking or spalling, while still adhering to both metal and ceramic surfaces. In addition, no tendency for these materials to migrate from fill interface due to excessive wetting was evident. The second function which requires the material provide a uniform contact surface seems to be met because of the large quantities of Cr_2O_3 fill. This prevents the glass from flowing out of the metal-ceramic interface, since this quantity of nonviscous fill material appears to all but eliminate viscous newtonian fluid behavior.

Figures 25 thru 33 show some of the other joint materials considered in this study in the as-fired and after exposure conditions.

3.2.4 Design and Analysis for Rig Test of Ceramic/Superalloy Nozzle

3.2.4.1 Design

Figure 34 illustrates a suggested 10kW nozzle design concept presented in the program proposal. The shrouds are made from 713LC superalloy and vanes are part 713LC (leading edge) and part ceramic (trailing edge). This type of bimaterial vane design is possible for improved erosion resistance because almost all vane erosion occurs at the trailing edge. This obviates the need for through holes in the ceramic because the 713LC leading edge will accommodate these.

TABLE 8

SUMMARY OF METAL SHROUD TO $HPSi_3N_4$ VANE FILL MATERIALS EXPOSED TO TEMPERATURE CYCLING

Material	Firing Temperature (°F)	As Fired Condition	After Exposure Cycle		Appearance and Comments
			1300°F Air Cool Two Times	1300°F Water Quench Two Times	
S5210	1700	OK	Debonded	--	Poor adherence and cracking
S5210, 47% Cr_2O_3	1700	Loose	Debonded	--	Poor adherence and cracking
B402	1500	OK	OK	OK	Crazed and excessive wetting
B402, 5% Cr_2O_3	1500	Debonded	--	--	
B402, 10% Cr_2O_3	1500	Debonded	--	--	
B402, 5% Cr_2O_3	1800	Debonded	--	--	
B402, 10% Cr_2O_3	1800	OK	OK	OK	Too soft at temperature
50% B402, 50% GN19	1800	OK	OK	OK	Will not resist extrusion
40% B402, 40% GN19, 20% Cr_2O_3	2000	Debonded	--	--	
35% B402, 35% GN19, 30% Cr_2O_3	2000	OK	OK	2 of 3 Samples OK	Resists extrusion
30% B402, 30% GN19, 40% Cr_2O_3	2000	OK	OK	OK	Resists extrusion
60% Pyrex, 40% Cr_2O_3	2100	Debonded	--	--	
Pyrex	2100	Debonded	--	--	
40% GN19, 20% B402, 40% Cr_2O_3	2100	--			Glass unstable
	1900	OK	Debonded	--	--
20% GN19, 40% B402, 40% Cr_2O_3	2100	--	--	--	Glass unstable
	1700	OK	OK	1 of 3 Samples OK	
332 (NBS)	1700	Debonded	--	--	Poor adhesion to ceramic
332 (NBS), 40% Cr_2O_3	1800	Debonded	--	--	Poor adhesion to ceramic
332 (NBS), 40% Cr_2O_3	1800	Debonded	--	--	Poor adhesion to ceramic
GN19	2100	OK	Debonded	--	Unstable
GN19, 40% Cr_2O_3	2100	OK	Debonded	--	
B402, 40% Cr_2O_3	1500	Debonded	--	--	

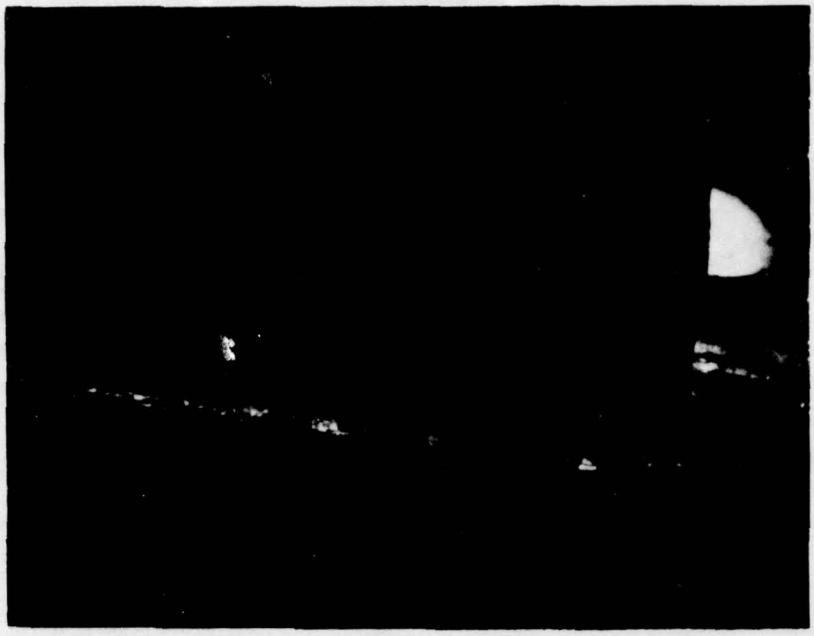

FIGURE 22. 30% B402, 30% GN19, 40% Cr_2O_3 AFTER EXPOSURE CYCLE (713LC TO $HPSi_3N_4$)

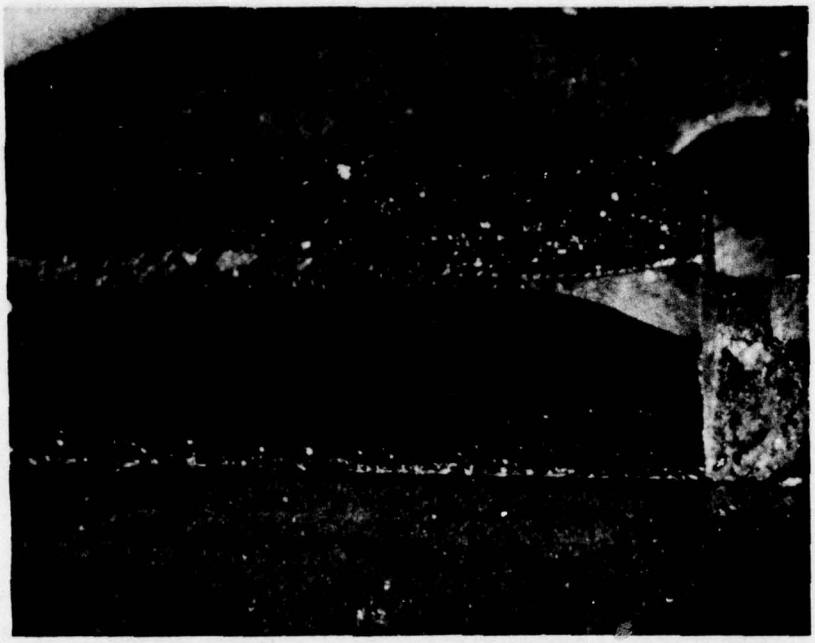

FIGURE 23. 35% B402, 35% GN19, 30% Cr_2O_4 AFTER EXPOSURE CYCLE (713LC TO $HPSi_3N_4$)

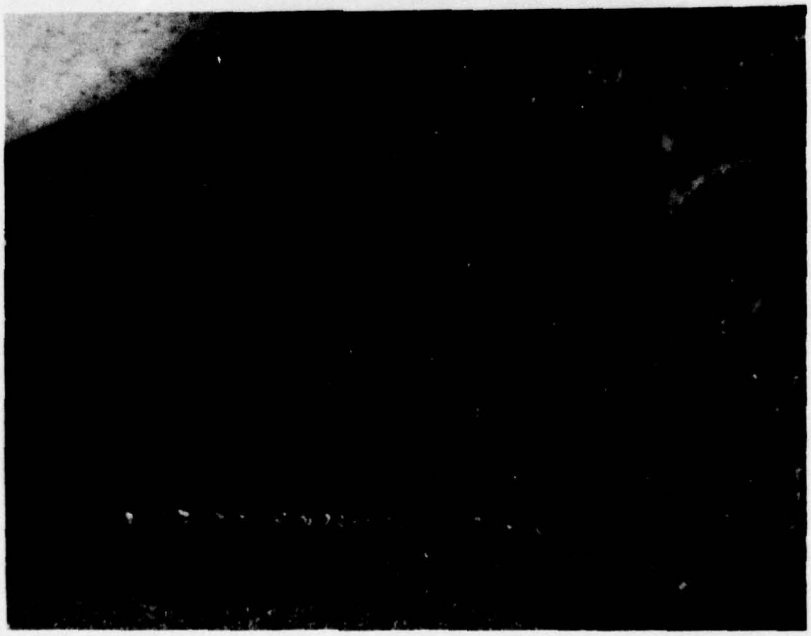

FIGURE 24. 20% GN19, 40% B402, 40% Cr_2O_3 AFTER EXPOSURE CYCLE (713LC TO $HPSi_3N_4$)

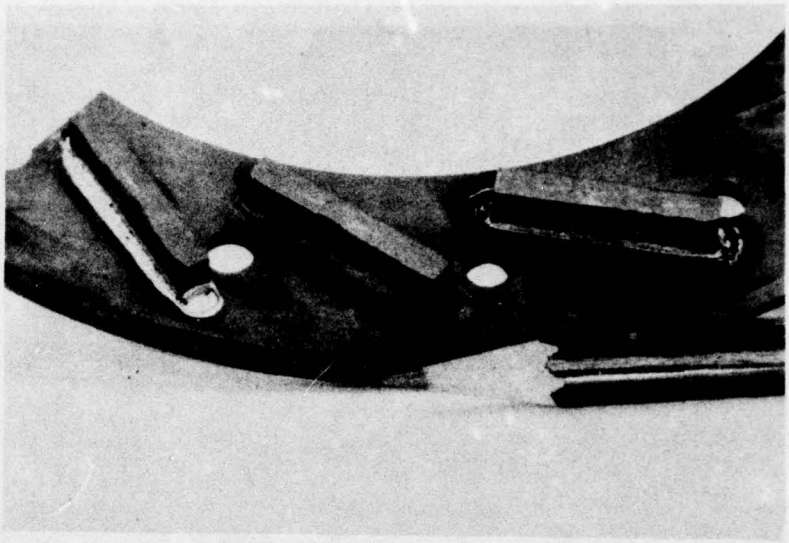

FIGURE 25. GLASS JOINT BONDS OF 713LC SHROUD SECTION AND HP Si_3N_4 - AS FIRED CONDITION. THE GLASSES ARE (Left to Right): TYPE S5210; TYPE S5210 WITH CHROME OXIDE FILL AND TYPE 402

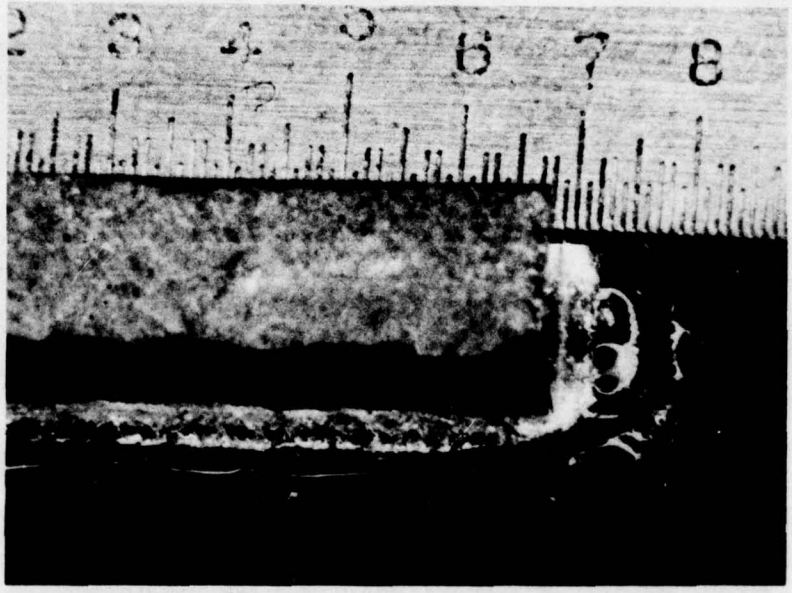

FIGURE 26. TYPE 402 GLASS JOINT - AS FIRED

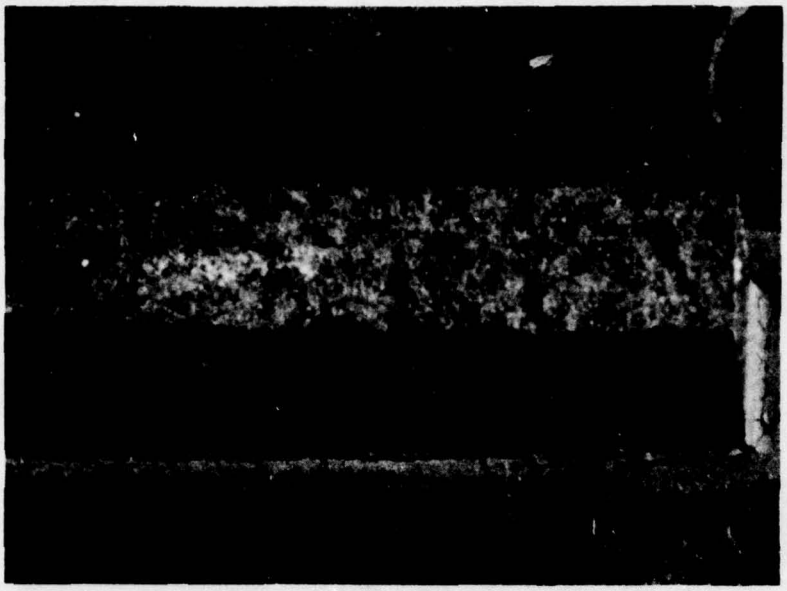

FIGURE 27. TYPE S5210 (With Chrome Oxide Fill) GLASS JOINT - AS FIRED

FIGURE 28. TYPE S5210 GLASS JOINT - AS FIRED

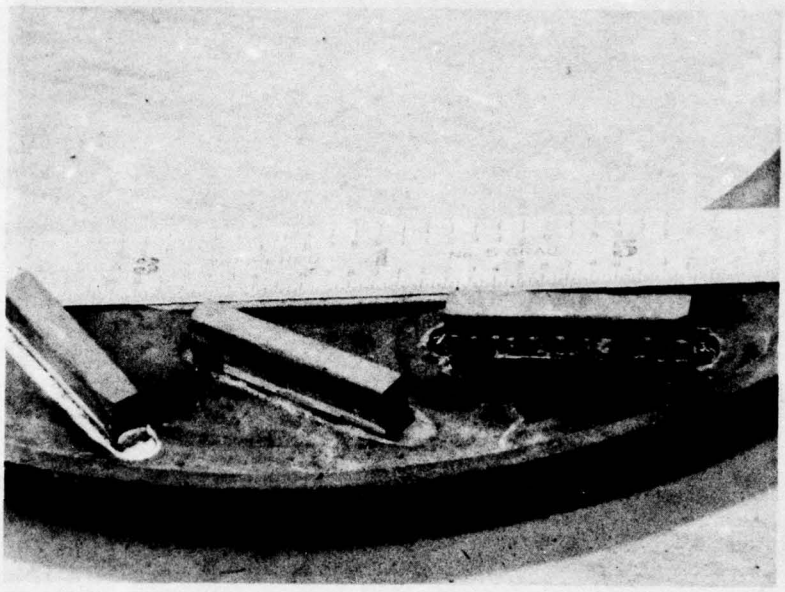

FIGURE 29. GLASS JOINT BONDS AFTER EXPOSURE. GLASSES ARE (Left to Right): TYPE S5210; TYPE S5210 WITH CHROME OXIDE FILL, AND TYPE 402

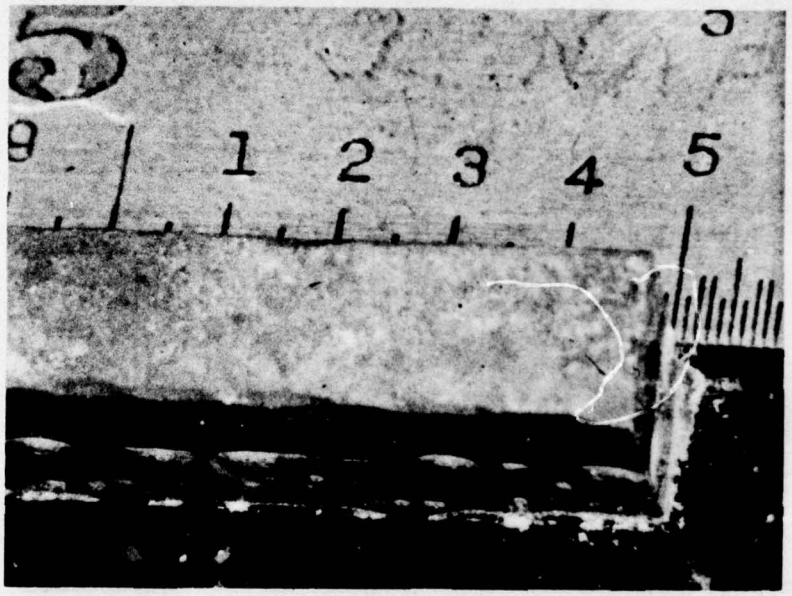

FIGURE 30. TYPE 402 GLASS JOINT AFTER EXPOSURE

A

B

FIGURE 31. TYPE S5210 GLASS JOINT WITH CHROME OXIDE FILL AFTER EXPOSURE

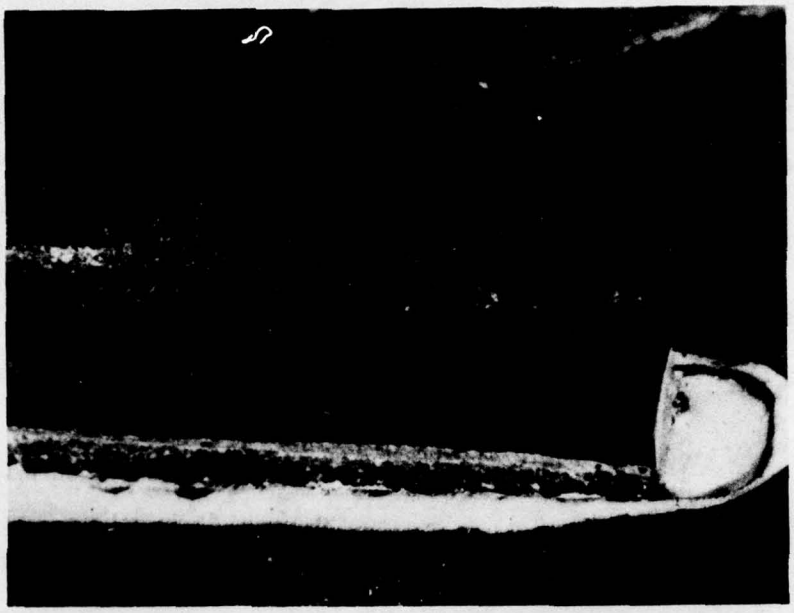

A

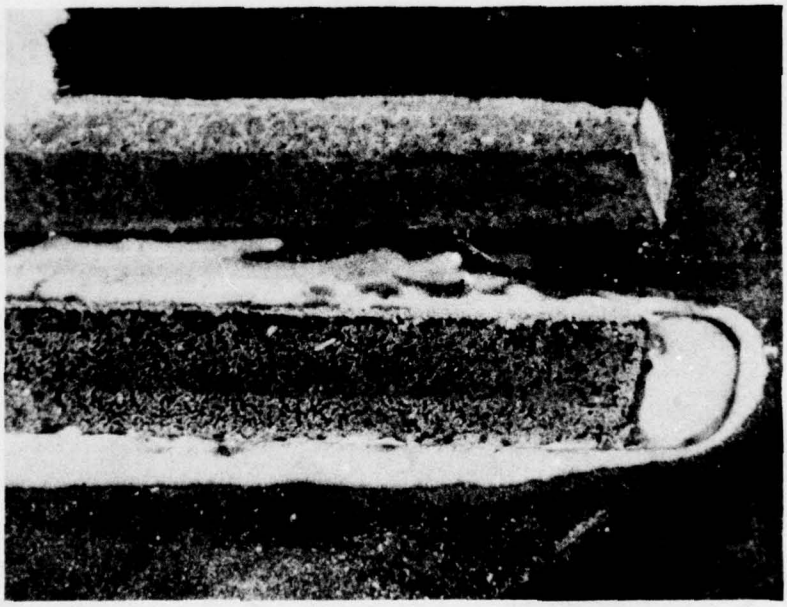

B

FIGURE 32. TYPE S5210 GLASS JOINT AFTER EXPOSURE

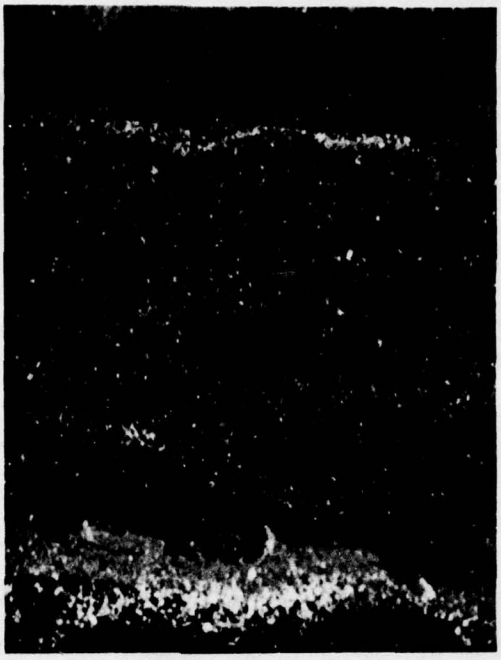

A. SHROUD RECESS SURFACE SHOWING S5210 GLASS WITH Cr_2O_3 AFTER EXPOSURE (Magnification 14X)

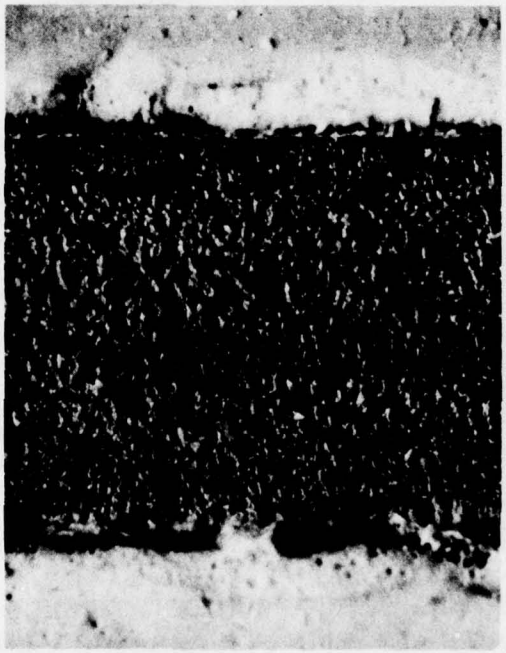

FIGURE 33B. SHROUD RECESS SURFACE SHOWING S5210 GLASS AFTER EXPOSURE. (Magnification 14X)

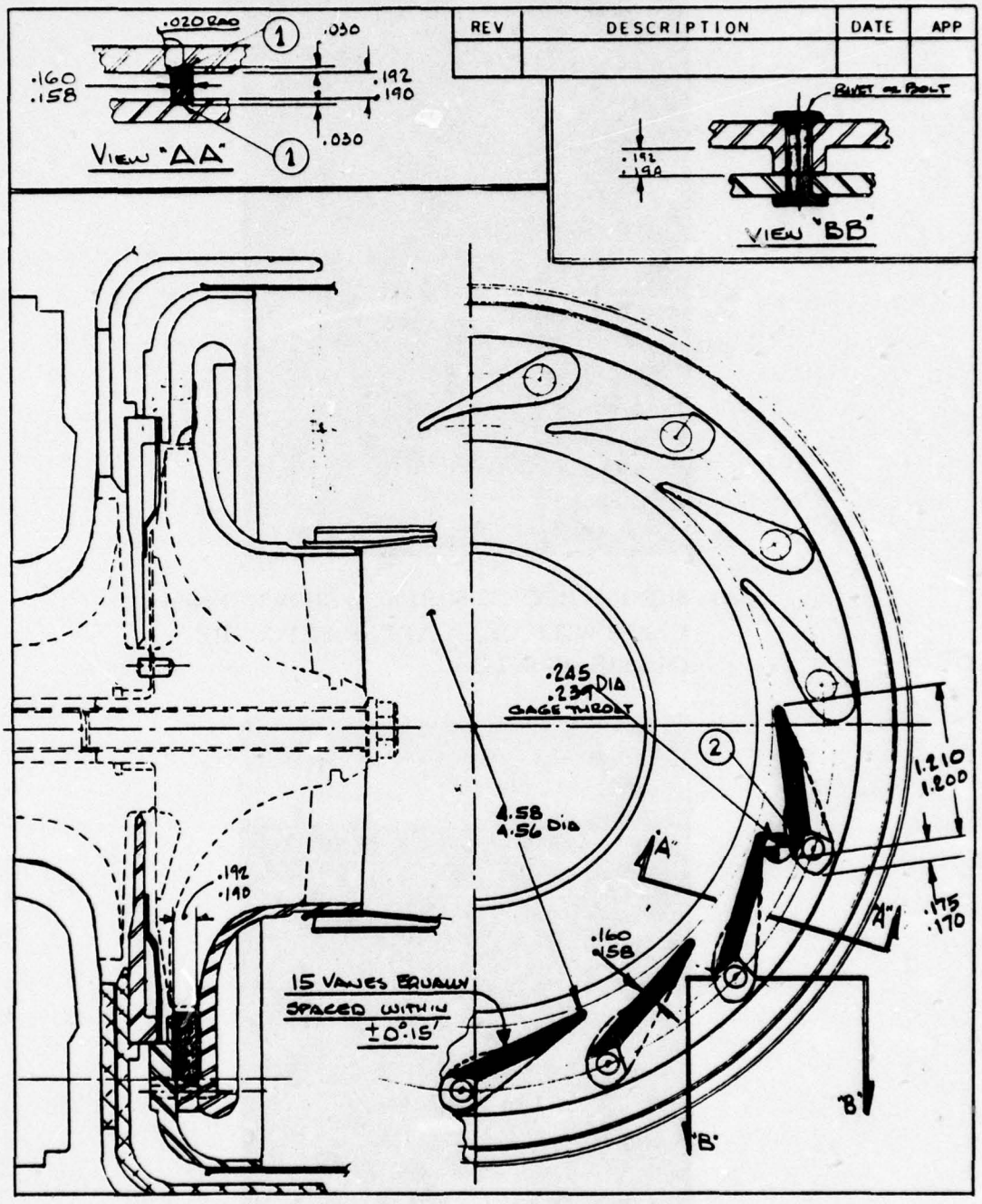

FIGURE 34. COMPARISON OF PRESENT NOZZLE DESIGN (UPPER) WITH REDESIGN FOR CERAMIC VANES AND METAL SHROUDS

The ceramic trailing edge is recessed into the shrouds. A softening glass may be applied at the ceramic interface for sealing and support of these ceramic vane section or the vane sections might be supported strictly by direct entrapment between shroud recesses.

Figure 35 presents two bimaterial vane designs (left and center vanes) which offer a number of advantages over the design in Figure 34. The ceramic section on the turbine wheel side of the vane is shorter, but is long enough to encompass the region of the vane which is observed to experience almost all of the vane erosion in the 10kW engine. The larger leading edge possible with this design allows location of vane rivet and engine through bolts to be the same as the standard engine design avoiding unnecessary redesign of existing engine components including nozzle shrouds and compressor diffuser sections. The aerodynamic shape of the existing vane can be adhered to more accurately without having to introduce curved surfaces on the ceramic vane section, (see Fig. 36).

The forward shroud of this engine has a tendency to distort in a manner that would cause a compressive stress at the vane trailing edge unless adequate stiffness is provided through the vanes. The bimaterial designs in Figure 35 provide much more stiffness via the vane leading edge than the Figure 34 design. This lessens the possibility of shroud distortion and lowers compressive stresses applied to ceramic trailing edge.

The design at the left in Figure 35 is preferred over the center design because of its obvious aerodynamic advantage and fewer surfaces which require machining. The philosophy of matching thicknesses of vanes to shrouds for better thermal transient stability resulted in the center design, however it is believed that the aerodynamic discontinuity and additional edges for this ceramic shape might cause greater difficulty in this regard.

The all-ceramic vane profile design shown at the right of Figure 35 was considered because it offered an avenue to avoid some of the problems expected to occur due to the differential thermal expansivities between 713LC

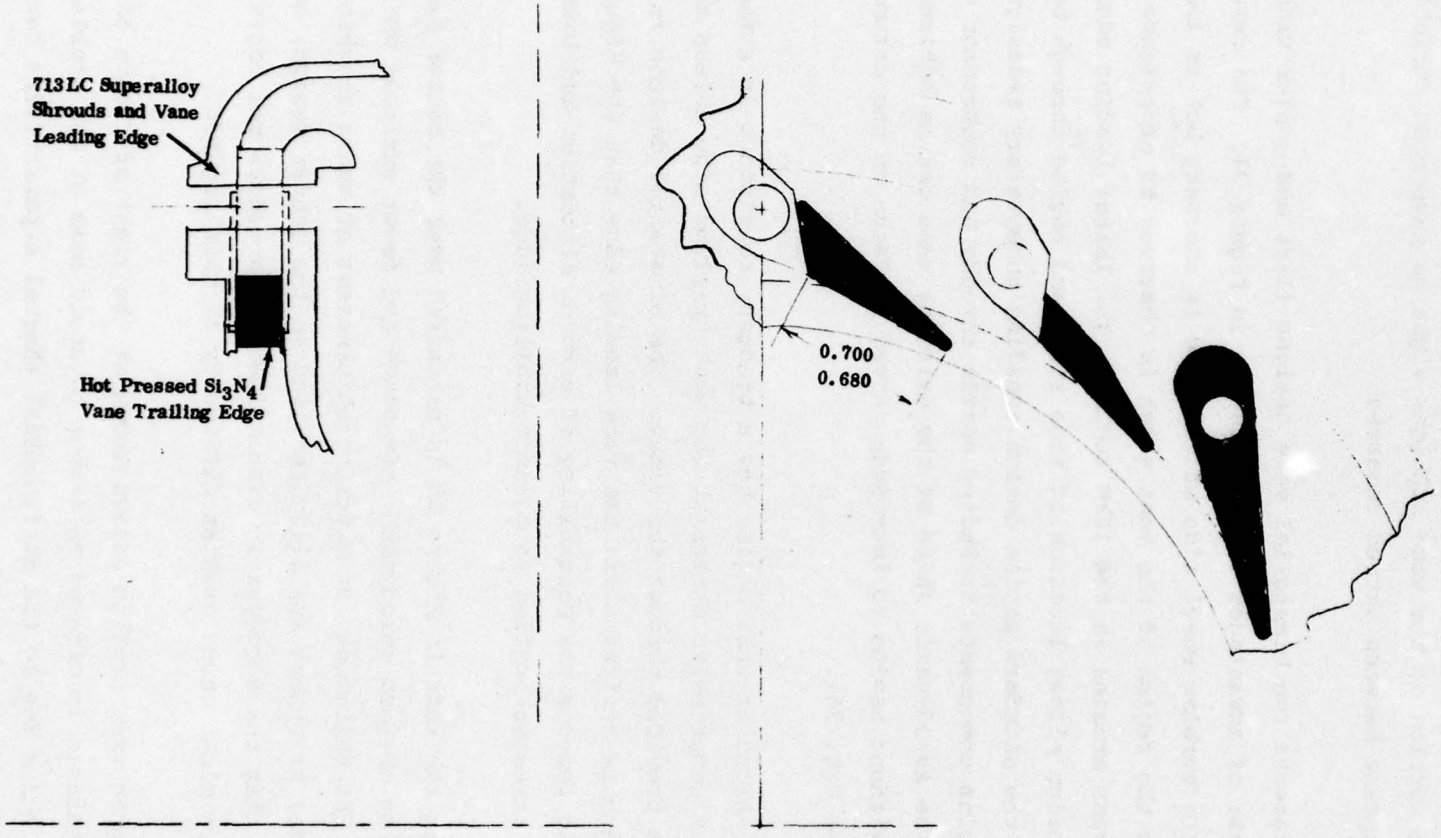

FIGURE 35. ALTERNATIVE VANE DESIGNS FOR METAL-SHROUD CERAMIC-VANE NOZZLE

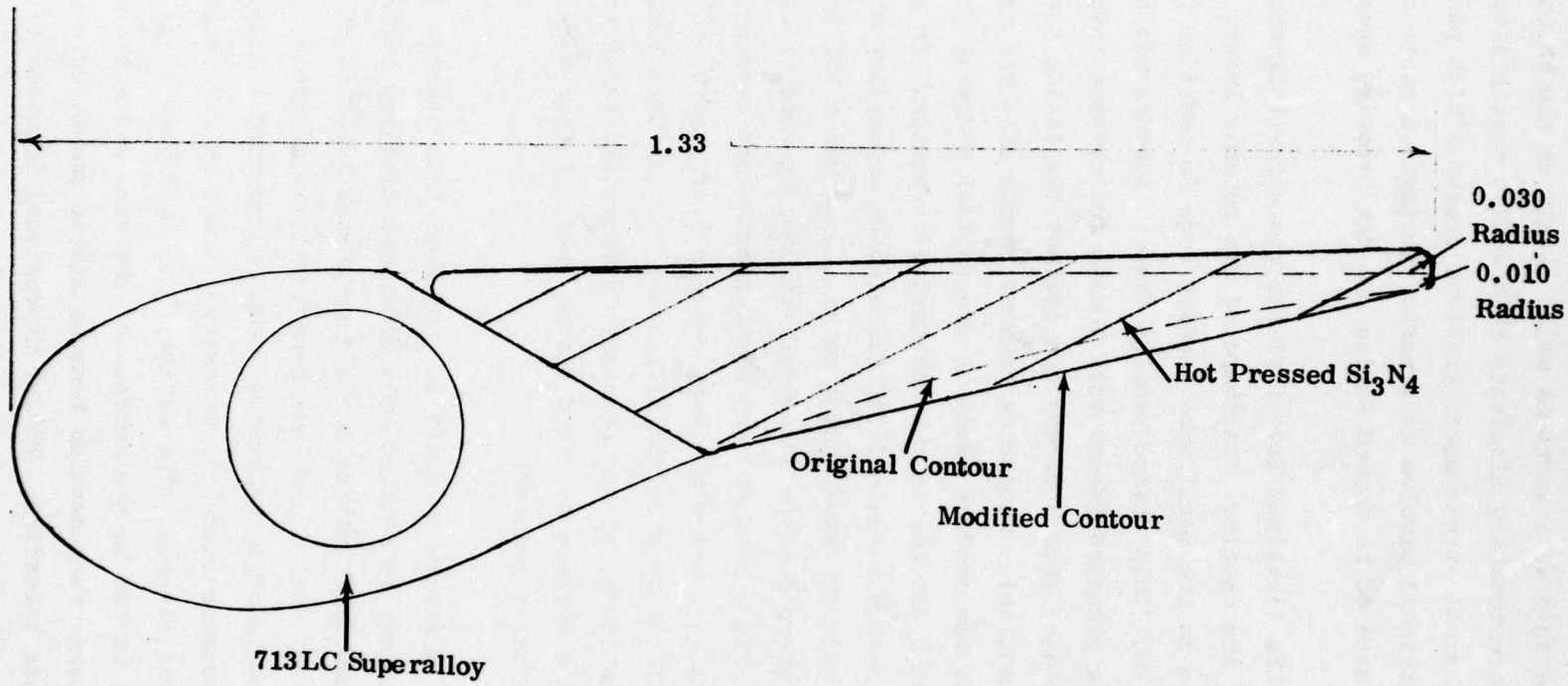

FIGURE 36. VANE AIRFOIL SECTION MODIFICATION DUE TO CERAMIC TRAILING EDGE

and HPSi$_3$N$_4$. The thin wall sections which result at the through bolt or rivet location unfortunately eliminate this design possibility because mechanical and thermal stress concentrations create a high probability of failure. An additional problem is greater fabrication costs since a hole of this type would have to be formed during the hot pressing operation.

Figure 37 shows the finalized layout of the ceramic/metal nozzle design for engine simulator rig testing. The shape of the ceramic insert and its position relative to the metal vane leading edge is modified from the design shown in Figure 36. This change results from an aerodynamic analysis which shows that static pressure forces will locate the ceramic insert at the downstream portion of shroud recess and against the inside surface (towards the axis of the engine). Clearance between recess size and ceramic insert size necessary to accommodate assembly dimensional stack-ups amount to between 0.010 and 0.030 in. in the lengthwise direction. In addition, differential expansion between 713LC nickel-base superalloy shrouds and hot pressed silicon nitride vanes amount to an additional 0.010 in. clearance. In the assembly where ceramic adhesives will not be used, a clearance will occur at the interface between vane metal section and ceramic section. Therefore, a total gap which can vary between 0.020 and 0.040 in. will result. This will cause substantial leakage through this interface since nearly the entire 18 psi static pressure differential taken across the nozzle exists across this surface at rated engine load. Performance of the nozzle would be substantially reduced.

The vane design in Figure 36 would tend to seal this leakage if the ceramic vane were long enough to contact only front and trailing surfaces. However, this presents some difficulties in holding radial location of ceramic section of vanes because of dimensional stack-up in nozzle assembly. (Approximately 0.050 in. maximum location tolerance would be expected.) Also, any sealing forces must be counteracted by compressive stress on the ceramic trailing edge, which is undesirable. The design shown in Figure 37 is expected to give a good seal at the bottom surface of the vane where the metal tab overlaps the ceramic vane section because static aerodynamic pressure forces tend to close this interface. Radial dimensional location of vane can be controlled more accurately (within 0.20 in.).

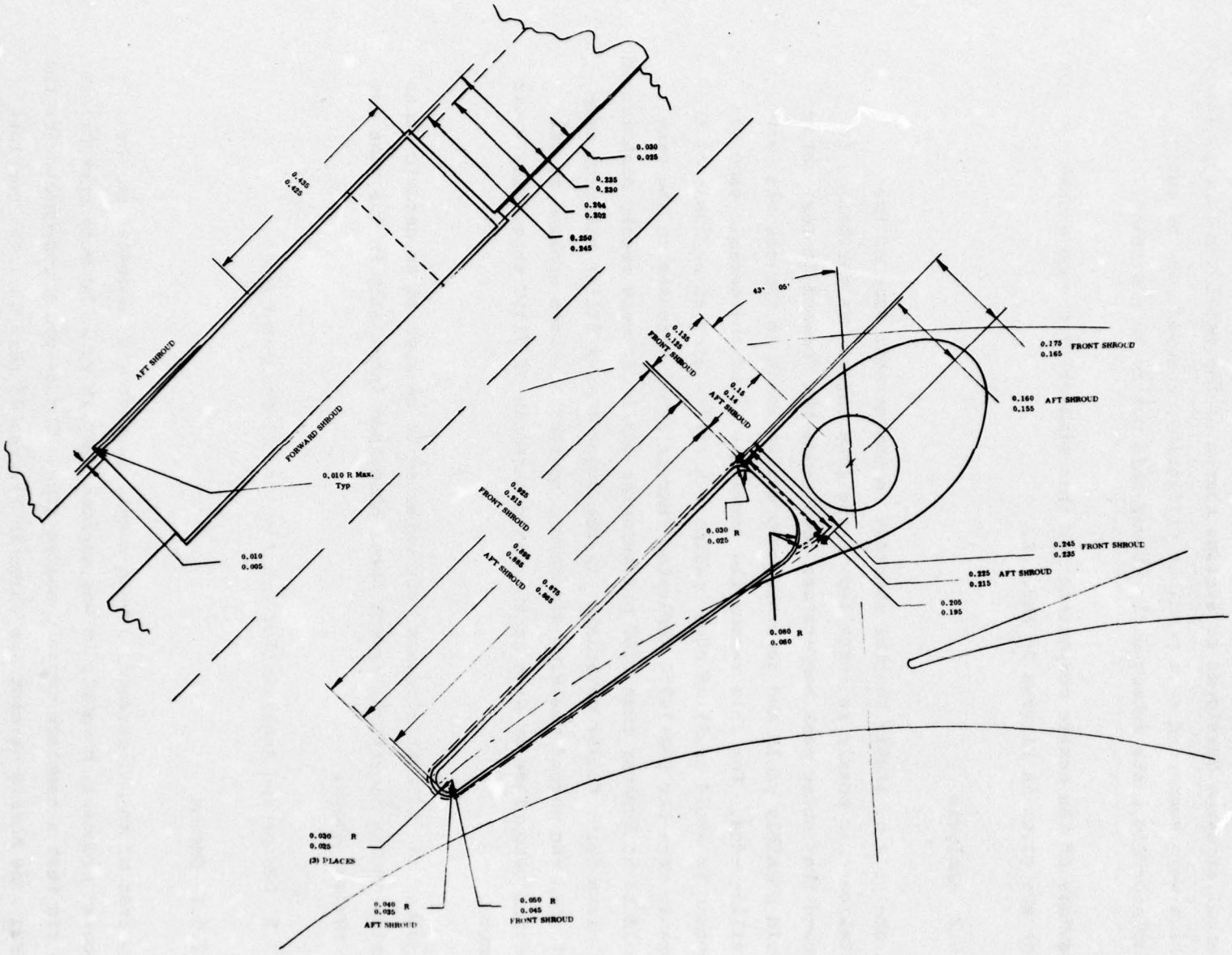

FIGURE 37. LAYOUT DRAWING OF VANE HP Si_3N_4 CERAMIC TRAILING EDGE INSERT

Thermal stresses developed at section change of the metal tab in this latest design were suspected as a possible difficulty, however, as the engine simulator rig tests subsequently showed this not to be a problem.

Drawings of the nozzle components for this bimaterial design chosen for rig test are given in Figures 38 thru 42.

3.6.2 Analysis

An analysis of static thermal stresses in the ceramic vane of the metal/ceramic nozzle as installed in the 10kW engine was performed. It showed that under peak temperature conditions the forward (outer) shroud could possibly yield and generate compressive loads on the ceramic vane trailing edge. For this reason the forward side of the ceramic vane was tapered to avoid trailing edge loading. A finite element analysis of the ceramic vane per DSK-14958 indicated that internal stresses in the vane would be no greater than 8600 psi assuming the loads were evenly distributed by glass joint filler material. In the event that a filler material were not used and shroud yielding did occur, contact stresses applied to the ceramic vane piece as high as the yield strength of 713LC superalloy could occur.

No other significant stresses were expected to be applied to ceramic vanes during engine operation, except those generated internally in the vane due to thermal shock.

3.2.5 Design and Analysis for Rig Test of All-Ceramic Nozzle

3.2.5.1 Design

Rig test of an all-ceramic, 3-vane nozzle segment was suggested in the program proposal, however, it was decided that it would be more appropriate to rig test a complete ceramic nozzle ring. The assembly components for the three vane nozzle segment are shown in Figures 43 thru 45. The complete ring design rig test nozzle components are shown in Figures 45 thru 47. One

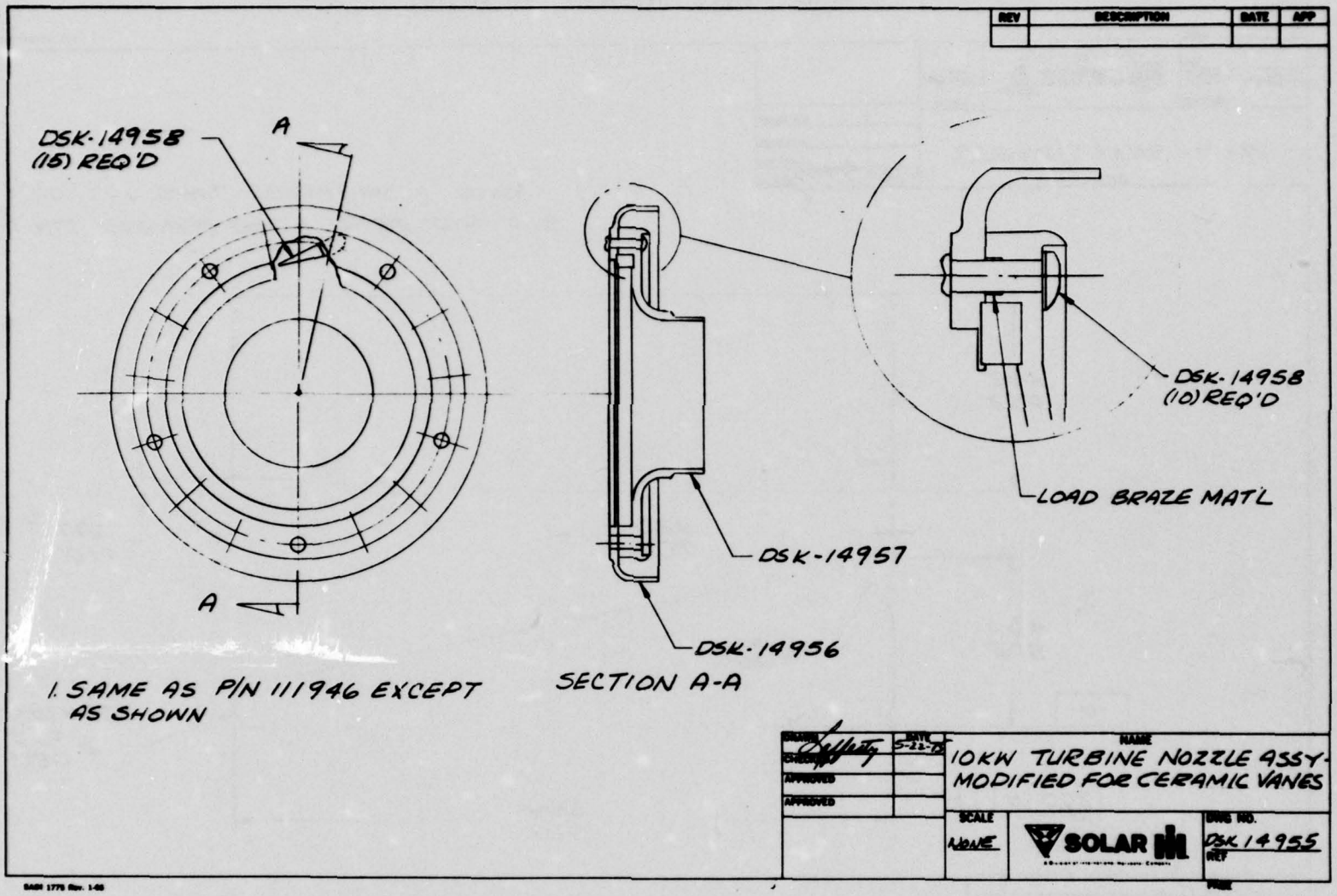

FIGURE 38. 10KW TURBINE NOZZLE ASSEMBLY MODIFIED FOR CERAMIC VANES

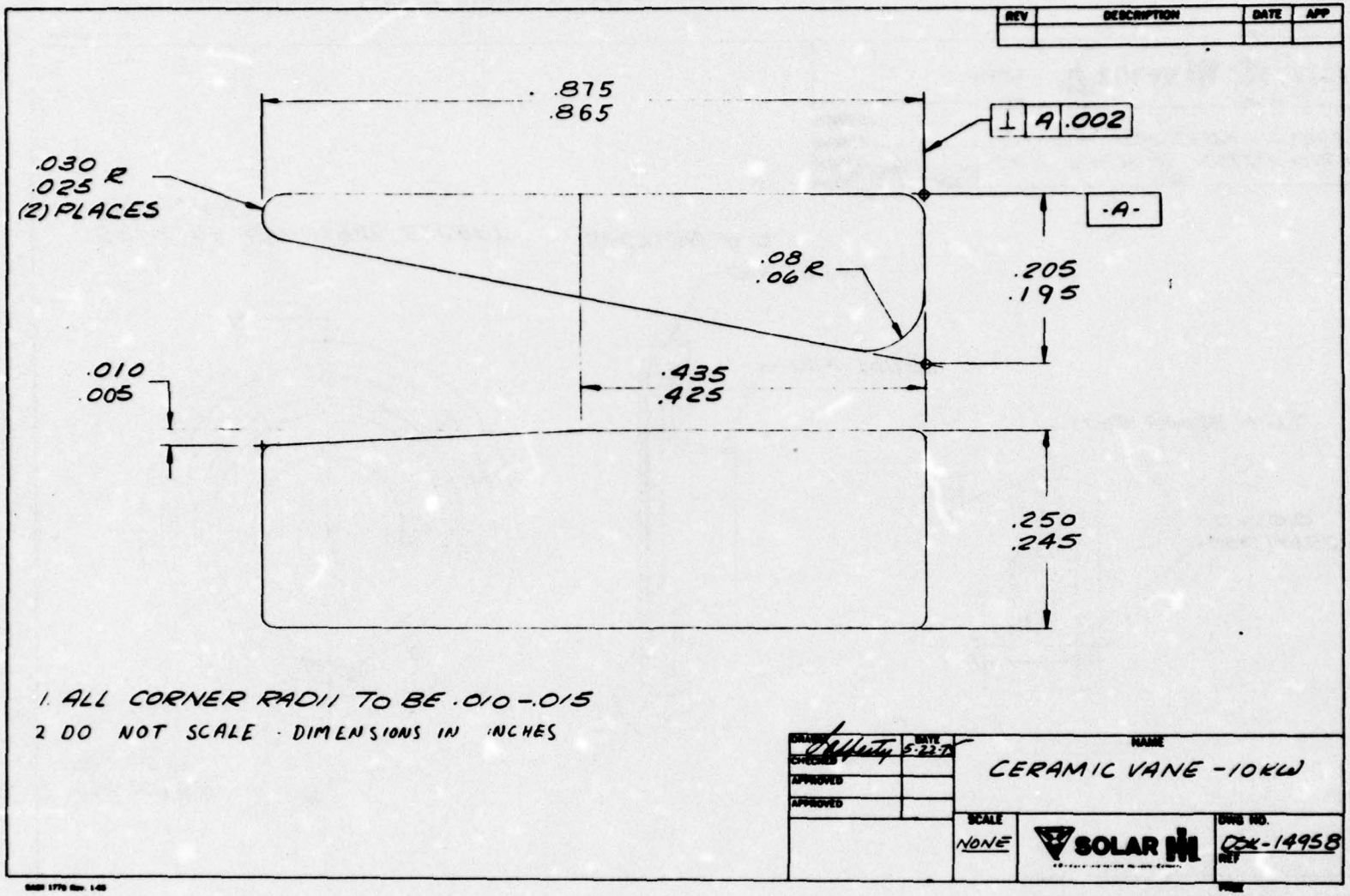

FIGURE 39. CERAMIC VANE - 10KW

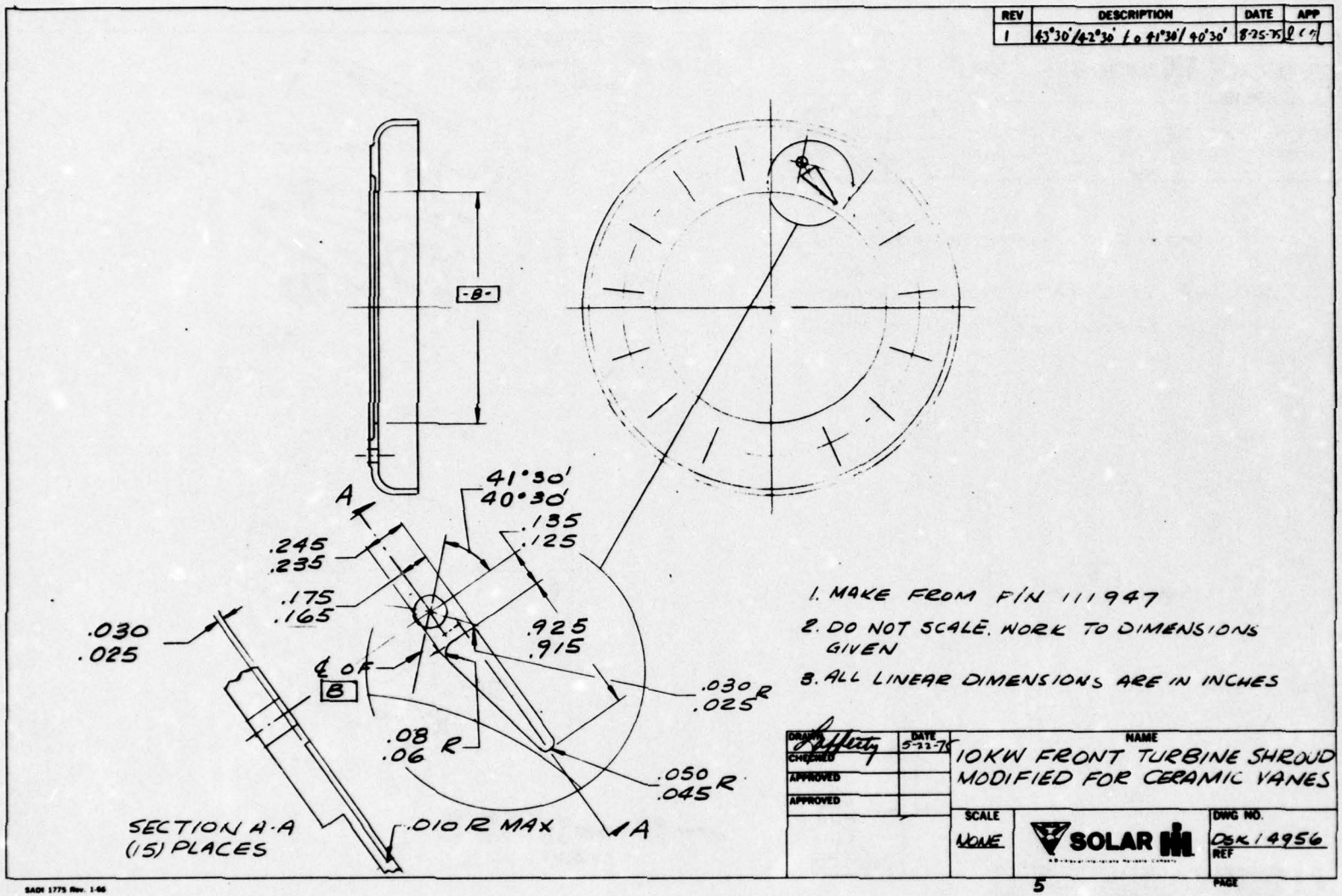

FIGURE 40. 10kW Front Turbine Shroud Modified for Ceramic Vanes

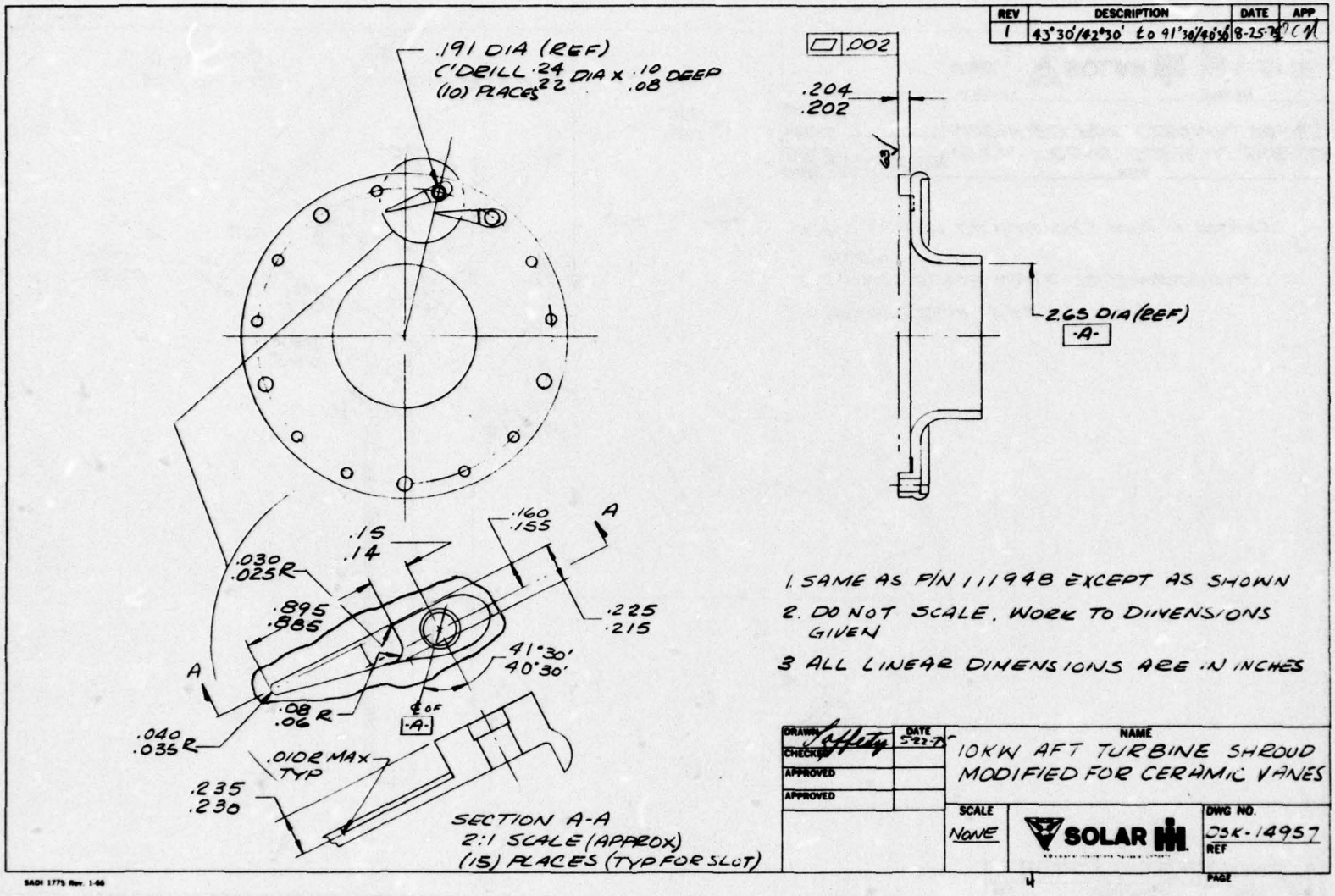

FIGURE 41. 10kW Aft Turbine Shroud Modified for Ceramic Vanes

SOLAR PART NO.	REVISIONS			
	LTR	DESCRIPTION	DATE	APPROVED

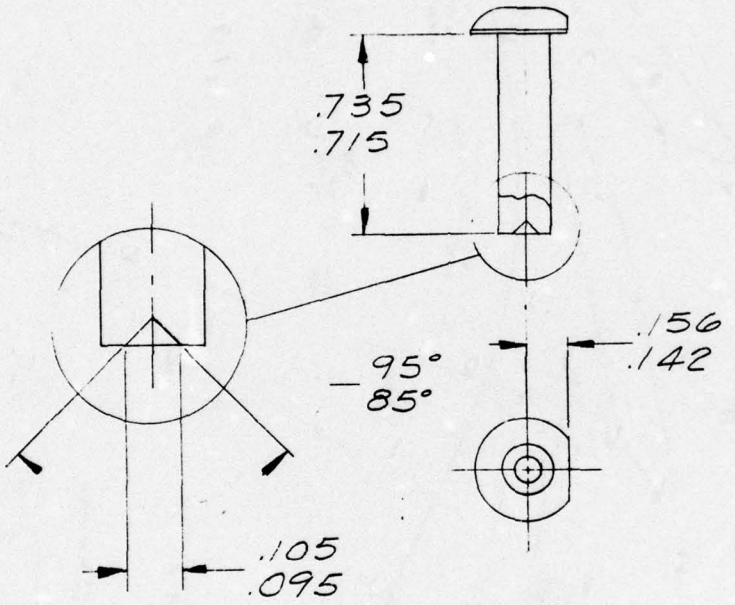

1. MAKE FROM P/N 45118
2. DO NOT SCALE DWG. WORK TO DIM'S GIVEN
3. ALL DIM'S IN INCHES

APPROVED BY	SOLAR — DIVISION OF INTERNATIONAL HARVESTER COMPANY, 2200 PACIFIC HIGHWAY · SAN DIEGO, CALIFORNIA 92112	
GOVT. CONTRACT NO.	DRAWING TITLE: RIVET, TURBINE NOZZLE	
PROJ / DES / CH / DB 5-27-75		
DESIGN ACTIVITY	SIZE: A; CODE IDENT NUMBER: 55820; DRAWING NUMBER: DSK-14959	
CUSTOMER	SCALE 2:1; TOTAL WT.; SHEET 1 OF 1	

FIGURE 42. RIVET, TURBINE NOZZLE

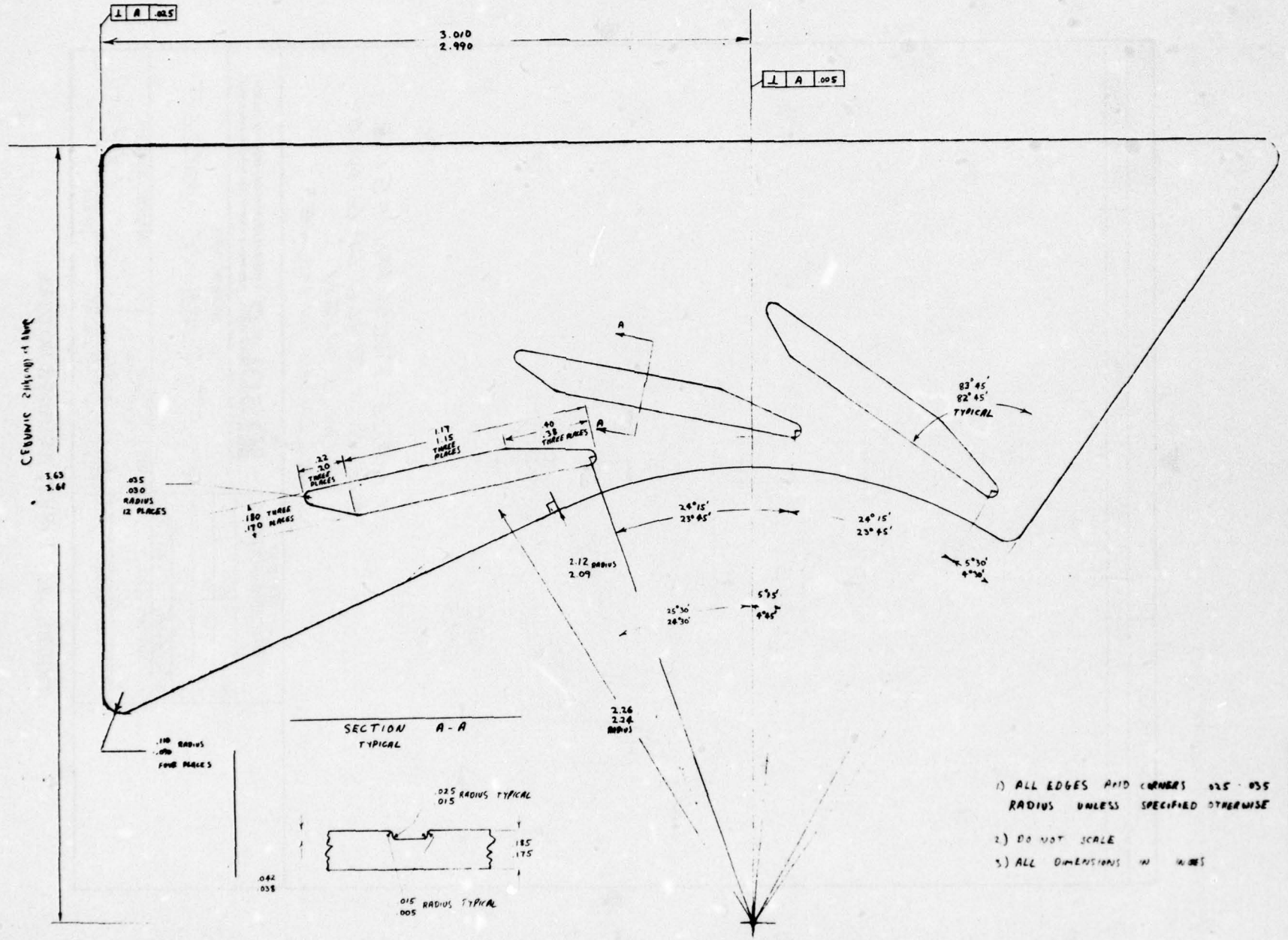

FIGURE 43. FORWARD SHROUD SECTION (RB Si_3N_4) CONSIDERED FOR RIG TESTS

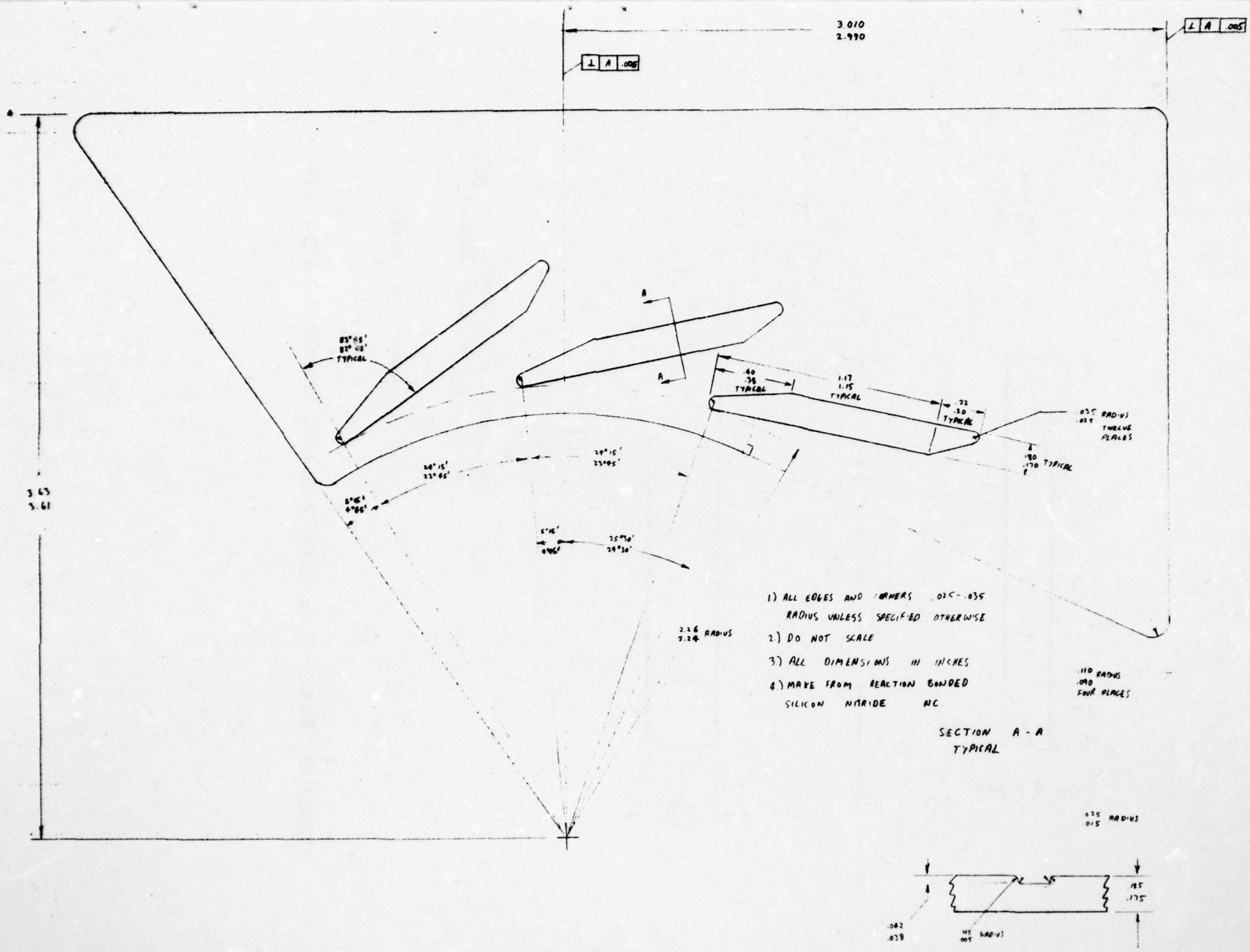

FIGURE 44. AFT SHROUD SECTION (RS Si_3N_4) CONSIDERED FOR RIG TESTS

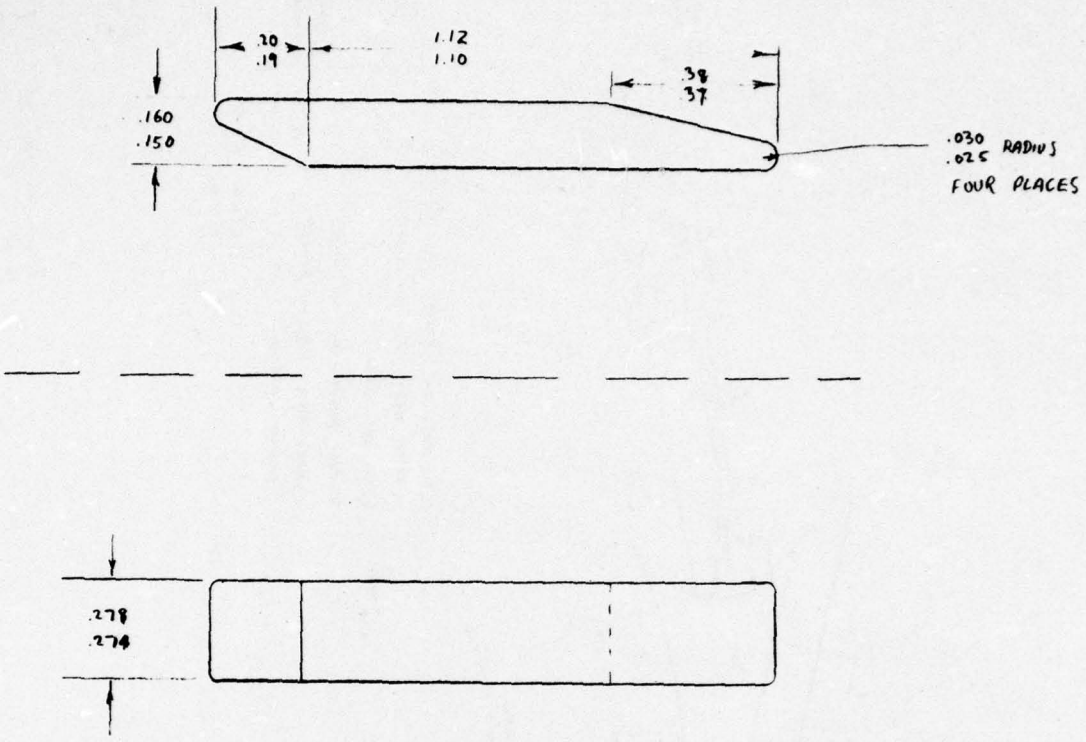

1) ALL EDGES AND CORNERS .025-.035 RADIUS UNLESS SPECIFIED OTHERWISE

2) DO NOT SCALE

3) ALL DIMENSIONS IN INCHES

FIGURE 45. VANE (HP Si_3N_4) FOR ALL-CERAMIC NOZZLE RIG TESTS

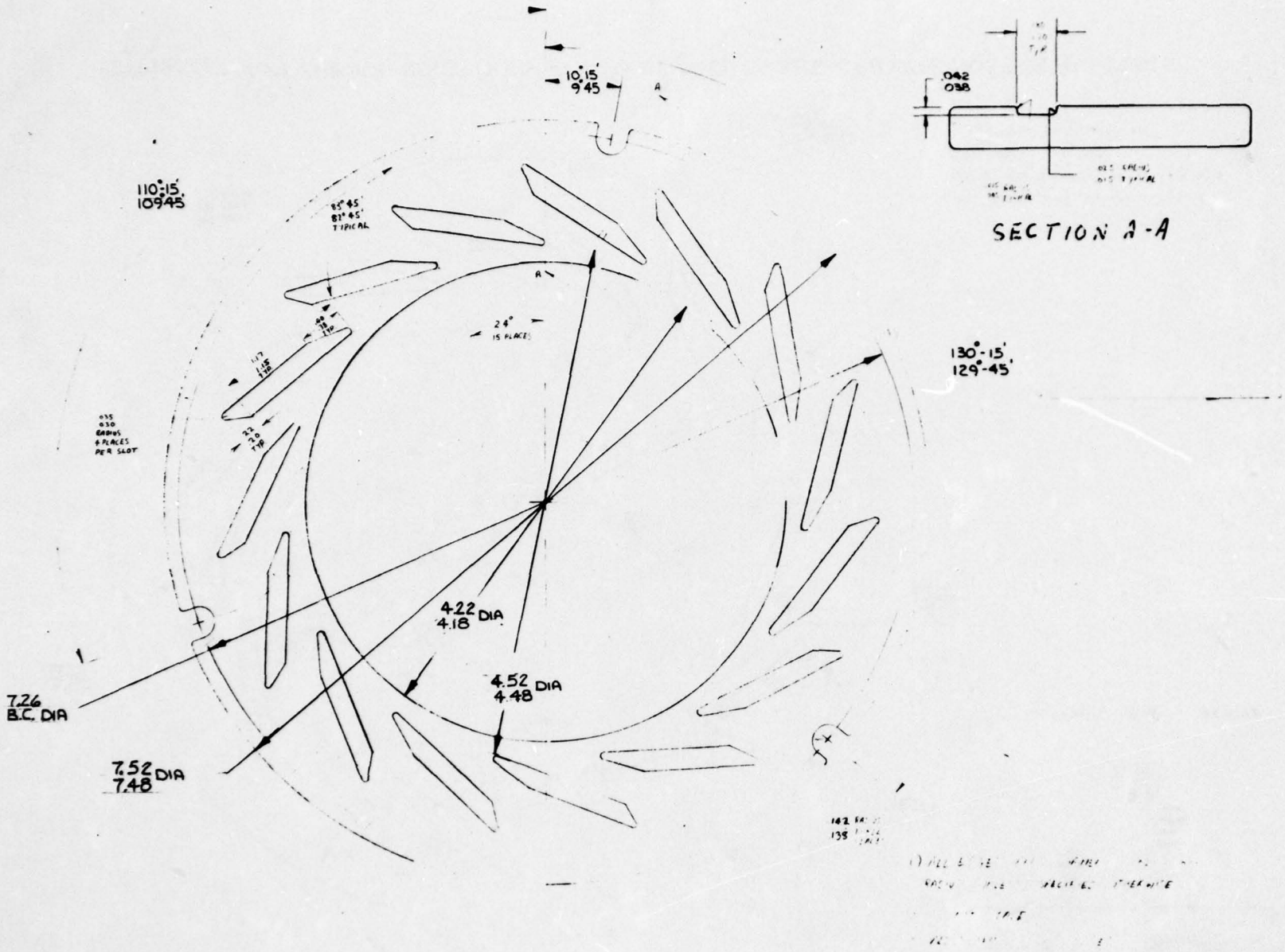

FIGURE 46. FORWARD SHROUD RING (RB Si_3N_4) TO BE USED IN ALL-CERAMIC NOZZLE RIG TESTS

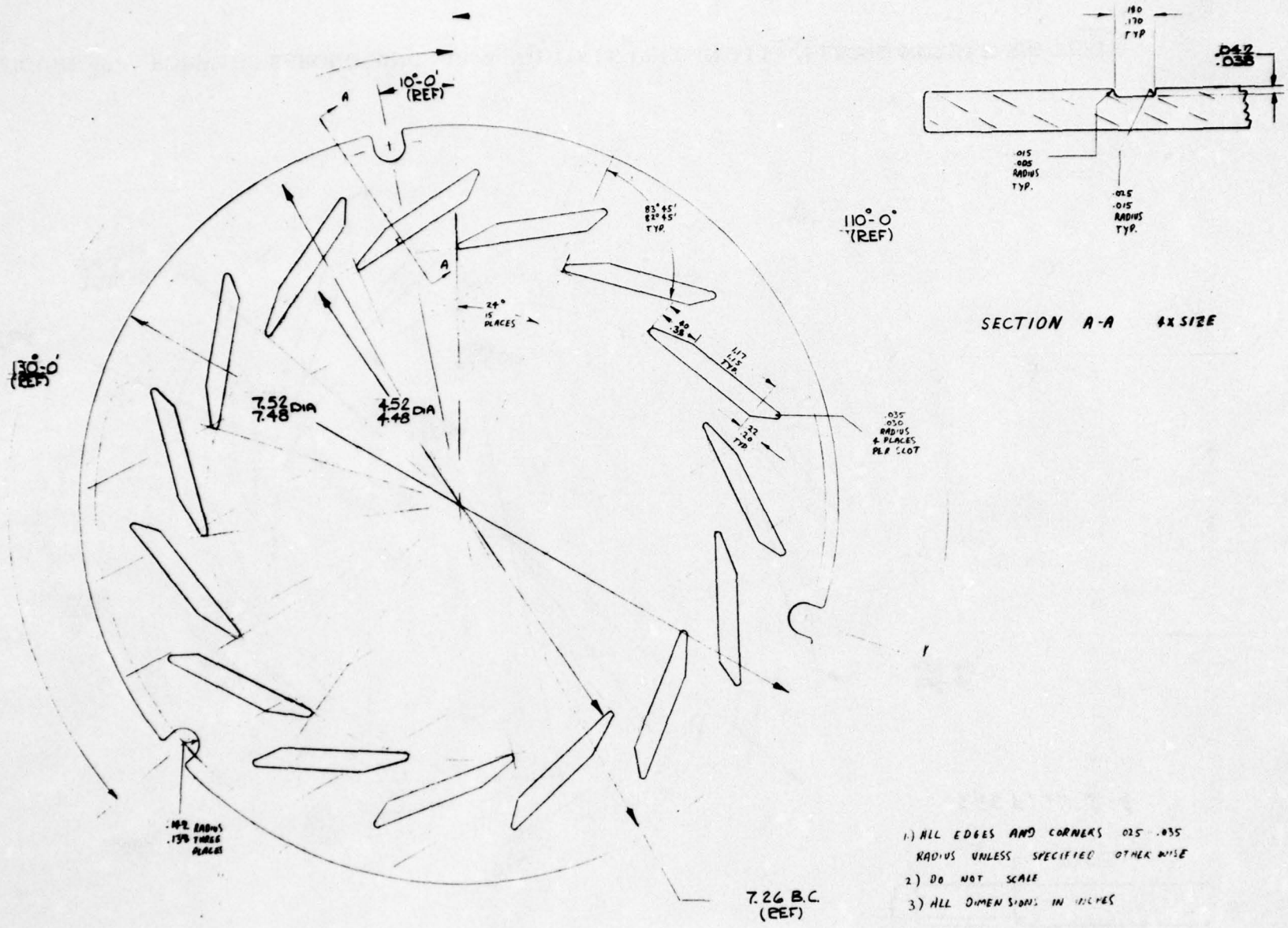

FIGURE 47. AFT SHROUD RINGS (RB Si_3N_4) TO BE USED IN ALL-CERAMIC NOZZLE RIG TESTS

advantage of the full ring design over the segmented one is that it avoids extraneous thermal stresses to shroud pieces which would not be characteristic of actual engine shrouds. Rig mounting of this assembly is simpler and more identical to actual engine conditions. The only drawback of this approach was considered to be cost of parts. A quotation from Norton Company showed cost differential to be relatively small in light of the advantages of this approach.

The HPSi_3N_4 ceramic nozzle vane as shown in Figure 45 are mechanically held in the shroud recesses. The entire shroud vane assembly is held in place for rig tests with three diameter piloted spring loaded Hastelloy X pins. Glass joining materials are applied at the vane shroud interfaces. (The assembly is pictured in Section 3.2.7.)

3.2.5.2 Vane Design

The shroud recess must restrict the vane from moving laterally, *longitudinally and from rotating.* View B-B of Figure 48 shows a recess type that could accomplish this, however the square sides of the recess which prevent rotation result in sharp radii and high stress concentration. (Total groove depth at sides is only approximately 0.030 in. which implies bottom corner radii to be less than 0.010 in. This results in approximately a 2.5 stress concentration factor for a transverse tensile load (Ref. 24).)

A variation on this design which is the design chosen for rig test, is given in Figure 49. The flat region at recess bottom offers resistance to rotation. Since the recess shape is not cylindrical the recess is deeper at the sides thus allowing for a greater radii. A 0.030 radius results in approximately 1.8 stress concentration factor. This configuration is regarded to be the least complex to fabricate of those considered here. Good vane location tolerances can also be achieved because static aerodynamic forces will locate the vane downstream and against the surface toward the engine axis.

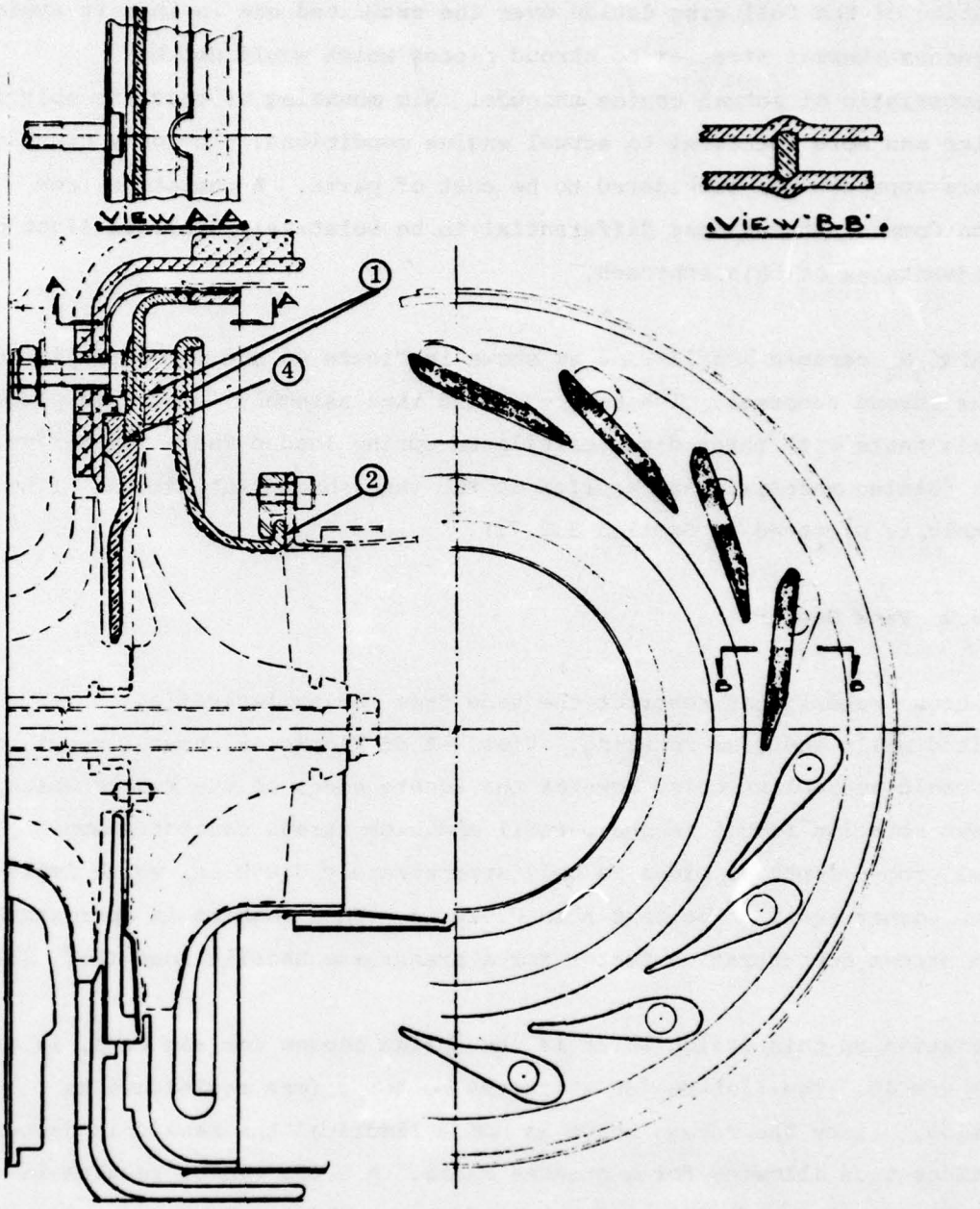

FIGURE 48. COMPARISON OF PRESENT NOZZLE DESIGN (LOWER) WITH REDESIGN FOR CERAMIC VANES, SHROUDS AND SEAL PLATE (UPPER)

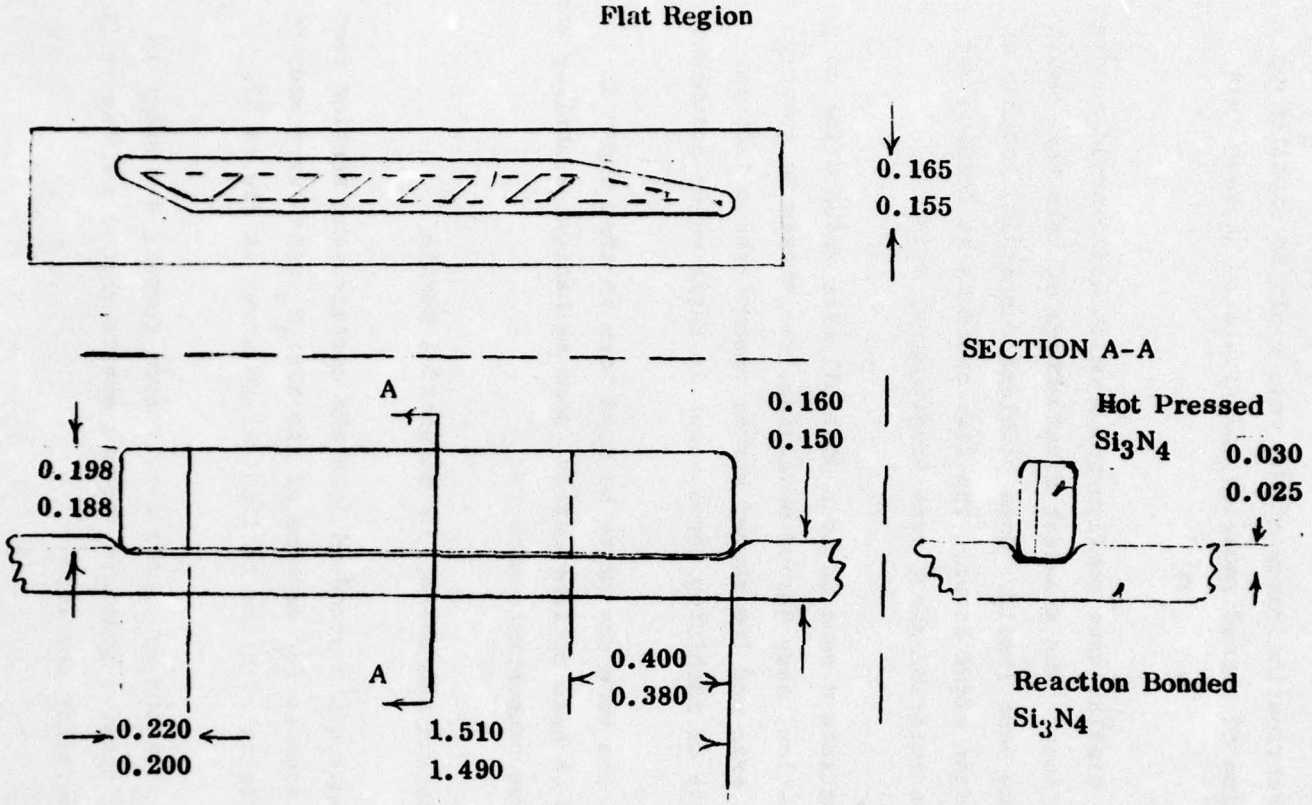

1. All Corners and Edges 0.030-0.040 Radius for Shroud
2. All Corners and Edges 0.020-0.030 Radius for Vane

FIGURE 49. POSSIBLE SHROUD RECESS AND VANES FOR ALL CERAMIC NOZZLE DESIGN

Figure 50 shows a vane shape which could be entrapped in a matching cylindrical recess in the shrouds. It offers a low stress concentration factor in shrouds (≈1.5), however little restraint for resisting vane rotation is offered. Fabrication costs of the vane would be expected to be reasonable, but machining of shroud recesses, particularly at vane ends, would be involved.

Figure 51 represents a similar vane configuration which would avoid complex shroud machining operations. The greatest disadvantage of this vane would be expense of making the vane itself. Some problems concerning leakage at leading and trailing edges might occur. The flat sections at leading and trailing edges restrain rotation about vane longitudinal axis.

Figures 52 and 53 illustrate a vane designs possibilities which offer better aerodynamic characteristics, easy shroud machining, resistance to rotation about the longitudinal axis and low shroud stress concentration factors (≈1.25). The complexity of machining these vanes is their major drawback.

The final selection of the vane design to be used here is that shown in Figure 49 and is based on ease of fabrication, good mechanical stability and reasonable shroud stress concentration factor.

3.2.6 Rig Test Fabrication and Assembly - Bimaterial Nozzle

Figures 54A and 54B compare the standard 10kW and ceramic vane section rear nozzle shrouds. The recesses for capture of the HPSi_3N_4 vanes were made by Electro Discharge Machining with the tooling set-up shown in Figure 55.

Typical ceramic vane sections as supplied by Norton Company are shown in Figure 56. Figure 57 shows a standard forward nozzle shroud and Figure 58 shows the ceramic/superalloy nozzle.

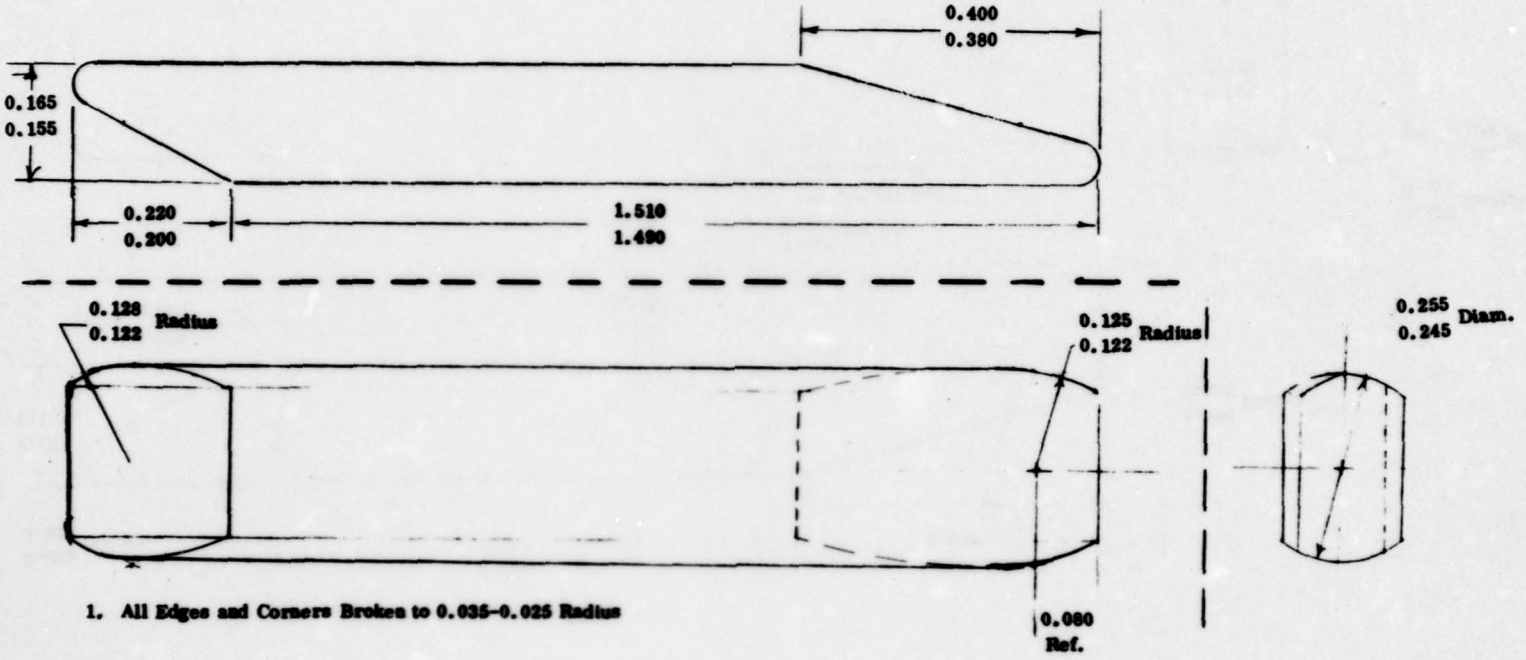

FIGURE 50. POSSIBLE VANE DESIGN FOR ALL CERAMIC NOZZLE

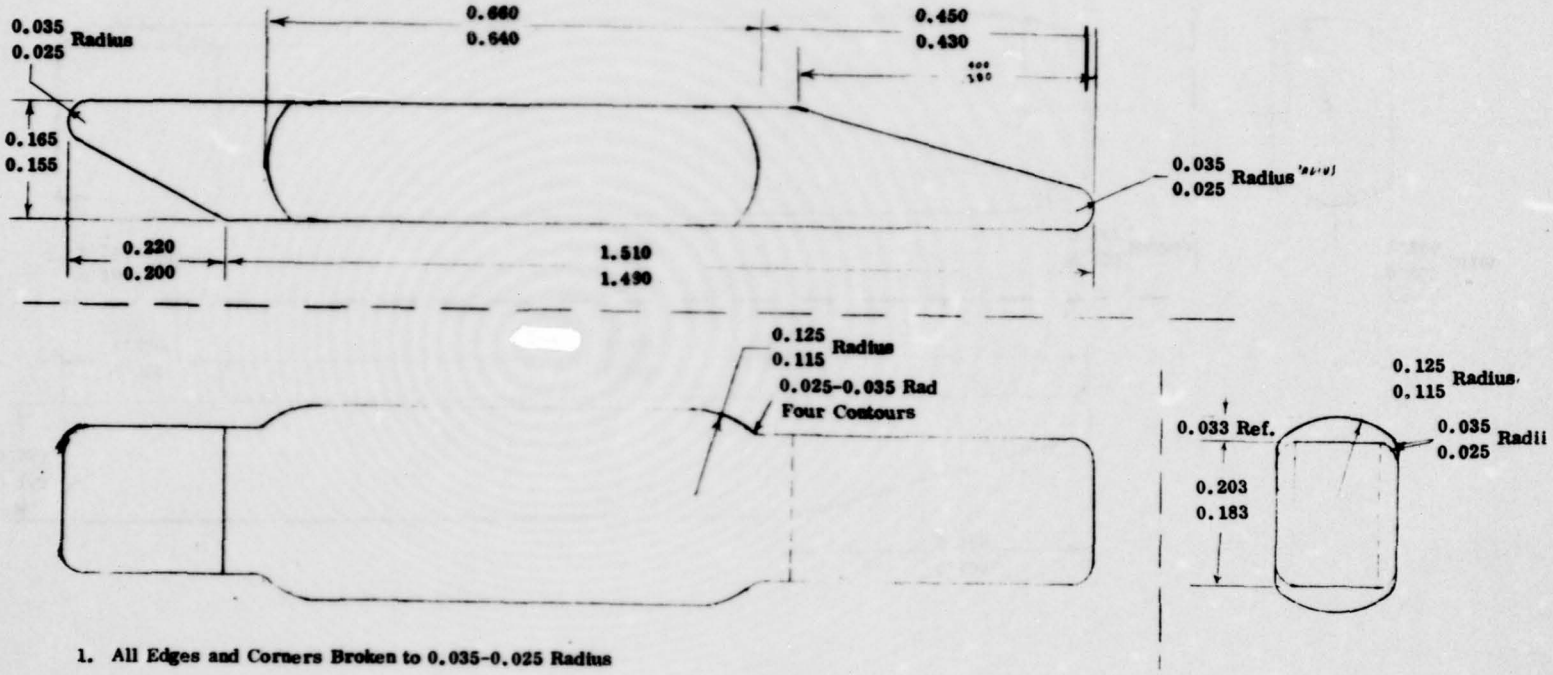

1. All Edges and Corners Broken to 0.035-0.025 Radius

FIGURE 51. POSSIBLE VANE DESIGN FOR ALL CERAMIC NOZZLE

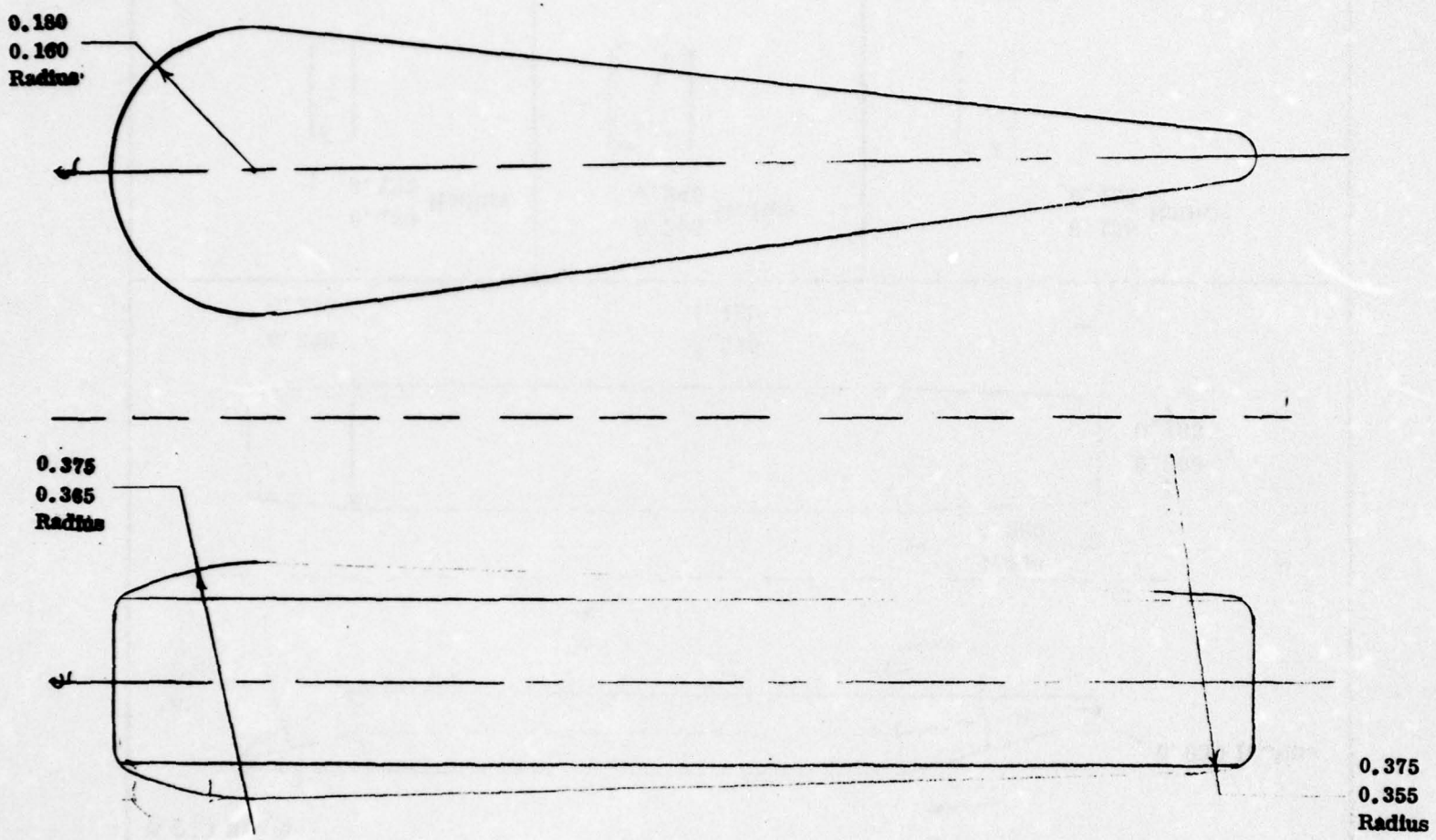

FIGURE 52. POSSIBLE VANE DESIGN FOR ALL CERAMIC NOZZLE

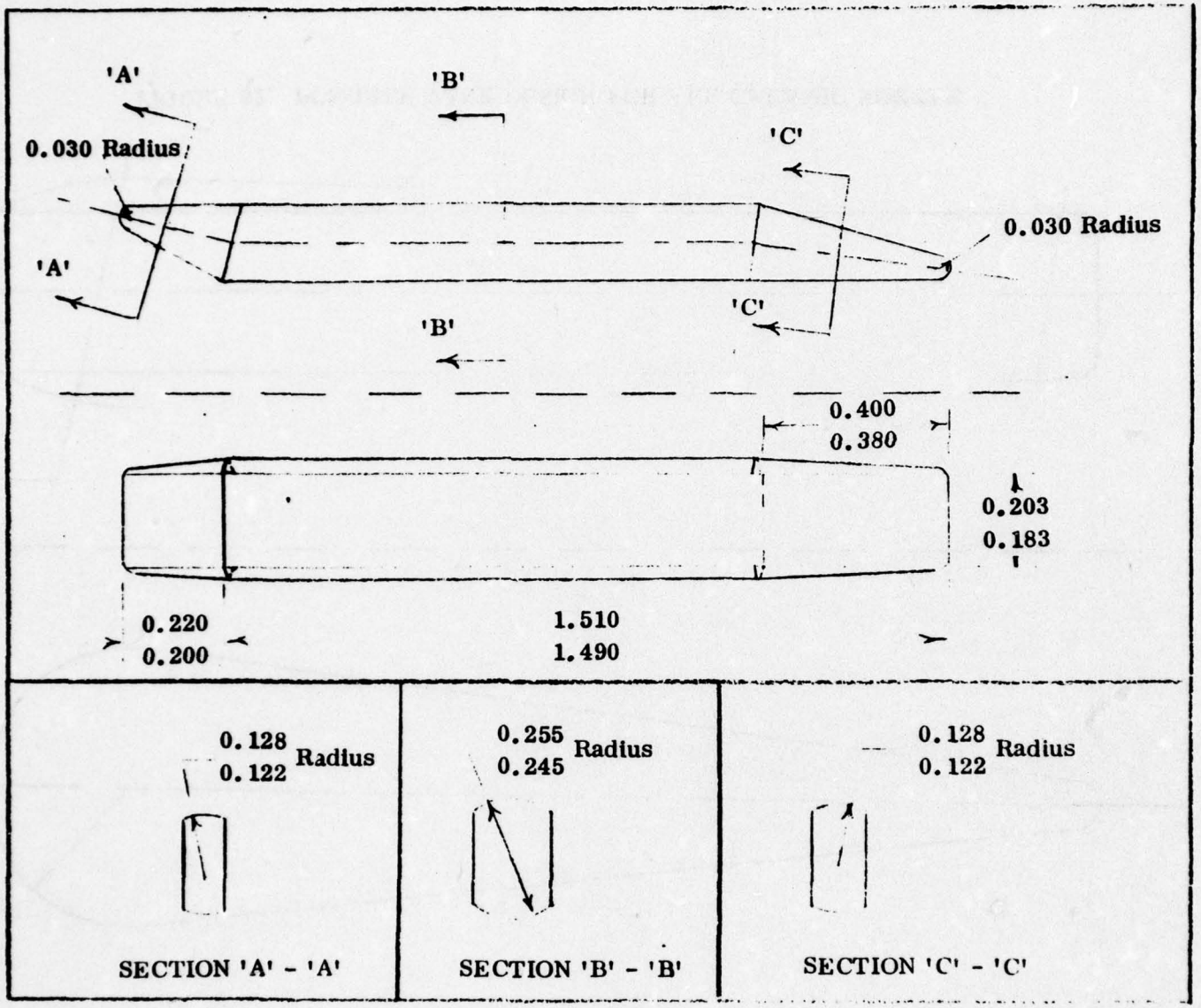

FIGURE 53. POSSIBLE VANE DESIGN FOR ALL CERAMIC NOZZLE

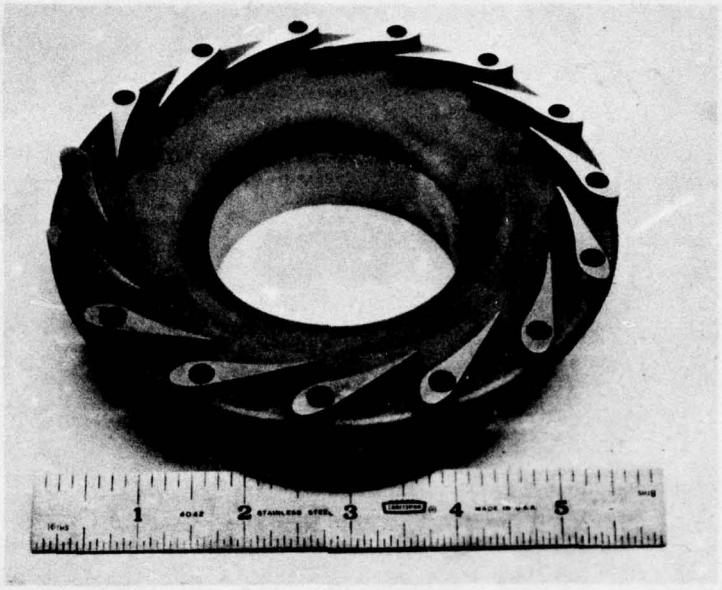

A.

STANDARD 10 kW REAR NOZZLE SHROUD (Part #107726-1)
(Turbine Seal Surface Not Machined)

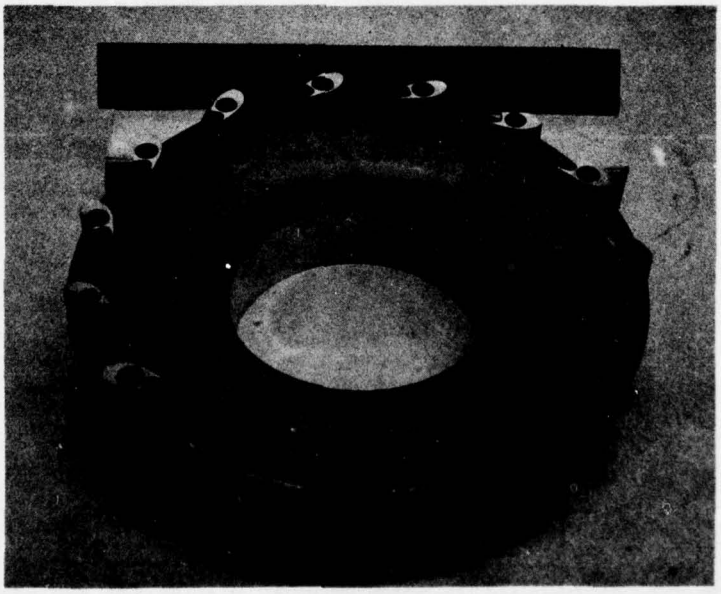

B.

FIGURE 54. 10 kW REAR NOZZLE SHROUD WITH TWO HPSi_3N_4 TRAILING VANE SECTIONS INSERTED (Per Drawing DSK 14957)

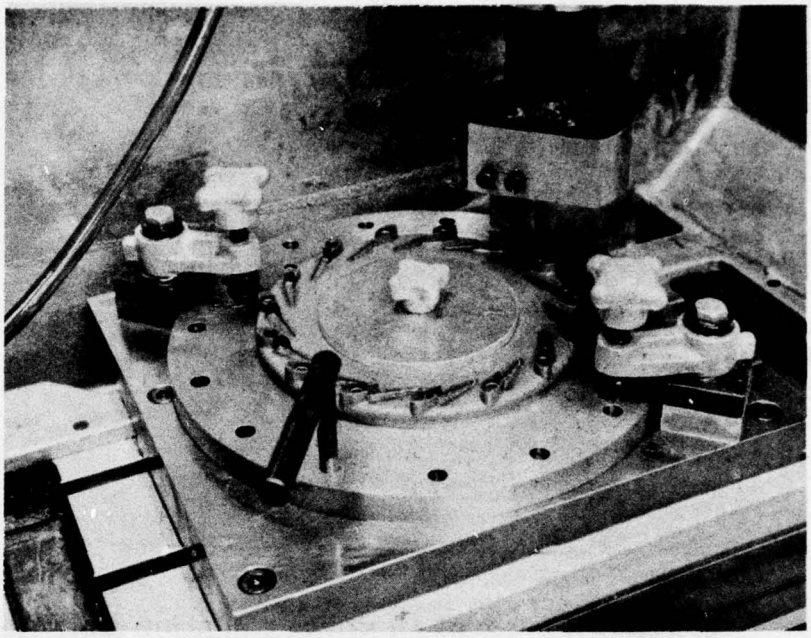

FIGURE 55. TOOLING SET-UP FOR EDM OF RECESSES IN NOZZLE SHROUD

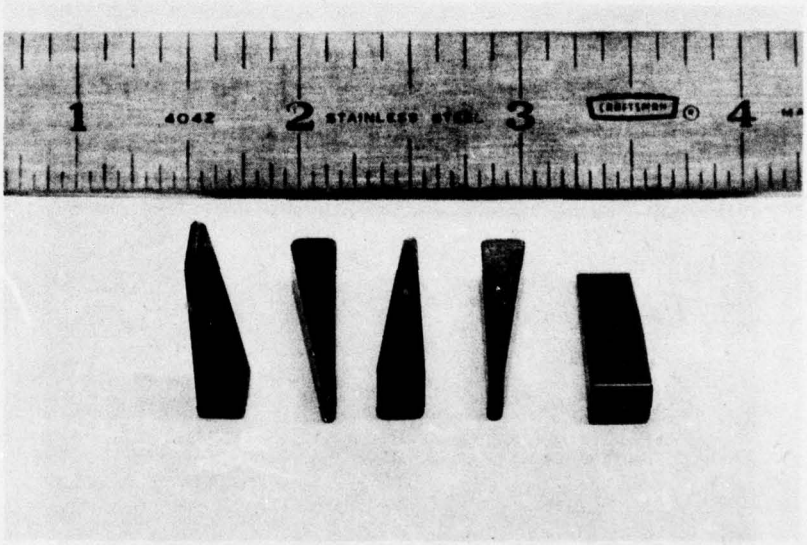

FIGURE 56. $HPSi_3N_4$ (NC-132) NOZZLE VANE TRAILING EDGE SECTIONS (Per Drawing DSK-14958)

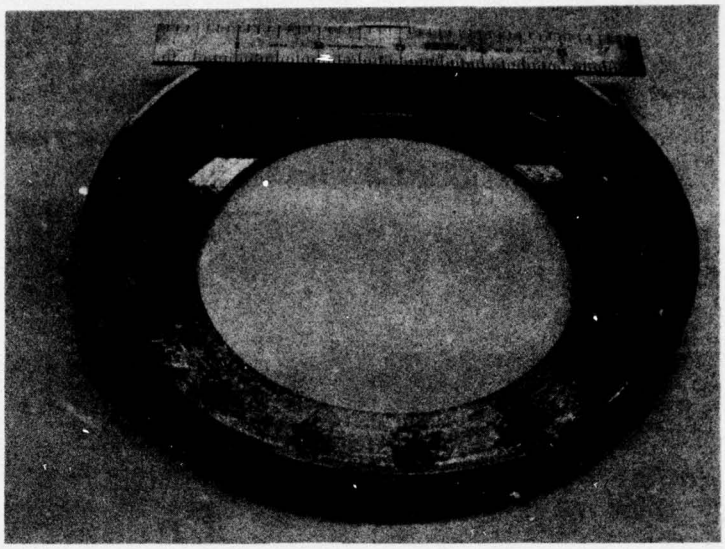

FIGURE 57. STANDARD 10 kW FORWARD NOZZLE SHROUD (Part #74-8006)

Figures 58A and 58B show the rear shroud with vane sections in place and glass interface material applied prior to firing. Table 9 gives the sequence of glass application starting with the top center vane (which has a reference arrow) and counting clockwise.

The glass slurries were applied to the appropriate recesses of the forward and rear shrouds as well as the ceramic vane sections. Both shrouds were then bolted together through each of the 15 rivet or bolt holes. The rivets, were then progressively set in each of the ten rivet holes following removal of the bolts one by one. The rivets were set statically on a tensile machine at ambient temperature with a maximum load of 15,000 pounds.

The assembly was then fired for one hour at 1038°C (1900°F) in an Argon atmosphere. The completed assembly, as installed in the rig test chamber before test, is shown in Figure 59.

Figure 60 shows the location of thermocouples used in rig testing.

Figure 61 illustrates the nozzle mounted to the water-cooled test chamber and location of thermocouples number 1 and 2.

AD-A035 329 SOLAR SAN DIEGO CALIF F/G 21/5
APPLICATION OF CERAMIC NOZZLES TO 10KW ENGINE.(U)
AUG 76 J C NAPIER, A G METCALFE DAAK02-75-C-0138
UNCLASSIFIED RDR-1797-16 NL

2 OF 2
AD
A035329

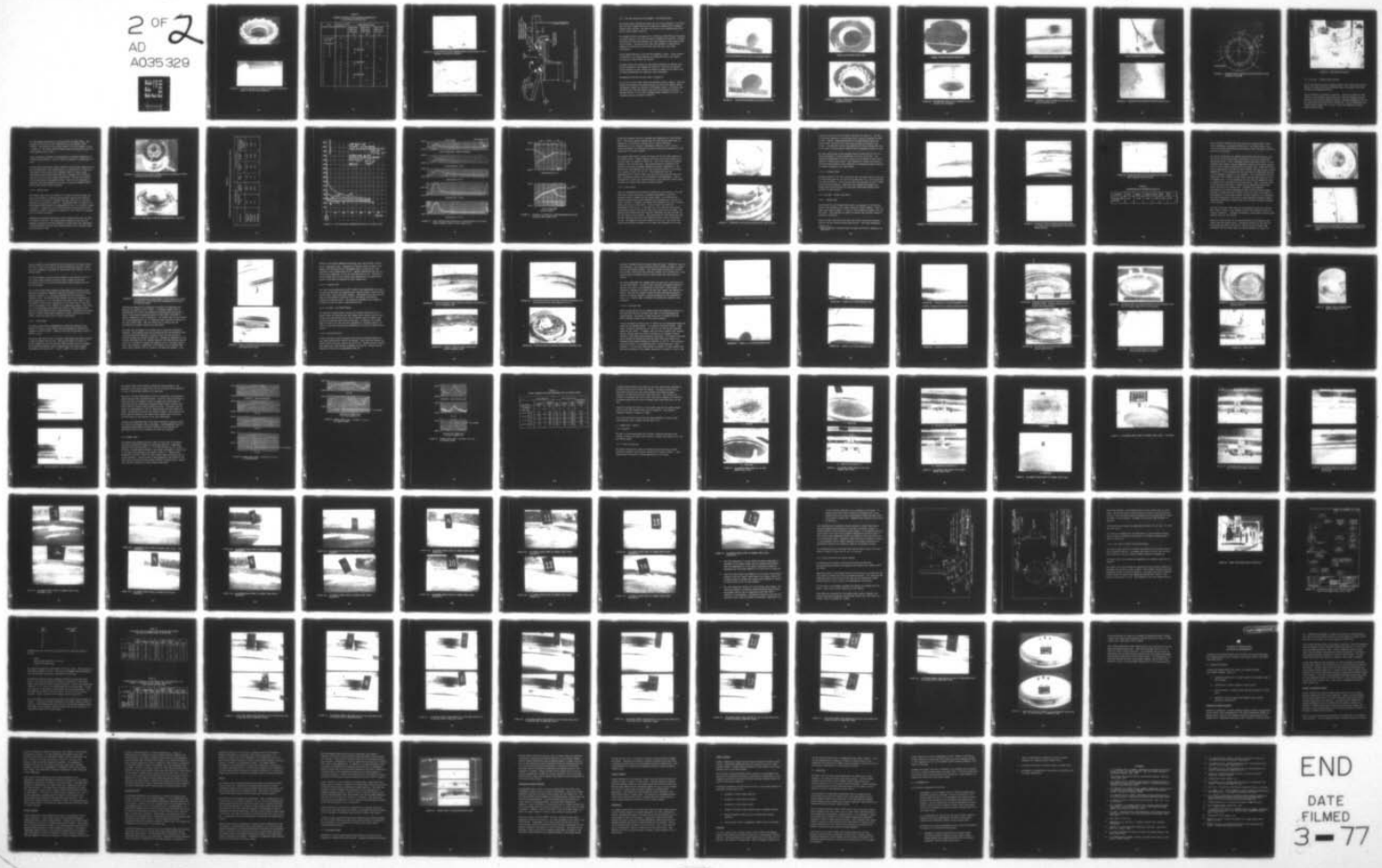

END
DATE
FILMED
3-77

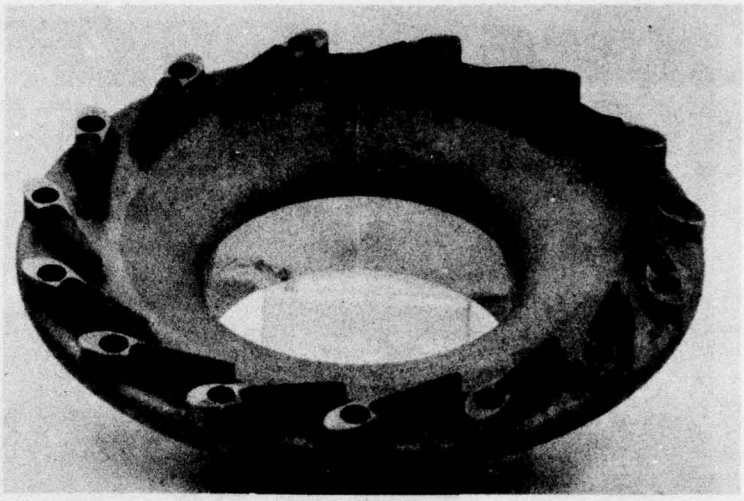

A.

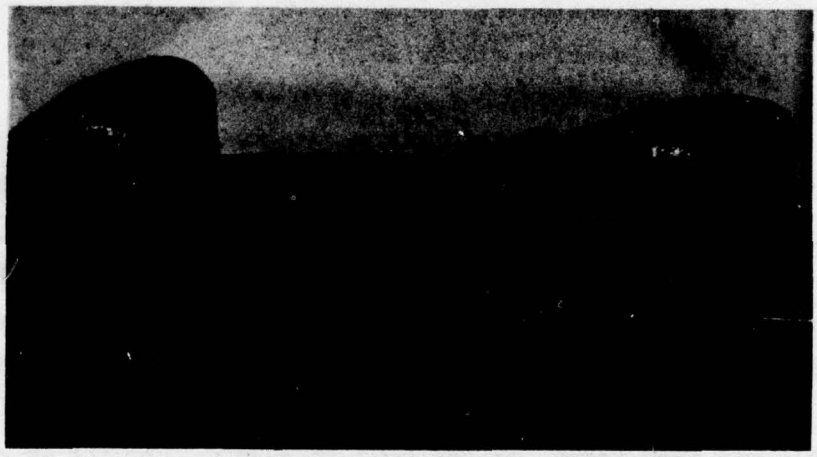

B.

FIGURE 58. CERAMIC/SUPERALLOY NOZZLE PARTIALLY ASSEMBLED PRIOR TO FIRING GLASS INTERFACE

TABLE 9

ASSEMBLY SCHEDULE FOR CERAMIC/SUPERALLOY
10 kW NOZZLE FOR RIG TEST

Vane Location Number	Ceramic Vane Identification	Glass Interface Type		
		30% B 402 30% GN 19 40% Cr_2O_3 (A)	35% B 402 35% GN 19 30% Cr_2O_3 (B)	40% B 402 20% GN 19 40% Cr_2O_3 (C)
1 (Top Center Fig. 58A)	B	X		
2 (Clockwise)	G		X	
3	H			X
4	I	No Glass Fill		
5	J	X		
6	K		X	
7	L			X
8	M	No Glass Fill		
9	N	X		
10	S		X	
11	P			X
12	Q	No Glass Fill		
13	R	X		
14	O		X	
15	T			X

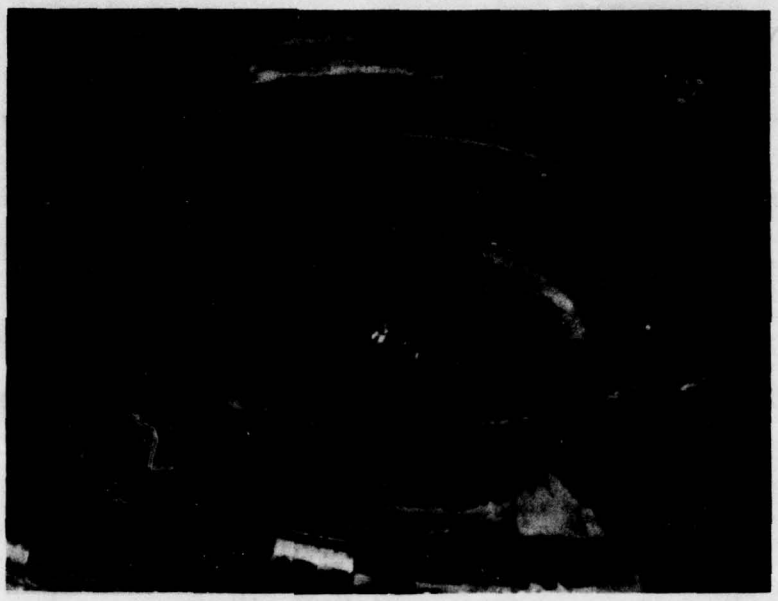

FIGURE 59. COOLED NOZZLE TEST CHAMBER WITH LID INVERTED TO SHOW UPSTREAM SECTION OF NOZZLE

FIGURE 60. 10 kW NOZZLE TEST RIG THERMOCOUPLE LOCATION

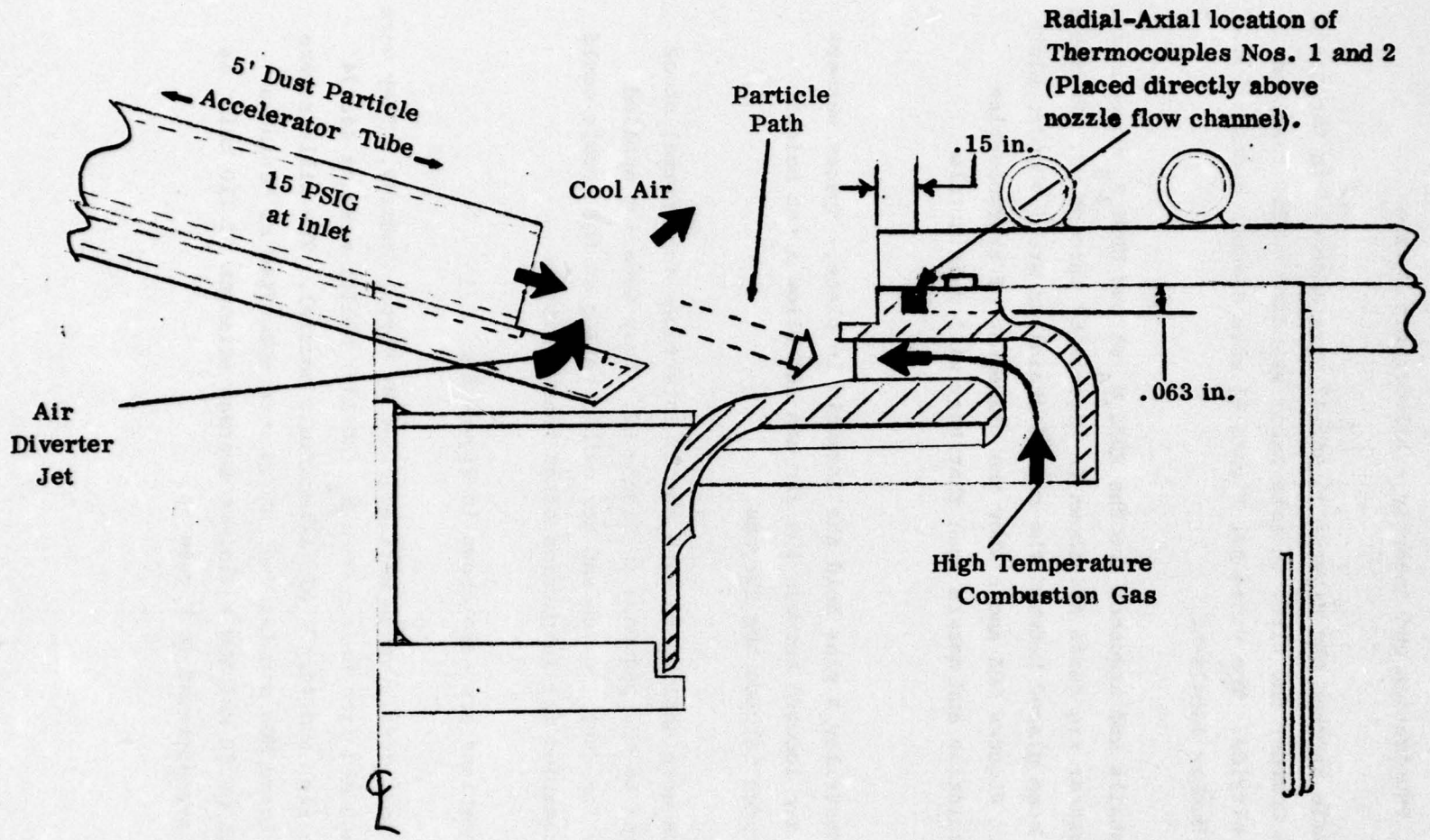

FIGURE 61. LOCATION OF THERMOCOUPLES NOS. 1 AND 2 IN RIG TESTS AND SKETCH OF DUST EROSION DEVICE

3.2.7 Rig Test Fabrication and Assembly - All-Ceramic Nozzle

The ceramic nozzle shrouds per Figures 46 and 47 were machined in the green state by Norton Company and fired to make their standard NC-350 reaction bonded silicon nitride. The vanes per Figure 45 were diamond ground from NC-132, Billet Number 446474-A2.

The assembly details and sequence for the $RBSi_3N_4$ shroud $HPSi_3N_4$ vane nozzle for engine simulator rig tests are shown in Figures 62 through 65. Refrasil insulation has been placed between the cooled stainless steel support plate and the nozzle. Figures 66A and B show the placement of thermocouples between the insulation and nozzle such that they will read nozzle temperatures.

Spring loaded Hastelloy X pins hold the assembly in place. Spacer washers of Hastelloy X are located between the shrouds and allow a net height clearance for vanes between the shrouds.

Relaxing glasses were applied to vane shroud interfaces for thermal shock testing according to the sequence in Figure 67. They were not applied during assembly for dust erosion and corrosion testing so the nozzle could be easily disassembled for inspection after these tests.

Thermocouple locations are also shown in Figure 68.

All of the rig test nozzle vanes were supplied by Norton Company. They were diamond tool machined from Norton $HPSI_3N_4$ (NC-132) billet numbers 446474 (bi-material nozzle) and 446474-A2 (all-ceramic nozzle). The billets were qualified with three MOR samples each which were specified as having a minimum strength of 80 ksi and a minimum average strength of 110 ksi. As received vanes are pictured in Figure 56.

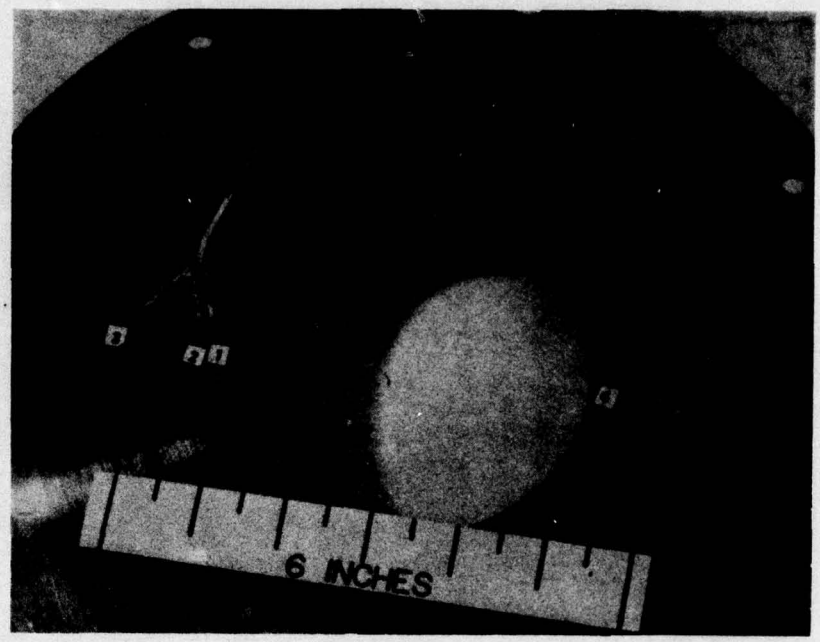

A.

COOLED MOUNTING PLATE FOR ALL-CERAMIC NOZZLE

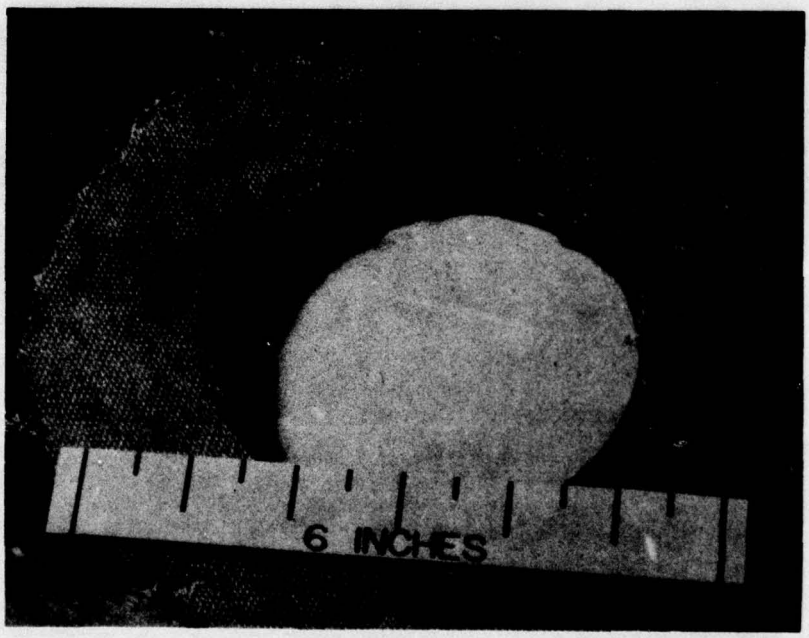

B.

FIGURE 62. PLATE WITH REFRASIL INSULATION IN PLACE

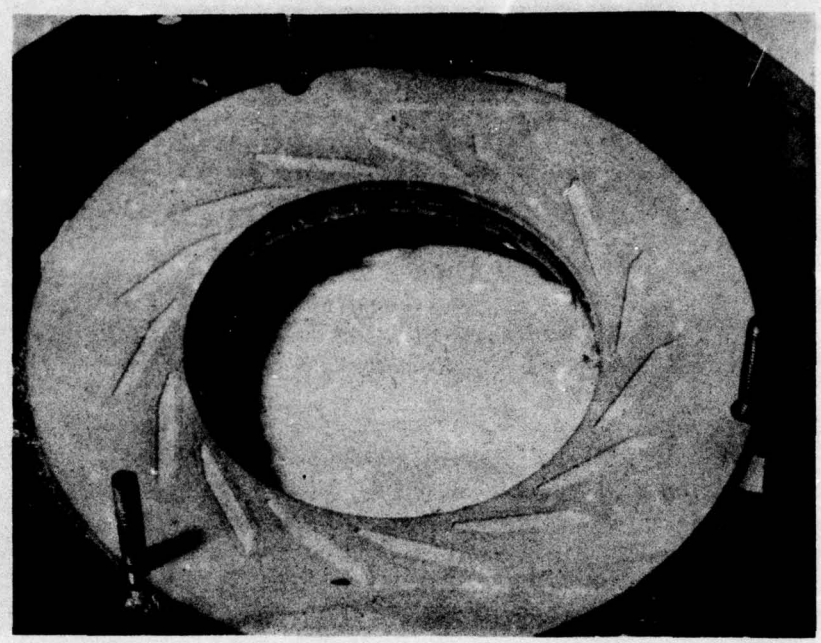

A.

$RBSi_3N_4$ EXIT SHROUD INSTALLED

B.

FIGURE 63. $HPSi_3N_4$ VANES INSTALLED WITH HASTELLOY SPACER WASHERS AND PINS

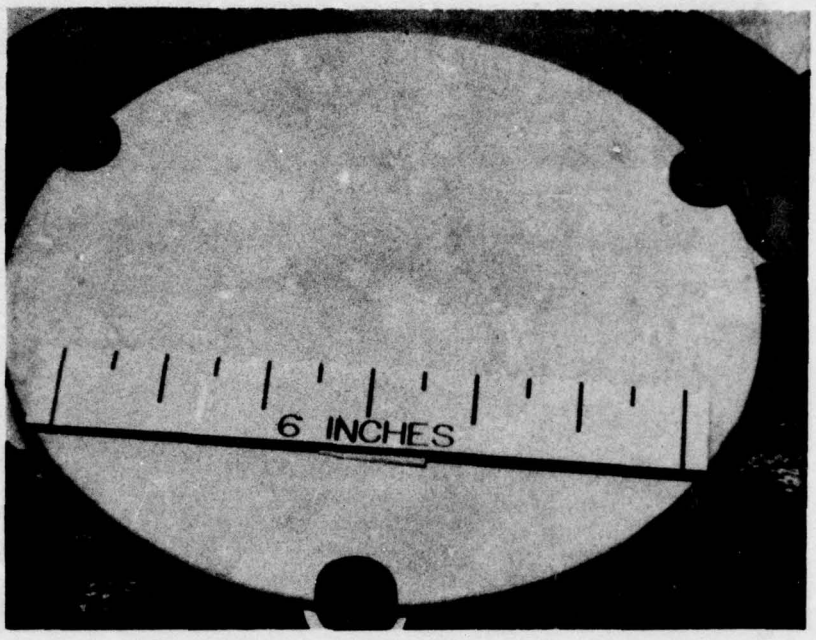

A.

$RBSI_3N_4$ UPSTREAM SHROUD INSTALLED

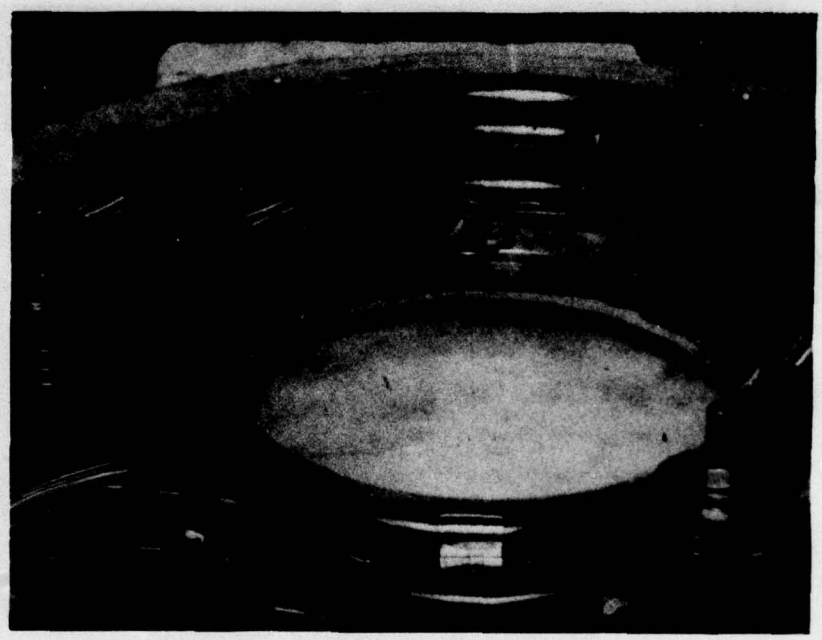

B.

FIGURE 64. DOWNSTREAM VIEW OF ALL CERAMIC NOZZLE IN COOLED TEST CHAMBER

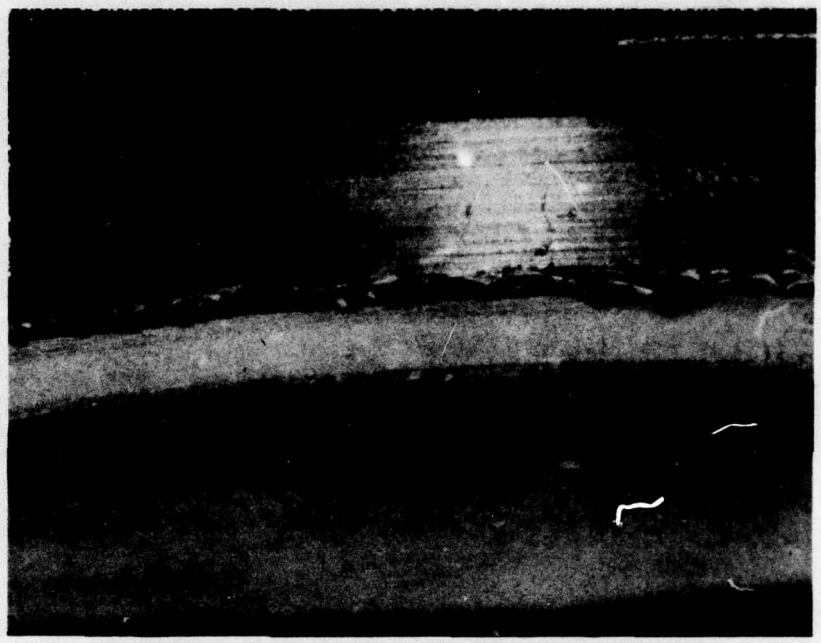

A. DOWNSTREAM VIEW OF TYPICAL VANE

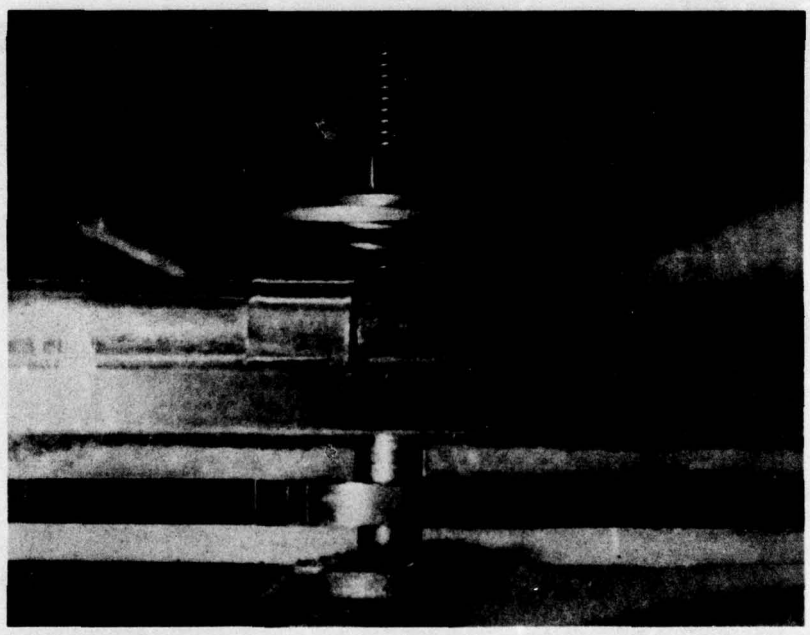

B.

FIGURE 65. UPSTREAM VIEW OF SPRING LOADED HASTELLOY NOZZLE SUPPORT PIN 'A'

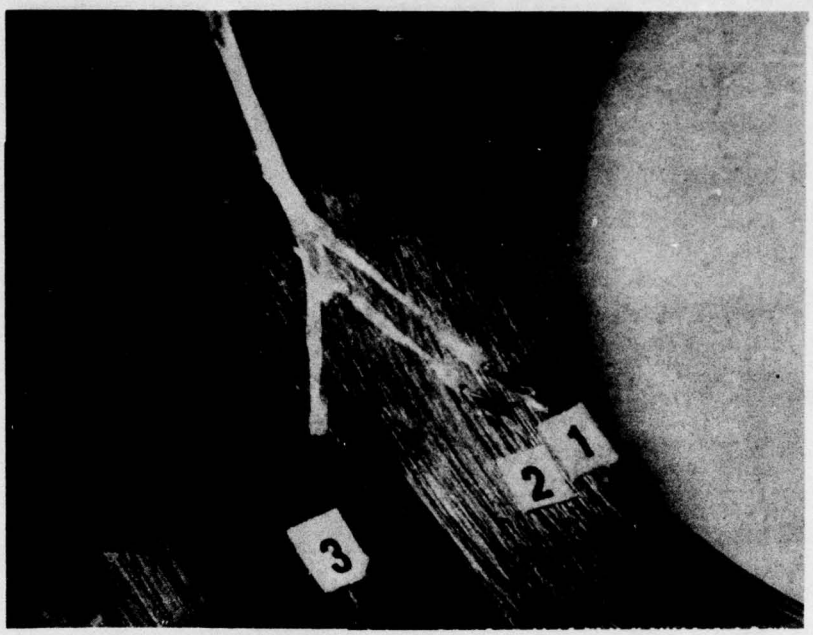

A. TYPE K THERMOCOUPLE LOCATION

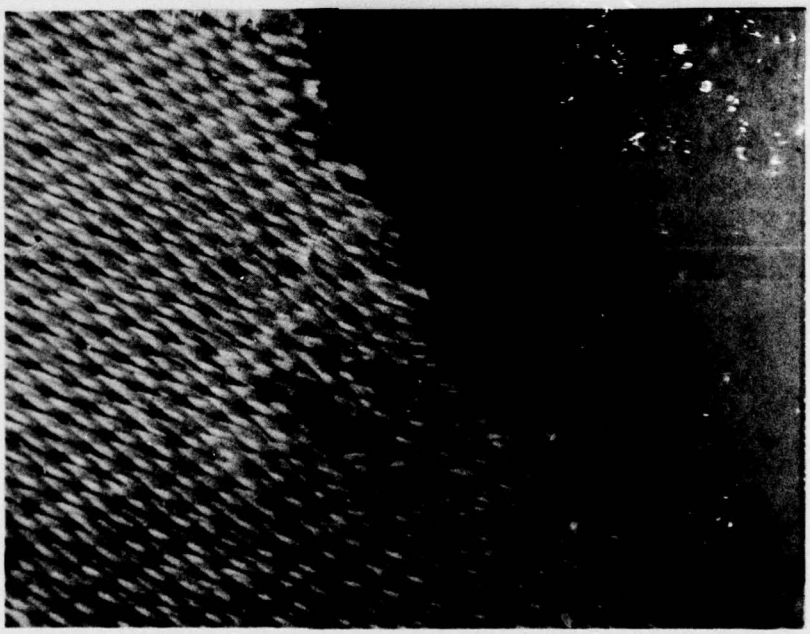

B.

FIGURE 66. THERMOCOUPLES INSERTED THROUGH INSULATION

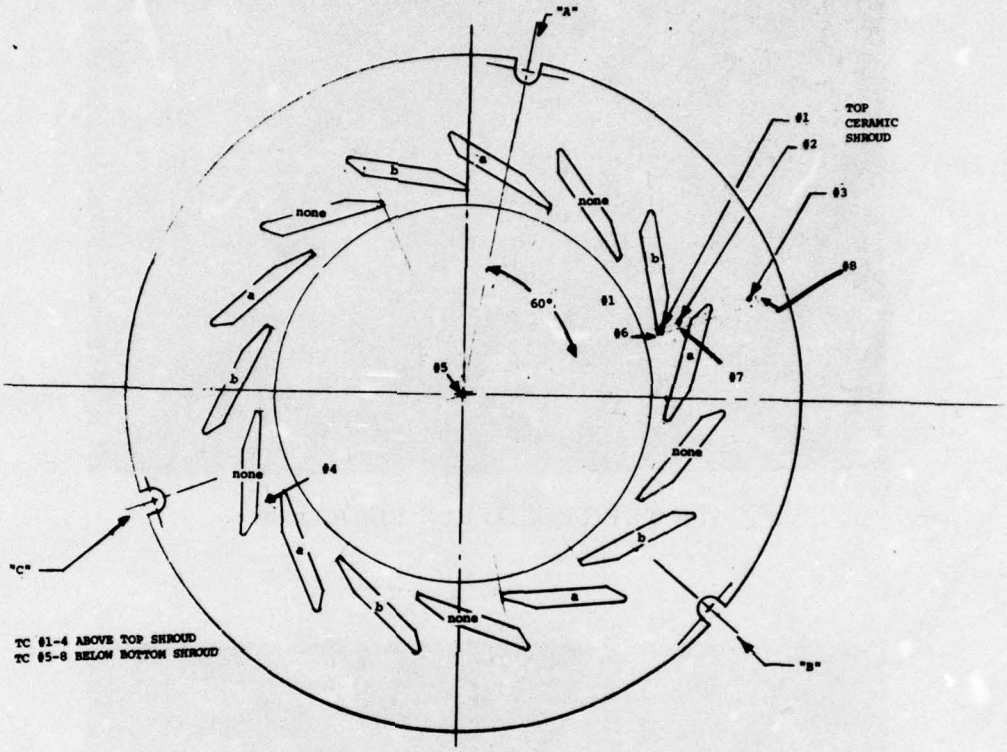

FIGURE 67. THERMOCOUPLE LOCATION AND GLASS JOINT FILLER MATERIAL LOCATION

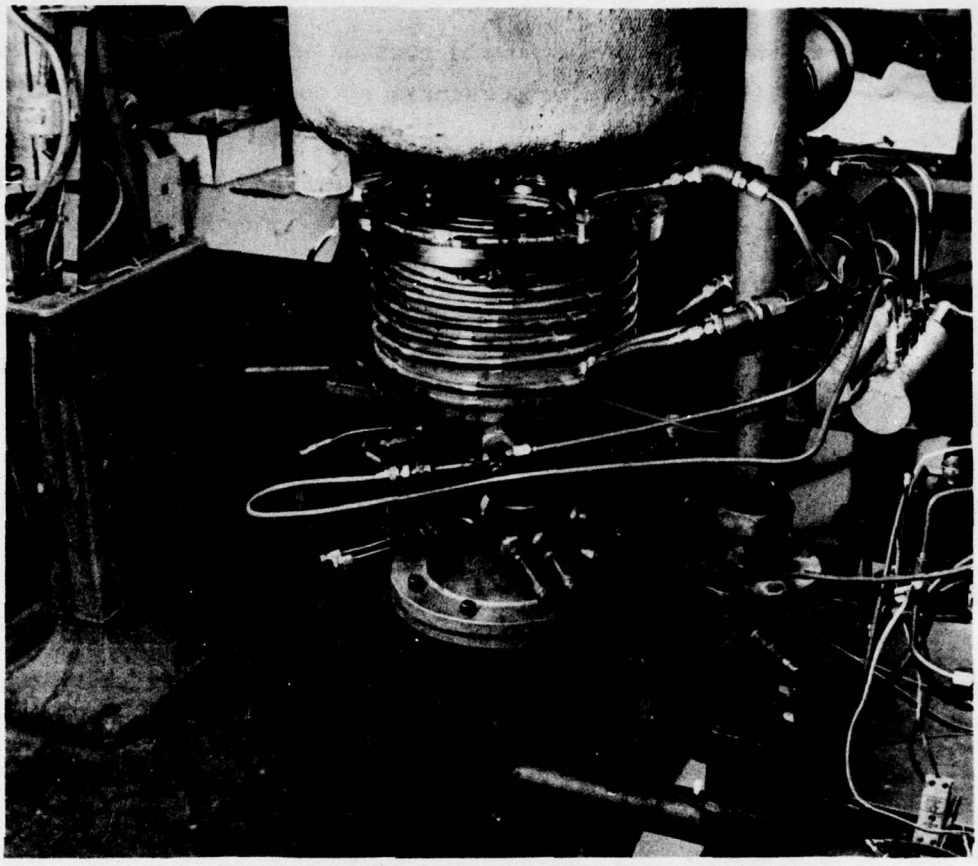

FIGURE 68. 10kW NOZZLE TEST RIG

3.2.8 Rig Test - Standard Nozzle Baseline

The rig test facility used for thermal cycling, dust erosion and corrosion testing of ceramic nozzles was calibrated using the standard 10kW nozzle configuration (Assembly #74-8005).

The test facility is pictured in Figure 68. Inlet air is heated to 538°C (1000°F) in the preheater with natural gas. The main combustor provides additional heat to bring combustion gasses to operating temperature and can be fired with either liquid fuel or natural gas. The rig experiments were conducted using natural gas in order to avoid low temperature flameout during thermal cycling.

The test chamber which holds the nozzle section was water cooled. This provides the facility for test temperatures up to or beyond 1400°C (2552°F). The position of the turbine nozzle in the test chamber is shown in Figure 69. The nozzle holder has been removed and turned such that the nozzle upstream side is seen.

Figure 70 shows the location of thermocouples at upstream, downstream and forward shroud positions. Figure 61 shows the position of thermocouples #1 and 2.

This rig test configuration closely simulates actual turbine temperature and gas flow conditions. The forward shroud is in proximity of a cooled metal plate which is the analog of the compressor shroud in actual engine installation and the rear shroud views and is immersed in hot combustion gases as it is in an actual engine installation. The major rig pressure drop is taken across the combustor nozzle. Table 10 lists temperatures, pressures, and flows observed for the test rig with the standard 10kW and ceramic vane section nozzles installed.

3.2.8.1 Thermal Shock

The thermal shock test cycle consists of a rapid up shock and slower cool down cycle designed to simulate the most severe thermal cycle condition which occurs for the 10kW on shutdown from full power with no load after shutdown as illustrated in Figure 71. (Thermocouple #95 is located at the same forward shroud position as thermocouples #1 and 2 in rig tests as shown in Figure 61. Temperature of the forward shroud at engine position 95 as indicated in Figure 71 undergoes an excursion of 300°C (540°F) at a maximum rate of 33°C/sec (60°F/sec).

Temperatures experienced during the rig test thermal shock cycle are shown in Figures 72A and 72B. The forward shroud temperature ramp rate and temperature excursion have been adjusted to closely match that experienced on engine shutdown, with the only difference being that an up-shock rather than down-shock is used.

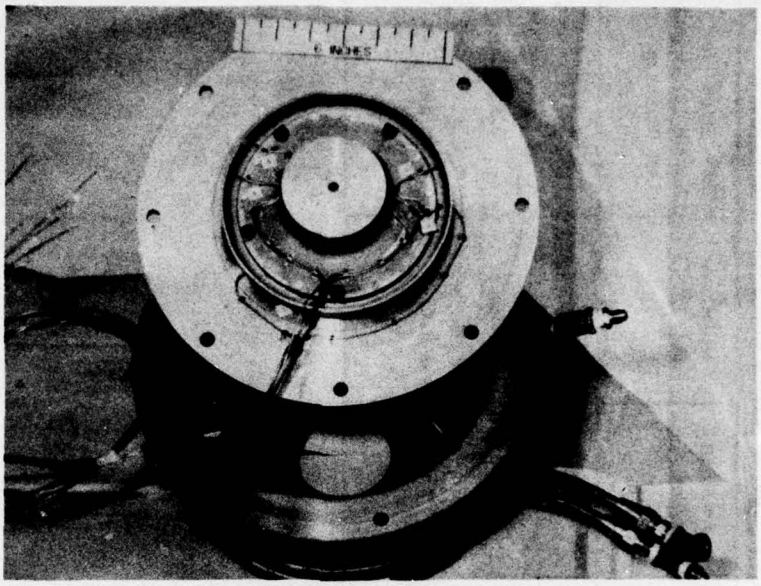

FIGURE 69. COOLED NOZZLE TEST CHAMBER WITH LID INVERTED TO SHOW UPSTREAM SECTION OF NOZZLE

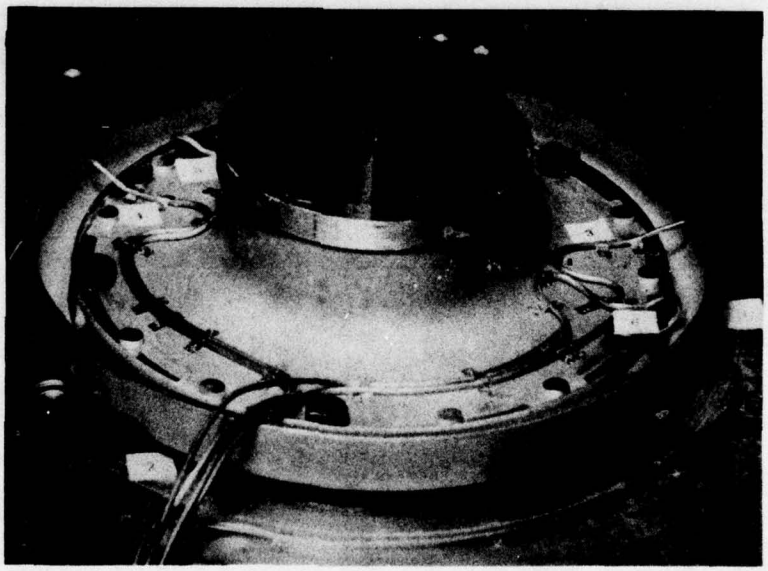

FIGURE 70. 10kW NOZZLE TEST RIG THERMOCOUPLE LOCATION

TABLE 10

TEST RIG FLOW CONDITIONS FOR STANDARD AND CERAMIC VANE NOZZLE TESTS

	Nozzle Upstream Flow		Nozzle Throat Conditions			
Test Condition	Total Pressure Psia	Total Gas Temperature °F	Mach Number	Gas Velocity Ft/Sec	Gas Density (Lb/ft^3)	Total Mass Flow + Nozzle Coefficient Of Discharge (Lb/Sec)
Thermal Shock High Fire	25.4	2500°F	0.919	2269	0.0157	0.173
Thermal Shock Low Fire	22.4	1160°F	0.80	1486	0.0276	0.1995
Dust Erosion or Hot Corrosion	22.9	1725°F	0.82	1768	0.0206	0.177

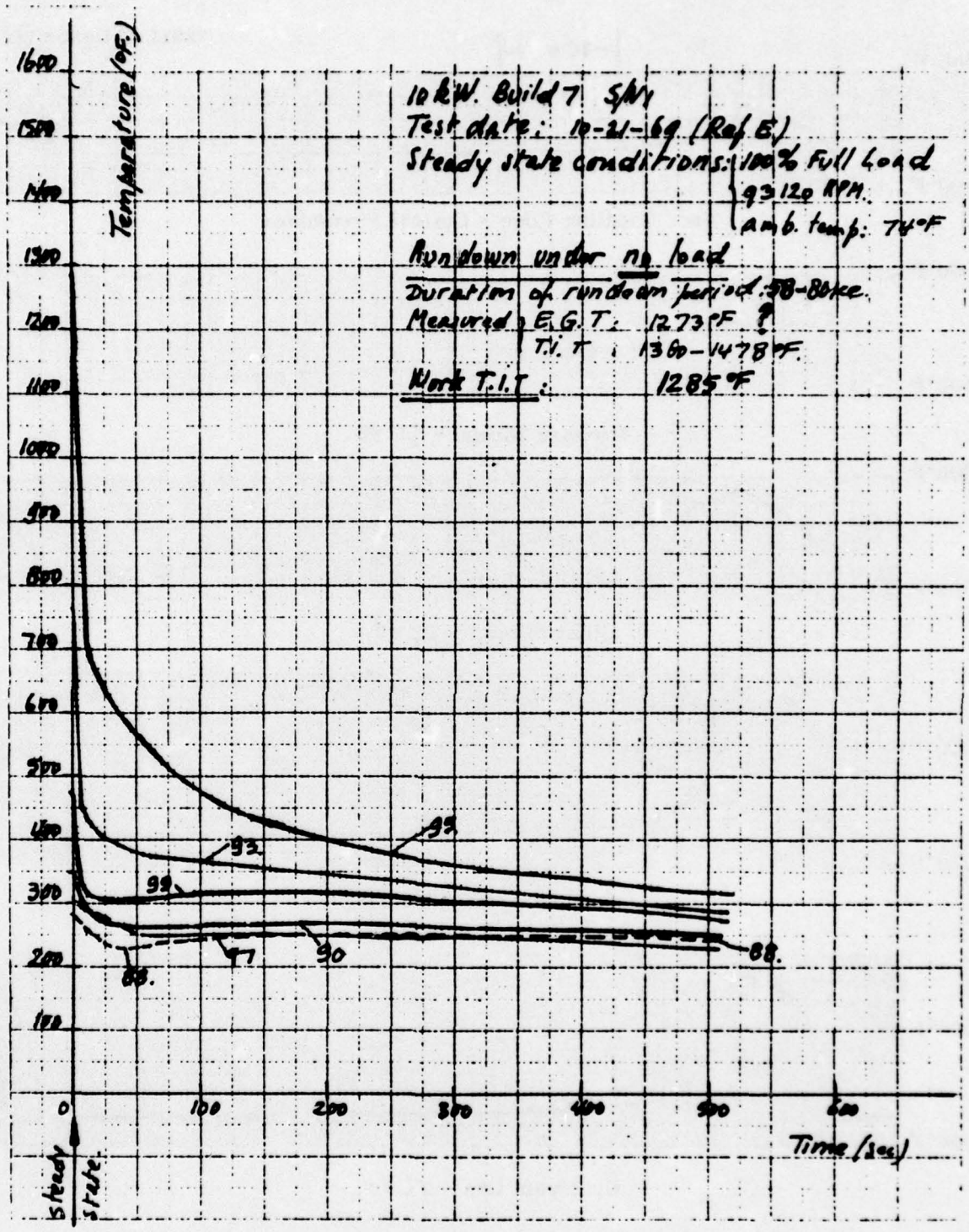

FIGURE 71. 10 kW SOAKBACK TEMPERATURES; Run Down Under No Load

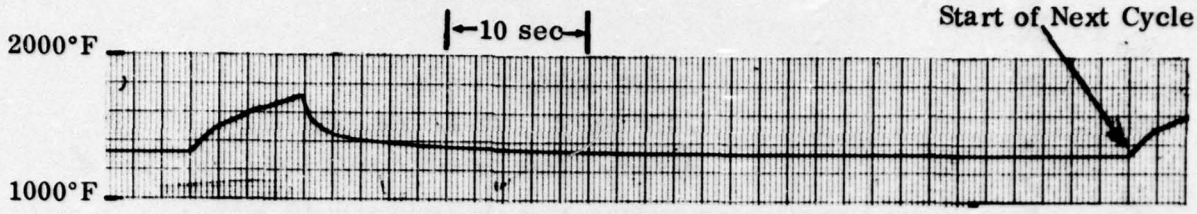

Vane Trailing Edge - Optical Pyrometer

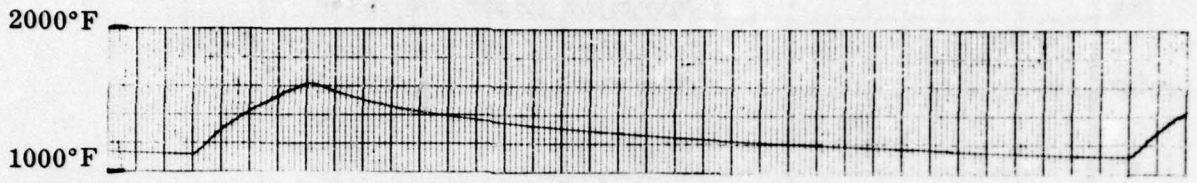

Forward Shroud - TC #2

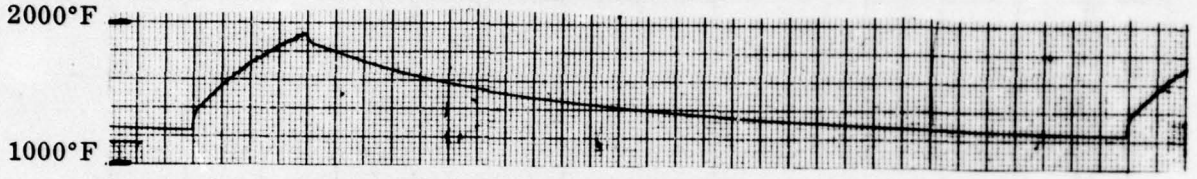

Rear Shroud - TC #7

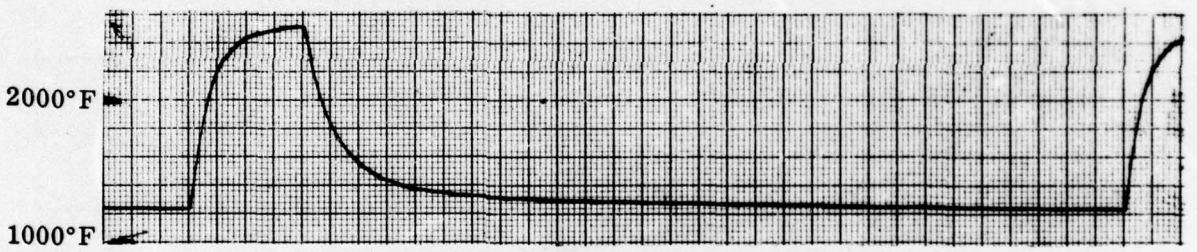

Upstream Gas - TC #3

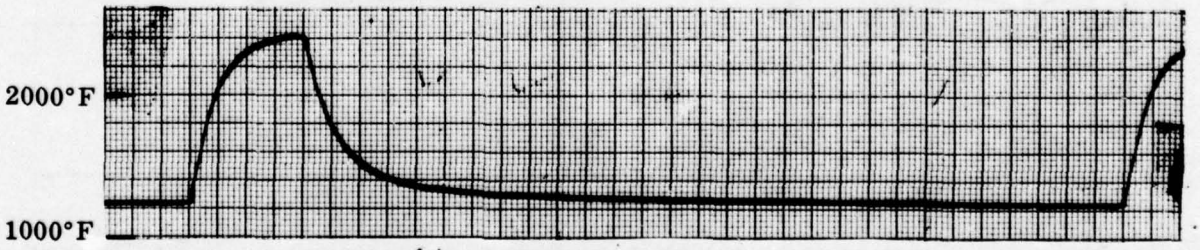

Upstream Gas - TC #4

A.

FIGURE 72. TIME TEMPERATURE PROFILES OF VARIOUS SHROUD LOCATIONS DURING THERMAL SHOCK CYCLE (Sheet 1 of 2)

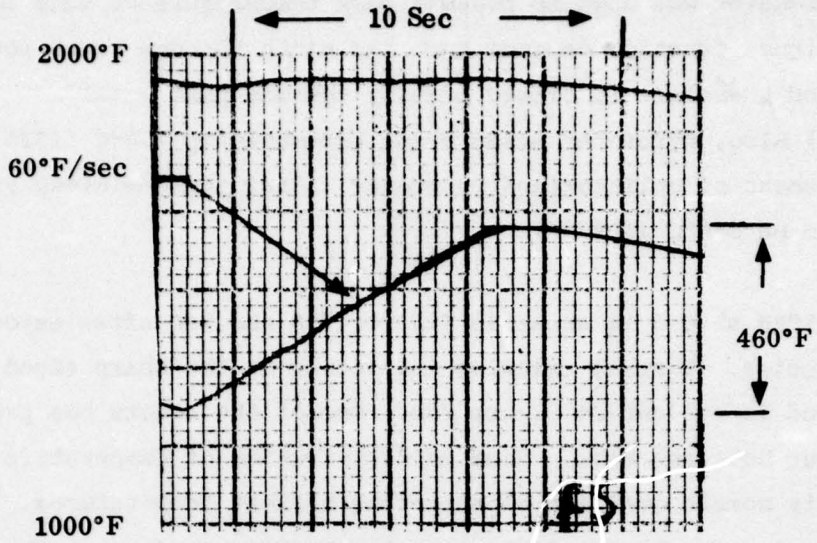

Forward Shroud TC #1

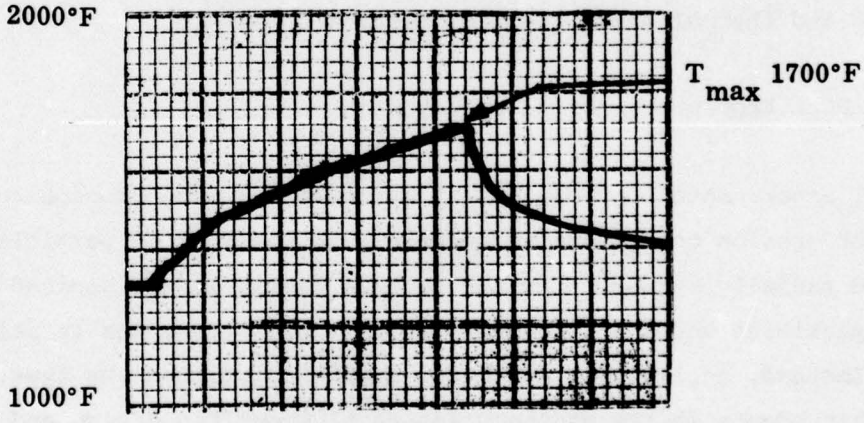

B.

Vane Trailing Edge
Optical Pyrometer

FIGURE 72. THERMAL UP-SHOCK OF FORWARD SHROUD AND VANE TRAILING EDGE (Sheet 2 of 2)

An optical pyrometer was used to measure peak temperature of vane trailing edge. (The signal function depends upon the ninth through tenth power of temperature and therefore is biased heavily towards peak metal temperatures.) Also, pyrometer measurement threshold is 716°C (1320°F). Direct measurement of unlinearized pyrometer signal shows minimum cycle vane temperature to be 588°C (1092°F).

The standard 10kW shroud is shown in Figures 73A and 73B after exposure to 500 thermal cycles. Thermal cracking initiating at the sharp edged lip of the rear shroud is evident in Figure 73B. One of the cracks has proceeded through a rivet hole and vane. Some maldistribution of temperature was noted with this nozzle quadrant experiencing highest temperatures. This location was reinstrumented and the time temperature profile at the shroud lip is shown in Figure 72A (TC #7). Since temperature here was approximately 93°C (200°F) higher than other sections monitored during the test, the thermal cracking can be attributed to overtemperature. The rig was modified to reduce this maldistribution to less than 38°C (100°F) during corrosion and thermal shock tests of ceramic nozzles.

3.2.8.2 Dust Erosion

Since all experimental and analytical evidence for vane erosion on the 10kW shows that erosion occurs due to secondary impingement of particles projected radially outward from the turbine wheel, it was decided that erosive particles would not be ingested in the upstream gas in initial rig tests. Instead, an impinger was devised which simulates the type of erosive attack that occurs in the engine. Figure 61 shows the design and arrangement of this device. A diverter jet of air redirects the particle accelerating stream so the hot gas nozzle flow would not be disturbed. The particles were Arizona Road dust and were classified such that they were in the size range of 43-74 microns. These particles are large enough that they are not redirected from their path toward the nozzle vane by the diverter air jet. The impinger outlet was located 4 cm (1.6 in.) from nozzle vane surface and particles impinged at a 60° angle from orthogonal to the vane.

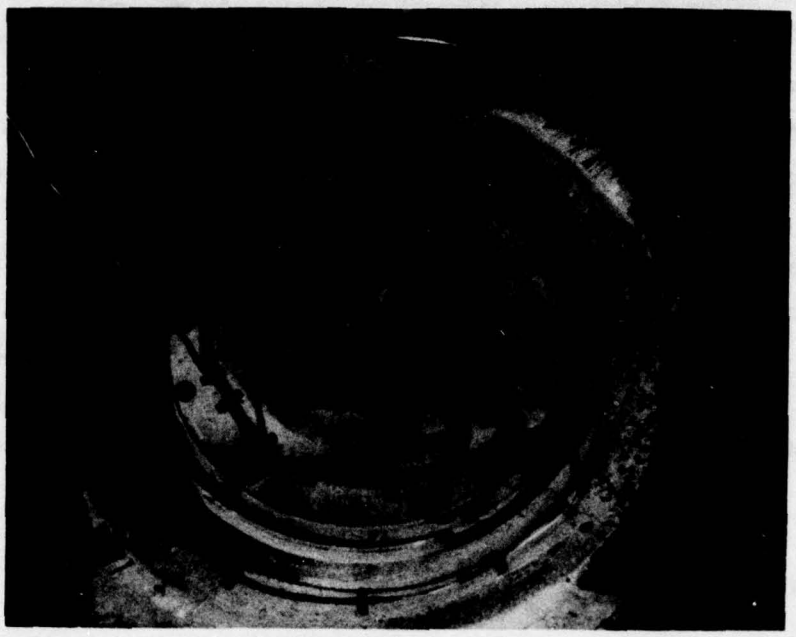

A.

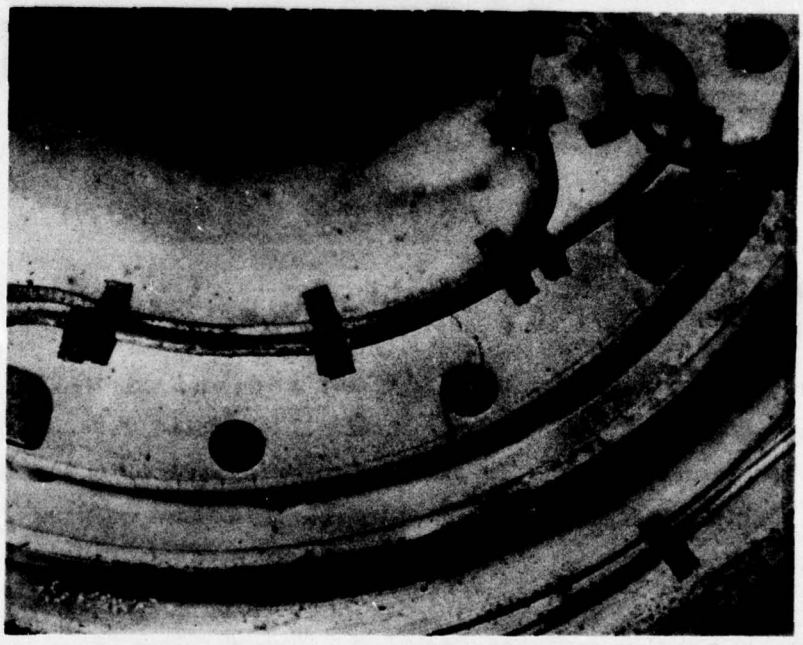

B.

FIGURE 73. STANDARD 10 kW NOZZLE AFTER 500 RIG TEST CYCLES

A ten hour test was run on the nozzle vane shown in Figure 74. The vane trailing edge temperature was monitored with an optical pyrometer and held at 927°C (1700°F). Dust concentration in the impinging gas stream was 0.0018 mg/cm^3 (50 mg/ft^3) with this stream flowing at 305 m/sec (1000 ft/sec). The particle velocity upon impinging the vane trailing edge falls in the range of 251-274 m/sec* (800-880 ft/sec) depending on particle size.

The vane trailing edge of the standard nozzle recessed 0.48 cm (0.19 in.) which corresponds to surface penetration of 0.14 cm (0.055 in.). The qualitative appearance of the vane erosion is very similar to vane erosion observed in actual engine tests. This technique of erosion is therefore a good qualitative analog to real conditions for determining erosion behavior of ceramics installed in the 10kW turbine.

3.2.8.3 Corrosion Tests

Corrosion testing of all test nozzles was done with three parts per million of artificially made sea salt per total stream mass flow. Salt constituents are given in Table 11. Vane trailing edges were monitored at 927°C (1700°F) with an optical pyrometer. These tests for standard and ceramic vane nozzles were run for 60 hours at which point significant surface attack occurred on 713LC shrouds.

3.2.9 Rig Test - Ceramic Vane Nozzle

3.2.9.1 Thermal Shock

Five hundred rig test thermal shock cycles, as described in the previous section, were applied to the ceramic superalloy nozzle assembly. Figure 75 shows vane location numbers 7, 8 and 14, which evidence no damage after the 500 cycles. This condition is typical of ceramic vane sections located in positions 1 through 14.

Figure 76 shows vane position #5 where the ceramic vane piece sustained a crack at the rear shroud trailing edge location. The lowest temperature

* These values were calculated using the method described in Appendix I of Reference 25.

a.

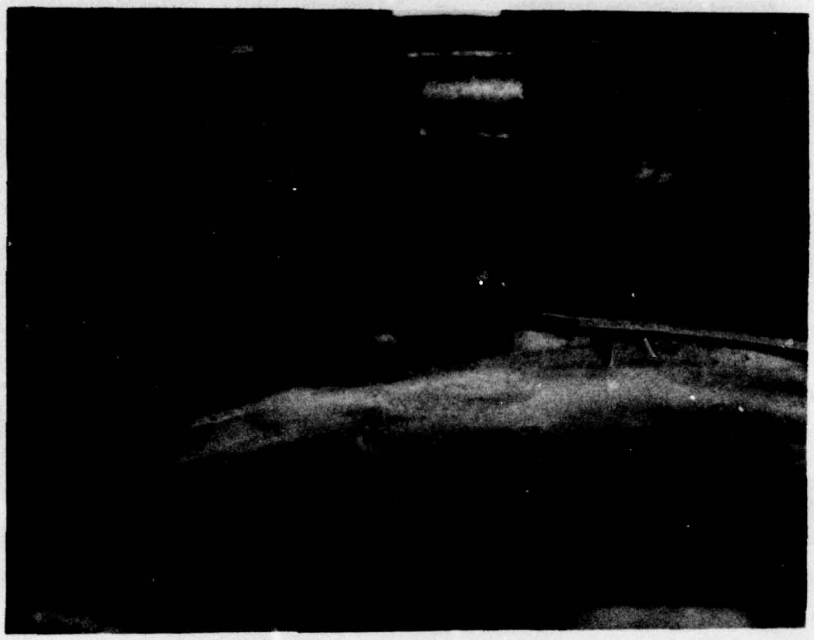

b.

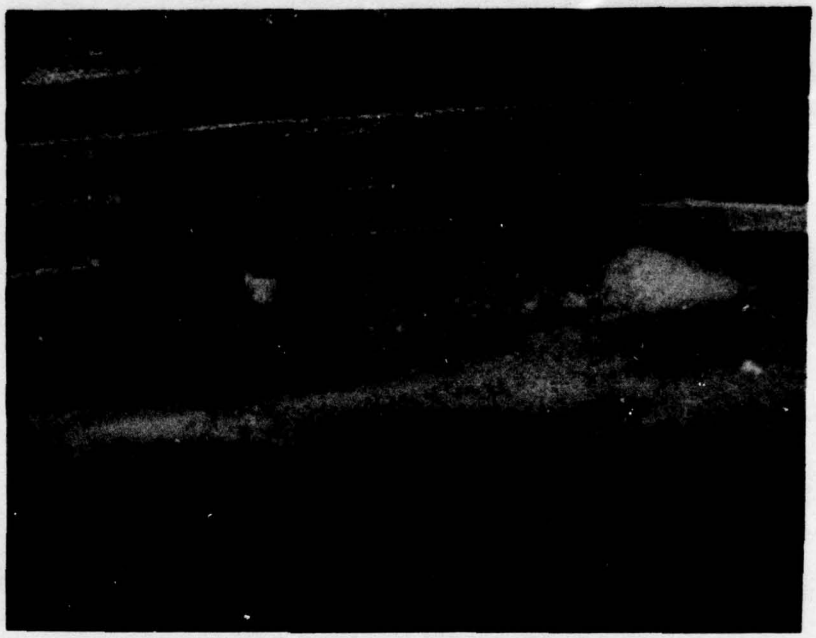

FIGURE 74. STANDARD 10 kW NOZZLE AFTER 10-HOUR RIG EROSION TEST

a.

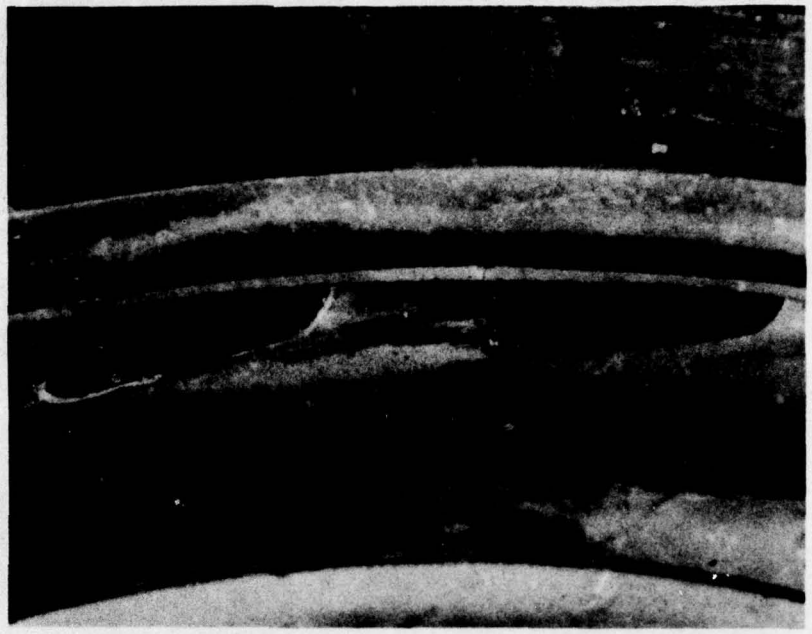

b.

FIGURE 75. CLOSE-UP VIEW OF NOZZLE VANE LOCATIONS (a) 7 AND 8, (b) 14, AFTER 500 RIG TEST THERMAL SHOCK CYCLES

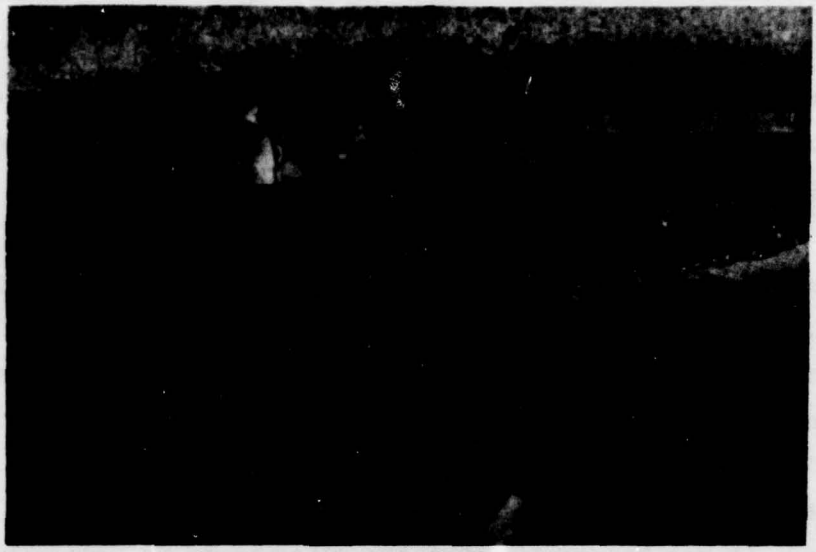

FIGURE 76. CLOSE-UP VIEW OF VANE LOCATION #5 AFTER 500 RIG TEST THERMAL SHOCK CYCLES

TABLE 11

CONSTITUENTS OF ARTIFICIAL SEA SALT

Constituent	NaCl	$MgCl_2$	Na_2SO_4	$CaCl_2$	KBr	KCl
PPM per total Gas Flow	2.04	0.455	0.310	0.099	0.080	0.018

glass (40% B402, 20% GN19, 40% Cr_2O_3) which has a nominal 927°C (1700°F) firing temperature, was applied to this vane. No flaws or defects were evident in the hot pressed silicon nitride vane insert from Zyglo inspection done prior to the test.

The failure initiates at the contact point between the vane trailing edge and the lip of the shroud recess, and appears to be due to longitudinal compressive forces. Static aerodynamic forces which tend to force the vane downstream only impose a 650 psi compressive stress at this region assuming that the load is evenly distributed at the contact area. Since peak thermal cycling temperature of the vane is 927°C (1700°F), the same the glass firing temperature, it can be assumed that the glass would not distribute stresses at this temperature because of low viscosity. It is believed that this low temperature glass promoted a higher stress condition than would occur with an unbonded vane. At peak temperature the vane would be expected to slide up against the trailing edge of the shroud recess. When a cool down cycle occurs the glass would begin to harden and the superalloy shroud would shrink relative to the ceramic vane. (Viscosity will change by approximately one order to magnitude per 84°C (120°F) for these glasses. Therefore, cooling from 927°C to 593°C (1700°F to 1100°F) will result in approximately a 100,000 times increase in glass viscosity.) It is believed that shear resistance of the glass at lower temperature tended to support compressive differential thermal loads on the trailing edge which resulted in this failure.

Only one of the four vanes using this low temperature glass has failed at this stage of testing. This probably reflects the statistical nature of failure of ceramics. Subsequent disassembly of this nozzle showed no other probable cause for this failure.

Figures 77A and 77B show the rear shroud section of the bimaterial test nozzle after 500 thermal cycles. The general condition of the nozzle is good except that each of the bolt or rivet holes has a thermal crack propagated from the shroud outer lip as shown typically in Figure 77B.

a.

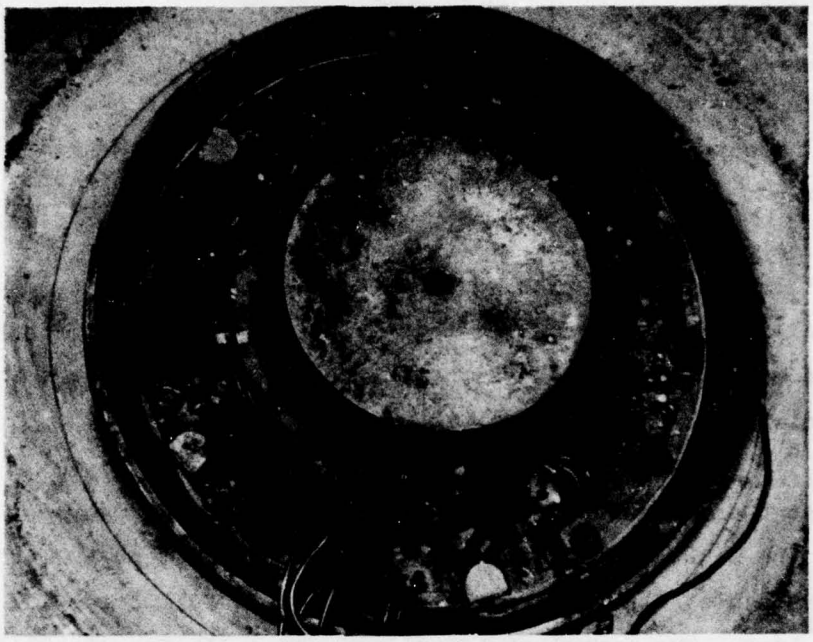

b.

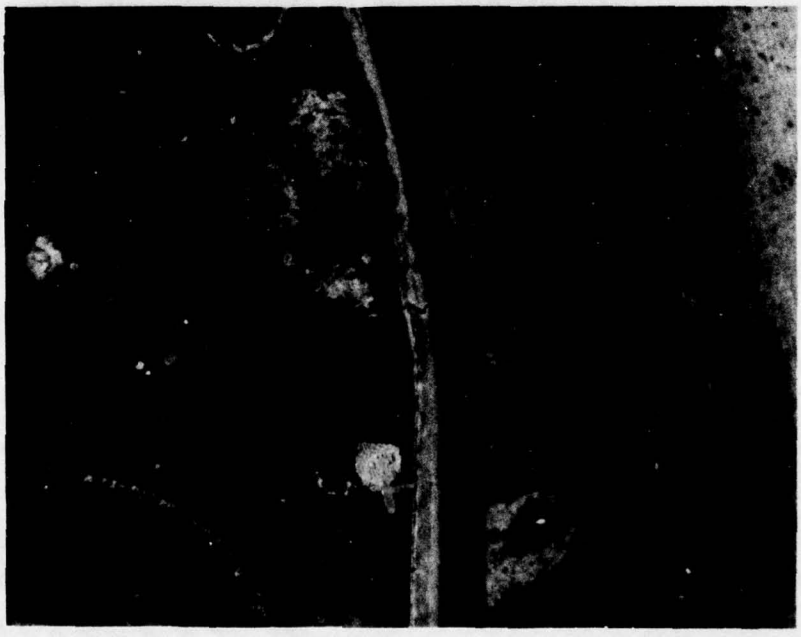

FIGURE 77. REAR SHROUD OF BI-MATERIAL NOZZLE AFTER 500 RIG TEST THERMAL SHOCK CYCLES SHOWING THERMAL CRACKING AT HOLES

Thermal cracking is also observed on the lip section of the forward shroud (see Figs. 75 and 76) at each of the vane trailing edge sections. These cracks are arrested at the change of section and do not continue into the forward shroud.

The thermal damage to the rear shroud attests to the severity of the rig test thermal shock sequence since this type of damage has not been encountered on any of the 10kW turboalternator engine packages that have been operational.

The rig test thermal shock sequence as described in the previous section duplicates the highest temperature ramp rates observed in the 10kW turbine operating sequence, i.e., emergency shutdown from full load with no alternator load. The normal shutdown sequence calls for stabilization of engine temperature at a no load condition and then rundown under no load. The "working" turbine inlet temperature in this latter case is only 492°C (920°F) as opposed to 732°C (1350°F) for an emergency shutdown. The result is a rig test sequence that exposes the nozzle to a more severe thermal shock than would normally occur on engine shutdown. Therefore, more thermal damage to ceramic vanes would be expected to result from the 500 rig test thermal shocks than would occur in engine installation.

3.2.9.2 Dust Erosion

The HPSi$_3$N$_4$ vane section corresponding to nozzle vane location #1 was exposed to 10 hours of dust erosion with vane temperature controlled by pyrometry to 927°C (1700°F). Details of the test are the same as given in Section 3.2.8.2.

During the first hour of test, a section of the nozzle rear shroud adjacent to vane #13 melted (see Fig. 78). This was the result of an error in control temperature and a high pattern factor caused by the dust impinger which aspirates combustion gasses preferentially from nozzle passages surrounding vane location #13. A 1122°C (2050°F) to 1149°C (2100°F)

FIGURE 78. MELTED SECTION OF REAR SHROUD IN THE VICINITY OF VANE LOCATION #13. (Photo Taken After Completion of Dust Erosion and Corrosion Tests.)

upstream gas temperature is necessary to maintain the downstream vane subjected to erosion at 927°C (1700°F). A pyrometer control error of approximately 65°C (150°F) and temperature maldistribution was enough to result in rear shroud temperature above the 1260-1286°C (2300-2350°F) melting temperature of 713 LC Superalloy. The ceramic vane at this location (#13) moved approximately 1/4 in. downstream which resulted in fracture of the vane trailing edge. This vane failure has no bearing upon the survivability of ceramic vanes in the 10kW engine.

The nozzle was not damaged to the extent that it could not be tested as scheduled. The pyrometer error was corrected and the nine additional hours of dust erosion were completed. Figures 79A and 79B show the vane at location #1 after the 10-hour erosion test. Microscopic examination of the trailing edge shows 0.005 in. maximum erosion at the vane trailing edge and 0.0035 in. of erosion at ceramic vane midpoint 0.19 in. from the trailing edge. This location is comparable to the location on the standard 10kW nozzle which suffered 0.055 in. erosion in the same test sequence. This

a

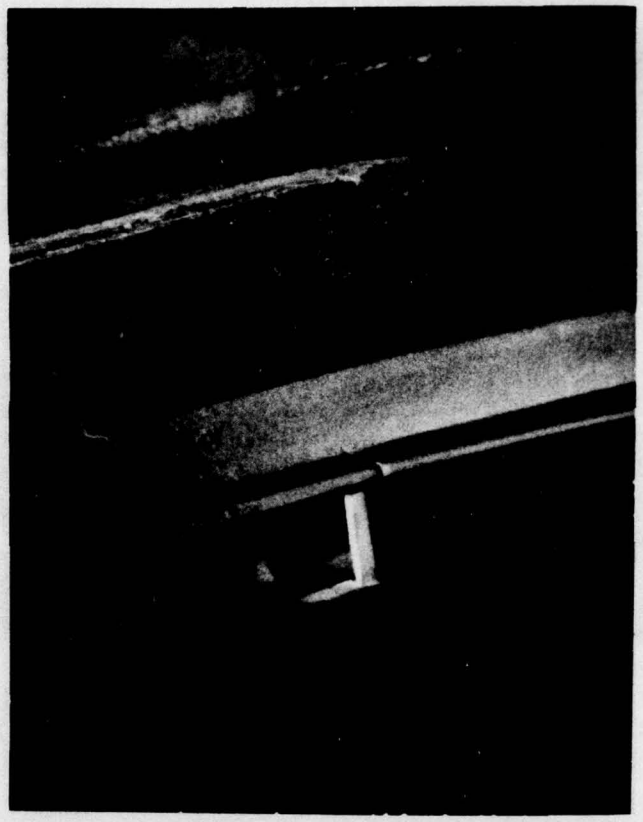

b

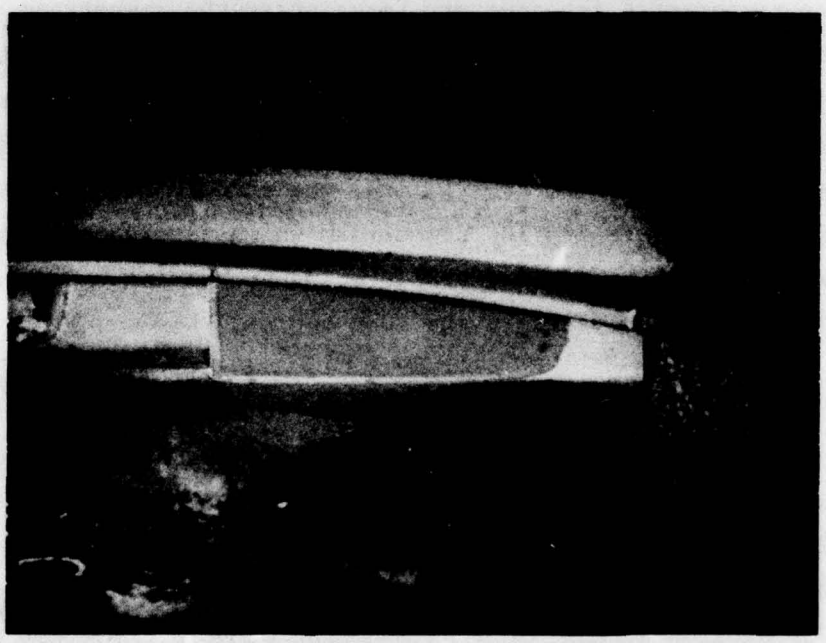

FIGURE 79. $HPSi_3N_4$ VANE SECTION AFTER 10 HOURS OF RIG TEST DUST EROSION AT 1700°F

implies a 16:1 erosion advantage for $HPSi_3N_4$ over 713LC at 927°C (1700°F) and 60° impingement angle. Examination of nozzles eroded in engine tests suggests that erosive particle impingement angle is less than 60° and approaches a more oblique angle of 30°. Ambient temperature tests show an erosion ratio comparison of 60:1 for these materials at 30°. Therefore it can be assumed that the 16:1 erosion ratio measured here is conservative. Values of 60:1 might be expected in actual engine test.

3.2.9.3 Corrosion Test

A 60 hour rig corrosion test at 927°C (1700°F) vane temperature with 3 ppm of artificial sea salt was completed after erosion testing. Figures 80A and 80B show vane 7 and 8 after this exposure. The details of the test are the same as those outlined in Section 3.2.8.3 The $HPSi_3N_4$ vanes show no evidence of corrosion attack. The superalloy shrouds do show evidence of corrosive activity as seen in Figures 81A and 81B.

3.2.10 Rig Test - All Ceramic Nozzle

The sequence of thermal shock, erosion and corrosion testing of the all ceramic nozzle was modified such that thermal shock exposure would be last. In the event that shrouds were to fail in thermal shock the results from erosion and corrosion tests would be obtained. In addition, the thermal shock test was run in four 125 cycle increments of increasing severity in order to obtain more quantitative information in the event of thermal shock failure.

3.2.10.1 Dust Erosion Test

Arizona road dust in the 43-74 micron size range was injected upstream to the nozzle during 1093°C (2000°F) rig testing. Total dust flow through the nozzle during a five hour erosion run was 557 gm. Average particle velocity upon impact with vanes has been estimated to be 600 fps. Nozzle exit gas velocity in this test is approximately 1800 fps.

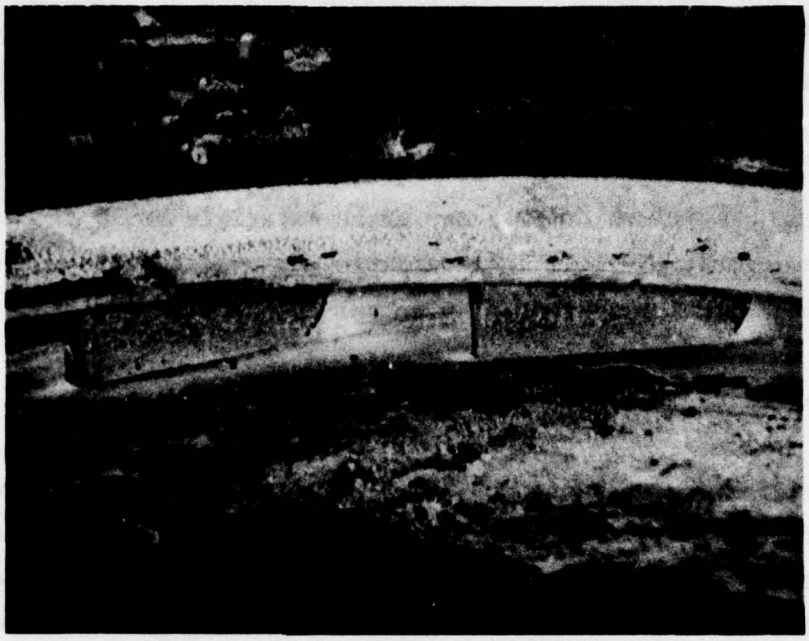

A.

FIGURE 80a. VANE LOCATIONS 8 AND 7 AFTER 60 HOURS, 3 PPM SEA SALT, 1700°F CORROSION TEST

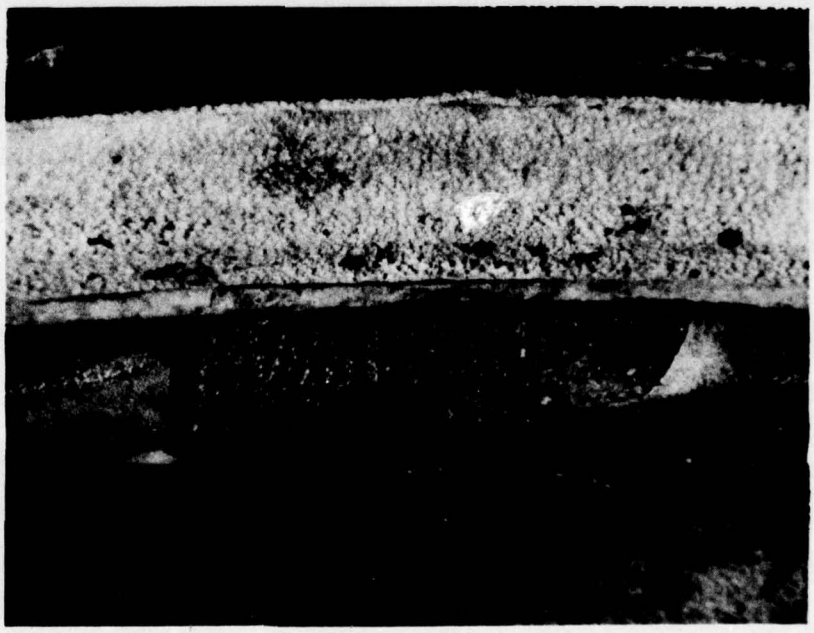

B.

FIGURE 80b. CLOSE-UP VIEW OF VANE LOCATION #7, AFTER CORROSION TEST

a

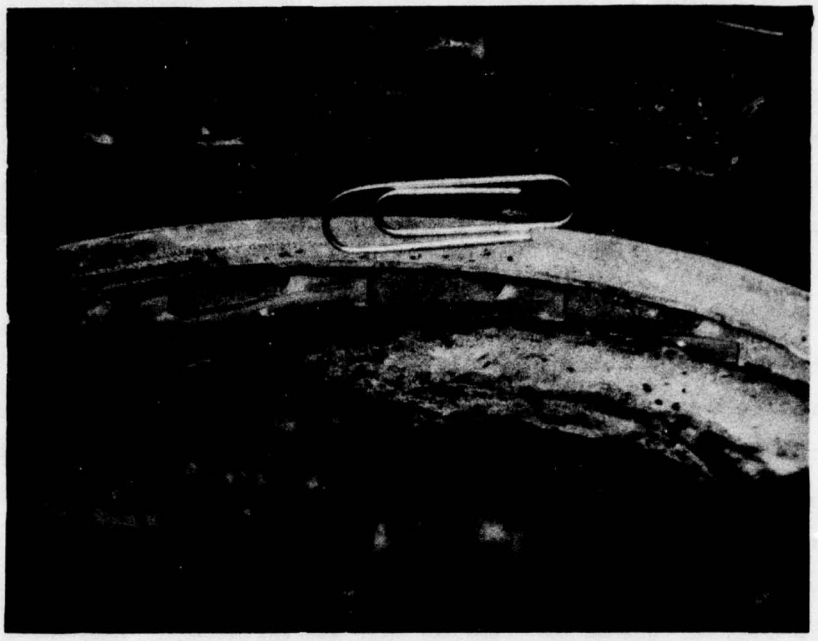

FIGURE 81a. DOWNSTREAM SIDE OF NOZZLE AFTER RIG CORROSION TEST (Vanes Shown are from Left to Right #9, 8, 7, 6 & 5)

b

FIGURE 81b. UPSTREAM SIDE ON NOZZLE AFTER RIG CORROSION TEST

Figures 82 through 84 show the nozzle after this test. Erosion of vanes was not measurable. The shrouds exhibited slight rounding of edges on inboard side of vane holding recesses. The shrouds might be expected to exhibit more erosion, except that dust particles impinge on the shrouds with a very shallow angle of incidence and as a result cause very little material removal.

The erosion experiment was stopped after five hours due to the failure of the dust feed system. In light of the time delay and expense required to continue this test, it was terminated at this point. Since erosion is expected to continue at a linear rate with time, results can therefore be scaled. The five hour exposure yields the same conclusions concerning erosion as would be reached by continuing testing for the prescribed 10 hours, i.e., neither vanes or shrouds are significantly eroded by dust injection.

3.2.10.2 Corrosion Test

After erosion testing, the all ceramic nozzle was exposed to 70 hours of 3 ppm artificial sea salt corrosion (see Table 11 for constituents and concentration). The nozzle is shown after test in Figures 85 and 86. Molten deposits formed on most of the nozzle surfaces.

A crack developed at locating pin 'B' during test and propagated towards the center of the upstream shroud. It is shown in Figures 87 and 88. Other cracks occurred at locating pin 'A' (see Fig. 89) but did not propagate beyond the pin region. It appears that the cracks resulted from localized thermal stresses since the pins run relatively cool because of direct mounting to the water cooled stainless steel plate. The refrasil insulation wafers between the holding pin head and lower shroud were found to be impregnated with molten products at locations 'A' and 'B'. The insulating wafer at location 'C' was relatively free of molten materials. Since location 'C' on the lower shroud showed no cracking it seems probable that the short circuiting of the thermal insulation at location 'A' and 'B' was

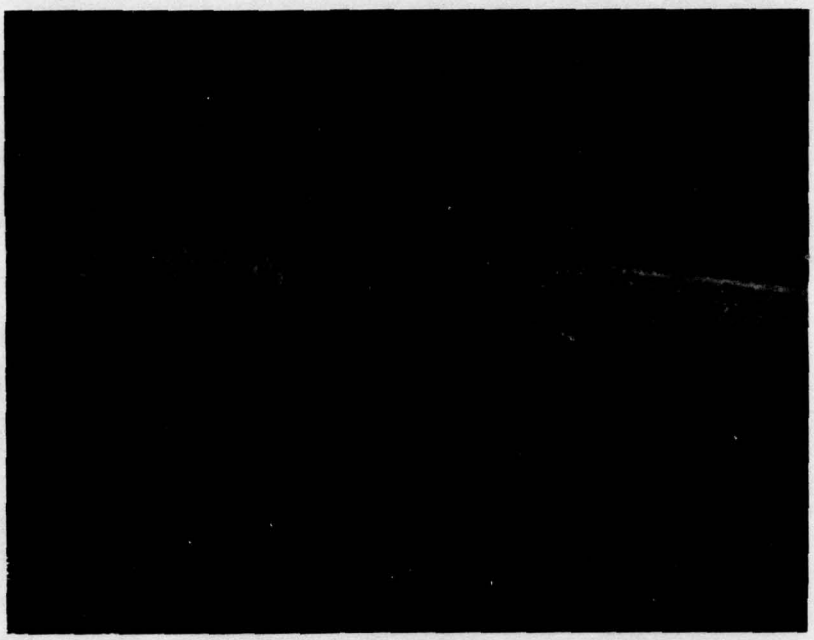

FIGURE 82a. VANES 5 & 6 AFTER 5 HOUR DUST EROSION TEST

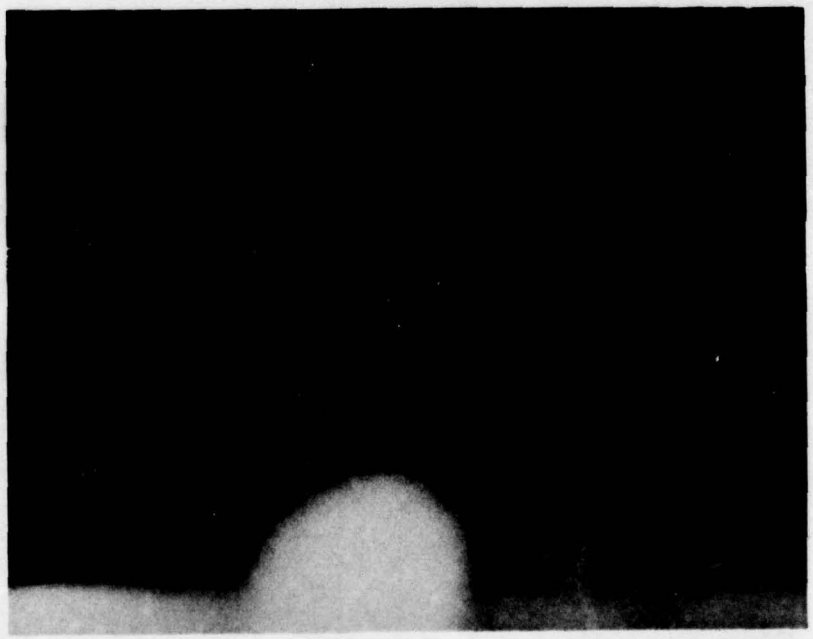

FIGURE 82b. VANES 1, 2 & 3 AFTER EROSION TEST

FIGURE 83a. VANES 4,5 & 6 AFTER EROSION TEST

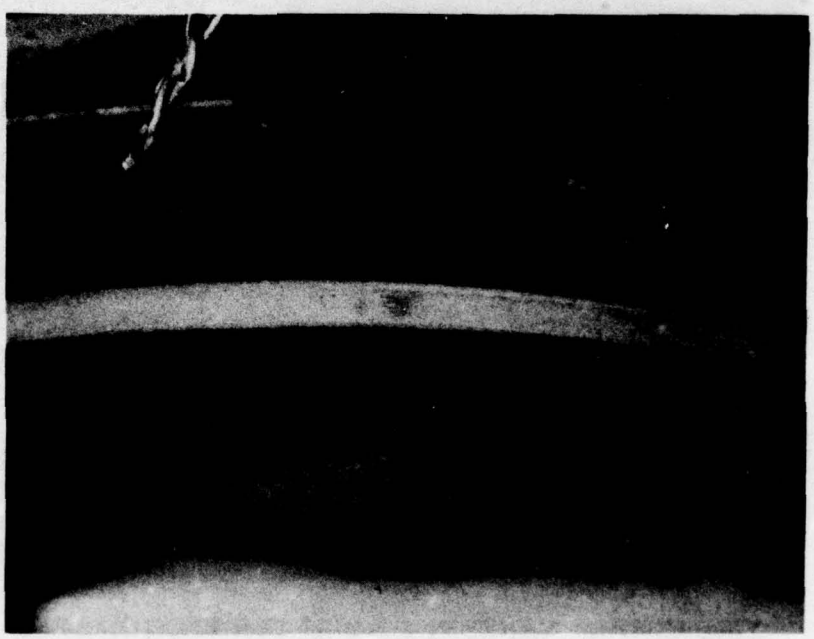

FIGURE 83b. VANES 7,8 & 9 AFTER EROSION TEST

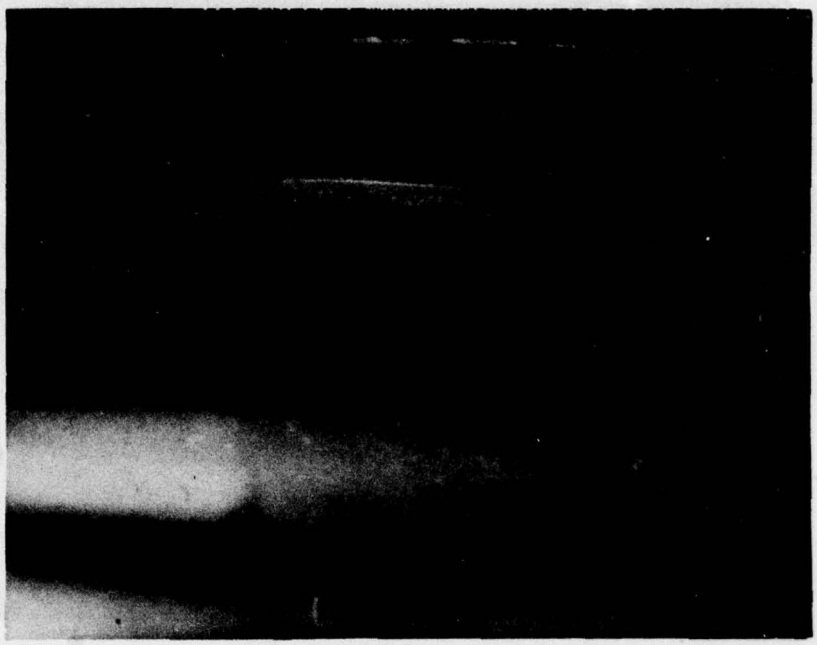

FIGURE 84a. VANES 10,11 & 12 AFTER EROSION TEST

(Surface Irregularity Due to Molten Arizona Road Dust)

FIGURE 84b. VANES 13,14 & 15 AFTER EROSION TEST

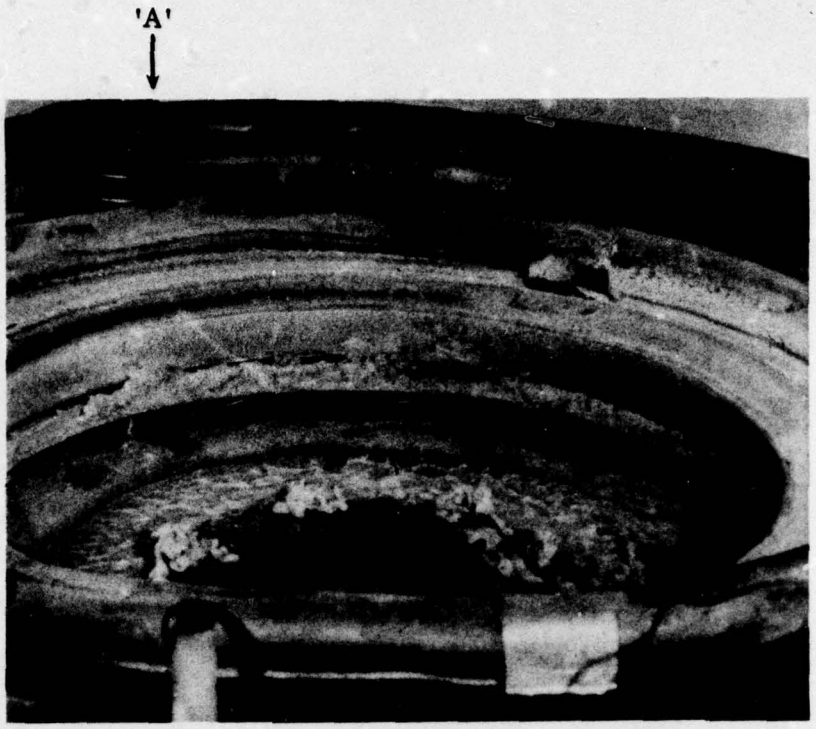

FIGURE 85a. CERAMIC NOZZLE AFTER 70 HOURS 3 PPM SEA SALT CORROSION TEST. (Nozzle Locating Spring Pin 'A' is Shown in Top Left of Picture)

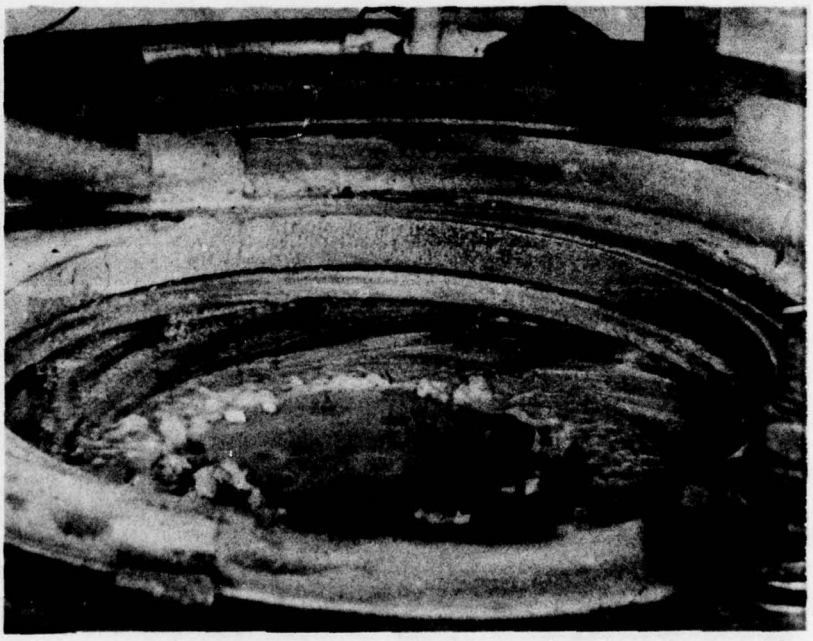

FIGURE 85b. SECOND VIEW OF NOZZLE (Spring 'A' is Shown in Bottom Right of Picture)

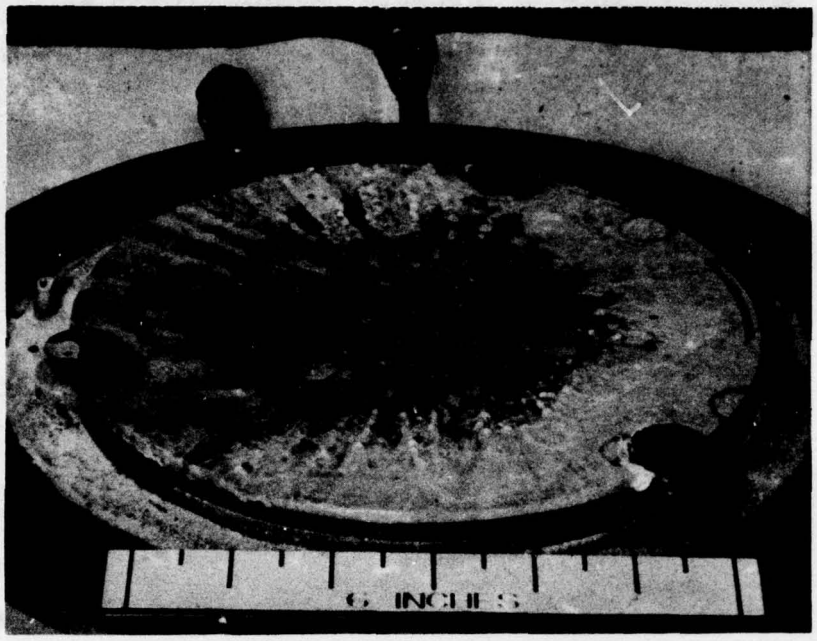

FIGURE 86a. UPSTREAM VIEW OF CERAMIC NOZZLE AFTER CORROSION TEST
(Pin 'A' At Bottom Right, Pin 'B' At Left Center)

FIGURE 86b. CRACK ORIGINATING AT HOLDING PIN 'B'
(Dye Penetrant Applied for Visibility)

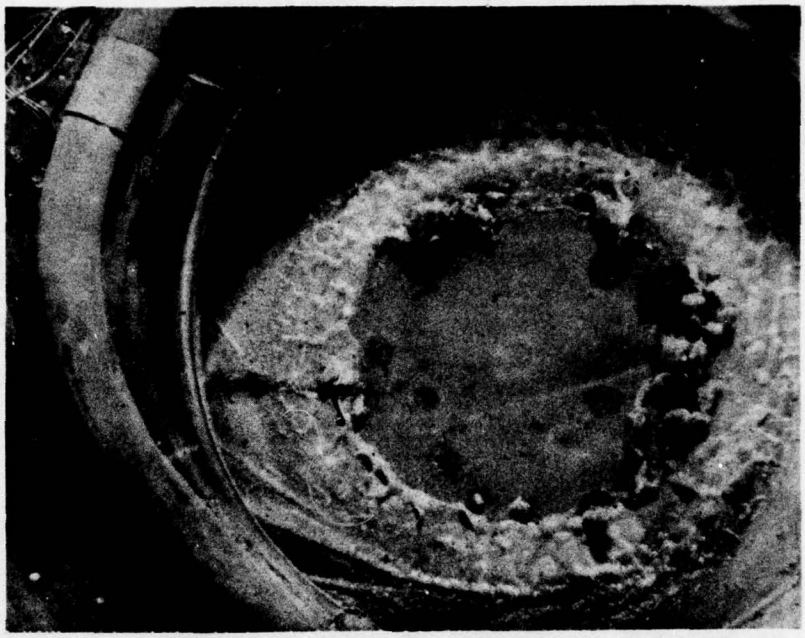

FIGURE 87a. VIEW OF CRACK FROM DOWNSTREAM SIDE OF CERAMIC NOZZLE

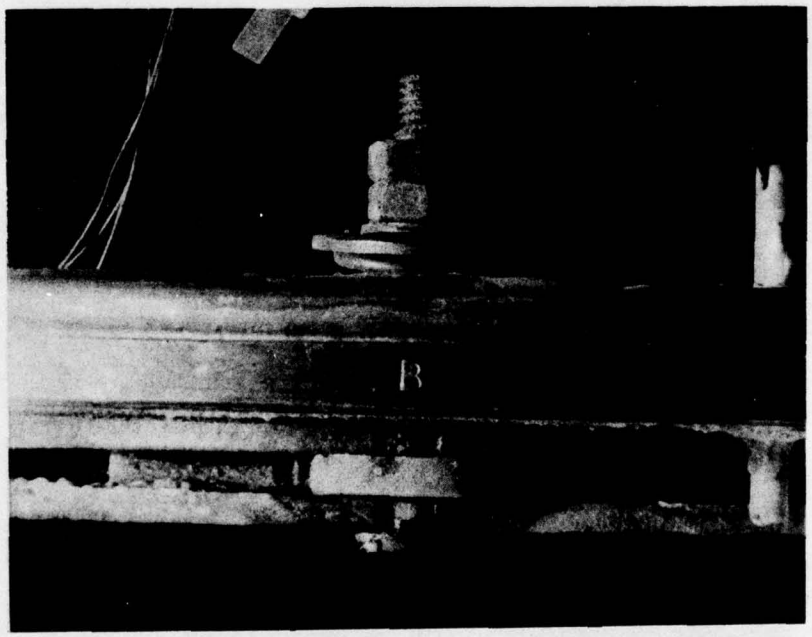

FIGURE 87b. CRACK ORIGIN

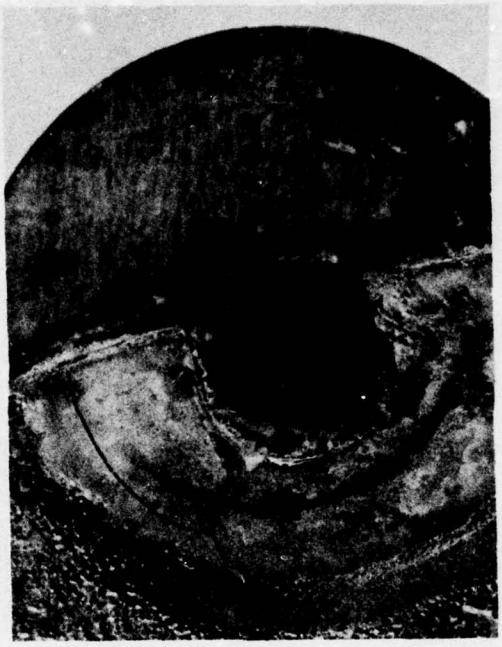

FIGURE 88. THERMAL CRACK IN BOTTOM CERAMIC SHROUD AT HOLDING PIN "B"

A

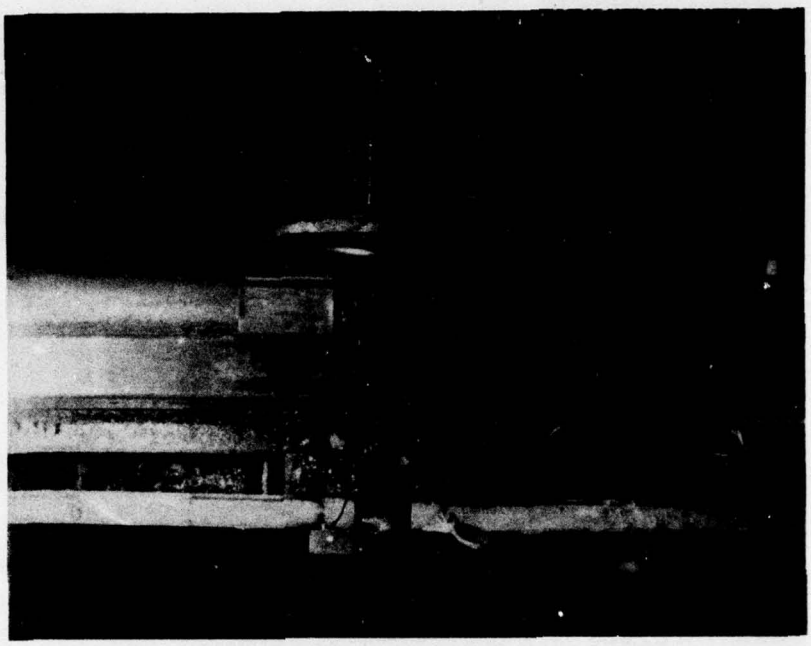

C

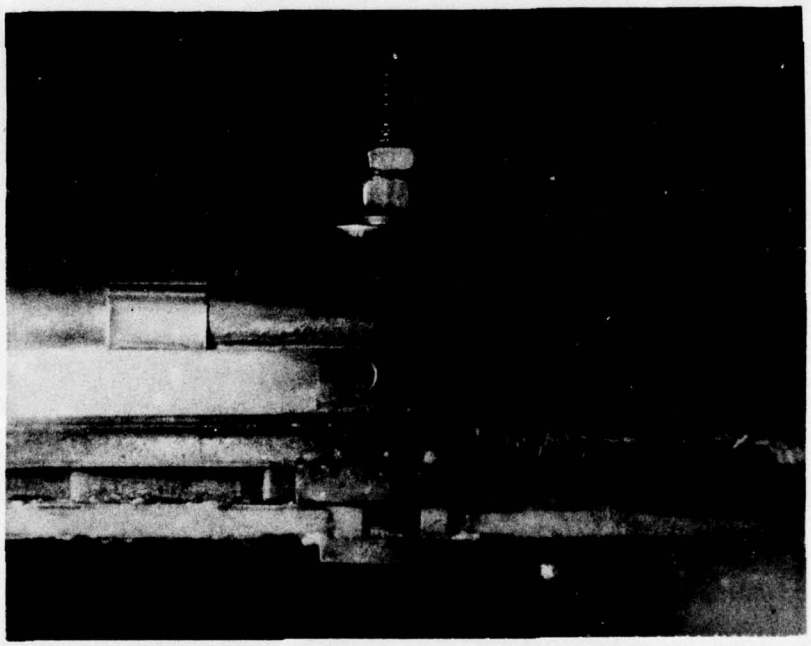

FIGURE 89. PIN LOCATIONS 'A' AND 'C' AFTER CORROSION TEST

the primary cause of high thermal stresses and shroud cracking. The appearance of the crack (shown in Fig. 88) as it follows the circumference of the pin head strongly supports this conclusion.

Some attack of vanes (approximately 0.010 in. penetration) was observed on inboard surfaces after corrosion testing. Since the products deposited in these areas were not soluble in water it appears that constituents of artificial sea salt combined with residual molten Arizona road dust from 1093°C (2000°F) erosion testing reacted with vanes. Localized attack of shrouds to approximately a 0.015 in. depth occurred near the holding pin heads. The deposits found here were soluble in water. This region of the nozzle would be expected to run cooler which suggests that this attack occurred because of the presence of sea salt constituents.

A steady state temperature map of the nozzle obtained by pyrometry during the erosion and corrosion tests is available. Time-temperature traces of thermocouple measurements at various locations of both upstream and downstream shrouds are also available for these test sequences.

3.2.11 THERMAL SHOCK

The thermal shock sequence was run in four 125 cycle sets of increasing severity and checked for damage or cracks after each set. Temperature transient rate was controlled to 8, 17, 25 and 33°C/sec (15, 30, 45 and 60°F/sec) at thermocouple locations 1 and 2 which correspond to location #95 in the 10kW engine transient trace shown in Figure 71. Maximum cycle temperature was 1093°C (2000°F) at vane trailing edge as monitored with an optical pyrometer. Figures 90 and 91 show temperature time traces for the least severe (15°F/sec) and most severe (60°F/sec) thermal cycles. Table 12 gives gas flow conditions for these thermal shock tests.

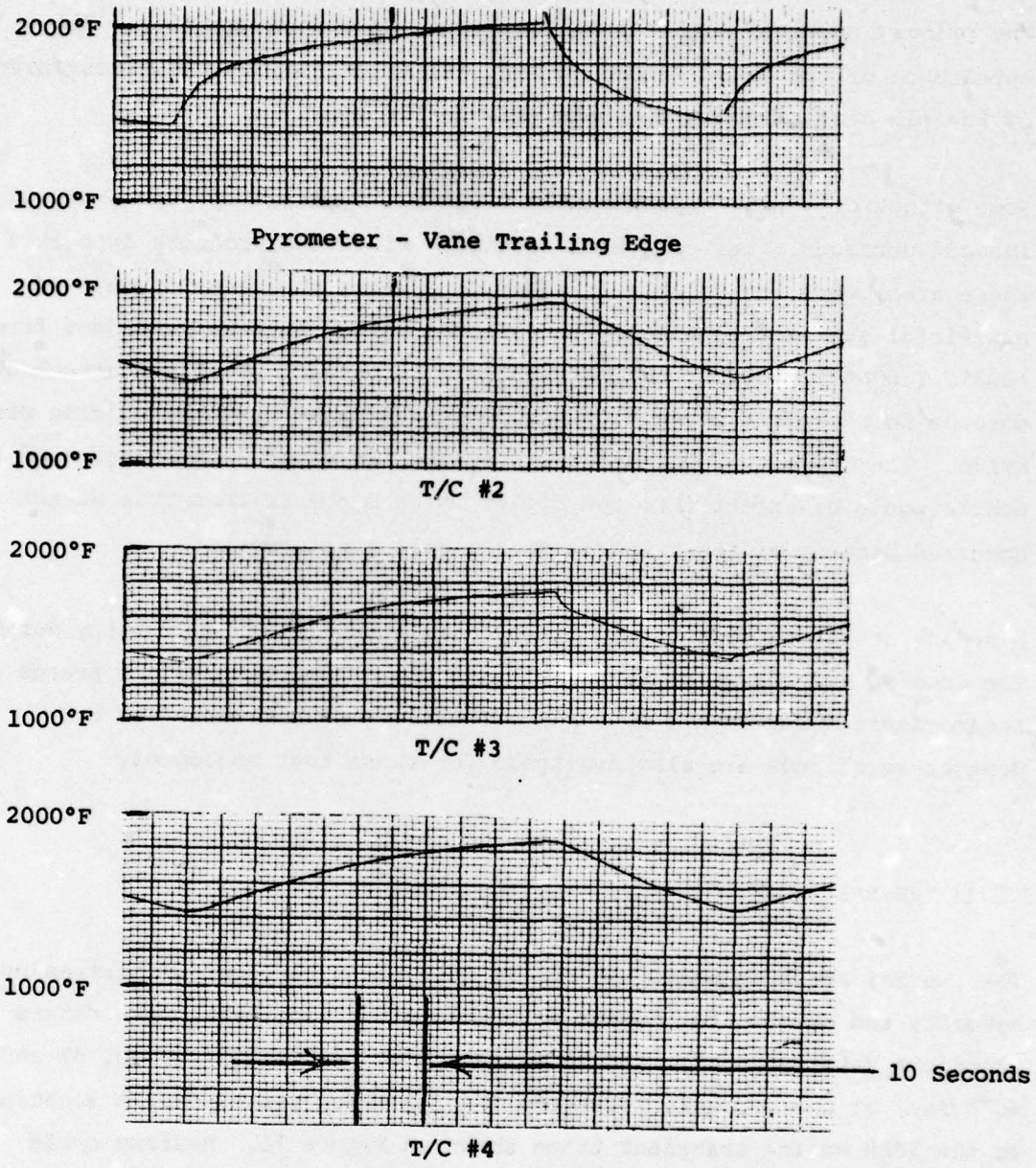

FIGURE 90a. THERMAL SHOCK CYCLE - 15°F/SEC. AT T/C #2 - ALL CERAMIC NOZZLE

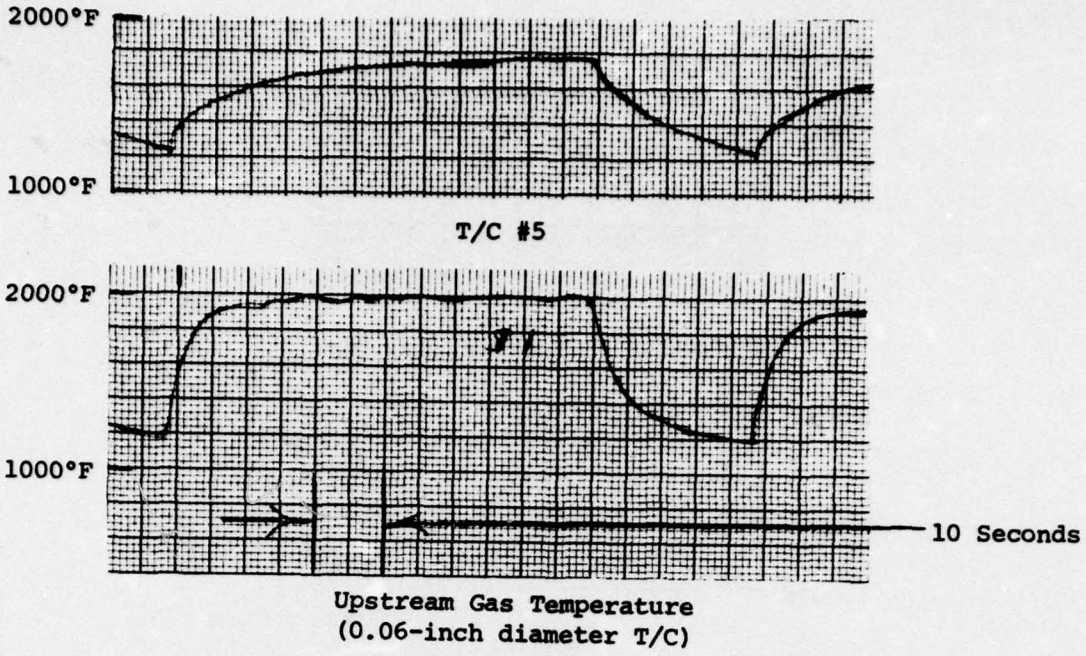

FIGURE 90b. THERMAL SHOCK CYCLE - 15°F/SEC. AT T/C #2 - ALL CERAMIC NOZZLE

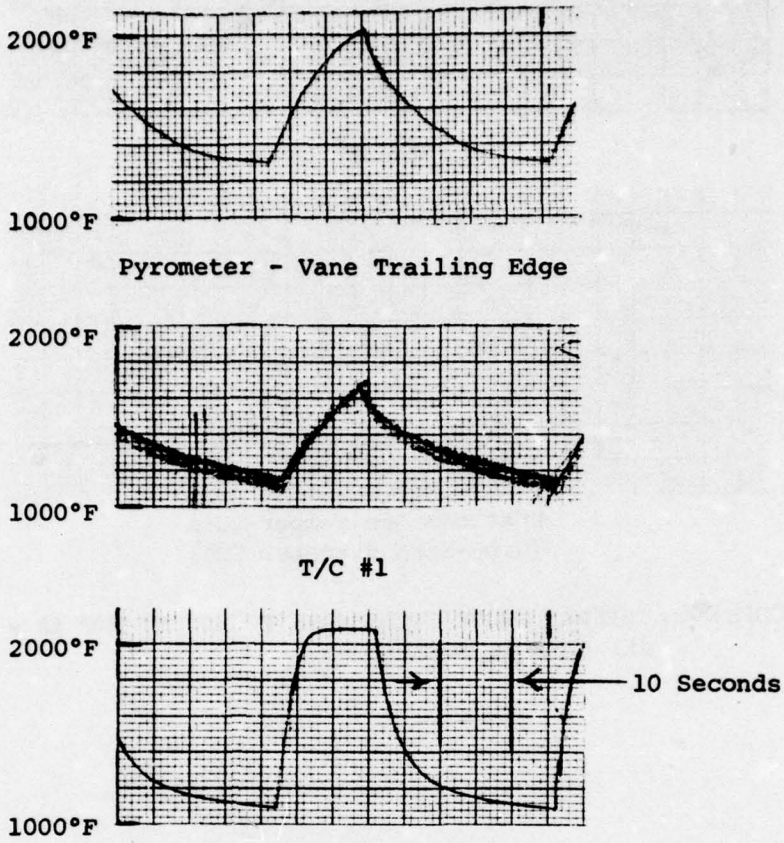

FIGURE 91. THERMAL SHOCK CYCLE - 60°F/SEC. AT T/C #1 - ALL CERAMIC NOZZLE

TABLE 12.

ENGINE SIMULATOR RIG FLOW CONDITIONS WITH ALL-CERAMIC NOZZLE

	Nozzle Upstream Flow		Nozzle Throat Conditions			
Test Condition	Total Pressure (psia)	Total Gas Temperature (°F)	Mach Number	Gas Velocity (ft/sec)	Gas Density (lb/ft^3)	Total Mass Flow × Nozzle Coefficient of Discharge (lb/sec)
Dust Erosion or Hot Corrosion	21.6	2000	0.76	1742	0.0180	0.173
Thermal Shock						
15°F/sec High Fire	20.7	2100	0.72	1693	0.0171	0.160
15°F/sec Low Fire	19.5	1200	0.65	1242	0.0259	0.178
30°F/sec High Fire	22.2	2240	0.79	1890	0.0165	0.172
30°F/sec Low Fire	20.4	1120	0.70	1297	0.0276	0.200
45°F/sec High Fire	23.9	2250	0.863	1983	0.0168	0.184
45°F/sec Low Fire	21.4	1240	0.75	1432	0.0260	0.206
60°F/sec High Fire	26.3	2250	0.951	2358	0.0173	0.225
60°F/sec Low Fire	22.8	1110	0.820	1489	0.0287	0.236

A second nozzle shroud set was used for this test since cracks sustained in corrosion testing would confuse the results. The $RBSi_3N_4$ shroud $HPSi_3N_4$ vane nozzle survived this test series without sustaining any damage. Figures 92 and 93A show the nozzle after 250 cycles. The cracking that occurred in corrosion test due to short circuiting of support pin insulation by molten products did not occur in thermal shock tests (see Figs. 93B and 94).

Figures 95 through 106 show all of the nozzle vanes and the nozzle shrouds after the 500 cycle thermal shock test was completed. Dye penetrant inspection showed no evidence of cracks.

All of the vanes were intact after the test regardless of type of glass joint material used or whether any was used at all.

3.3 ENGINE TEST - PHASE II

3.3.1 Objective

The goal of this program phase was to design, fabricate and engine test evaluate a ceramic and engine test evaluate a ceramic vane nozzle in the 10kW gas turbine engine.

3.3.2 Design and Analysis

The nozzle configuration chosen for engine test was the $HPSi_3N_4$ ceramic vane-713LC superalloy shroud design rig which was tested in Phase I. Three modifications were made for engine application of this design.

A. Upstream

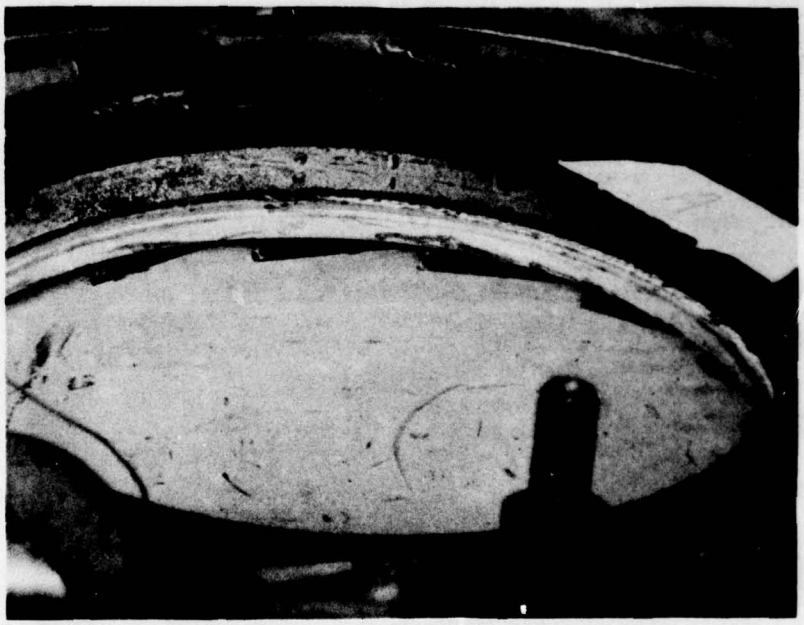

B. Downstream

FIGURE 92. ALL-CERAMIC NOZZLE AFTER 250 RIG TEST THERMAL SHOCK CYCLES

A. Downstream

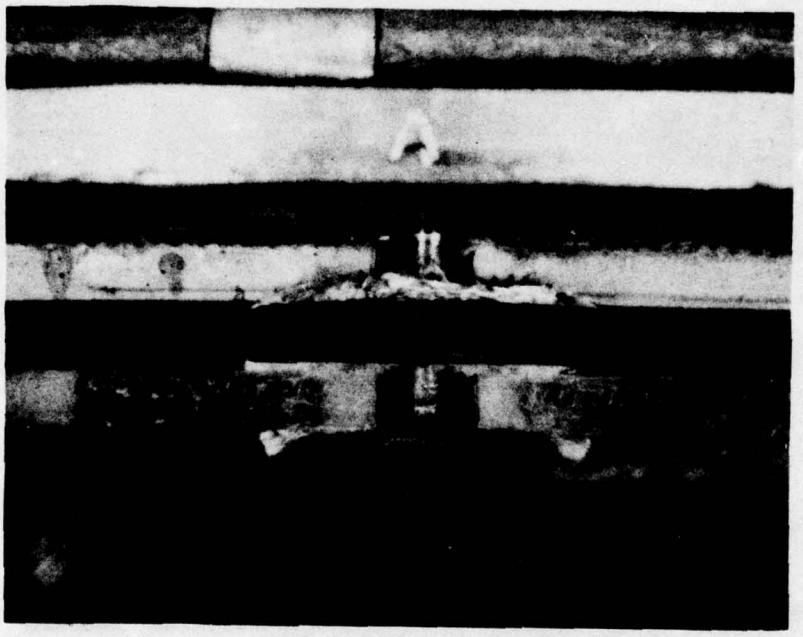

B. Holding Pin Location "A"

FIGURE 93. ALL-CERAMIC NOZZLE AFTER 250 RIG TEST THERMAL SHOCK CYCLES

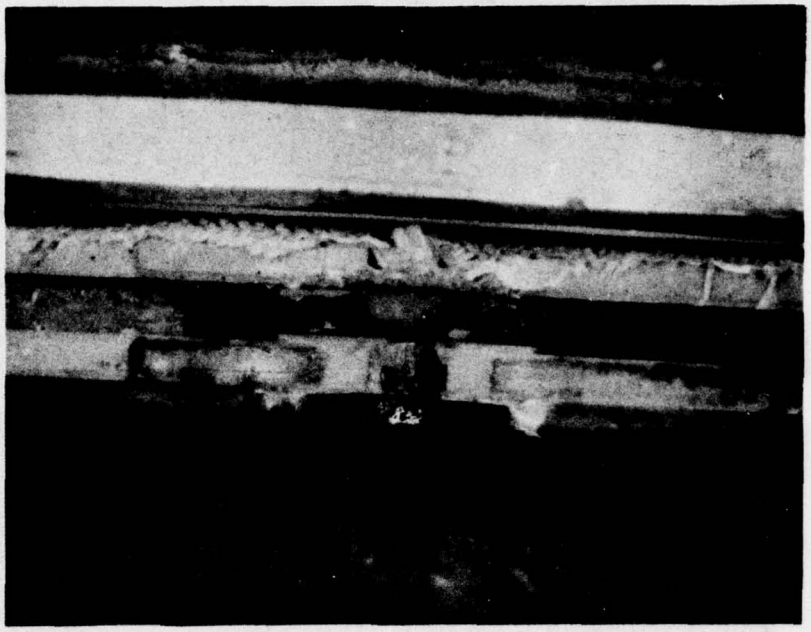

A. Holding Pin Location "B"

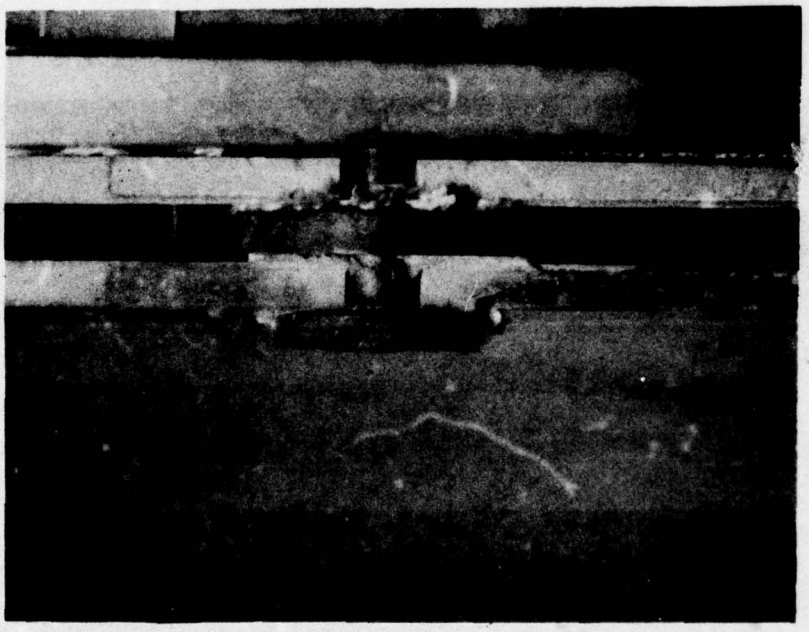

B. Holding Pin Location "C"

FIGURE 94. ALL-CERAMIC NOZZLE AFTER 250 RIG TEST THERMAL SHOCK CYCLES

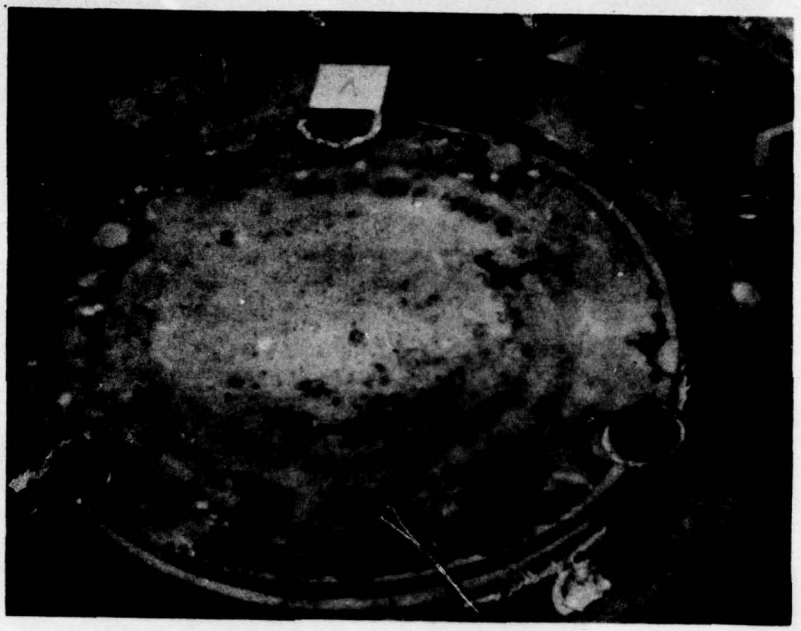

A. UPSTREAM

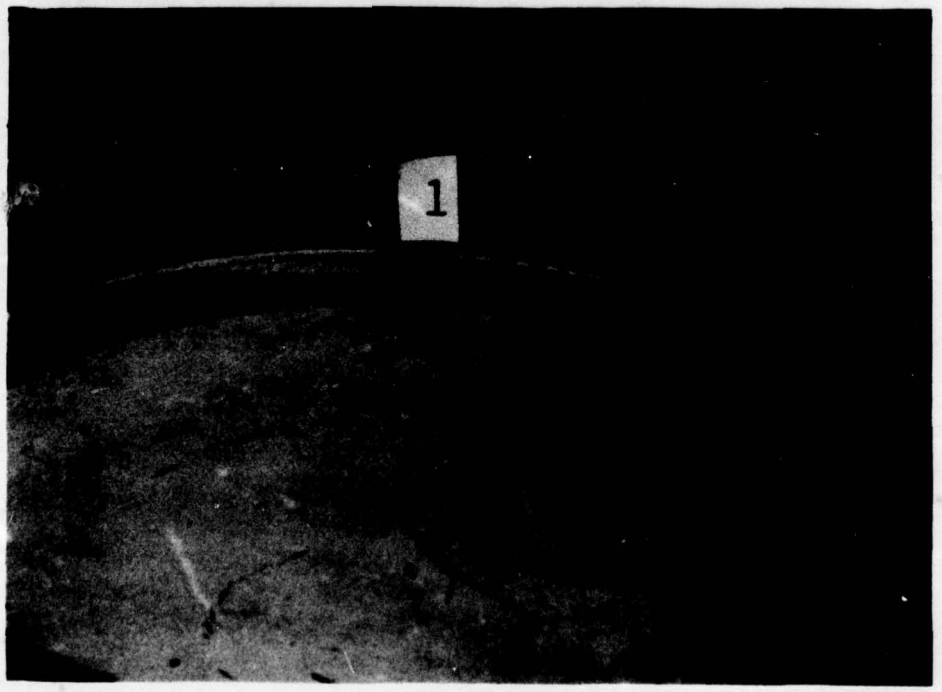

B. DOWNSTREAM

FIGURE 95. ALL-CERAMIC NOZZLE AFTER 500 THERMAL SHOCK CYCLES

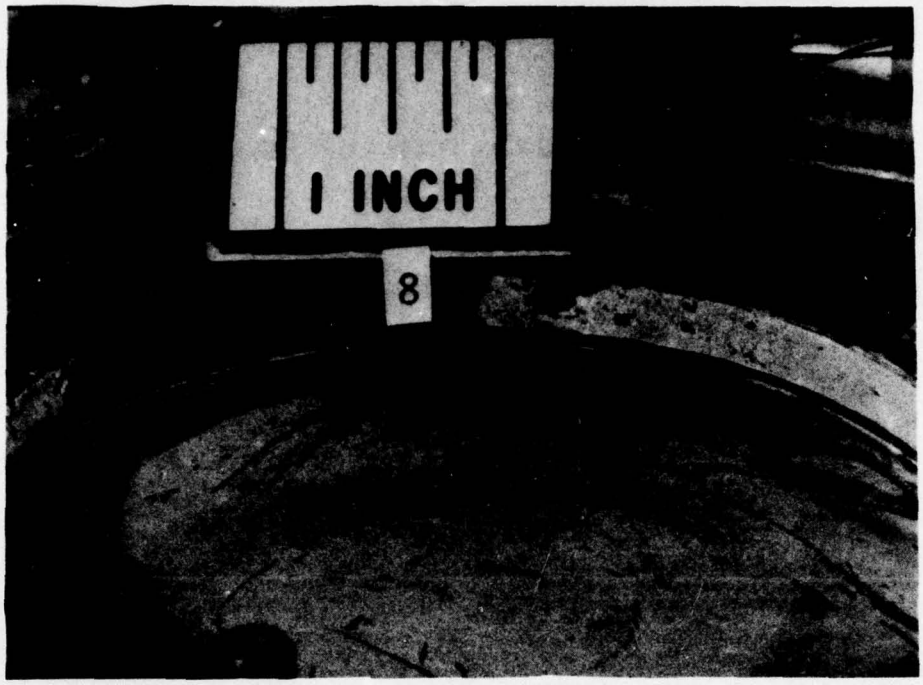

FIGURE 96. ALL-CERAMIC NOZZLE AFTER 500 THERMAL SHOCK CYCLES - DOWNSTREAM

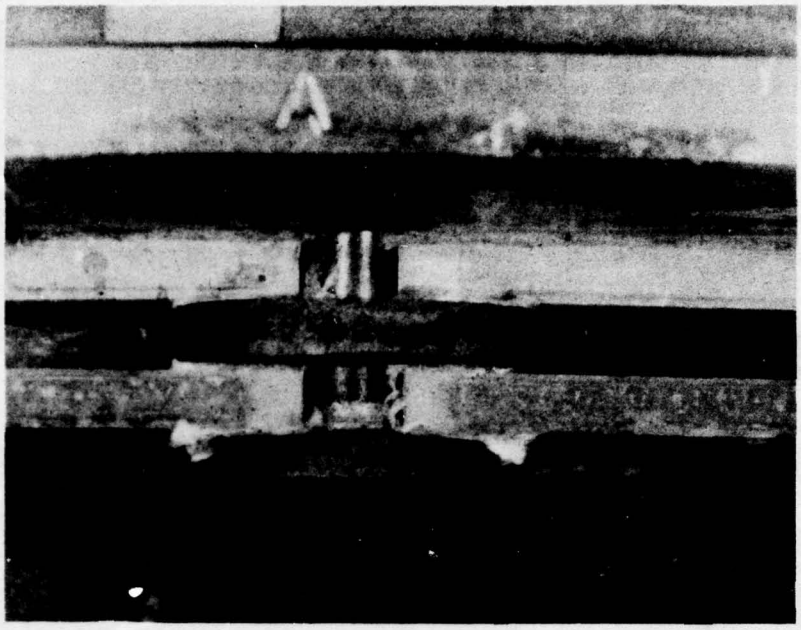

A.

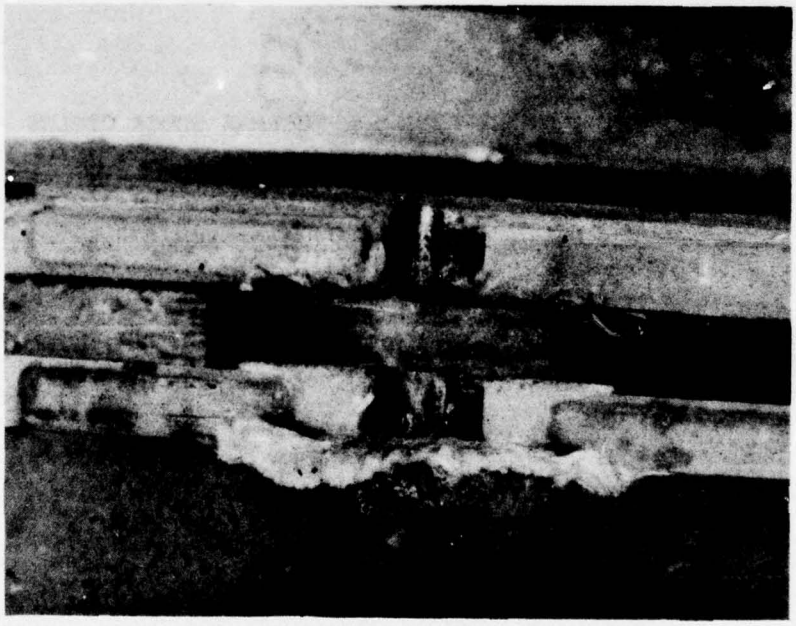

B.

Figure 97. All Ceramic Nozzle at Pin Locations "A" and "B" After 500 Thermal Shock Cycles

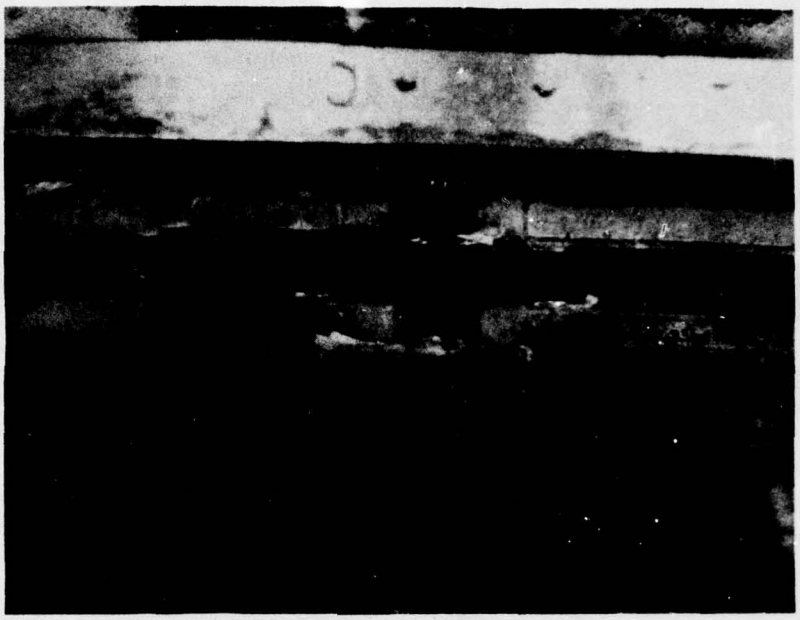

A.

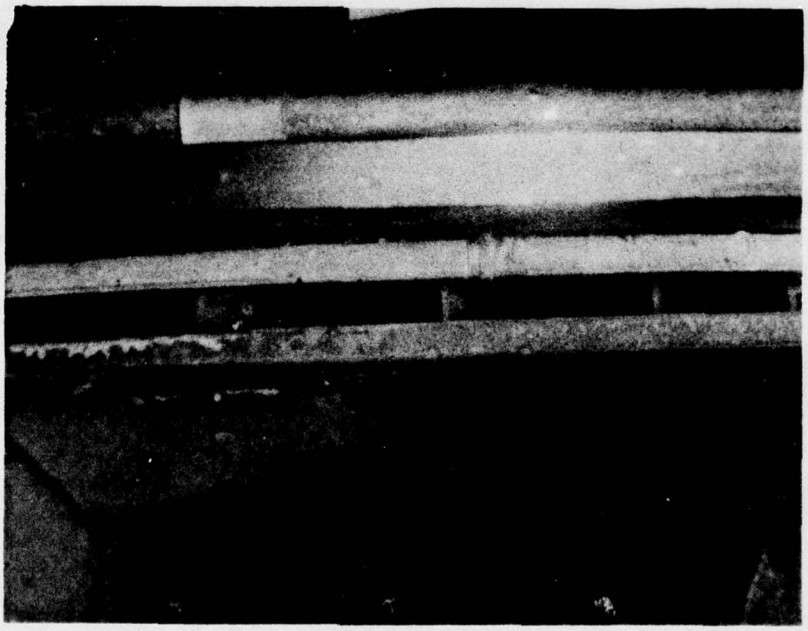

B.

FIGURE 98. All Ceramic Nozzle at Pin Location "C" and Between Pins "A" and "C" After 500 Thermal Shock Cycles

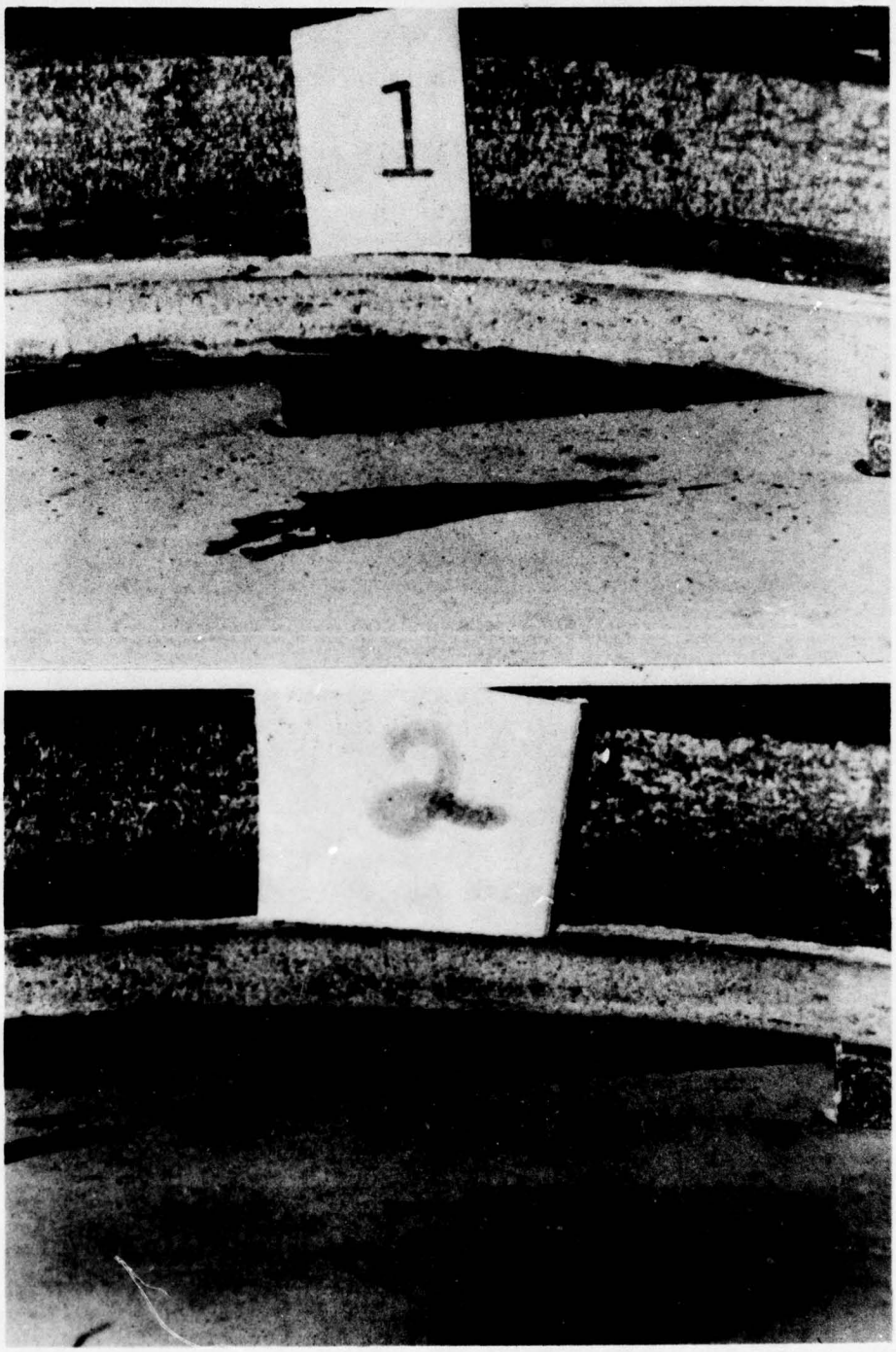

A.

B.

FIGURE 99. ALL-CERAMIC NOZZLE AFTER 500 THERMAL SHOCK CYCLES - LOCATIONS 1 and 2

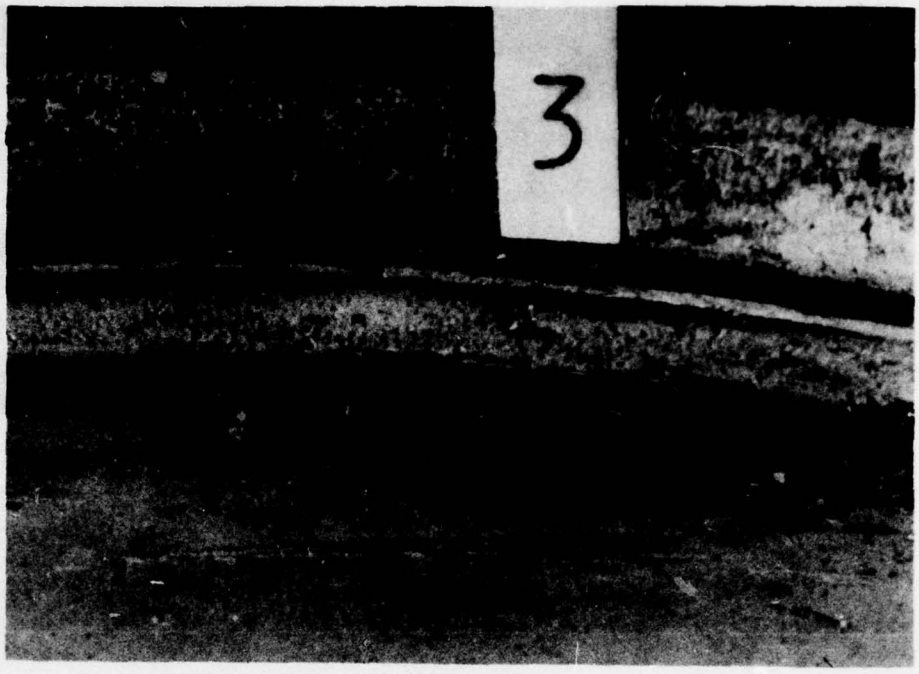

FIGURE 100a. ALL-CERAMIC NOZZLE AFTER 500 THERMAL SHOCK CYCLES - VANE LOCATION #2

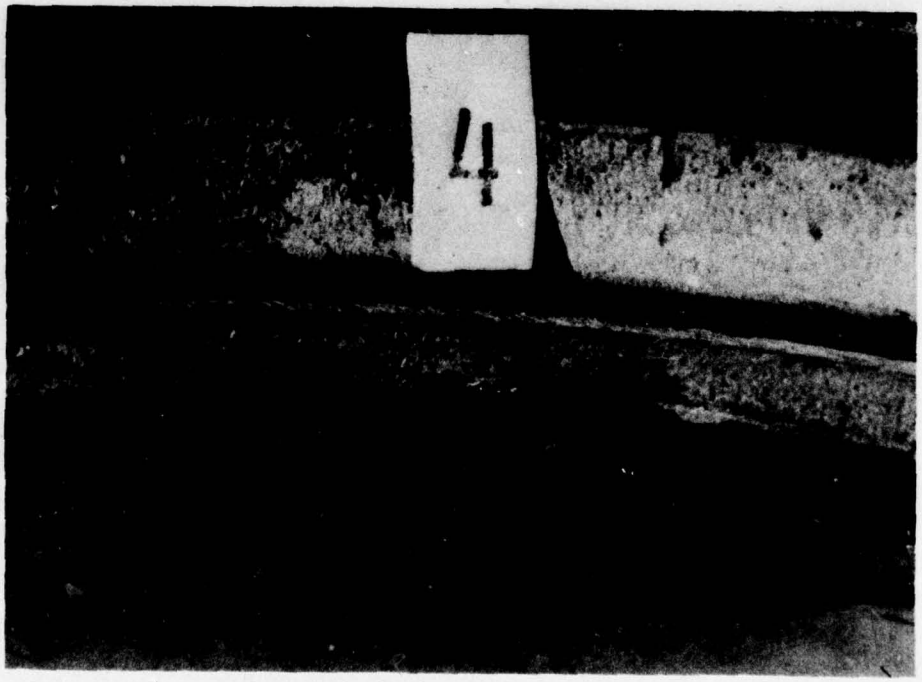

FIGURE 100b. ALL-CERAMIC NOZZLE AFTER 500 THERMAL SHOCK CYCLES - LOCATION #3

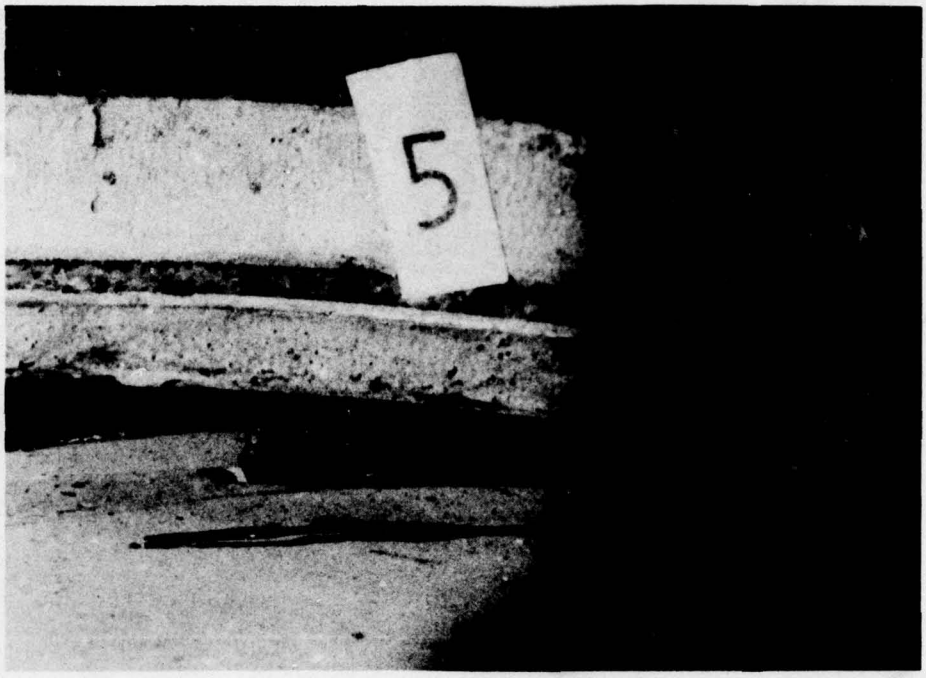

FIGURE 101a. ALL-CERAMIC NOZZLE AFTER 500 THERMAL SHOCK CYCLES - LOCATION #5

FIGURE 101b. ALL-CERAMIC NOZZLE AFTER 500 THERMAL SHOCK CYCLES - LOCATION #6

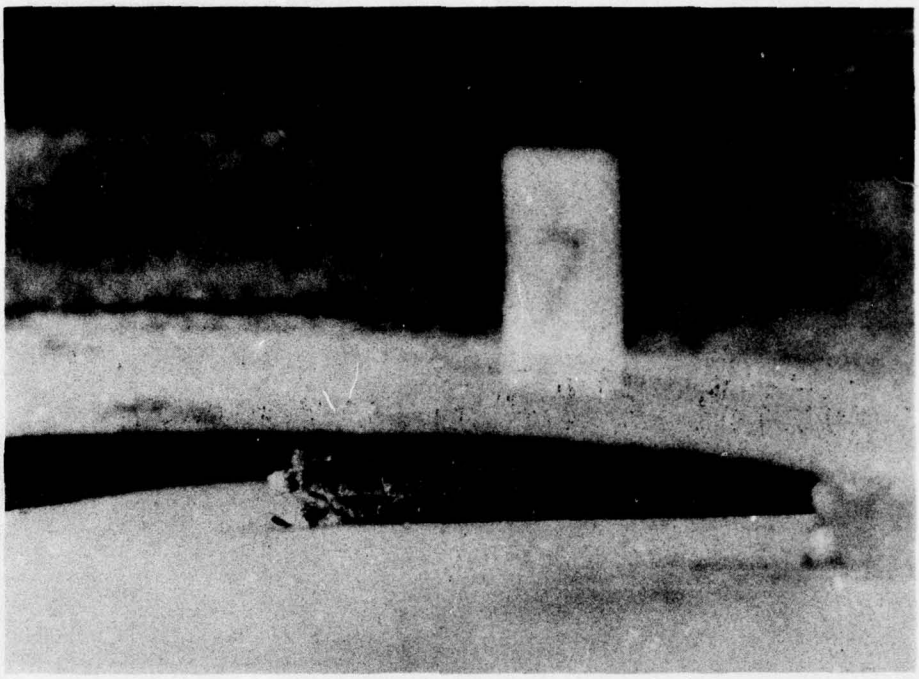

FIGURE 102a. ALL-CERAMIC NOZZLE AFTER 500 THERMAL SHOCK CYCLES - LOCATION #7

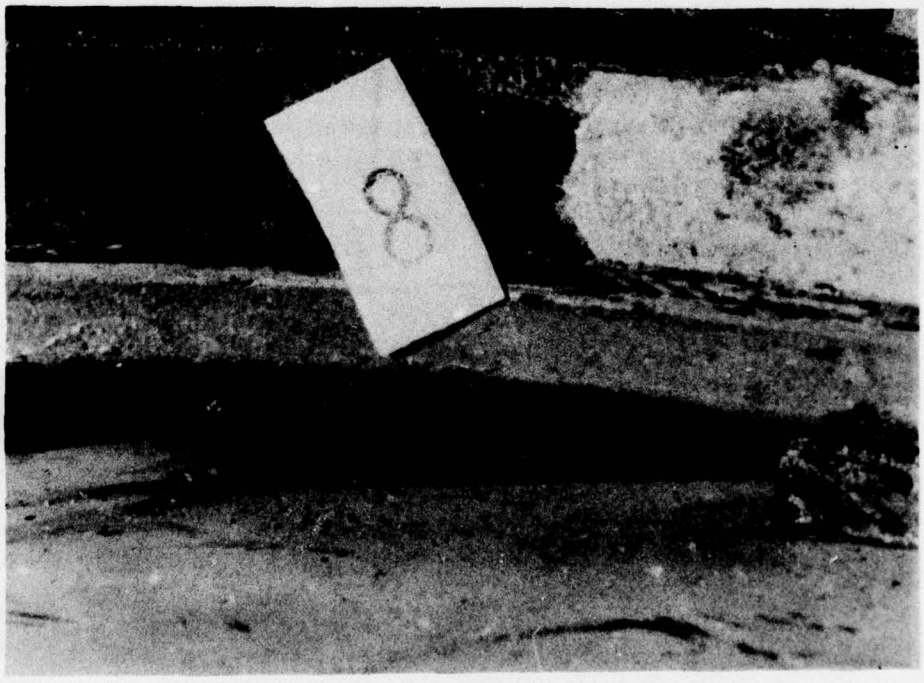

FIGURE 102b. ALL-CERAMIC NOZZLE AFTER 500 THERMAL SHOCK CYCLES - LOCATION #8

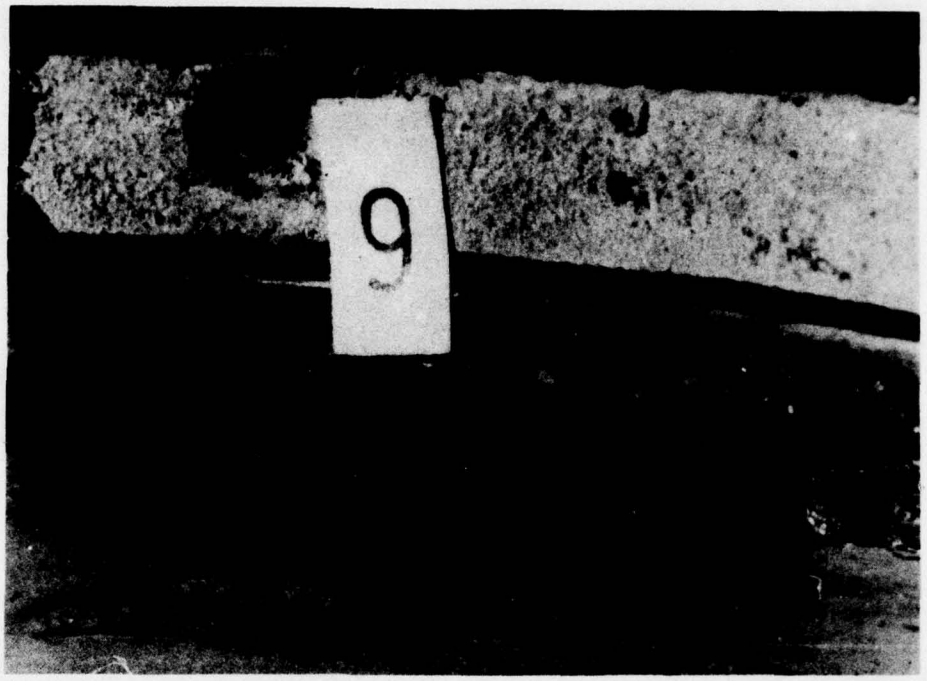

FIGURE 103a. ALL-CERAMIC NOZZLE AFTER 500 THERMAL SHOCK CYCLES - LOCATION #9

FIGURE 103b. ALL-CERAMIC NOZZLE AFTER 500 THERMAL SHOCK CYCLES - LOCATION #10

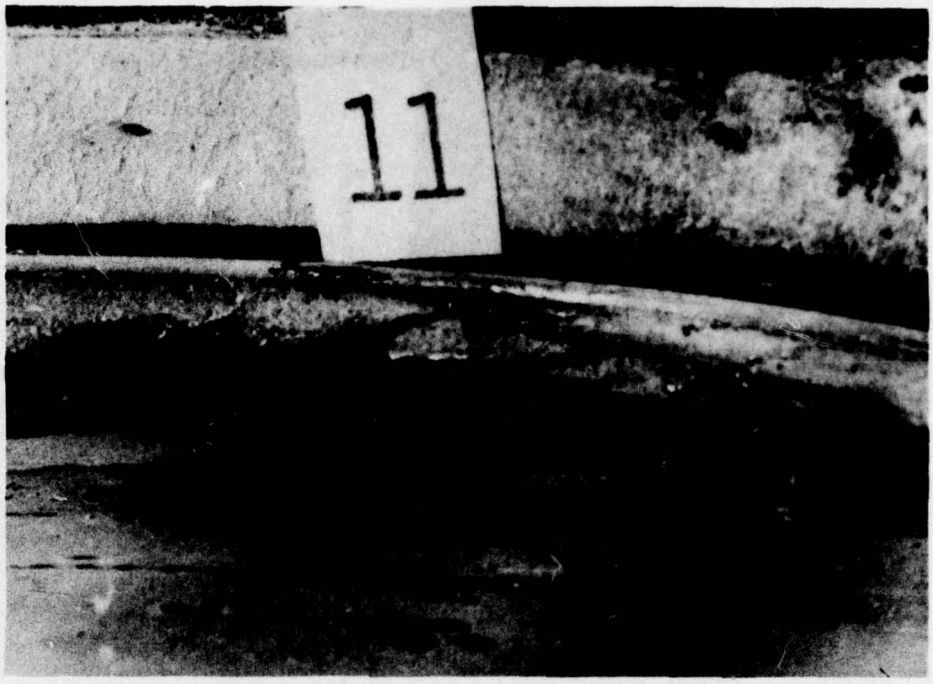

FIGURE 104a. ALL-CERAMIC NOZZLE AFTER 500 THERMAL SHOCK CYCLES - LOCATION #11

FIGURE 104b. ALL-CERAMIC NOZZLE AFTER 500 THERMAL SHOCK CYCLES - LOCATION #12

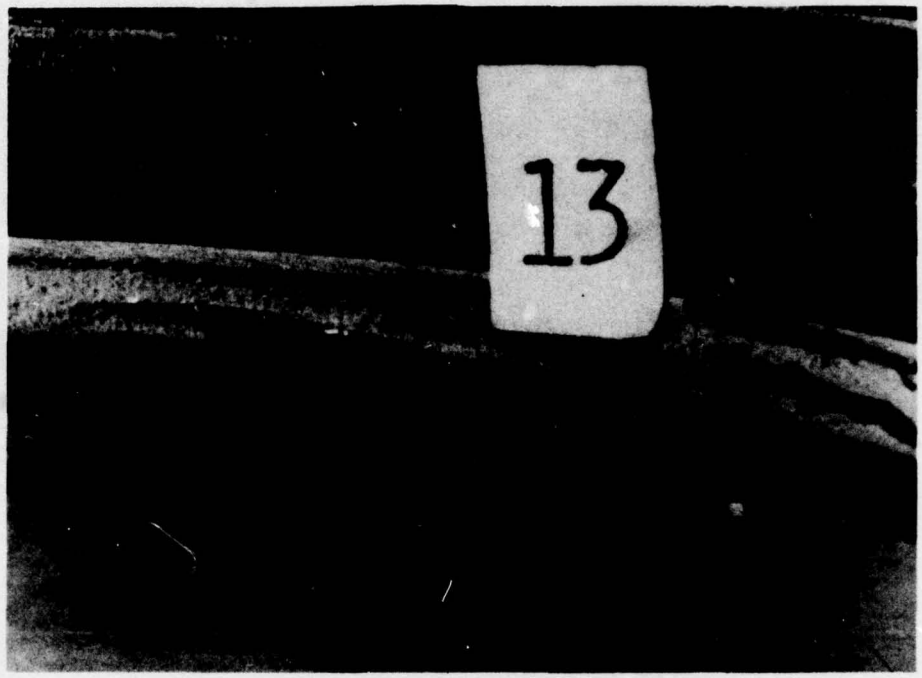

FIGURE 105a. ALL-CERAMIC NOZZLE AFTER 500 THERMAL SHOCK CYCLES - LOCATION #13

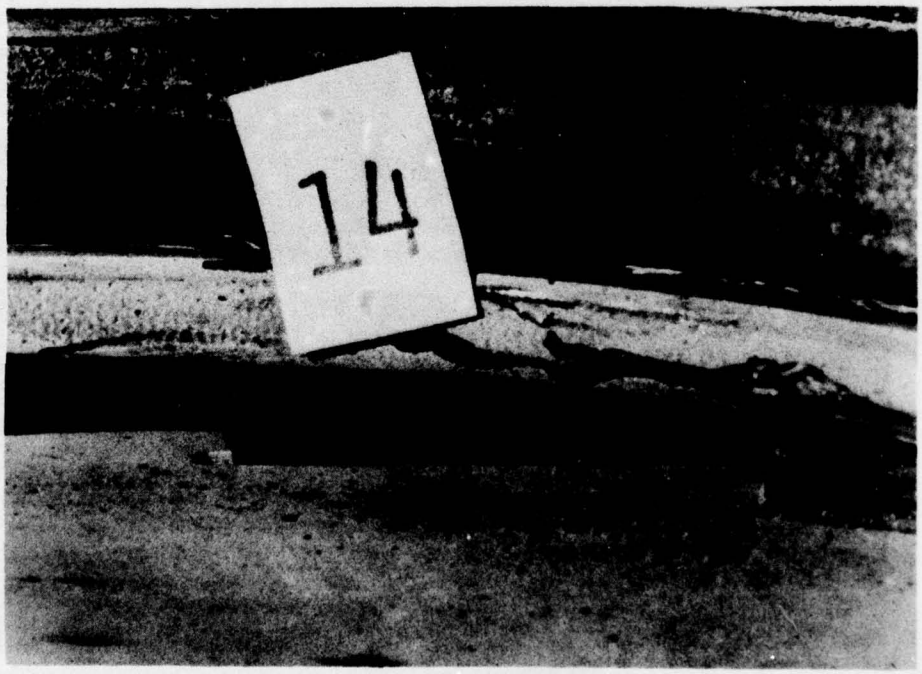

FIGURE 105b. ALL-CERAMIC NOZZLE AFTER 500 THERMAL SHOCK CYCLES - LOCATION #14

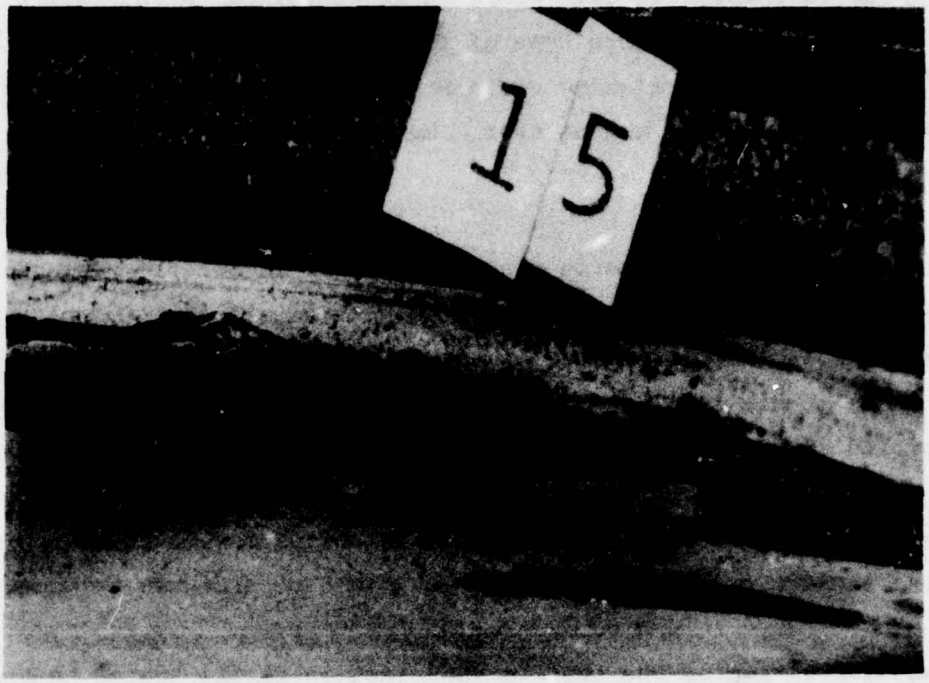

FIGURE 106. ALL-CERAMIC NOZZLE AFTER 500 THERMAL SHOCK CYCLES - LOCATION #15

1. Flow data generated in rig test showed the nozzle coefficient of discharge to be slightly higher than the standard nozzle design. This was compensated for in the engine installation design by decreasing the vane height dimension of 0.204/0.202 to 0.186/0.184.

2. Since the nozzle throat area depends on the location of the inboard surface of the rear (inner) shroud nozzle vane recess, some of the tolerances used in locating this surface were tightened in relation to those called out for rig test hardware.

3. Rig tests showed one failure out of the fifteen vanes tested. The cause was assigned to constraint introduced between metal shrouds and ceramic vanes by the low temperature glass bond [927°C (1700°F)] in the interface. Differential strains on cool down were believed to have caused an excessive longitudinal compressive load

on vane trailing edge where it is contained in the recess. In order to avoid this type of failure in an engine test, it was decided that relaxing glass bonds between shrouds and vanes would not be used in engine test. Unbonded vanes survived rig test with no failures.

Even distribution of transverse contact stresses on ceramic vanes due to possible forward shroud distortion is the most significant function of relaxing glasses in this bimaterial nozzle design. It was expected that the engine tests at sea level and low ambient temperatures would not result in high turbine inlet temperatures during the planned 25 hour engine test run and 50 stop/start cycles. Therefore, nozzle distortion, because of yielding of shroud material due to thermal gradients and excessive temperature as predicted in Section 3.6.2, Analysis, would not be expected to occur.

The finalized design of the ceramic vane section nozzle tested in the 10kW engine is shown in Figures 38, 39, 42, 107, and 108.

3.3.3 Nozzle Fabrication and Engine Assembly

The forward and rear nozzle shrouds per DSK 14956 and 14957 were electro-discharged machined from standard 10kW castings (Part Numbers 11947 and 11948).

Vanes were placed in the recesses and AMI 100 braze alloy was loaded into the rear shroud at counter bore holes per standard procedure. The rivets per DSK 14959 were static cold set with 12,000 load and the assembly was vacuum furnace brazed at 1162°C (2125°F) for approximately five minutes.

At this point in the assembly procedure the HPSi$_3$N$_4$ vane segments were all loose. (This is the correct condition for this design.)

Final machining operations for the turbine wheel contour, combustor and exhaust pipe sealing diameters, and piloting surfaces were then done by an outside vendor per Drawing No. 74-8005.

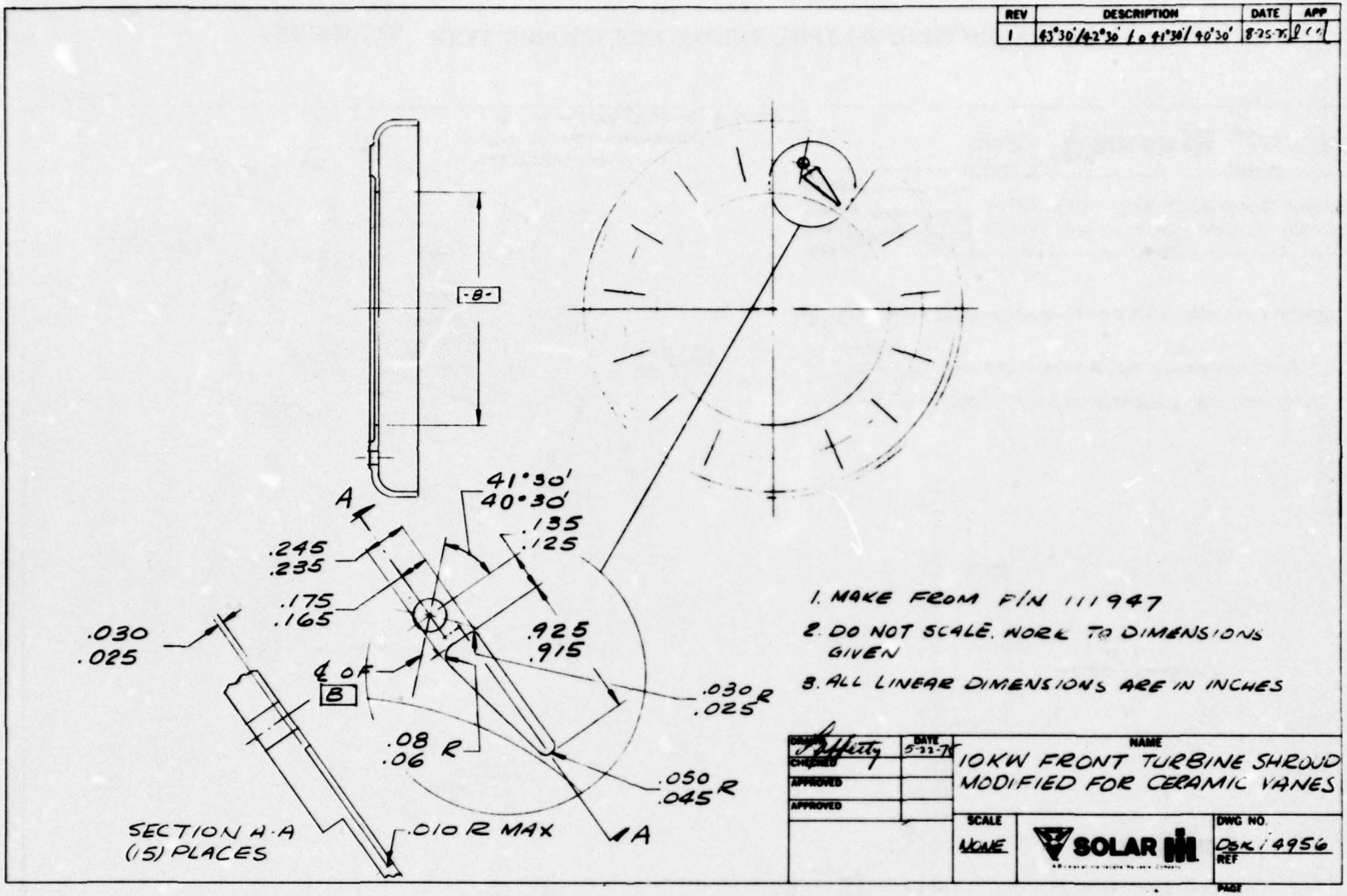

FIGURE 107. FORWARD SHROUD FOR ENGINE TEST OF CERAMIC VANES

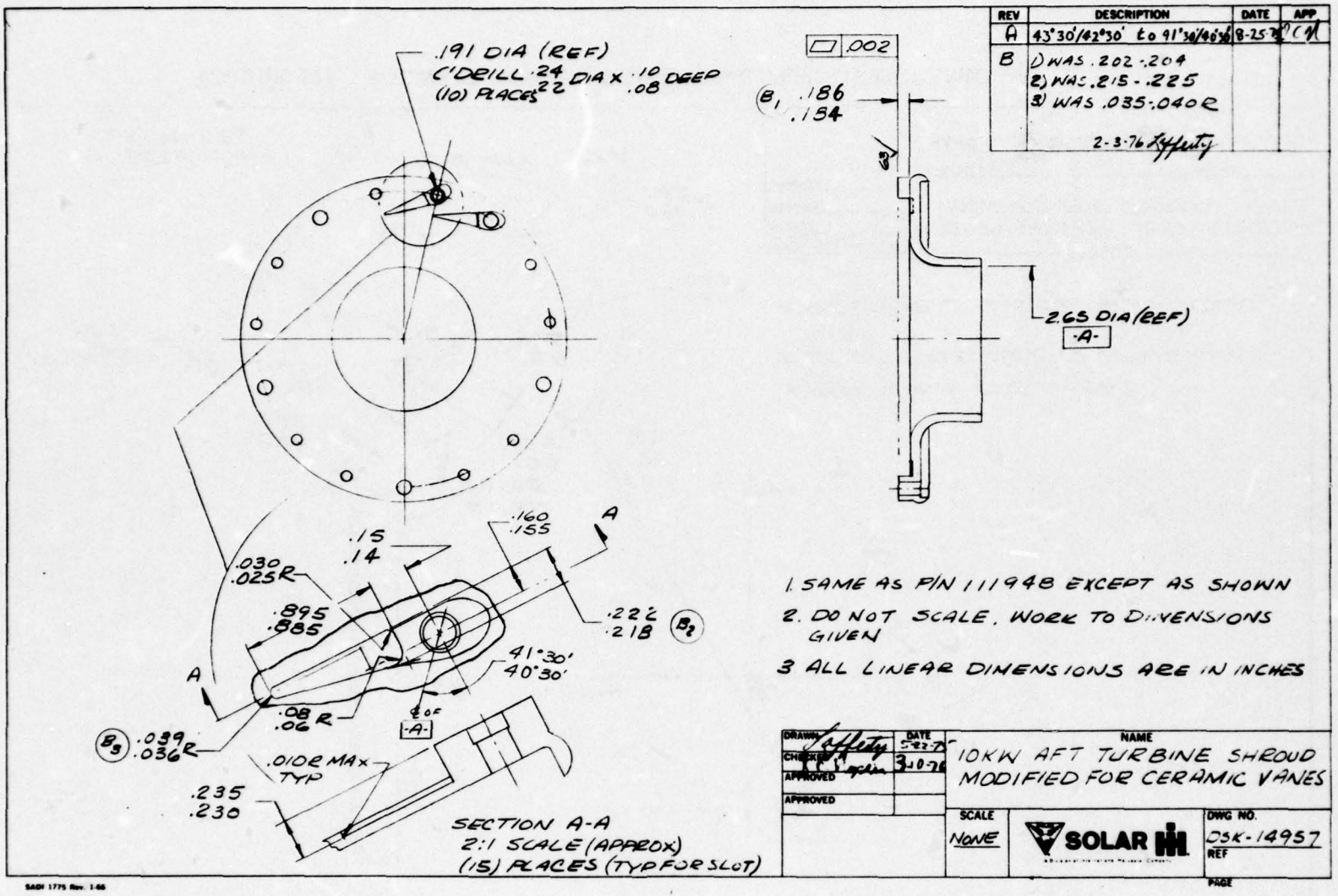

FIGURE 108. REAR SHROUD FOR ENGINE TEST OF CERAMIC VANES

After this operation it was observed that the vane sections were no longer loose. The forward (outer) shroud piloting lip (which is final machined to 0.040 to 0.050) had been distorted by machining tool pressure and had trapped the vanes in their recesses. No damage to the ceramic vane sections was observed.

This distortion was repaired by mechanically bending the lip back. The vanes were then loose.

The nozzle was assembled into the 10kW engine in turbo-alternator package Serial #5 which is pictured in Figure 109. An assembly clearance chart is given in Figure 110.

3.3.4 Engine Test of Ceramic Vane Section Nozzle

The engine package was test run before installation of the ceramic nozzle in the as received condition. Performance was found to be poor and load could not be applied to the unit without excessive exhaust gas temperature.

The nozzle section was removed and inspected but no abnormal conditions were observed.

The ceramic vane section nozzle was installed and the alternator package was calibrated The raw data is given in Table 13 and standard condition corrected performance figures are given in Table 14. Full power could not be developed without generating turbine inlet temperature beyond 898°C (1650°F). Full power for this engine is 12 kW. The following 25 hour test sequence was run:

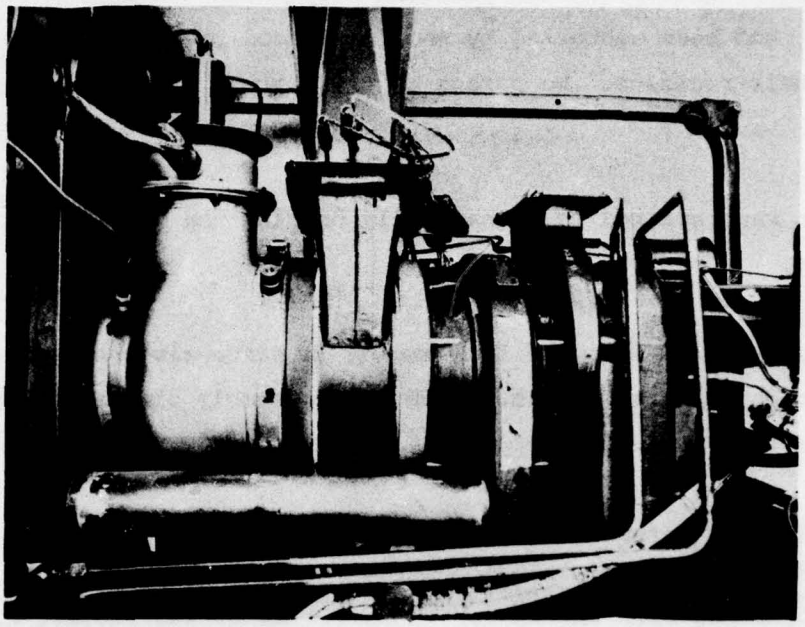

FIGURE 109. MERDC 10KW ENGINE SET-UP IN TEST CELL

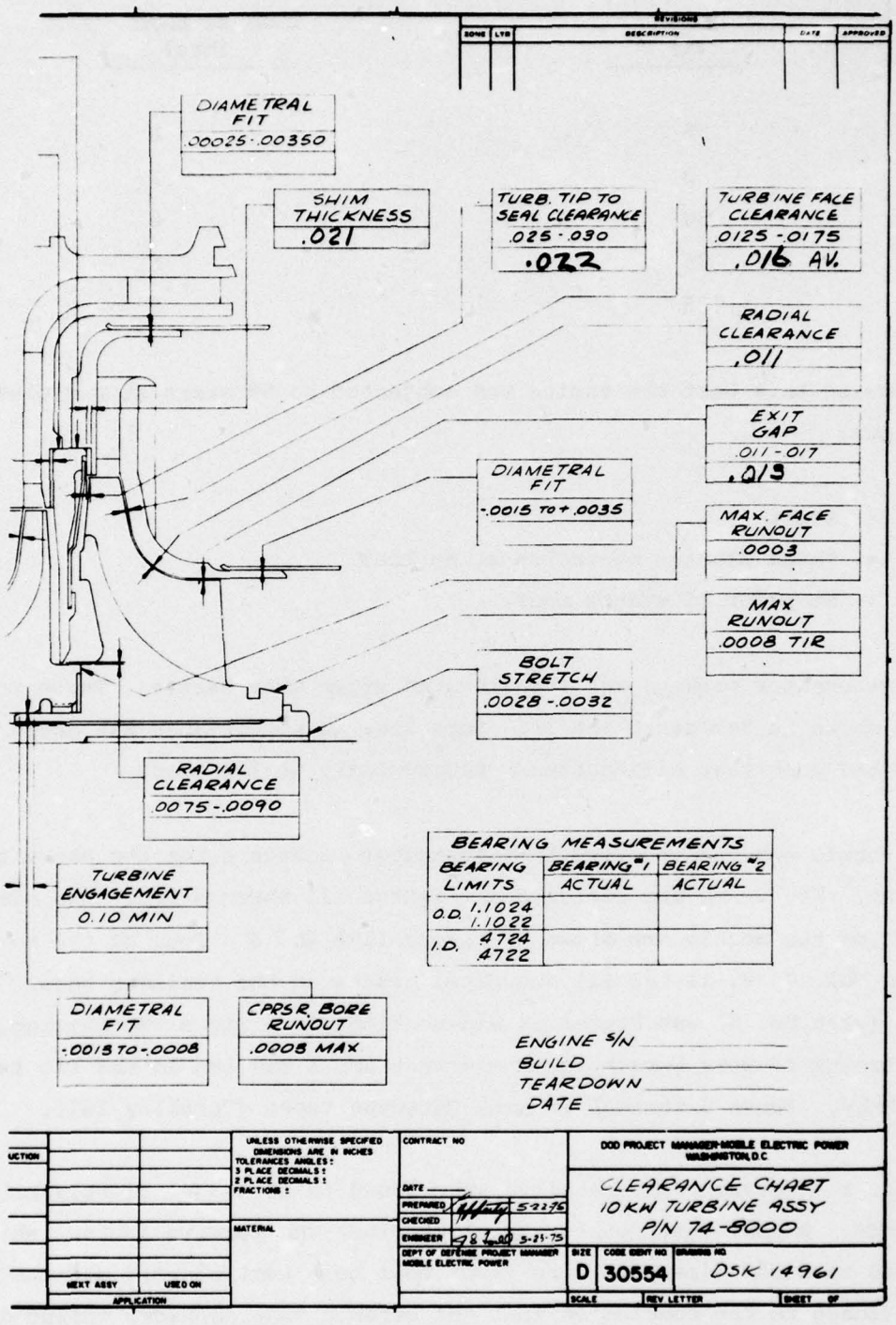

FIGURE 110. CLEARANCE CHART 10 kW TURBINE ASSEMBLY (June 15, 1976 Engine Serial #5) P/N 74-8000

Load (%)	Time at Load (hrs)
75	6
0	1
50	6
25	6
25	6

Following this test the engine was subjected to 50 start/stop cycles as follows:

- Start
- Three minutes operation at no load.
- Stop for 12 minute soak.

The alternator package was recalibrated after this series. These results are also shown in Tables 13 and 14. Some loss in performance was noted between pre- and post-test calibrations, particularly at low load.

The nozzle was removed from the alternator package after the above test series. The vanes are pictured in Figures 111 through 118. Two overall views of the nozzle are shown in Figure 119A and B. Four of the nozzle vanes (vane Nos. 7, 9, 11 and 15) sustained cracks at the trailing edge. A fifth vane (vane No. 5) was broken at mid-section and a piece was missing. (Vane #1 through #5 were Norton vanes and vane No. 5 was run in the rig test sequence. Vanes 6 through 15 were Ceradyne vanes (Ceralloy 147).

All of the ceramic vane sections were found to be wedged tightly between the shrouds. A post test inspection showed that the forward (outer) shroud lip (0.040 to 0.050 dimension) and rivet bolt hole section were deformed inward. This leads to the conclusion that the ceramic vane sections failed due to compressive loads at the trailing edges.

Table 13

CALIBRATION DATA FOR CERAMIC 10KW ENGINE SN5 WITH CERAMIC VANE SECTION NOZZLE BEFORE AND AFTER TEST

Test Condition		Turbine Inlet Temperature (°F)	Exhaust Gas Temperature (°F)	Power Output (kW)	Fuel Flow (pph)	Compressor Inlet Temperature (°F)	Compressor Inlet Pressure (in. H_2O)	Data Point Number	Pressure Ratio
Pre-Test	0 Load	1071	795	-	15.6	88	-5.5	1	3.09
	25% Load	1232	925	-	18.6	92	-5.2	2	3.12
	50% Load	1412	1070	-	22.3	-	-5.1	3	3.14
	75% Load	1550	1174		25.9	90	-4.8	6	3.24
After 26 Hour Run and 50 Start/Stop Cycles	0 Load	1120	828	-	19.9	92	-5.0	154	3.19
	25% Load	1290	975	-	20.1	97	-4.1	157	3.08
	50% Load	1445	1095	-	23.0	98	-4.3	156	3.17
	75% Load	1615	1230	-	25.9	98	-4.1	155	3.21

Table 14

CALIBRATION DATA (Corrected to 59°F and 14.7 psi inlet conditions) FOR CERAMIC 10kW ENGINE SN5 WITH CERAMIC VANE SECTION NOZZLE BEFORE AND AFTER TEST

Test Condition		Turbine Inlet Temperature (°F)	Exhaust Gas Temperature (°F)	Power Output (kW)	Fuel Flow (pph)	Compressor Inlet Temperature (°F)	Compressor Inlet Pressure (in. H_2O)	Data Point Number	Specific Fuel Consumption
Pre-Test	0 Load	985	726	0	15.4	59	0	1	-
	25% Load	1130	840	4.00	18.3	59	0	2	2.80
	50% Load	1296	977	6.99	21.9	59	0	3	1.92
	75% Load	1433	1080	10.56	25.5	59	0	6	1.478
After 26 Hour Run and 50 Start/Stop Cycles	0 Load	1014	750	0	19.6	59	0	154	-
	25% Load	1163	875	4.01	19.6	59	0	157	2.99
	50% Load	1302	984	7.18	22.46	59	0	156	1.912
	75% Load	1459	1110	10.42	25.3	59	0	155	1.484

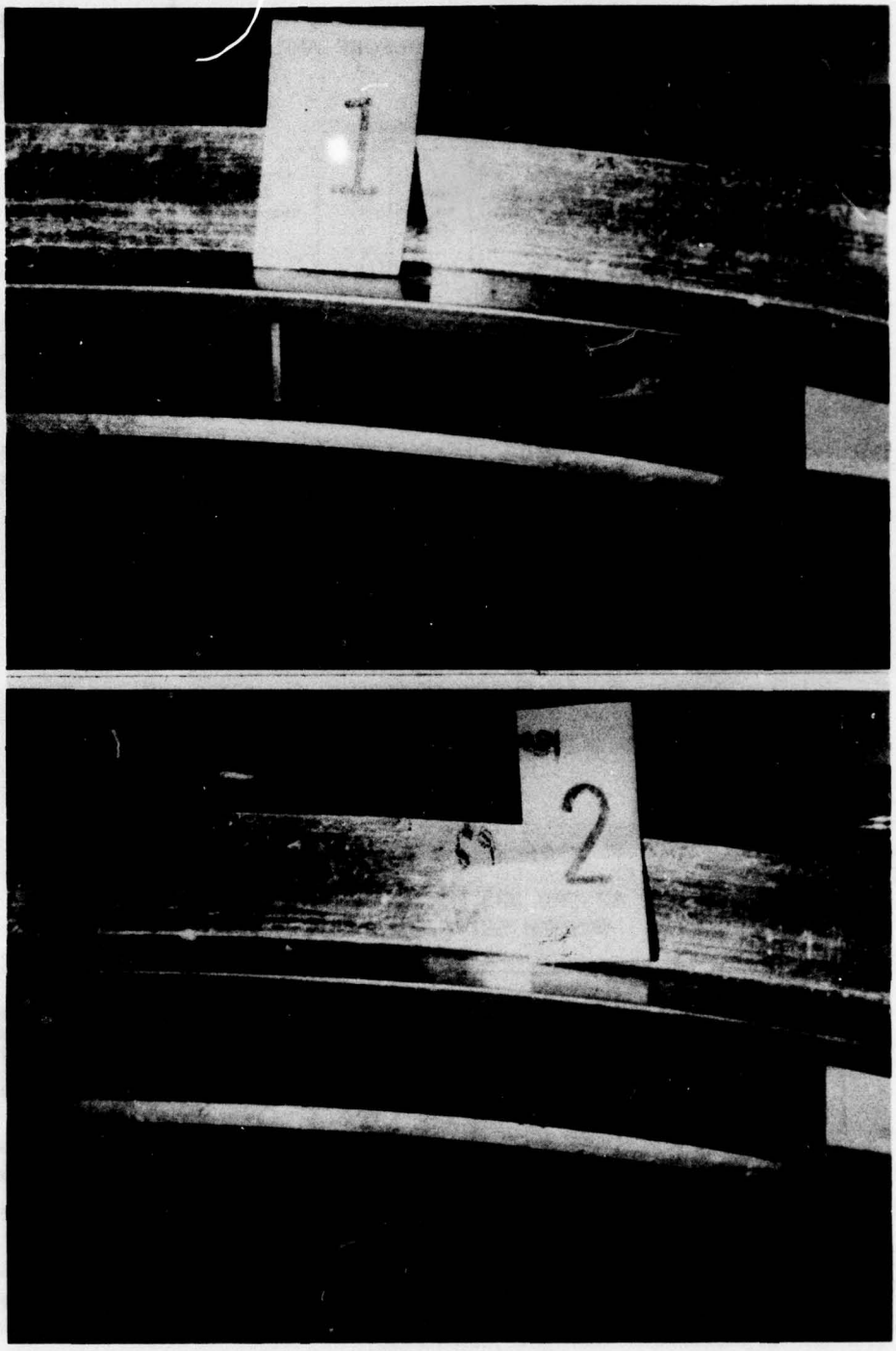

#1

#2

FIGURE 111. 10kW NOZZLE CERAMIC VANE SECTIONS #1 AND #2 AFTER ENGINE TEST - 25 HOUR RUN PLUS 50 START/STOP CYCLES

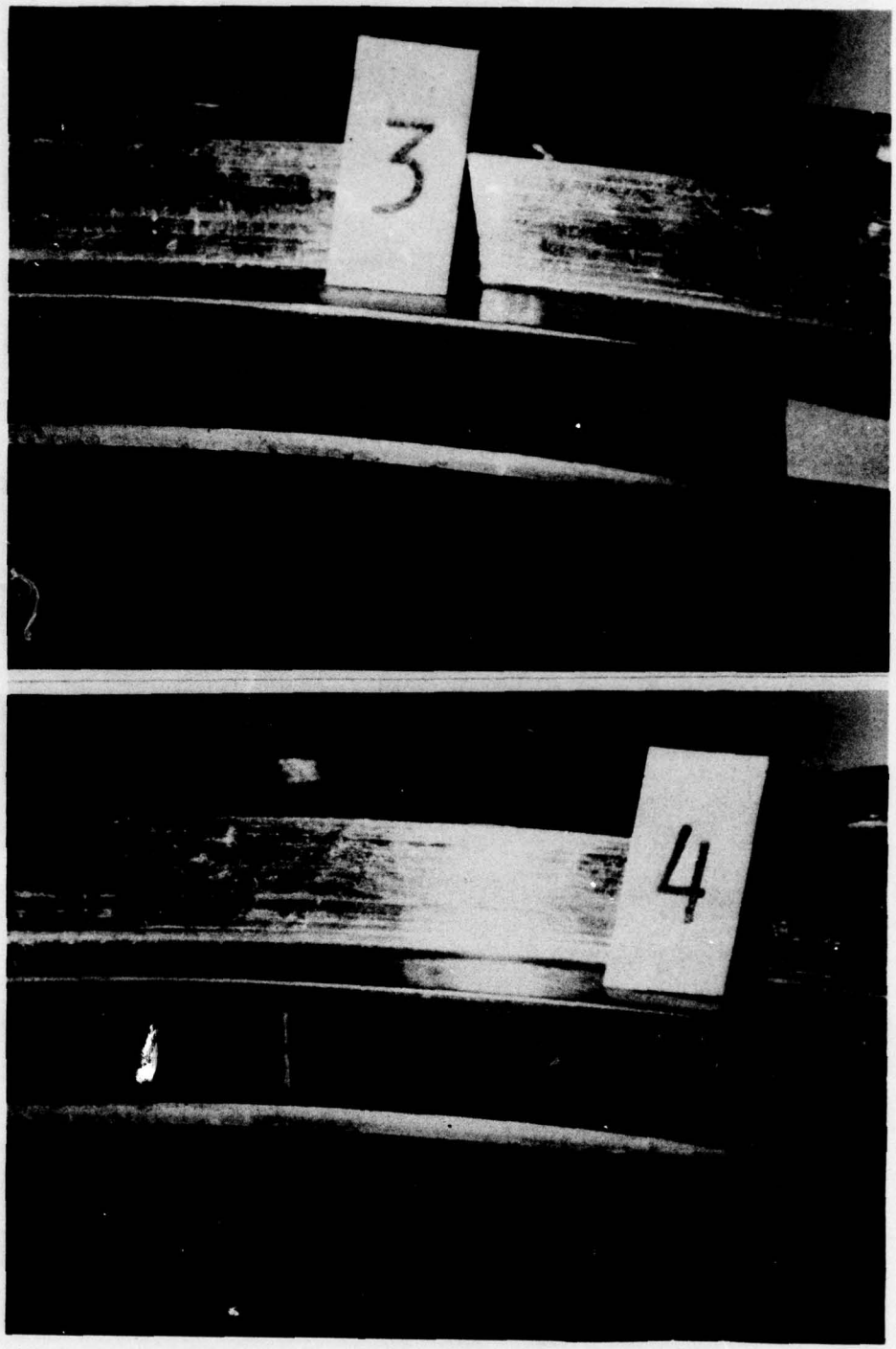

FIGURE 112. 10kW NOZZLE CERAMIC VANE SECTIONS #3 and #4 AFTER ENGINE TEST - 25 HOUR RUN PLUS 50 START/STOP CYCLES

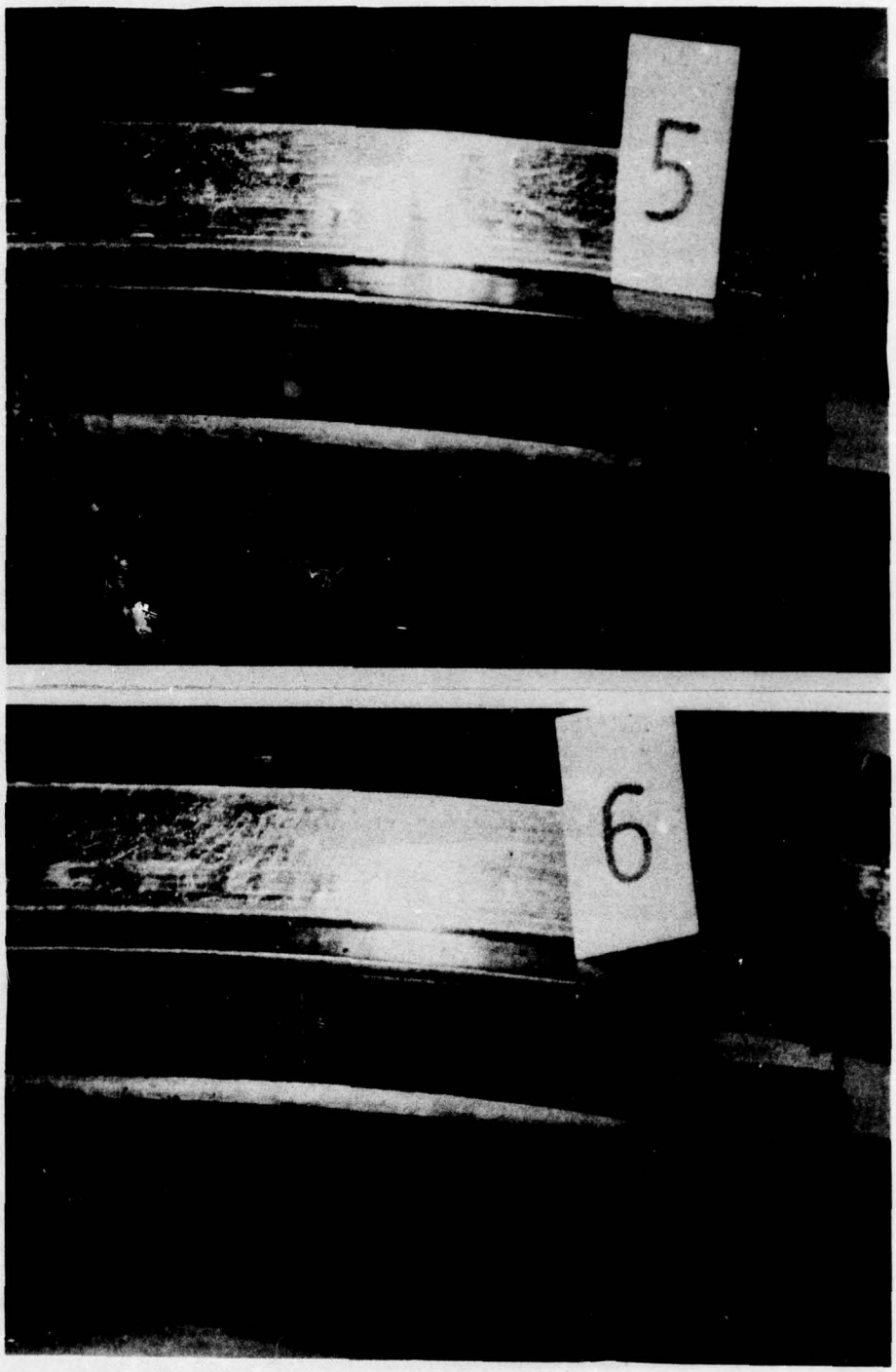

#5

#6

FIGURE 113. 10kW NOZZLE CERAMIC VANE SECTIONS #5 and #6 AFTER ENGINE TEST - 25 HOUR RUN PLUS 50 START/STOP CYCLES

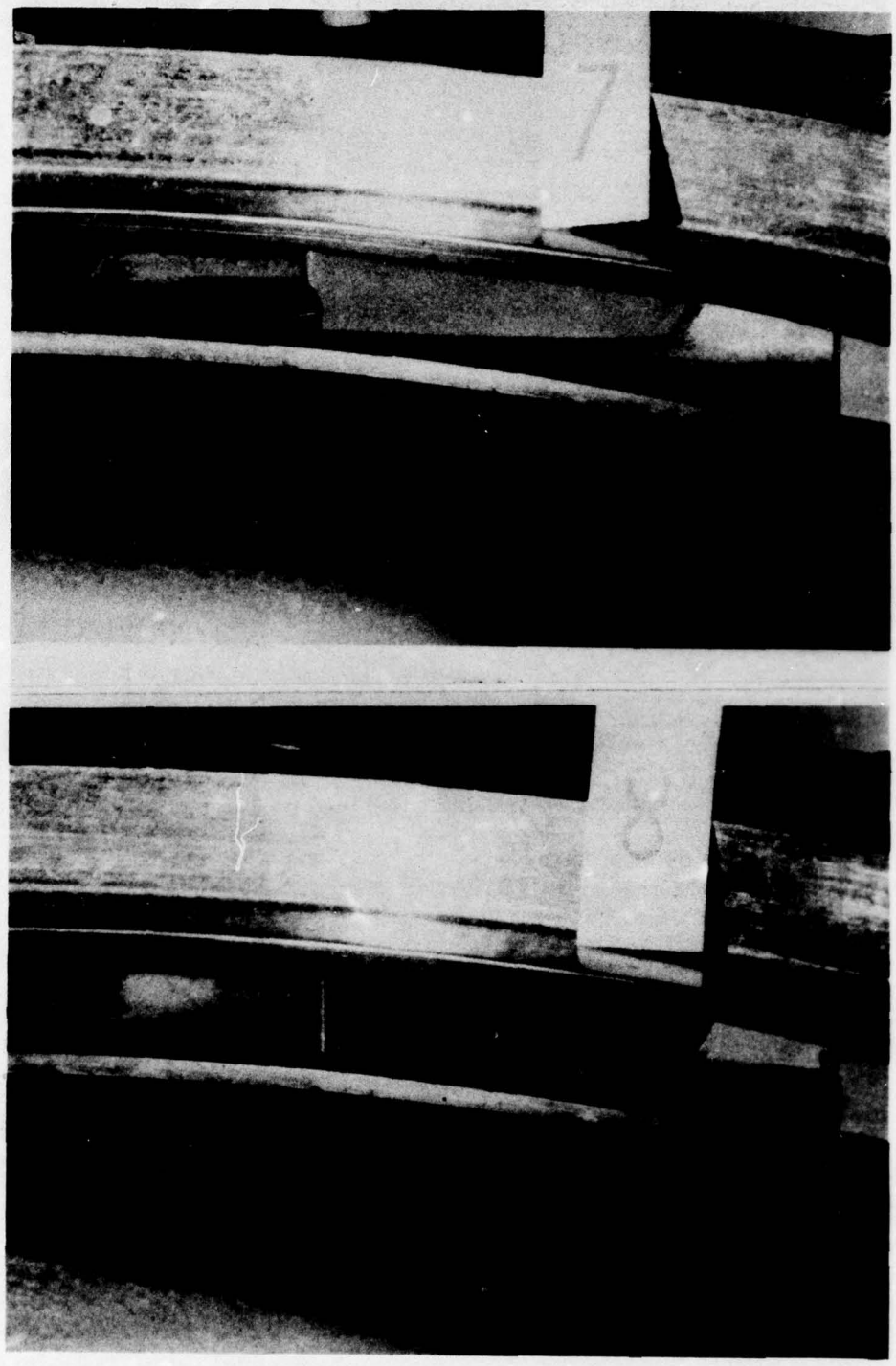

FIGURE 114. 10kW NOZZLE CERAMIC VANE SECTIONS #7 AND #8 AFTER ENGINE TEST - 25 HOUR RUN PLUS 50 START/STOP CYCLES

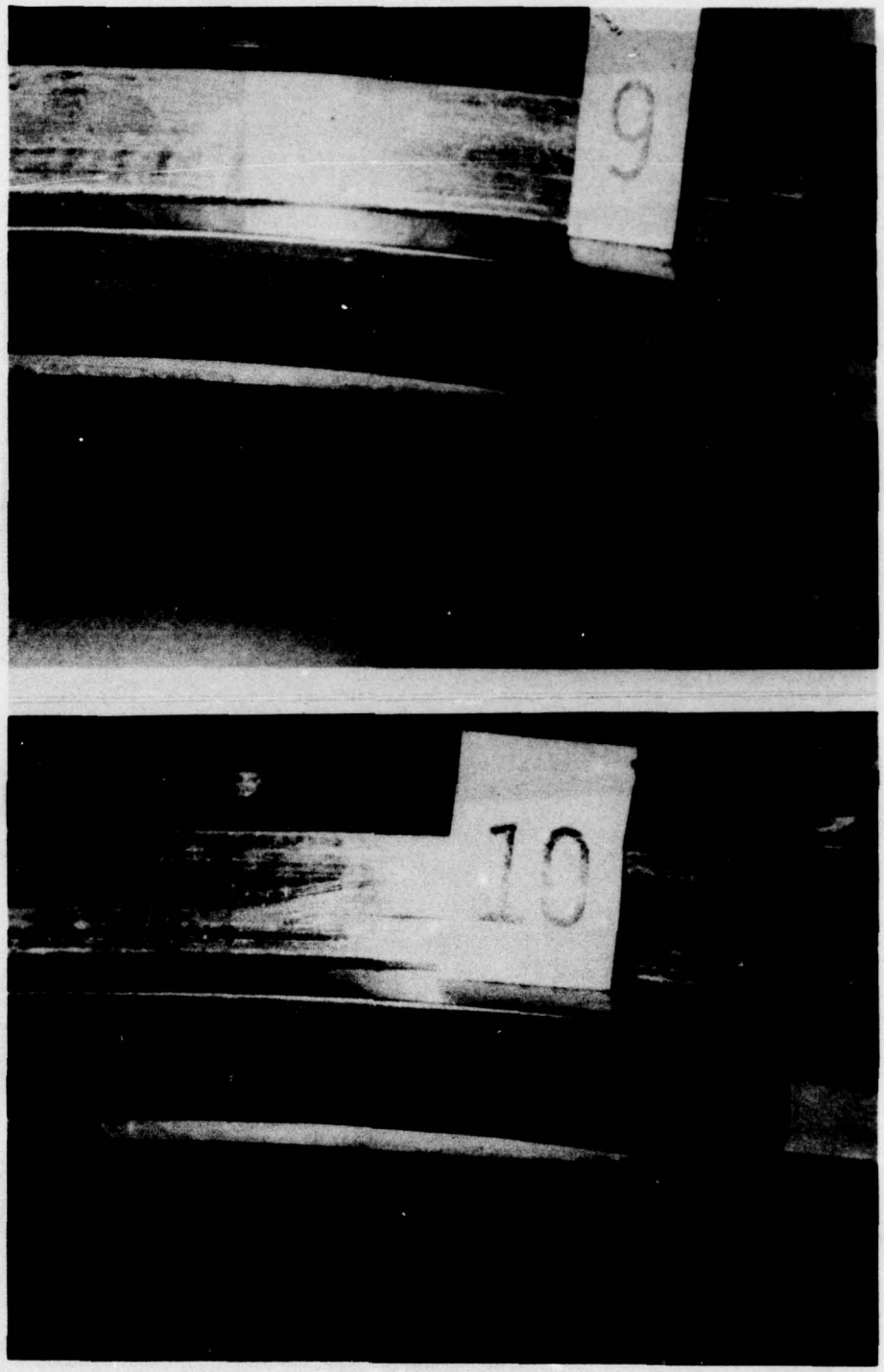

#9

#10

FIGURE 115. 10kW NOZZLE CERAMIC VANE SECTIONS #9 and #10 AFTER ENGINE TEST - 25 HOUR RUN PLUS 50 START/STOP CYCLES

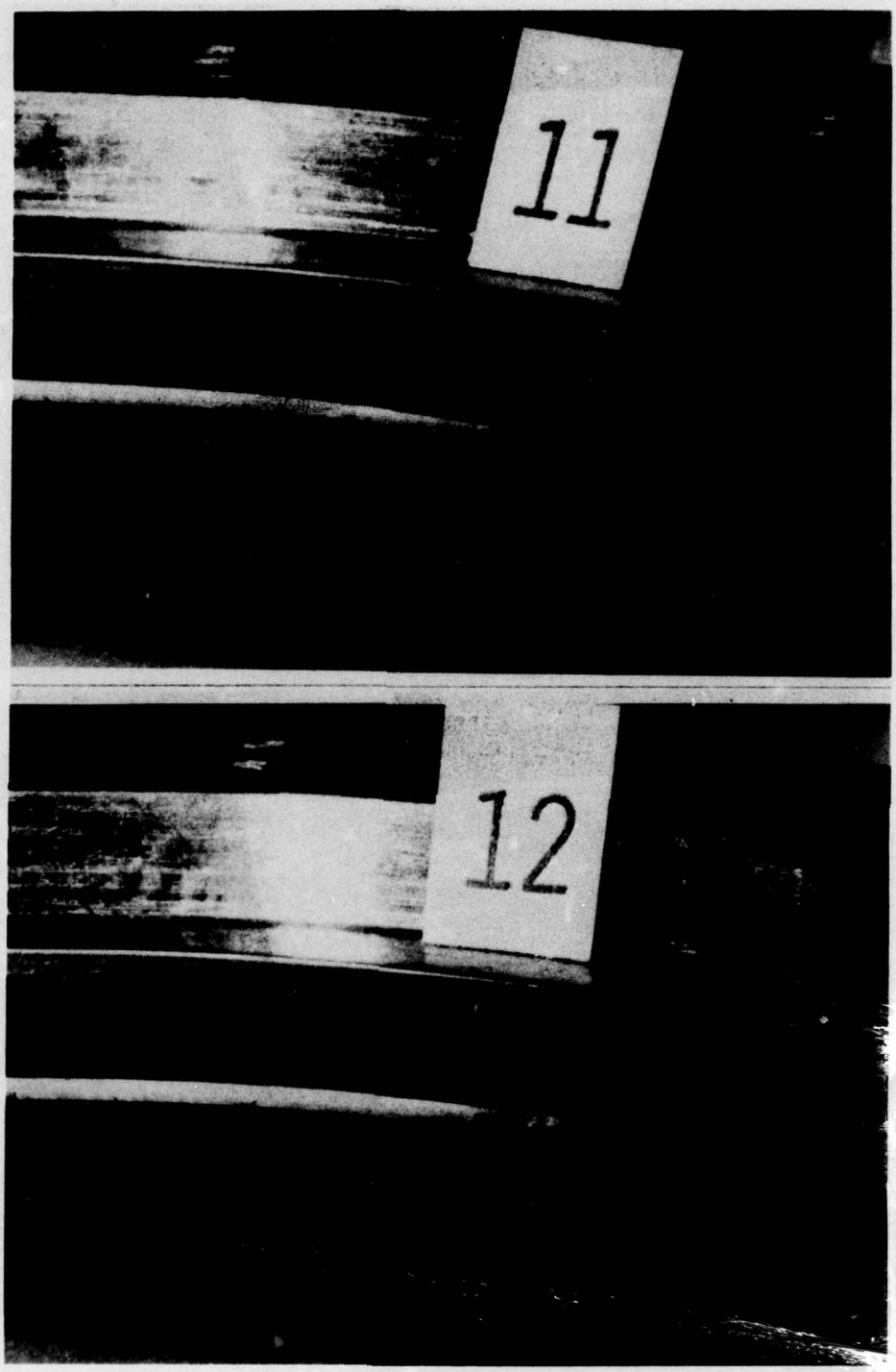

#11

#12

FIGURE 116. 10kW NOZZLE CERAMIC VANE SECTIONS #11 AND #12 AFTER ENGINE TEST - 25 HOUR RUN PLUS 50 START/STOP CYCLES

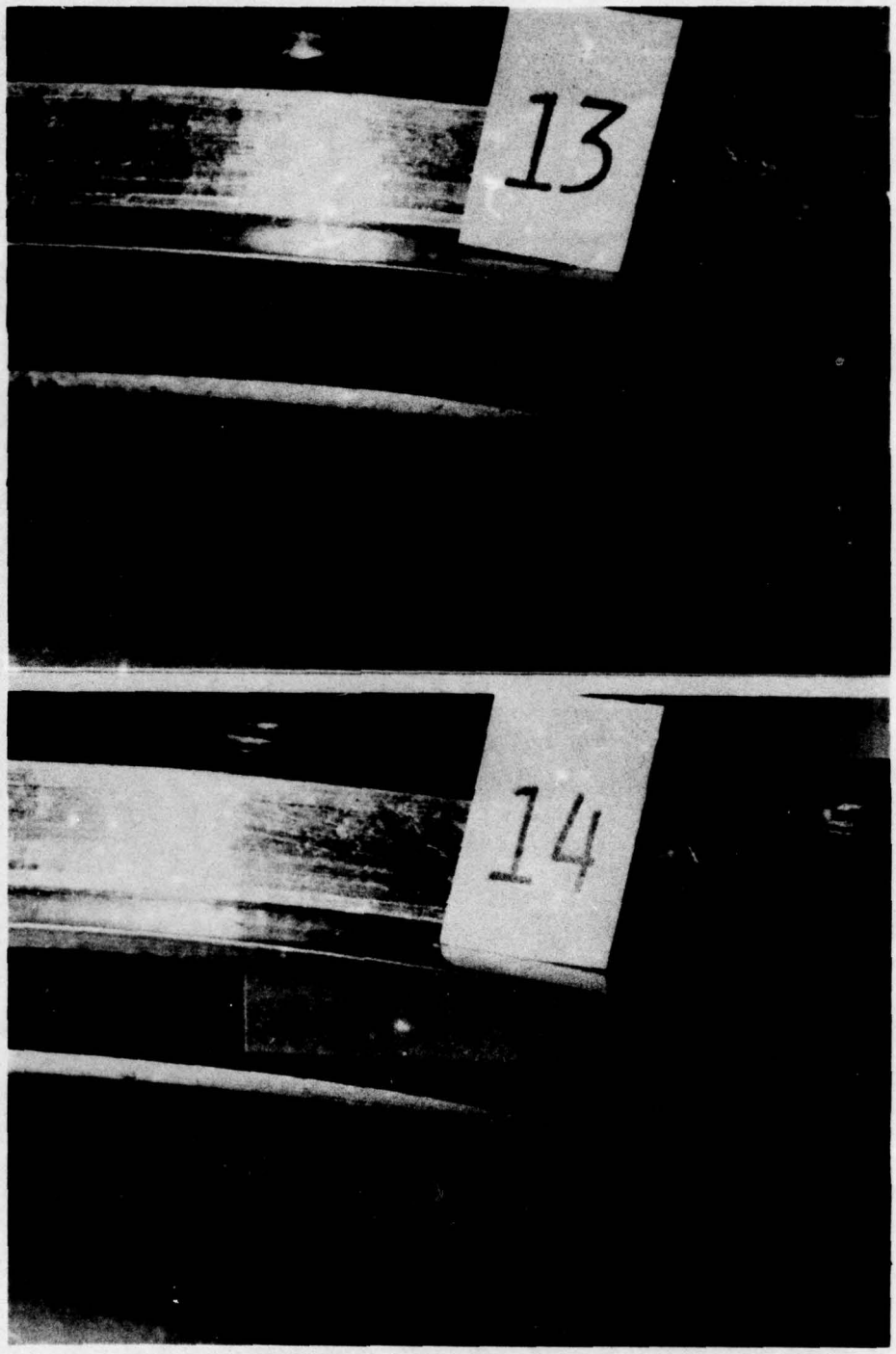

#13

#14

FIGURE 117. 10kW NOZZLE CERAMIC VANE SECTIONS #13 AND #14 AFTER ENGINE TEST - 25 HOUR RUN PLUS 50 START/STOP CYCLES

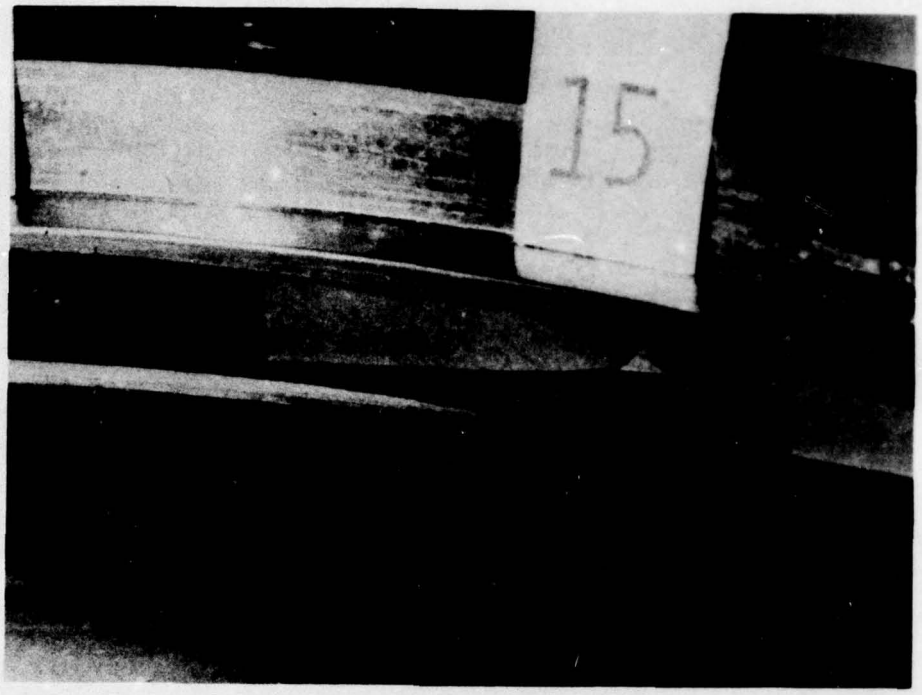

#15

FIGURE 118. 10kW NOZZLE CERAMIC VANE SECTIONS #15 AND #16 AFTER ENGINE TEST - 25 HOUR RUN PLUS 50 START/STOP CYCLES

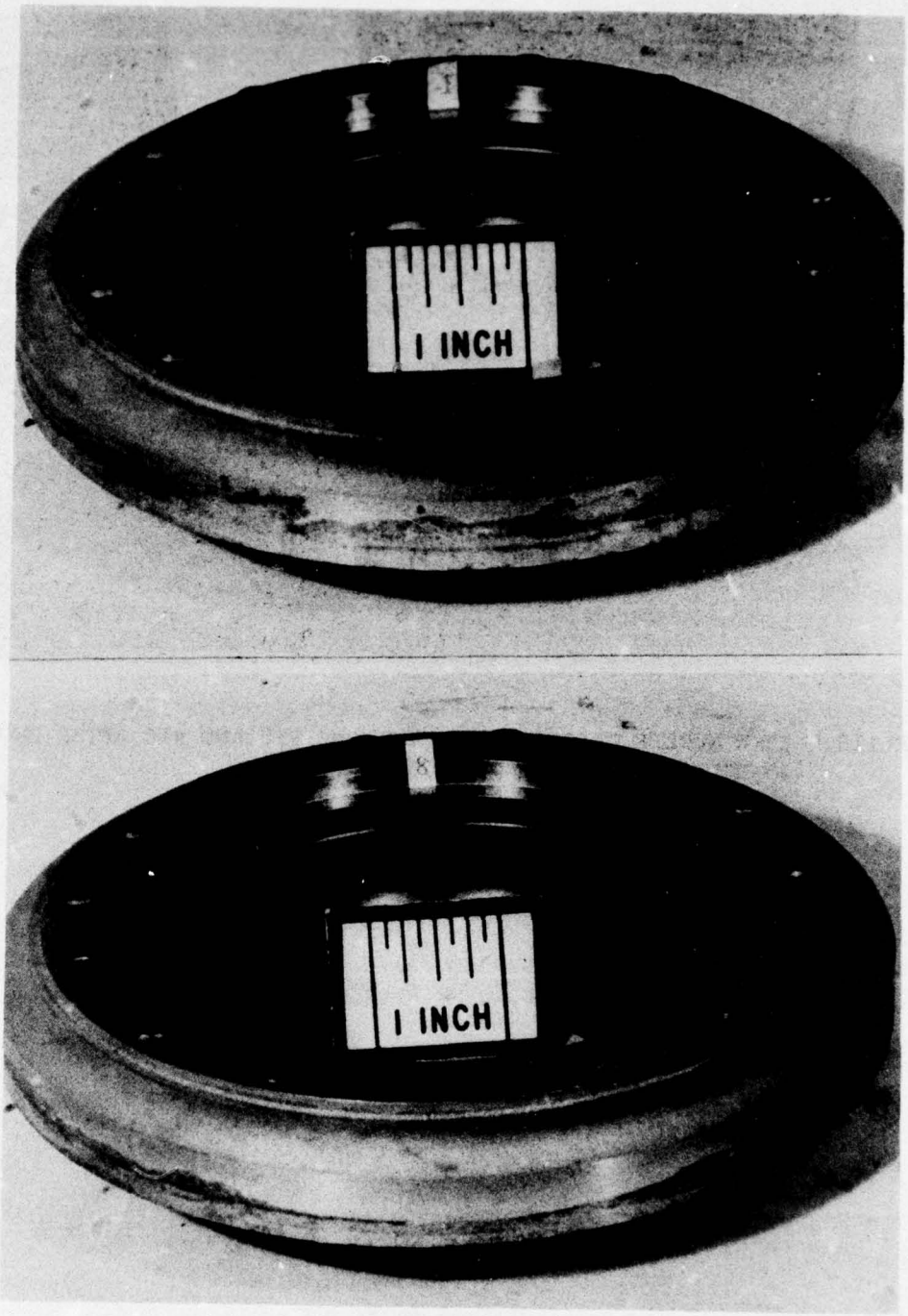

A.

B.

FIGURE 119. 10kW NOZZLE WITH HOT PRESSED Si_3N_4 VANE SECTIONS AFTER ENGINE TEST - 25 HOUR RUN PLUS 50 START/STOP CYCLES

Shroud deformation was shown to be probable by analysis because of thermal stresses and lowered yield strength of the shroud material (713LC) at higher turbine inlet temperatures ∿871°C (1600°F).

Also, forces generated by nozzle mounting bolts are counteracted at the lip which was deformed during test. These nozzle assembly forces are on the order of 5,000 to 10,000 lb per bolt. It is believed that the shroud lip deformation that occurred resulted primarily from this assembly arrangement which applies bending loads to this shroud section. This deformation could also have resulted partially from residual stresses induced during final machining of this lip and subsequent bending back to its original position.

4

DISCUSSION OF PROGRAM RESULTS
CONCLUSIONS AND RECOMMENDATIONS

Discussion of the program results forms the basis for interim conclusions and recommendations on use of ceramics in the nozzle section of the small 10kW radial engine.

4.1 CERAMIC VANE NOZZLE

A radial gas turbine nozzle with ceramic vane segments presents some inherent problems. They are:

1. Dissimilar coefficients of thermal expansion from ceramic vanes to metal shrouds.

2. Difficulties in bonding ceramics to metal alloys.

3. Brittle behavior of ceramics which make them sensitive to contact loads.

4. Fabrication costs of ceramic vane segments and/or limited fabrication capabilities.

Differential Thermal Expansion

Dissimilar coefficients of thermal expansion between ceramics and superalloys require special design considerations. The length differential between the $HPSi_3N_4$ ceramic vane and 713LC superalloy shroud as engine tested in this program due to a temperature excursion to 927°C (1700°F) is 0.242 mm (0.0095

in.). Mechanical containment of ceramic vane sections in shroud recesses must allow for shroud growth and still not allow leakage to develop between the front of the ceramic vane section and metal leading edge.

This problem was dealt within this program by providing a metal tab extending from the inboard section of the metal leading edge (see Fig. 37), such that cross vane leakage would not occur. Static aerodynamic pressure forces locate the vane against this metal tab section and provides a self-sealing metal ceramic interface regardless of relative thermal growth. The same problem and solution also applies to leakage at vane recess in shrouds.

By the above method of vane entrapment it is still possible to accomplish accurate vane location (and nozzle shroud size) while providing an oversized vane recess. Pressure forces locate the vanes downstream and against the recess surface nearest engine axis. Location of this recess surface and vane thickness are the only dimensions that must be controlled for accurate nozzle throat opening. Cross vane thermal expansion difference from HPSi$_3$N$_4$ ceramic to 713LC superalloy results in 0.030 mm (0.001 in.) more growth in nozzle throat than would normally occur. This is not a significant variation in nozzle throat size.

Ceramic to Superalloy Bonding

Another technique for avoiding leakage across vanes is to use a joining material between metal and ceramic components. However, high differential thermal growth makes bonding or joining of ceramics to most metal alloys, including superalloys, very difficult. Any bond must have capability to deform considerably while still maintaining its function. (While it is possible to formulate metal braze alloys which will wet both ceramic and superalloy, these braze materials will not relax sufficiently and failure of the braze or ceramic usually results.)

Metal to ceramic joints have been applied in the program by use of relaxing glass adhesives. At high temperature [$\sim$600°C ($\sim$1100°F)] they will relax and

conform to differential thermal strains while still adhering to both ceramic and superalloy surfaces. At lower temperature the glasses become less flexible and will not relax plastically, however, certain compositions (30% B402 - 30% GN19 - 40% Cr_2O_3 and 35% B402 - 35% GN19 - 30% Cr_2O_3) will maintain a bond through low temperature excursions. The mechanism is believed to be that the glass forms micro-cracks which allow localized mechanical rotations and accommodation of substantial shear strain without loss of bond. When taken back to operating temperatures, these cracks tend to heal themselves.

These relaxing glass adhesives do have certain limitations at low temperature. Actual bond strength is relatively low because of the cracking phenomena and inherently low strength of the glass itself. High temperature strength is limited because the glass behaves like a Newtonian fluid (with very high viscosity). Sufficient time at elevated temperature will allow parts bonded with relaxing glass to change position and locate at the point of lowest energy. (In the case of ceramic vanes in recesses, this is not an entirely undesirable phenomena since the vane will locate itself at the inboard downstream surface which provides proper vane location.) This implies that relaxing glasses are suitable to fulfill only certain functions, which include sealing of potential gas leakage interfaces and provide control of contact stresses.

Contact Stresses

Ceramic materials are very susceptible to contact stress because of their lack of plasticity. Contact loads on metal alloys normally distribute themselves because of local plastic behavior. Ceramics do not yield locally and therefore, are subject to extremely high contact stresses. Micro-cracks form if stresses become high enough. This stress sensitizes the part to the applied loads and results in crack propagation and failure. The relaxing glass-based adhesives cited in the previous paragraph have the potential of being very useful in solving the problem of contact stresses in ceramics. They are capable of flowing and conforming to surface irregularities but also

contain a significant amount of finely dispersed Cr_2O_3. (Cr_2O_3 is undissolved at all temperature ranges considered here and therefore will resist extrusion from contact interfaces and successfully avoid excessive contact stresses under prolonged load). However, one possible difficulty in using relaxing glasses for joining of ceramics to metal alloys is generation of extraneous loads on ceramics. For example, the lower temperature glass (40% B402 - 20% GN19 - 40% Cr_2O_3) used in rig tests may be associated with failure of a vane trailing edge in these tests (see Section 3.2.9 for details). For this reason, relaxing glasses were not used in engine tests. Also, it was felt that a metal-ceramic structure would not be as sensitive to contact stresses as an all-ceramic structure because some stress relaxation can be expected at the metal contact. However, five ceramic vane section failures due to excessive contact loads in the engine tests might have been avoided if the higher temperature glasses had been used to distribute contact loads.

Fabrication Costs

An important consideration in application of ceramics for reduced nozzle erosion is material cost of the nozzle assembly. If hot pressed materials are used, the cost of 15 vane sections substantially impact the total price of the nozzle. Currently, the cost of these vanes in limited quantities, is approximately equal to twice the finished cost of a standard nozzle. One vendor has estimated that the price of these HPSi_3N_4 and ceramic vanes could be reduced to approximately one quarter of their current cost if they were made in quantities of thousands. Unfortunately, the potential for cost reduction of hot pressed vanes is limited because they must be diamond ground to shape from hot pressed billets. Even the simple vane section configuration used here requires significant grinding time. The diamond tool consumption rate also adds to vane section cost.

A possible alternative to the high cost of hot pressed ceramic vane sections exists and that is use of a silicon filled type recrystallized silicon carbide for vane sections. This material offers the potential for lower fabrication costs since it can be slip cast. Although the erosion resistance of NC 430 (Norton's designation for the above material), for example, is

reduced from HPSi_3N_4 it still offers an advantage over 713LC superalloy. (Ambient temperature 30° impingement angle erosion tests show a 60:1 advantage of HPSi_3N_4 over 713LC compared to a 10:1 advantage for NC 430.) While thermal shock resistance of silicon filled silicon carbide is less than HPSi_3N_4, it appears to be comparable to HPSiC. The thermal loading environment of the 10kW engine may not be overly severe for application of this easily fabricated material. The most cost effective use of ceramics for increased nozzle erosion resistance is probably application of a lower cost ceramic like NC 430 for an order of magnitude increase in erosion resistance.

Results

The portion of this project dealing with the ceramic vane nozzle concluded with an engine test. Although no significant deterioration in engine performance occurred after 25 hours operation and 50 start/stop cycles, five vane sections failed due to mechanical loads. Distortion of the forward (outer) 713LC shroud seems to be the direct cause of these failures.

Rig testing did not generate nozzle distortion. This is probably due to one of two or both of the following reasons: the lip at the outer shroud inner diameter which normally bears against the seal plate to counteract mounting bolt forces was not used in rig tests to take up these loads; and the outer ring section of the outer shroud was immersed in hot combustion gasses as compared to the engine installation which has a dead air space on the outside of this ring. The outer ring section of the outer shroud runs cooler in the engine installation which would be expected to accentuate the shroud warping problem.

Shroud warping has been experienced in standard nozzle installations of the 10kW engine. A nozzle material change from Hastelloy X to 713LC for higher elevated temperature yield strength improved this situation for the standard nozzle. The ceramic vane nozzle does not have as much section stiffness at the nozzle throat as the standard configuration because of the abbreviated length of the metal vane section. Deformation at temperature seems therefore likely with the ceramic vane section nozzle.

There are measures which could be used to counteract this problem. Inspection of the outer shroud after test show that most of the distortion that resulted in vane failures occurred in the thin lip that bears against the seal plate. Deformation of this lip appears to be the result of yielding under load at peak temperatures. An analysis of stresses developed in the lip because of assembly bolt torque alone shows that the lip experiences bending stresses near the 713LC ambient temperature yield point. Reduction in yield point due to high temperature operation of the nozzle causes an overstress condition. Several design modifications of the metallic shroud to minimize this distortion have been considered and could be used if required.

Engine simulator rig tests conducted in program Phase I demonstrated that $HPSi_3N_4$ vanes can resist a minimum of 500 thermal shock cycles which are more severe than that typically encountered in engine operation. The cycle was designed to simulate thermal shock equivalent to that occurring in an emergency shutdown situation. Figure 120 gives a pictoral display of this thermal upshock sequence which raises ceramic vane trailing edge temperature from 593°C to 937°C (1100°F to 1700°F) in 7.7 seconds. This shock cycle involves total gas temperature of 1121°C (2500°F) and nozzle throat velocity of 2270 fps (See Section 3.2.9.1 for details.)

Engine simulator rig erosion tests conducted with a standard 10kW nozzle using 713 LC vanes and ceramic vane nozzle in a parallel test show a minimum of 16:1 advantage of the ceramic nozzle in 927°C (1700°C) dust erosion.

A 60 hour, 3 ppm, sea salt corrosion test conducted in the engine simulator at 927°C (1700°F) demonstrated that $HPSi_3N_4$ vane sections are unaffected by this environment. As a comparison, the 713LC nozzle shrouds showed significant surface attack.

4.2 ALL-CERAMIC NOZZLE

Application of an all-ceramic nozzle involves many of the same types of problems as a ceramic vane section nozzle. Dissimilar expansion coefficients

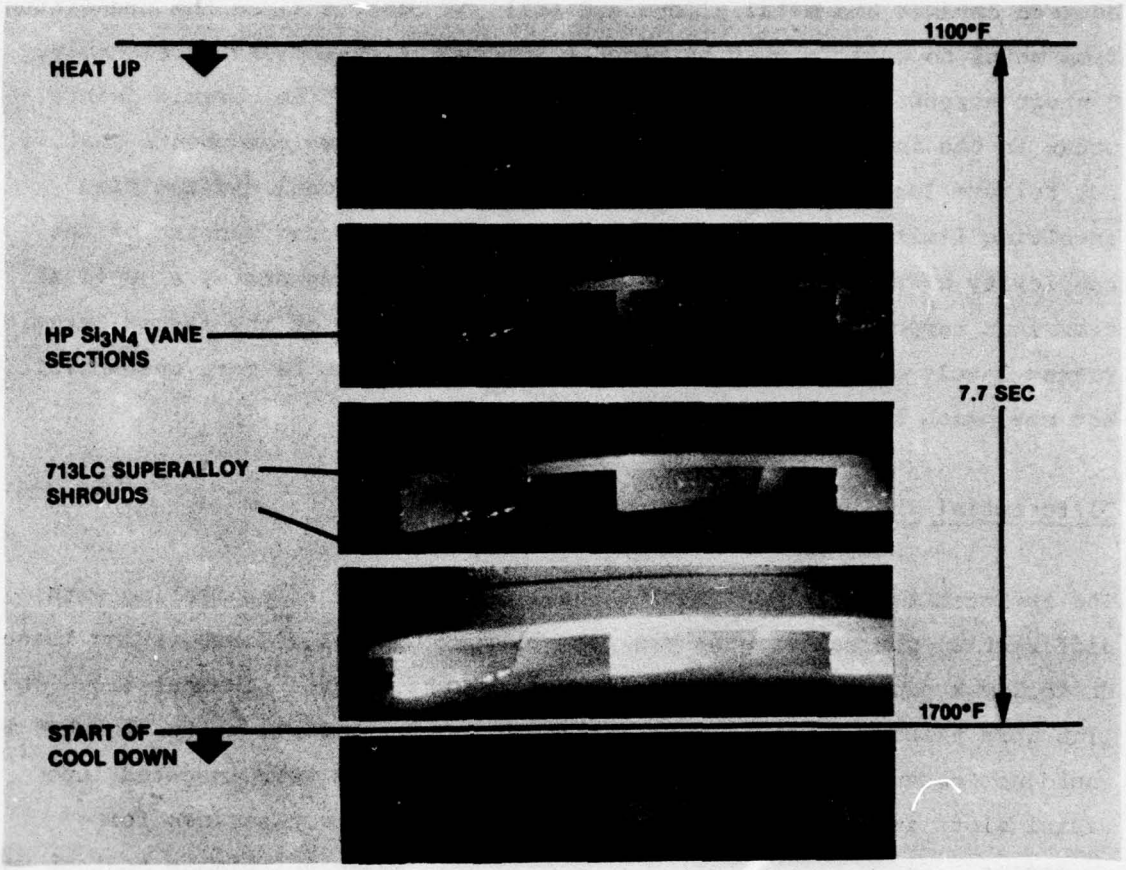

FIGURE 120. THERMAL SHOCK OF CERAMIC/SUPERALLOY NOZZLE

between ceramic and metal alloys are still of concern since the transition from metal to ceramic must be made at some point in the engine assembly. Contact stresses become more critical because ceramic to ceramic joints as occur in the interface of vanes to shrouds involve two components that will not relieve localized stress concentrations. Additional difficulties involving limits on fabrication capabilities are imposed because of the complexity of shrouds. Thermal stresses due to steady state, as well as transient temperatures, become more critical because of the larger ceramic pieces involved. Also, reaction bonded Si_3N_4 seems to be more susceptible to hot corrosion than $HPSi_3N_4$.

Differential Thermal Expansion

The approach taken in design of the all ceramic nozzle for dealing with differential thermal strains was primarily mechanical. Three spring loaded Hastelloy X pins held the nozzle plates against the test chamber lid. The pins were piloted on their diameter at the mounting plate to assure that they would not become misaligned. The three holding pins were inserted into radial slots in the $RBSi_3N_4$ shrouds. The slots allow clearance for expansion. Since the Hastelloy X holding pins were in intimate contact with the cooled holding plate they would be expected to run cooler than gas stream temperature. Refrasil insulation was used to the face between holding pin heads and ceramic shrouds to avoid any local thermal gradients there.

During the course of 1093°C (2000°F) sea salt corrosion testing cracks developed at holding pin locations. One crack proceeded to the center of the bottom shroud. Dissassembly of the nozzle showed that only the two pin locations where cracks had occurred had molten products impregnated into the refrasil insulation (see Section 3.2.10.2 for details). The nature of the failures at these pins led to the conclusion that short circuiting of the insulation caused excessive local thermal gradients in the ceramic shroud.

In order to verify this, a second set of nozzle shrouds was used in thermal shock tests. Insulation was placed at locating pin heads and on both sides of Hastelloy spacers which are located between shrouds on holding pins. This proved effective in eliminating the cracking problem on ceramic shrouds at locating pins.

Contact Stresses

Contact stresses at the interface of ceramic vanes and ceramic shrouds are a potential source of failure in these pieces. The same approach in dealing with this problem as taken for the ceramic superalloy nozzle was taken here. Relaxing glass adhesives with substantial amounts of Cr_2O_3 fill were applied to 10 of the 15 vanes tested in engine simulator rig thermal shock experiments. The compositions were suitable for higher temperature than those used in metal to ceramic bonds. No difference in performance between either type of bond used for vane or unbonded vanes was noted, because no vane or shroud failures occurred due to joint contact stresses.

Fabrication

The ceramic shrouds used in rig tests were relatively simple shapes compared to what would be required for shrouds appropriate for engine installation. However, considerable accuracy of location and detail was required for the 15 vane recesses in each of the shrouds. $RBSi_3N_4$ was chosen as the ceramic material best able to meet the required fabrication capabilities along with adequate strength and physical properties needed for the shrouds. $RBSi_3N_4$ can be easily machined to shape in the green state. Final firing does not result in distortion, change in volume or loss of surface finish. This material can also be injection molded or formed by other processes prior to final firing.

Thermal Stresses

Thermal stresses are probably the most critical problem for ceramic nozzle shrouds. Fabrication capabilities and costs require the use of a lower strength ceramic. Thermal loads are prone to be high because of the large physical size of the nozzle shrouds.

Despite these anticipated problems engine simulator rig experiments have shown that the simulated nozzle design considered for demonstration in this program can survive the most severe thermal transients expected during the course of 10kW engine operation.

The design incorporates the principles set forth in the program proposal for philosophy of design which are:

1. Avoidance of heavy ceramic sections.
2. Avoidance of rapid change in section.
3. Avoidance of large ceramic pieces.
4. Attempt to maintain uniform heating rates on adjacent sections.
5. Thermal expansion relief by use of relaxing glass joining materials.
6. Design ceramic parts in compression loading as much as possible.

Corrosion

A 70 hour 3 ppm sea salt corrosion test at 1093°C (2000°F) with RBSi$_3$N$_4$ nozzle shrouds showed that corrosion attack was not insignificant with this material. Surface penetration at certain regions was of the same order as that for 713LC shrouds in the same test. There is evidence, however, that

sea salt corrosion occurs only at temperatures below 1093°C (2000°F). It has not been demonstrated the $RBSi_3N_4$ is inferior in these tests to 713LC superalloy and therefore this ceramic would be expected to perform as well as the existing nozzle material in the sea salt corrosion.

4.3 CONCLUSIONS

The Phase I and II program results demonstrate the feasibility of using ceramics in the 10kW gas turbine engine nozzle section. Silicon nitride ceramics have been shown to have adequate thermal shock and sea salt corrosion resistance for use as nozzle vanes and shrouds. Erosion resistance of hot pressed silicon nitride 10kW nozzle vanes has been shown to be far superior to that of high temperature metal alloys.

Engine simulator rig experiments demonstrated that hot pressed silicon nitride vanes can survive 500 thermal shock cycles representing the most severe thermal transient that could occur in the 10kW operating schedule. Reaction bonded silicon nitride in the form of simplified nozzle shrouds also survived 500 engine simulator thermal cycles.

Since the engine simulator thermal cycles used in test of the above ceramic nozzle components were more severe than the normal engine operating sequence and represented an extraordinary operating event, it is reasonable to assume that ceramic nozzle components of these materials possess the properties necessary to endure a normal engine life cycle. Other simulator test results (erosion, corrosion tests) demonstrate that survivability of $RBSi_3N_4$ nozzle shrouds depends heavily upon proper design precautions, particularly the method of connecting ceramic shrouds to metal components.

Engine test of hot pressed ceramic vane sections shows that even high strength ceramics are very susceptible to failure due to contact stresses. (Mechanical compression of hot pressed silicon nitride vanes between 713LC superalloy shrouds resulted in fracture of trailing edges in 5 of 15 ceramic vane sections.

Engine simulator rig erosion experiments at 927°C (1700°F) of the HPSi$_3$N$_4$ ceramic vane section nozzle show that erosion rate can be reduced over that of 713LC superalloy by use of hot pressed silicon nitride by between 1 and 2 orders of magnitude.

Informal cost studies show that a substantial cost advantage can be realized by use of a non-hot pressed ceramic for nozzle vanes. Literature study shows that silicon filled recrystallized silicon carbide has a high probability of meeting this need for the 10kW turbine engine.

4.4 RECOMMENDATIONS

The following recommendations are made:

- Development of an all-ceramic nozzle for 10kW gas turbine engine application should be continued. This work is outlined in the project phases III and IV. The development plan includes analysis and design for selection of two alternative all-ceramic nozzle concepts. The two concepts will be tested progressively in static thermal cycling and engine simulator thermal cycling experiments. This is to be followed by a design selection and engine test of an all-ceramic nozzle.

- It is recommended that the ceramic vane section nozzle concept be retested after design modifications are made to avoid shroud distortion and compressive loading of vane trailing edges.

- Additional work should be performed to aid in practical application of ceramics to the 10kW gas turbine engine:

  1. Refinement of ceramic nozzle design for improved nozzle efficiency relating to leakage at static seals, dynamic leakage between rear shroud and turbine wheel and improved aerodynamic form for ceramic nozzle vanes.

2. Study of alternatives for reduction in cost of ceramic components and completed engine assembly costs.

3. Statistical definition of strength limits of ceramic parts.

4. Development of nondestructive test method for qualifying parts for engine installation.

REFERENCES

1. H.E. Shoemaker and C.P. Shumate, "Techniques for Reducing Sand and Dust Erosion in Small Gas Turbine Engines," SAE Paper 700706, Society of Automotive Engineers (Sept. 1970).

2. "Gas Turbine Sand and Dust Effects and Protection Methods," SAE Paper 700705, Sept. 1975.

3. W.A. Compton and K.P. Steward, "Dust Erosion of Compressor Materials - Experience and Prospects," ASME Paper 68-GT-55, The American Society of Mechanical Engineers (March 1968).

4. C.E. Smeltzer, M.E. Gulden and W.A. Compton, "Mechanisms of Metal Removal by Impacting Dust Particles," ASME Paper 69-WA/Met-8, The American Society of Mechanical Engineers (1969).

5. C.E. Smeltzer and W.A. Compton, "Mechanisms of Sand and Dust Erosion in Gas Turbine Engines," Final Report on Contract DAAK02-68-C-0056 (1968).

6. I. Finnie, "Erosion of Surfaces by Solid Particles," Wear, Vol. 3, pp. 87-103 (1960).

7. H.M. Consylman, C.P. Shumate and W.M. Owen, "Product Support Program," Final Report on Contract N00019-71-C-0311 for the Naval Air Systems Command, Solar Report ER 2429 (Feb. 1973).

8. K.H. Jack, "The Production of High Temperature, High Strength Nitrogen Ceramics," Proceedings of the Second Army Materials Technology, Brook Hill (1974).

9. C&EN, June 14, 1976, p 8.

10. Baumgartner, H.R., Norton Co., Industrial Ceramics Div., Personal Communication.

11. Campbell, ed. "HIgh Temperature Technology," New York: John Wiley & Sons, Inc., 1956, p. 460.

12. R.J. Beck, "Evaluation of Ceramics for Small Gas Turbine Engines," SAE 740239, March 1974.

13. S.E. Mumford and C.R. Booker, "Testing of Ceramic Stator Vanes to 2500F (1371C)," ASME 75-GT-103.

14. S.A. Sanders and H.B. Probst, "Behavior of Ceramics at 1200°C in a Simulated Gas Turbine Environment," SAE 940240.

15. A.F. McLean, et al., "Brittle Materials Design, High Temperature Gas Turbine," Interim Report, AMMRC CTR 73-9.

16. A.F. McLean, et al., "Brittle Materials Design High Temperature Gas Turbine," Interim Report, AMMRC CTR 73-32.

17. Norton Co., Industrial Ceramics Division, "Ceramics for Engine Components," Product Bulletin.

18. International Nickel Company, Inc.

19. A.F. McLean, et al., "Brittle Materials Design, High Temperature Gas Turbine," Interim Report AMMRC CTR 74-26.

20. Torti, M.L., "Ceramics for Gas Turbines Present and Future," SAE 740242.

21. R.J. Lumby, et al., "The Development of Silicon Nitride to Achieve Higher Inlet Temperatures in Land Based Gas Turbines," SAE 720170.

22. A.G. Metcalfe, "Application of Ceramics to Radial Flow Gas Turbines at Solar," presented at Army Materials Technology Conference Series, Ceramics for High Performance Applications, November 1973.

23. "Ceramic Materials for Gas Turbine Environment," AMMRC CTR 73-52.

24. Black, Machine Design, McGraw Hill, 1955.

25. C.E. Smeltzer, M.E. Gulden, S.S. McElmury, and W.A. Compton, "Mechanisms of Sand and Dust Erosion in Gas Turbine Engines, USNAVLABS Technical Report 70-26 (1970).

26. International Nickel Company, Inc.

27. Sanday, S.C. et al, "Design and Analysis of a Ceramic Stator Vane," ASME 75-GT-100.

28. McLean, A.F. et al, "Brittle Materials Design, High Temperature Gas Turbine," Interim Report AMMRC Ctr 75-29.